

THE UNIVERSITY OF HULL

Magnetic Forces for Surface-Based Bioanalysis in Microfluidic Devices

being a Thesis submitted for the Degree of

Doctor of Philosophy

in the University of Hull

by

Sally A. Peyman BSc (Hons) MRSC

April 2010

Contents

Contents	1
Acknowledgements	8
Glossary	10
Abstract	14
1 Microparticle handling on-chip	16
1.1 Microparticles for surface-based bioanalysis	16
1.2 Microfluidics and micro-Total Analysis Systems	21
1.3 Particle handling on-chip – literature survey	23
1.3.1 Retention of microparticles in channels	23
1.3.2 Retention using adhesion and patterning	27
1.3.3 Retention using externally applied forces	28
1.3.4 Continuous flow separation of particles.....	43
1.3.5 Continuous flow particle processing.....	63
1.4 Summary of particle handling in microfluidic devices	65
1.5 Scope and aim of the thesis	66

2	Theory of on-chip magnetic particle handling	69
2.1	Stable particle suspensions	69
2.2	Magnetic theory.....	73
2.2.1	Magnets and units	73
2.2.2	Magnetic materials	76
2.2.3	Measuring magnetism – the <i>M/H</i> curve.....	81
2.3	Deflecting magnetic particles in flow	83
2.3.1	Magnetophoretic mobility.....	83
3	Experimental	89
3.1	Chemicals and solutions	89
3.2	Magnetic particle Suspensions	93
3.2.1	Magnetic particle suspensions for particle comparison investigation.....	93
3.2.2	Magnetic particle suspensions for bioassays	95
3.2.3	Vibrating Sample Magnetometer (VSM) for measuring magnetisation curves of magnetic particles.....	96
3.3	Permanent magnets.....	100
3.3.1	Hall sensor for measuring magnetic flux	100

3.4	Microchip fabrication	102
3.5	Particle comparison investigation.....	103
3.5.1	Microchip design.....	104
3.5.2	Microchip set-up	105
3.5.3	Magnetic set-up	106
3.5.4	Experimental procedures.....	109
3.5.5	Data acquisition and analysis	110
3.6	One-step bioassays	111
3.6.1	Microchip design (MLF1).....	111
3.6.2	Magnetic set-up	113
3.6.3	Experimental set-up for one step bioassays	115
3.6.4	Experimental procedures for MLF1 design	117
3.6.5	Data acquisition and analysis	120
3.7	Two-step bioassays.....	125
3.7.1	Microchip design (MLF2).....	125
3.7.2	Experimental set-up of two step bioassays	126
3.7.3	Magnetic set-up of two step bioassays.....	127

3.7.4	Experimental procedures.....	128
3.7.5	Data acquisition and analysis	133
3.8	Diamagnetic manipulation of particles.....	134
3.8.1	Chemicals and polystyrene particle suspensions for diamagnetic repulsion 135	
3.8.2	Microfluidic set-up.....	136
3.8.3	Particle trapping investigation.....	137
3.8.4	Diamagnetophoresis.....	140
4	Magnetic particle selection	146
4.1	Comparison of permanent magnets used for particle deflection	146
4.2	Particle selection.....	151
4.2.1	Comparison by free-flow magnetophoresis	151
4.2.2	Comparison by VSM measurements.....	169
4.2.3	Comparison of free-flow magnetophoresis and VSM results	173
4.2.4	Summary of particle selection.....	176
4.2.5	Discussion	177
5	Development of a one-step streptavidin – biotin continuous flow binding assay.	180

5.1	Characterisation of flow in MLF1	181
5.2	Deflection of M-270 particles	187
5.3	Streptavidin – biotin binding assay	192
5.3.1	Initial assay experiments and optimisation	194
5.3.2	Effect of biotin concentration.....	202
5.3.3	Summary and discussion of the one-step bioassay	209
6	Two – step sandwich immunoassay	211
6.1	Characterisation of flow in the chip design MLF2 (Multi-Laminar-Flow-2)	212
6.2	Diffusion investigations	215
6.3	Optimisation of magnetic particle deflection	219
6.4	Mouse IgG sandwich immunoassay	221
6.4.1	Initial investigations into two-step binding assay	222
6.4.2	Effect of 1 ^o antibody concentration.....	231
6.4.3	Summary of mouse IgG immunoassay	234
6.5	C-reactive protein sandwich immunoassay	234
6.5.1	Proof of concept for CRP sandwich immunoassay	235
6.5.2	Summary of CRP immunoassay	241

6.6	Discussion of two-step immunoassays	241
7	Diamagnetic repulsion for on-chip manipulation	244
7.1	Diamagnetic plugs for simultaneous bioanalysis	244
7.1.1	Diamagnetic forces for trapping polymer particles.....	245
7.1.2	Diamagnetic particle plugs for simultaneous streptavidin – biotin binding assay	250
7.1.3	Formation of simultaneous diamagnetic and paramagnetic plugs	254
7.1.4	Summary of diamagnetic repulsion forces for trapping particles	259
7.2	Size - selective diamagnetophoresis.....	260
7.2.1	Diamagnetic repulsion for deflecting particles	261
7.2.2	Separation of 5 μm and 10 μm sized polymer particles.....	262
7.2.3	Diamagnetic repulsive forces for the size-selective separation of two particle populations.	263
7.2.4	Summary of size-selective diamagnetophoresis	272
7.3	Discussion of diamagnetic repulsion forces for manipulating particles.....	272
8	Conclusions and future outlook	275
8.1	Particle selection.....	275
8.2	One step bioassays.....	277

8.3	Two-step bioassays.....	279
8.4	Diamagnetic repulsive forces for particle handling.....	281
8.5	Outlook for the future	283
	References	285
	Appendix	294

Acknowledgements

This project was funded by the University of Hull and the EPSRC and I would to thank them both for the opportunity to study for this PhD.

Firstly and foremost I would like to thank my supervisor, Nicole Pamme for her continued and unwavering support through-out this PhD and beyond. I can safely say that the work contained within these pages, my own professional development and the success that I have enjoyed with this project over the last 3 and a half years, is a direct and positive result of her supervision and mentoring. I think with any good supervisor, some of their style and professionalism is impressed upon the student and I can never imagine now creating an image without a scale bar, drawing a poster without spending three hours using the align tool or writing a good report without blasting out the 'gap' in the research. Thank you Nicole, I hope that long after this thesis has been examined we will remain good friends in the years to come. There are scores of people I wish to thank who have helped me over the last four years, either personally or professionally. To name a few: Alex Iles for his support and ideas, whether slightly way-out or not, they've always encouraged me to think about my work from a different angle and often solved many frustrating problems. Also for his quick and very thorough last minute proof-reading of this thesis, thank you Alex. Lou Evans, who has been there for me the longest. Thank you for being my best friend and my biggest supporter since those early days in the Chemistry department back in 2002. Those trips to the Rez, the Gardeners, the OGM or the Sanctuary have been invaluable over the years and some of my sanity through-out the PhD I most definitely owe to you. Thanks to Tom 'Ice' Dearing and

Acknowledgements

Gareth Pearson, who showed me the ropes when I first started my PhD and continued on to being two of my best friends. Thanks also to Sam, Jane, Martin, Francesco, Entesar and the number of MSc students that have passed through lab C217. All of you have shared various ups and downs with me, but have all created an atmosphere at Hull that I will never forget. Last but by no means least of the Hull crew I would like to give a special thanks to Mark Tarn and Kirsty Evershed for all their support both in and outside the lab, but also for being super friends and for helping me with the final submission of this thesis. Outside of the University, my thanks go to Charly Rees and Aisling Creedon, for support and encouragement I would have wavered many a time without. Thank you.

My deep and sincere gratitude go to my family, my Dad, Roger Peyman and my brother John, who despite the years of teasing me for being 'a student', I know I have always had your support and I hope all the years of 'claiming off the tax-payer' will finally make you proud! Thanks also go to the rest of my family, Malc, Liz, Mark and Sophie and especially to my Mum, Annie Ives, without whom I most certainly would not be here. Thanks for pushing me from day one, I may have scowled and stuck my heels in from time to time, but I realise now that you above anyone saw my potential and knew, even when I didn't, that I would not be happy in my later life if I did not aim for the stars. Lastly, I would like to acknowledge those family members that cannot see my achievements. My Grandad, Edgar Kennington and in particular, my Grandma, Audrey Peyman, whose resilience always has and will always remain a huge inspiration to me. The last conversation I had with you was late one balmy New Zealand evening, in December 2004, and I promised you then I would not give up on doing a PhD. Well, Grandma, this is for you.

Glossary

1° Ab	Primary Antibody
2° Ab	Secondary Antibody
Ag	Antigen
AC	Alternating Current
AGC	Automatic Gain Control
APTS	Aminopropyltriethylsiloxane
BSA	Bovine Serum Albumin
CAD	Computer Aided Design
CCD	Charged Coupled Device
CRP	C-reactive Protein
DEP	Dielectrophoresis
nDEP	negative Dielectrophoresis
pDEP	positive Dielectrophoresis
DC	Direct Current

DNA	Deoxyribose Nucleic Acid
emu	Electromagnetic Units
ELISA	Enzyme Linked Immunosorbant Assay
FFA	Free-Flow Acoustophoresis
FFD	Free-Flow Diamagnetophoresis
FFM	Free-Flow Magnetophoresis
F_{mag}	Magnetic Force
FITC	Fluorescein Isothiocyanate
GSB	Glycine Saline Buffer
IgG	Immuno-Globulin
IPA	Isopropanol
LOD	Limit of Detection
Mag1-4	Magnet set-up one to four
MLF1	Multi-Laminar Flow 1 device
MLF2	Multi-Laminar Flow 2 device
NdFeB	Neodymium-Iron-Boron magnet
Oer	Oerstead (magnetic unit)

PBS	Phosphate Buffered Saline
PCR	Polymerase Chain Reaction
pI	Isoelectric Point
RMM	Relative Molecular [#] Mass
SEM	Scanning Electron Microscopy
SNP	Single Nucleotide Polymorphism
SPLITT	Split-Flow-Thin Fractionation
μ TAS	Micro- Total Analysis Systems
TBE	Tris-Borate EDTA
TIRF	Total Internal Reflection Microscopy
U_{mag}	Magnetically Induced Velocity
U_{hyd}	Hydrodynamic Induced Velocity
UV	Ultra-Violet Light
VSCEL	Vertical Cavity Surface Light Emitting Laser
VSM	Vibrating Sample Magnetometer

Abstract

Biochemical analysis is a critical part of clinical diagnostics, forensic science and environmental monitoring. Typically, this form of analysis involves the use of bioanalytical procedures which are extremely sensitive and highly specific. However, such assays often involve many different reaction and washing steps, which means that a single analysis could take hours or even days to perform. There is an urgent demand for high through-put analysis systems that are rapid, simple to use and can be utilised in the field or at the point-of-care. Microfluidic technology has gone some way to producing such systems, however many of the current devices still incorporate batch methods of analysis, which are still time consuming or do not integrate all steps of the analysis on one device.

Two aspects of particle handling utilising magnetic forces were investigated. 1) The use of single magnetic particles as mobile solid-supports in a continuous flow system for bioanalysis. 2) The use of diamagnetic repulsion forces for label-free on-chip particle handling.

For the continuous flow system, a magnetic particle type was selected from eight commercially available brands of particles and characterised using on and off-chip measurements. Dynabead M-270 particles were ultimately used as mobile solid-supports for performing entire bioanalytical processes in continuous flow, for the first time. This was achieved by generating multiple laminar flow streams along the length of a rectangular chamber and applying a magnetic field gradient perpendicular to flow. Each reagent stream contained reagents for a molecular binding assay and

functionalised magnetic particles were deflected across the width of the chamber. As the particles were deflected through reagent streams, washing and reaction steps were performed on the surface of the particle in one operation in continuous flow. The system was used to perform a one-step streptavidin – biotin binding assay with an LOD of 20 ng mL⁻¹, a two-step mouse IgG immunoassay with an LOD of 0.1 µg mL⁻¹ and a qualitative sandwich immunoassay for C-reactive protein (CRP). All three procedures were performed within one minute with no manual intervention.

For the diamagnetic repulsion forces for label-free particle handling, 10 µm polystyrene particles were trapped into plugs on a glass capillary by suspending them in a paramagnetic solution and creating an area of high magnetic field gradient between two magnets. Particles were repelled by the field and formed a plug upstream from the magnets. The system was used to simultaneously perform positive and negative controls on a sample of fluorescently labelled biotin using two plugs; one containing streptavidin functionalised polystyrene particles and one containing plain polystyrene particles. In addition, diamagnetic repulsion was used to deflect polystyrene particles from flow inside a square deflection chamber. A particle mixture of 5 µm and 10 µm particles were separated into different exits at a flow rate of 20 µL h⁻¹ based on the difference in their volume, termed free-flow diamagnetophoresis. Potential applications include label-free cell manipulation.

1 Microparticle handling on-chip

Micrometer and sub-micrometer sized polymeric particles have been used in a wide variety of applications for many years. In industry, these applications include paints and glues in which the microparticles are commonly referred to as polymeric colloids. In clinical diagnostics and other biochemical based analysis methods such as forensic science and environmental monitoring, microparticles have found uses in an assortment of applications including bioseparations, immunoassays, DNA sequencing, blood flow tracers and in drug delivery systems.[1] More recently, microparticles have also become a popular and common solid-support in the relatively new technology of microfluidics.[2, 3] In these scaled down systems, microparticles can be handled more conveniently, resulting in greater efficiency for batch processes but also handling on a particle by particle basis in continuous flow systems, the latter being more advantageous in terms of shorter procedural times and real time monitoring.

In the following two sections, two subject areas will be explored. 1) The motivations for the use of microparticles in surface-based bioanalysis will be introduced; this will be discussed for bulk practices and for use in microfluidic channels. 2) A literature survey over the last 10 years on the different techniques employed by researchers to handle microparticles inside microchannels and the development of continuous flow particle handling for the realisation of true micro-Total Analysis Systems.

1.1 Microparticles for surface-based bioanalysis

The term microparticle typically refers to spherical particles with diameters of 0.5 μm to

several tens of micrometers. Microparticles are usually made from polymers, most commonly polystyrene, other materials include glass, silicon, silver or gold depending on their ultimate application and they can be synthesised to give a uniform size distribution. Some microparticles can also be purchased with added physical properties, such as magnetic microparticles which have a core of magnetic material, usually oxides of iron, surrounded by a polymer shell (figure 1.1). Microparticles made from soft polymers allow the penetration of water into the polymer which facilitates their movement through aqueous media. Microparticles of temperature sensitive polymers, can switch between hydrophobic and hydrophilic properties at a critical temperature. [1]

In addition to the variety of substrates, the particle surface can also be modified to exhibit a wide range of surface functionalities. These include chemical reactive groups, such as amines, carboxylic acids or epoxy groups which allow the immobilisation of almost any desired biomolecule by simple protocols. Particles are also available with specific biomolecules, such as antibodies and nucleic acids. Furthermore, particles can be purchased in an array of colours or with fluorophores immobilised on their surface. The variety in physical properties and surface functionality make these microparticles an enormously diverse solid-support for many solution-based reactions, as packing materials for chromatography applications or as drug delivery vesicles.

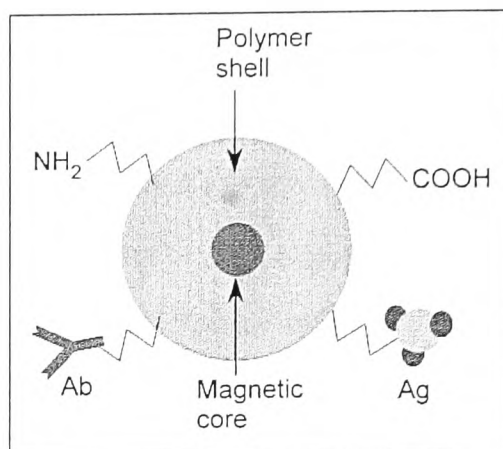


Figure 1.1. Microparticles can exhibit a wide variety of surface functionalities i.e. chemical reactive groups, biomolecules such as DNA, antigens (Ag) and antibodies (Ab). In addition, they can be tailored to have specific physical properties, such as a core of magnetic material.

Another advantage of using microparticles as solid-supports is their high surface to volume ratio. For instance, 1 g of particles, with a 100 nm diameter has a total surface area of around 60 m². [1] This means that just a small amount of particles can have many reactive groups or proteins immobilised on their surface, far more than what would be achieved on the planar wells of a microtitre plate (figure 1.2).

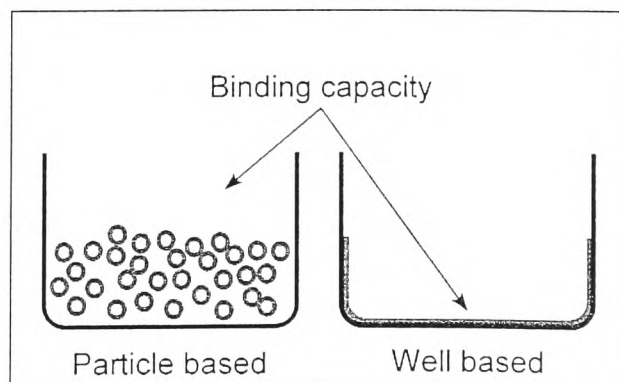


Figure 1.2. Binding capacity of a suspension of microparticles compared to that of a well based technique.

A high density of reactive groups results in a greater binding capacity and an overall preconcentration effect of the target analyte. The binding of an analyte to a solid-support is usually traced by a fluorescent or enzyme label, and a higher concentration of these labels results in an amplified signal compared to the same result in a well or in free solution, which inevitably increases efficiency and sensitivity.[3]

Conventionally, particles are separated from solution by using a centrifuge or a filter, both of which can be time consuming and not grossly efficient. The magnetic particles mentioned above can be easily and conveniently separated from solution by applying an external magnetic field (figure 1.3). Particles can be separated from solution anywhere from a few seconds to a few minutes depending on the strength of the magnet. Table 1-1 shows companies supplying magnetic particles for surface based bioanalysis and figure 1.4 shows a Scanning Electron Microscopy (SEM) image of the Dynabead MyOne range of particles.

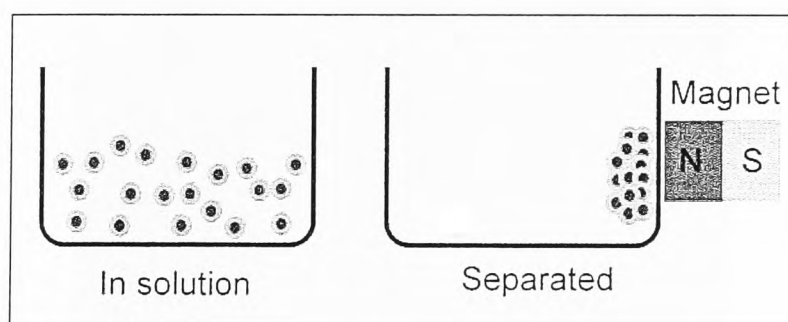
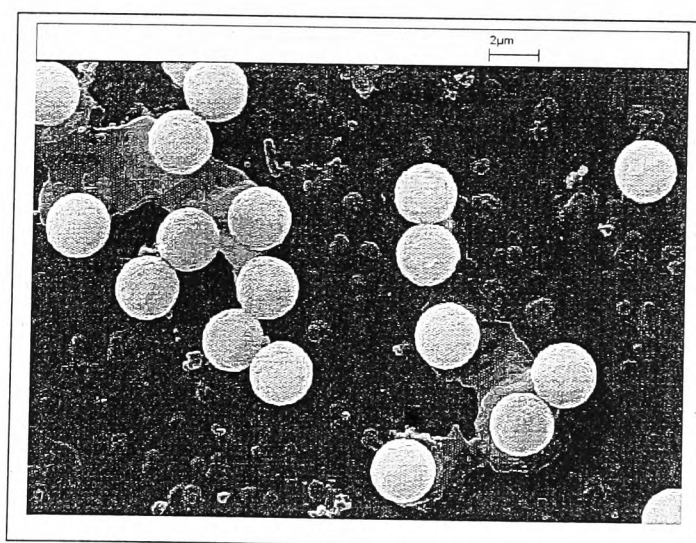


Figure 1.3. The separation of magnetic particles from solution requires a simple external magnetic field.

Table 1-1. Suppliers of magnetic particles and their locations.

Brand name (manufacturer)	Location
Dynabeads (Invitrogen)	Paisely, UK
Compel (Bangslabs)	Fisher, USA
Adembeads (Ademtech)	Pessac, France
MACS (Miltenyi Biotech)	Bergisch Gladbach, Germany
Micromer (Micromod)	Rostock-Warnemuende, Germany

**Figure 1.4. SEM image of Dynabead, MyOne magnetic particles. Particles are spherical and uniform in size.**

1.2 Microfluidics and micro-Total Analysis Systems

Micro-Total Analysis Systems, also known as μ TAS was an ambition first proposed by Manz *et al.* in the early 1990's.[4] The idea involved the down scaling of bench-top laboratory processes onto small, planar microfluidic devices in which networks of micro-channels and micro-reaction chambers could be fabricated. Micro-channels typically range from 5 μm to 500 μm in width and up to 100 μm in depth and, depending on design layout, can be several centimetres in length. Internal volumes of fluid depend on the dimensions of the channels but are usually within the nano-litre range or lower. Figure 1.5 shows multiple laminar streams inside a microfluidic device.

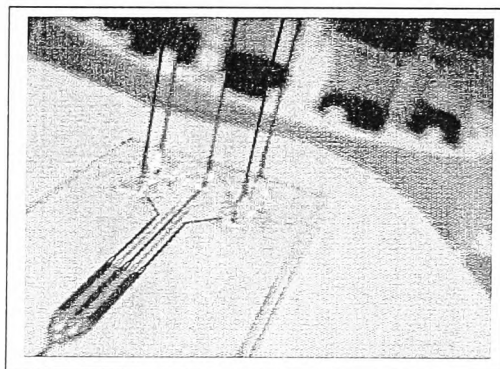


Figure 1.5. Laminar flow streams in a microfluidic device using alternating red and blue ink.

Manz *et al.* anticipated that entire analytical and bioanalytical procedures could be miniaturised down to these small devices, including sample pre-treatment, analyte separation and detection such that a single device could replace entire conventional bench top systems. The motivations for this idea quickly become obvious;

- The first, and probably the most obvious, is the reduction in reagent

consumption and consequently the reduction in the production of waste. Typically for a bench top immunoassay in an Eppendorf tube, the volumes of expensive reagents used is in the mL range. For the same assay on a microfluidic device the volume of reagents used are likely to be around the μL or even nL range.

- The micrometer sized dimensions of the channels reduce the distances reagent molecules have to diffuse in order to react with one another, therefore reducing reaction and incubation times. For a procedure such as an immunoassay, this results in a shortening from several hours to only a few minutes. When flow is continuous over a solid-support then mass transfer is increased as waste products and unreacted molecules are removed quickly and more efficiently by flow.
- The microchannels feature a high surface to volume ratio so there is increased contact between a channel wall and the fluid. For separations this results in greater efficiency and shorter separation times. Reaction conditions such as temperature control can also be managed with better accuracy than in large vessels. Due to the laminar flow regime in microfluidics, there is greater control over fluids so mixing of reagents and manipulation of objects can be finely tuned.
- In addition to this, separations and reactions can be performed in continuous flow which can improve through-put and allow for real time monitoring of reaction efficiency, with the potential for feedback control. This is not generally achievable with traditional batch methods.

Once a procedure has been optimised on a prototype chip then there is the potential for

out-scaling. Many chips can be fabricated in parallel, and with added automation, comes the realisation of portability which would be advantageous for all areas of analysis, such as clinical diagnostics, forensic applications and environmental monitoring. By taking the device to the point of analysis, and taking into account the advantages discussed above, the realisation of μ TAS systems could revolutionise modern day chemical and biochemical analysis.

1.3 Particle handling on-chip – literature survey

The advantages of using microparticles for surface-based bioanalysis and the use of microfluidics for miniaturising bioanalytical processes have been outlined separately above. Therefore it comes as no surprise that combining the two together further improves the advantages of both. The combinational benefit of using microparticles inside microfluidic channels has been reviewed by Peterson[2] and Verpoorte[3]. In the following sections literature from the last 10 years (1999 to 2009) on the most popular current methods for handling particles in microfluidic devices are described.

1.3.1 Retention of microparticles in channels

By far the most frequent method for utilising microparticles inside microfluidic devices has been to retain or trap particles inside channels or chambers to form packed beds, plugs or particle arrays for surface based bio-processing. This has been achieved either by the use of physical barriers, patterning techniques, or external forces. These methods are discussed in more detail in the following sections. An excellent recent review by Nilsson and Laurell explored the extensive and varied particle and cell trapping techniques in microfluidics.[5]

1.3.1.1 Retention of particles using physical barriers

A relatively simple method of retaining microparticles in microfluidic channels is the use of physical barriers in the form of microstructures fabricated into the microchip substrate. The primary aim of these micrometer sized structures is to retain particles against flow within a specific area of the chip, creating a packing effect much like that of a chromatography column. A simple dam structure was described by Sato *et al.* in 2001 in which a 90 μm high barrier was fabricated in a 100 μm deep channel in quartz. A suspension of 45 μm polystyrene particles were retained against the dam and utilised in an immunoassay for Human Secretory Immunoglobulin (s-IgA). The authors reported a reduction in antigen – antibody incubation time from 24 h to 1 h due to the ‘liquid microspace’ produced between the particles (figure 1.6). This dam technique was reported again the following year but instead of using a single channel design, the authors reported a multiplexed system in which particles were retained by four dam structures in a branched microchannel system. Here it took 50 min to analyse four samples using a sandwich immunoassay simultaneously on the trapped particle surface for interferon- γ . [6-8]

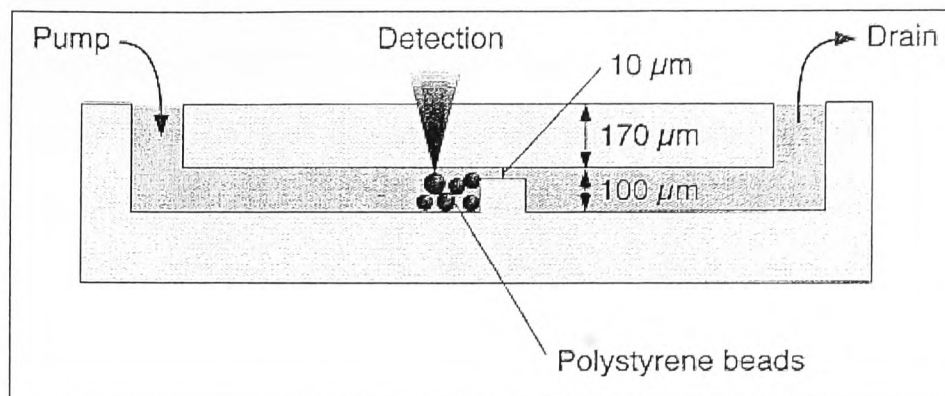


Figure 1.6. Retaining particles inside a microchannel by the fabrication of a dam structure. Here, 45 μm polystyrene particles were retained for use in a surface based immunoassay.[6]

The system was also adapted for trapping cells in following years.[9] In another example, Oleschuk *et al.* utilised two weirs fabricated into a glass device to create a cavity or chamber to trap silica particles for solid phase extraction (figure 1.7). The gap between the weirs and the top plate of the device was 1 μm and particles with diameters between 1.5 μm and 4 μm were introduced into the chamber via a particle loading channel using electro-osmotic flow until the chamber was packed.[10]

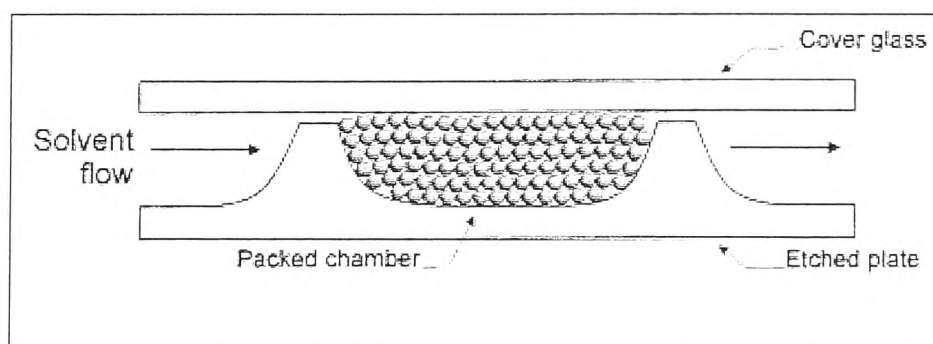


Figure 1.7. The packing of a channel using two weirs and a side loading channel. Particles of 1.5 μm and 4 μm were retained in the channel.[10]

The work by Sato and Oleschuck are good examples of the effectiveness of using a

simple dam structure fabricated into the microfluidic channel. However, disadvantages of blocking a large cross sectional area of a channel in this way are the creation of back pressures when pumping particle suspensions and other fluids through the channel. To reduce this effect the flow rate can be lowered, however this in turn can produce long procedural times as it takes longer to load particles and flush reagents through.

Another popular method which alleviates some of the above disadvantages is to fabricate a particle filter inside the microchannel which retains the particles without causing as much obstruction to flow. These miniature filters are usually solid pillar like structures fabricated inside a channel or chamber that are spaced such that liquid can flow through easily, whilst particles are too large to pass between them and are retained (figure 1.8). A first example of this method was described by Andersson *et al.* in 2000, in which a square filter chamber was designed, fabricated and characterised for the retention of 5.5 μm diameter particles.[11, 12]

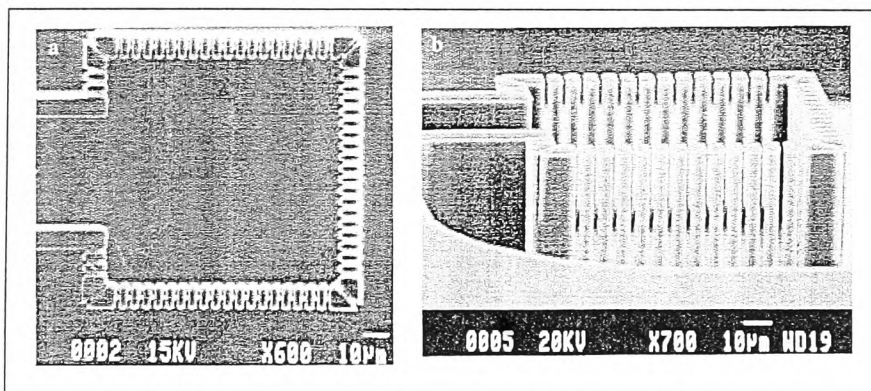


Figure 1.8. Square particle filter chamber fabricated into a silicon microfluidic device. The filter allowed flow to move through the channel with minimal clogging, whilst retaining particles. A drop of 40 % of the flow rate was reported once the chamber was full.[12]

Since these initial investigations, many groups have investigated dam structures and

pillar arrays for the retention of beads for use in bioanalytical procedures including enzyme kinetics,[13] proteomics,[14] DNA analysis[15, 16] and other immunoassay type procedures.[17-20]

1.3.2 Retention using adhesion and patterning

Retention of particles in channels can also be achieved by the patterning of particles onto a functionalised channel wall or by chemically modifying the particles surface.

Breadmore *et al.* packed a single 60 μm deep microchannel with 15 μm silica beads and immobilised them with sol-gel for use in DNA purification. The particles acted as a solid-support for DNA to absorb onto and after removal of PCR inhibitors the target DNA was eluted. The efficiency of the purification was comparable to traditional centrifuge techniques but the procedure was performed much faster and with less sample than conventional methods.

Malmstadt *et al.* reported the use of latex particles functionalised with a temperature sensitive polymer. When the temperature was raised above 28 $^{\circ}\text{C}$ the polymer went through a reversible hydrophilic – hydrophobic transition. Inside heated areas of a microchannel this caused aggregation of the particles and immobilisation. The particles were also surface functionalised for an immunoassay to detect digoxin. To release the particles for regeneration, the heat was removed and dis-aggregation of the particles ensued.[21]

Recently, Sivagnanam and Gijs reported a device in which lines of aminopropyltriethoxysilane (APTS) were micro-patterned onto glass. Particles of 1 μm in diameter, were found to adhere to the APTS strips by electrostatic forces as they

were pumped over the surface. The device was used for an immunoassay application by surface functionalising the particles.[22]

1.3.3 Retention using externally applied forces

Using physical barriers to retain microparticles and cells in microchannels remains a common technique to date, however there are inherent problems associated with such methods, such as the complex fabrication of microstructures, blockages from narrow channel structures and difficulty in removing particles once they have been trapped in order to recycle the device.

As an alternative, external forces can be used to manipulate particles inside microchannels. Forces on particles can be generated by magnetic fields, electric fields or acoustic waves by exploiting differences between the physical properties of the particles and their surrounding medium. The manipulation is contactless and particles can be trapped or released with relative ease. The entrapment area is not limited to specific areas of the chip and the channel design is often simple and fabrication of the device easier. The following section contains an overview of literature published in the area of trapping particles using externally applied forces inside microfluidic devices.

1.3.3.1 Dielectrophoresis (DEP)

Dielectrophoresis forces can be used to manipulate particles inside microfluidic devices. In dielectrophoresis, a non-uniform, high frequency alternating current (AC) is applied to the particle suspension. A particle experiences an attraction or repulsion from an area of high electric field density depending on the difference between the dielectric permittivity of the particle and that of the surrounding medium. The force, F_{DEP} , can be

expressed as;

$$F_{DEP} = 2\pi\epsilon_m R^3 \text{Re}[K(\omega)] \nabla E_{rms}^2 \quad \text{Equation 1}$$

Where R is the radius of the particle, E_{rms}^2 is the root mean square of the value of the electric field and $K(\omega)$ is the Clausius-Mossotti factor determined by the difference in complex permittivity of the particle, ϵ_p^* , and the medium, ϵ_m^* :

$$K(\omega) = \frac{\epsilon_p^* - \epsilon_m^*}{\epsilon_p^* + \epsilon_m^*} \quad \text{Equation 2}$$

In positive DEP (pDEP) $K > 0$ the particle experiences an attractive force to an area of high electric field intensity. The opposite is true for negative DEP (nDEP), where $K < 0$ and the particle is repelled from an area of high electric field intensity.[5, 23] The dielectric properties of the material very much depend on its composition, and therefore the application of the force can be selective to one object or another. Both pDEP and nDEP have been used by researchers to manipulate particles, cells and even biomolecules. In a very early example, Müller and Fuhr trapped and handled cells and latex particles in PBS buffer using nDEP in 1999.[24] Li *et al.* used an electrode array to create areas of high and low field intensity in a fluidic device to capture and separate particles with both pDEP and nDEP. This was also used separate biological species from each other depending on their intrinsic dielectric constants.[25] In 2006, Yasukawa *et al.* trapped 6 μm particles in a DEP cage area in a microchannel for a surface-based immunoassay using nDEP.[26] Much work has been published over the last 10 years on using DEP for trapping particles and cells,[27-29] and the volume of

work is testament to DEP forces being an efficient way of utilising the intrinsic properties of objects to facilitate their contactless handling on-chip. However, in order to perform particle trapping with DEP forces, an external power supply is required to generate electric fields, which can be bulky and difficult to miniaturise. In addition, contact is required between electrodes and buffer, which can cause the formation of bubbles and heat, both of which are disadvantageous in a microfluidic system.

1.3.3.2 Optical forces

Optical trapping, more commonly known as optical tweezing, has also gained much attention within microfluidic research. The technique utilises focussed laser beams to manipulate single molecules up to micrometer sized objects. The laser beams, usually focussed through a microscope objective, are used to exert a force on a dielectric object, such as a particle or cell, by the transfer of momentum from the scattering of photons. Calculating the force acting on a particle depends on the size of the particle in relation to the wavelength of light and differences in refractive index. The total force exerted on a dielectric particle can be calculated if the sphere of the particle is less than the wavelength of incident light and is split into two sub-forces. The scattering force which exerts a force on the particle in the direction of light propagation and a second gradient force in the direction of light gradient produced by a typical Gaussian beam. The following references provide a more detailed look into the calculation of these forces for the interested reader. [30-32]

An example of early work with optical tweezers for trapping objects inside microfluidic platforms was demonstrated by Birkbeck and Ozkan, in which a vertical cavity surface emitting laser (VCSEL) with the highest beam intensity is concentrated around the

outside of the beam, as opposed to the Gaussian beam intensity of conventional lasers. This was used to manipulate a variety of cell types inside a microchannel fabricated.[33, 34] Optical tweezers have been used for applications such as trapping cells and particles for interrogation by Raman spectroscopy[35-37], for force extension investigations of DNA,[38] or for particle sorting applications.[39, 40] Recently, some groups have moved away from bulky optical set-ups and investigated more miniaturised alternatives. Cran-McGreehin *et al.* reported fabrication of a device in which the microfluidic platform was directly integrated onto a semi-conductor laser material. The laser was directed straight into the device negating the need for a microscope set-up. The system was used to trap 2.4 μm sized spheres.[41] Another promising alternative is the use of fiber optics integrated into devices.[42-44]

1.3.3.3 Ultrasonic standing waves

Ultrasonic standing waves, or acoustic radiation force, generated across a microfluidic channel or chamber is another emerging and useful tool for particle and cell handling. Ultrasonic forces are another contact-less and label free technique and require a simple transducer to generate an ultrasonic wave. As the standing wave is stationary, particles or cells are pulled towards the pressure node or anti-nodes, depending on their acoustic contrast factor, ϕ , which is a function of the densities and compressibility of the particle and of the medium it is suspended in.[5] The force, F_r , acting on a particle can be expressed by;

$$F_r = -\left(\frac{\pi \rho_0^2 V_p \beta_m}{2\lambda}\right) \phi(\beta, \rho) \sin(2kx)$$

Equation 3

Where the acoustic contrast factor, ϕ , is described as:

$$\phi = \frac{5\rho_p - 2\rho_m}{2\rho_p + \rho_m} \frac{\beta_p}{\beta_m} \quad \text{Equation 4}$$

The densities of the particle and medium are denoted by ρ_p and ρ_m , respectively and the compressibility by β_p and β_m . V_p is the volume of the particle, p_0 is the pressure amplitude and λ is the wavelength of the ultrasonic wave. x is the distance from the pressure node.

In 2000, Yasuda *et al.* used ultrasonic standing waves for ‘lining up’ 7 μm sized polystyrene particles along the pressure node inside a fluidic device (figure 1.9). This system was also used for mixing erythrocytes in laminar flow. Notably, the standing wave was not observed to damage the cells.[45]

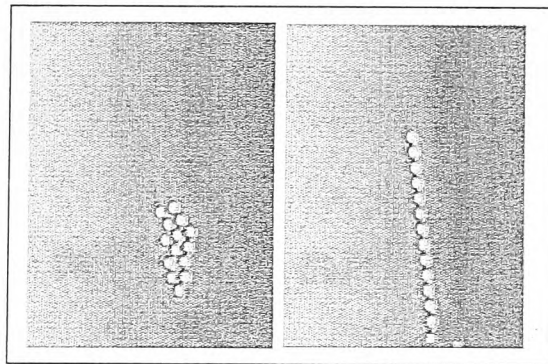


Figure 1.9. Images of 7 μm particles lining up with the application of an acoustic standing wave. Particles line up in the pressure node of the wave.[45]

In 2005, Lillihorn and Laurell developed a microfluidic device into which micro-transducers were fabricated into one of the channel walls. This device was used to trap 5 μm polyamide particles from flow at nodes of pressure minima.[46] More recently, in

2008, Svennebring *et al.* used confocal ultrasonic ‘cavity’ to select and retain 10 μm fluorescent particles and a sub-population of cells from a sample flow for optical characterisation.[47] In the same year, Manneberg *et al.* reported a three – dimensional ultrasonic cage generated by dual frequencies. Particles were trapped as either 2D monolayers or 3D particle aggregates and the system was also utilised for the trapping and enrichment of cells.[48]

1.3.3.4 Hydrodynamic forces for trapping

In addition to the applied force fields discussed above, some work has been reported on the use of hydrodynamic fluid effects to trap particles. In 2003, Lettieri and Verporte published work on the trapping and preconcentration of particles with diameters between 1 and 6 μm by opposing electro-osmotic flow and hydrodynamic flow to create miniature vortices into which the particles were trapped.[49] Trapping of particles in micro-vortices has also been reported by Lin (figure 1.10)[50] and Lutz,[51] in these examples the authors created fluid oscillations by means of an electrical component to generate fluid vortices.

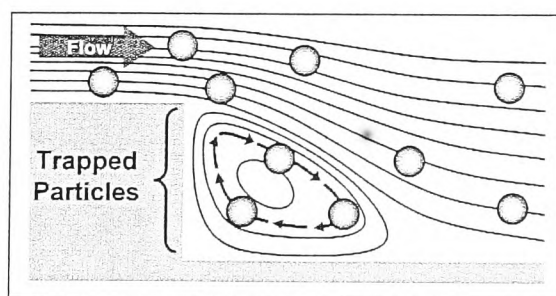


Figure 1.10. An example of using hydrodynamic forces in conjunction with channel geometries to trap particles in mini-vortices or 'eddys'. [50]

1.3.3.5 Magnetic forces

The use of magnetic forces to manipulate magnetic particles inside microfluidic devices for separations and surface based bioanalysis has become increasingly popular over the last ten years. Figure 1.11 shows the number of article publications over the last ten years for a search of magnet* AND particle* AND microfluid*.

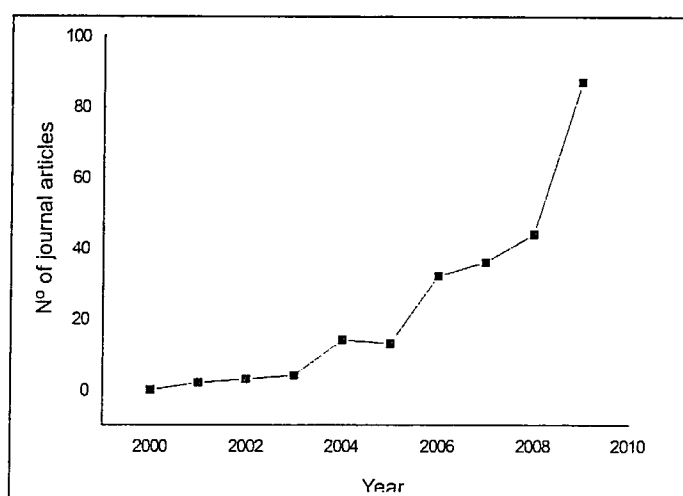


Figure 1.11. The increase in popularity of using magnetic particles in microfluidic devices over the last ten years. A search was performed using the Web of Science and the search parameters magnet* AND particle* AND microfluid*.

Magnetic forces are independent of pH, buffer ionic strength and temperature. The object to be manipulated requires being susceptible to magnetic forces and in the case of microparticles, (see table 1.1), polystyrene microparticles with a magnetic core consisting of a cluster of magnetic nanoparticles are employed. The use of magnetic particles in microfluidic devices was reviewed in detail by both Gijs[52] and Pamme.[53] The forces experienced by magnetic particles in a magnetic field are

discussed in some detail later in section 2.3.

One of the first examples of the use of magnetic particles to form a packed bed in a microchannel using a simple permanent magnet was demonstrated for DNA hybridisation by Fan *et al.* in 1999. Here, paramagnetic particles functionalised with a single-stranded DNA probe (ssDNA) were prepared off-chip and then pumped into a device where they were localised in eight parallel channels by applying a magnetic field. The particle beds were used to simultaneously investigate eight samples with the same probe and successful DNA hybridisation was performed on the surface of the particles.[54] Hayes *et al.* also utilised a simple magnet to trap a plug of magnetic particles 1 to 2 μm in diameter against a channel wall. The magnet was placed to one side of the channel so the plug was formed to one side of the channel. By doing this the authors claim that the flow was not obstructed by the plug and immunoassays for parathyroid hormone and interleukin-5 were successfully performed from blood plasma.[55] This use of permanent magnets being placed in close proximity to a microchannel is a very simple and effective method for trapping particles from flow.[56-58] In 2008, Bronzeau and Pamme demonstrated a similar system using several sets of magnets for trapping multiple plugs of magnetic particles, each with different surface functionalities. By placing sets of permanent magnet pairs with attractive poles facing across a glass capillary and loading particles with three different surface functionalities one by one, a mixed sample of biotin and IgG was successfully probed simultaneously as shown in figure 1.12.[59]

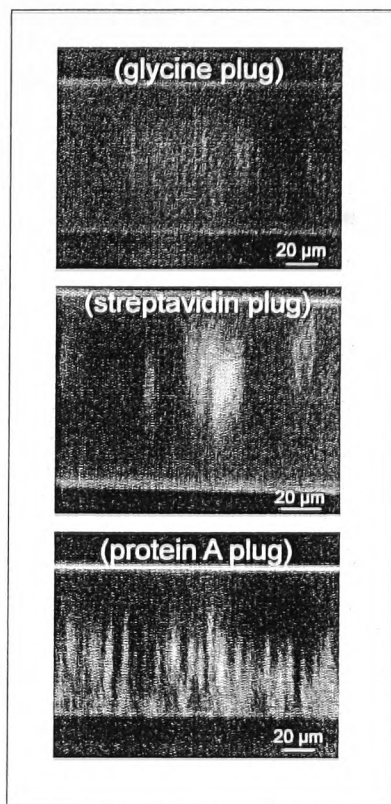


Figure 1.12. Three separate magnetic particle plugs with different surface functionalities were created by having three sets of magnets along a glass capillary. A sample was probed with streptavidin coated particles, protein A coated particles and glycine coated particles as a negative control simultaneously.[59]

While the use of small permanent magnets is simple and easy to implement, some groups have utilised more complex set-ups with integrated magnetic elements for precise spatial control of particles and electromagnets which can be tuned and switched on and off when required. In an early example, Choi *et al.* presented a device with a planar electromagnet fabricated onto the bottom of a silicon device by electroplating a permalloy of nickel and iron metals into a serpentine design. When a DC current was

applied to the serpentine a magnetic field was generated to trap magnetic particles 0.8 μm to 1.3 μm in diameter. Particles formed a uniform layer across the planar device and were easily released by turning off the electromagnet.[60] This same design was later utilised in a polymeric device for a surface based sandwich immunoassay in which a layer of 2.8 μm particles functionalised with a primary antibody was trapped against the magnet and used to capture the complementary antigen from flow. Detection of the antigen was performed with electrochemical detection (EC) and the entire procedure was performed within 20 min (figure 1.13).[61]

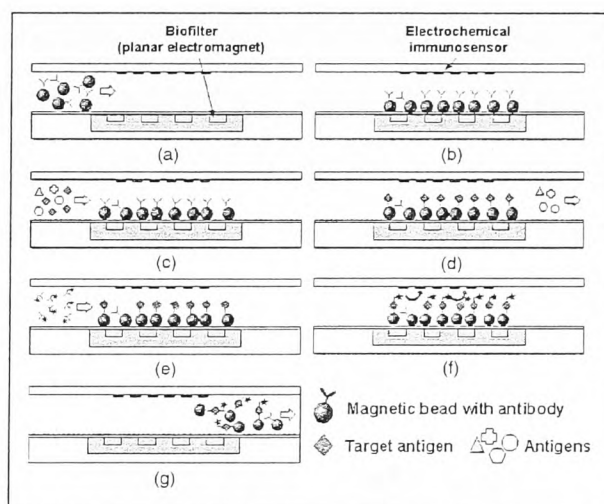


Figure 1.13. Magnetic particles were trapped into a bead bed using an electromagnet and a permalloy feature electroplated onto the chip. The device was used for an immunoassay procedure with electrochemical detection.[61]

Deng and Whitesides also reported the trapping and controlled movement of 4.5 μm magnetic particles using the field from a permanent magnet superimposed onto a microfabricated current carrying microcircuit. By changing the DC current to the

microcircuit the field maxima could be moved along the circuit such that the trapped magnetic particles moved with the maxima. Whilst the currents used for this system (~ 3 A) generated too much heat for compatible use with biomolecules, the system was an early example of the precision that can be achieved using magnetic forces.[62]

Smistrup *et al.* demonstrated microfluidic devices onto which 4.5 mm long and 50 μm wide soft magnetic elements were electroplated along both sides of a microchannel. An electromagnet with a field of 50 mT was used to magnetise the strips of nickel and iron permalloy in order to trap 1 μm fluorescently labelled magnetic particles from flow. This system was used to trap particles of two different populations by utilising a device with three inlets feeding a single microchannel. Particles of different surface functionalities were introduced via the two outside inlets. The middle inlet was used for a buffer solution with a higher flow rate which was used to focus the particles against the channel walls. By applying a magnetic field the particles were then trapped against each strip and used to simultaneously probe a sample for SNP analysis. Figure 1.14 shows plugs of fluorescent particles trapped against each magnetic element.[63, 64]

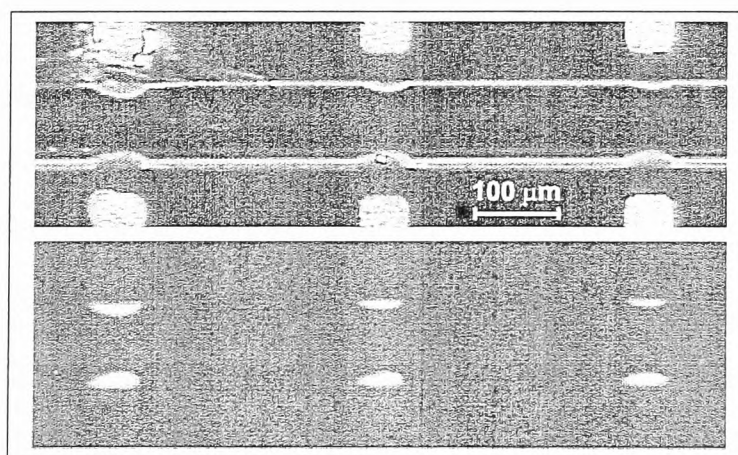


Figure 1.14. Strips of soft magnetic elements were electroplated along a channel to trap small plugs of particles with different functionalities. The system was used to simultaneously probe a sample for SNP analysis.[63, 64]

A similar system was developed by Abonnenc *et al.* in 2009 but instead of electroplating permalloy into strips, trenches were fabricated into a polymeric device and filled with a 'magnetic liquid'. Two permanent magnets were used to magnetise the magnetic strips and up to 34 strips were fabricated along a single channel, capturing up to 34 particle plugs.[65]

Viovy's group utilised magnetic particles for a slightly different type of bioassay. In this work the authors used 600 nm sized superparamagnetic particles to form an array of magnetic columns by injecting a suspension of particles into a PDMS device and applying a homogeneous magnetic field, either by a permanent magnet or a cooled magnetic coil. The particles self-assembled into an array the authors called an 'Ephesia' system. This was used as an obstacle array for the separation of different sized fragments of DNA.[66, 67] Another example of using magnetic particles in self-assembled chains was reported by Lacharme and Gijs in 2008. Here, the authors used a homogeneous field produced by a permanent magnet to trap magnetic nanoparticles into self-assembled chains. The particles were used as a solid-support for an immunoassay with fluorescence detection, for which all steps were performed on chip.[68, 69]

Another magnetic force based technique that is less known than that of magnetic attraction, is the phenomenon of diamagnetic repulsion (see Section 2.3.1). Diamagnetic materials such as water, polymers and wood are repelled from areas of high magnetic field. These forces are much weaker than magnetic attraction, and early work involved the use of very high magnetic field gradients produced by specialised superconducting magnets. However, advancements in the area of microfluidics has allowed high gradients to be produced on a much smaller scale and brought closer to the diamagnetic object of interest. In addition, the use of paramagnetic solution, such as complexes of

manganese and gadolinium, can enhance the force acting on the particles. A few specific groups have utilised diamagnetic forces for manipulating particles and cells inside microdevices.

In 2001, Watarai *et al.* demonstrated the trapping of 6 μm sized polystyrene particles suspended in paramagnetic manganese(II) chloride inside a glass capillary using two permanent magnets with attractive poles facing each other. Under stop-flow conditions the magnetophoretic velocity from the repulsion of the particles from the magnetic field was investigated.[70] This same system was also used to trap red blood cells in 0.1 M MnCl_2 . Here the magnetic field was focussed to a smaller area on the capillary by using two iron blocks attached to the permanent magnets, 400 μm apart.[71] Winkleman and Whitesides demonstrated particle and live cell trapping using an adjustable 3D magnetic trap. They trapped a variety of cells, including fibroblasts and yeast cells in solutions of gadolinium, which is considered less toxic than manganese.[72]

Recently, our group demonstrated the use of magnet pairs with attractive poles facing to create an area of high magnetic field gradient across a glass capillary. Diamagnetic polystyrene particles, 10 μm in diameter, were suspended in paramagnetic buffer MnCl_2 and pumped through the capillary. The particles were repelled from the high field gradient and did not flow between the magnets, forming a trapped plug. This simple set up was used for a particle based binding assay.[73]

Diamagnetic repulsion forces are a relatively new and promising method for on-chip particle and cell manipulation, as they combine the simplicity of using external magnets with microfluidics but also they are label free, and rely on the intrinsic diamagnetic properties of target object. However, forces are generally much weaker than magnetic

attraction forces, and paramagnetic buffers are often incompatible for biological applications.

1.3.3.6 Summary of retaining microparticles in channels

Microparticles are a common solid-support in microfluidic devices, and this chapter has explored the use of physical barriers and the use of externally applied magnetic, dielectrophoretic and ultrasonic forces for retaining microparticles and cells into designated areas in microfluidic devices. The methods allow for contactless and reversible trapping often relying on the intrinsic properties of the object in question, negating the need for labelling. Table 1.2 summarises the methods discussed in this chapter for retaining particles in microfluidic devices.

Table 1-2. Summary of particle trapping techniques including a brief description of the advantages and disadvantages of each.

Type of trap	Advantages	Disadvantages	Reference
Physical barrier	Integrated on-chip	Complex microfabrication Difficult to regenerate Limited to specific areas on-chip	[6-9, 12-20]
Patterning	Precise control over number of particles in bead bed Make distinct arrays	Complex chemical modifications required Often immobilisation is permanent	[22]
Diamagnetic force	Label – free and contactless	Forces are weak Often requires paramagnetic solution	[70, 71]
Electrical force	Label-free	External power supplies Electrodes require contact with solution Joule heating	[24-29]
Optical force	Label-free and contactless	Requires external laser source Microscope to focus laser beam	[29-42]
Acoustic force	Label free, contactless and biologically gentle	Requires transducer and an external power supply	[43-46]
Hydrodynamic effects	Label-free, contactless and integrated on-chip	Often requires complex microchip design and fabrication	[47-49]

Magnetic force	Simple and easy to manipulate No contact with solution required	Limited to magnetic particles or labelled cells	[52-67]
----------------	--	---	---------

The examples described above, in which particles are retained or trapped in beds or as single particles, are essentially batch procedures. Miniaturisation has reduced incubation times and the consumption of reagents, however the potential of these systems is still held back by disadvantages associated with batch procedures. These include lengthy procedural times as reagents have to be changed consecutively; which involves the removal of syringes, or the switching of valves. Some examples are automated, however much of this is still performed manually. Batch procedures are also restricted by a limited sample volume and detection is performed after the entire procedure has been completed, so any changes to system parameters to improve separation resolution or assay sensitivity can only be implemented by starting the entire procedure all over again. These considerations make batch procedures generally unsuitable for high through-put analysis, a feature of biochemical analysis that is in great demand.

1.3.4 Continuous flow separation of particles

An exciting advancement in microfluidics is the development of continuous flow devices in which samples are continuously injected into a system and subjected to a manipulation mechanism such as a force field. The separation or detection is thus performed in real time. In the following sections the development of continuous flow devices for microparticle and cell sorting and for continuous flow bio-processing are

discussed.

1.3.4.1 Focussing and guiding of microparticles

There have been a substantial number of publications concerning the focussing and manoeuvring of particles and cells in flow using external forces. Whilst this is a convenient and contactless method of pre-concentrating and pre-positioning of particles in microfluidic devices, they will not be covered in detail in this thesis literature survey. Similar to the trapping techniques described above, forces have been used to focus and guide particles in microfluidic devices, for example via obstacle arrays,[74] hydrodynamic forces,[75-81] electrical forces,[82-84] magnetic[73] and optical forces.[74, 85-88]

Many of the continuous flow microfluidic devices developed to date have been employed almost exclusively in the separation and sorting of microparticle and cell suspensions. In these examples, a sample mixture is continuously injected into a device and subjected to a force field, usually perpendicular to the direction of flow or an obstacle array that fractionates the sample mixture into separate components. Continuous flow separation holds many advantages over batch separation techniques, as an infinite sample volume can be injected with separation efficiency being monitored in real time (figure 1.15). This allows parameters affecting the resolution to be tuned whilst the separation is taking place. A recent review by Pamme highlights the advancements and benefits of using continuous flow approaches to particle, cell and molecule separations.[89]

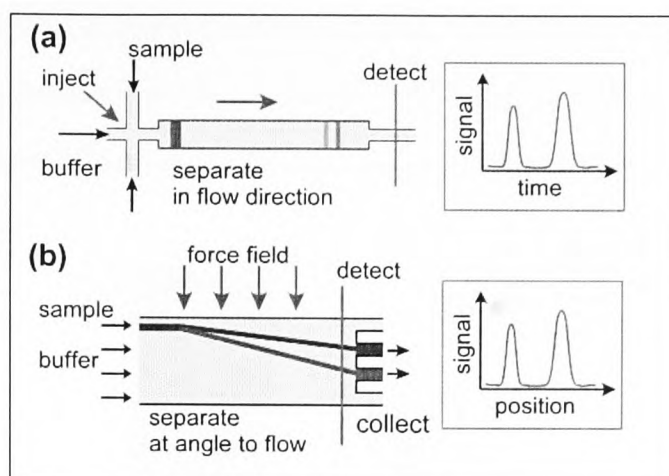


Figure 1.15. Motivations for continuous flow separations. a) In a batch situation a limited sample volume is injected into the system with detection after the separation is completed. Changes to improve efficiency have to be made after separation run is completed. b) In continuous flow, the sample is injected continuously and detection is made in real time, so optimisation of parameters can be done by feedback control. [89]

1.3.4.2 Physical obstacles

Physical obstacles combined with laminar flow streams have been used to separate particles on a size basis. An early asymmetric obstacle array was used in 2000 was demonstrated by Chou *et al.* for the separation of different sized fragments of DNA.[90] In 2004, Huang and Sturm published a paper based on a similar design for the sorting and separation of different sized microparticles. Here, a technique termed ‘deterministic lateral displacement’ utilised an array of micrometer sized obstacles in a chamber. The array was made up of rows of obstacles; each row was slightly shifted horizontally from the row upstream such that laminar flow flowing through the device always bifurcated on hitting the next obstacle. Small particles following laminar flow followed the stream line in which they were positioned around the obstacles, whereas a large particle, which

could not flow in close proximity to the posts were shunted along stream lines and were continuously separated from the smaller particles (figure 1.16). This array was used to successfully separate particles 0.8, 0.9 and 1.0 μm in diameter.[91]

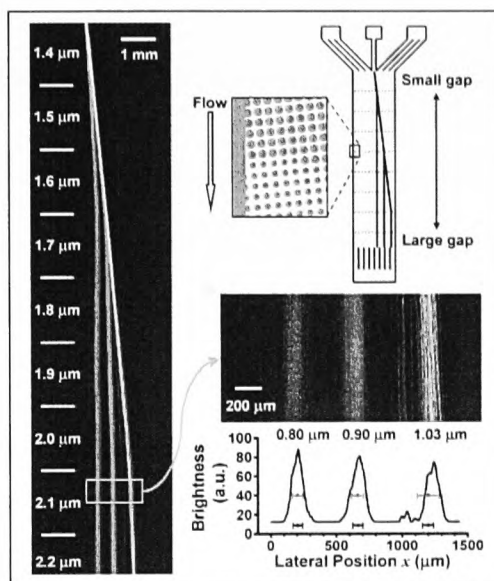


Figure 1.16. ‘Deterministic lateral displacement’ array for continuously separating particles according to size. Particles above a ‘critical particle size’ are bumped along the array and displaced by the obstacles, whereas particles smaller than this size pass straight through with laminar flow. [91]

Inglis and Sturm further characterised and improved the design and efficiency of the deterministic lateral displacement array in the following years, with applications to cell sorting for disease state cells by size alone.[92-95] In a slightly different physical arrangement, Vankrunkelsven *et al.* demonstrated a device for the separation of nano- and microparticles using shear flow through a tapered step-wise channels.[96]

Separating particles using laminar flow and physical obstacles is a passive and label free

process, whose mechanism of separation is independent of surface charge, ionic strength and the pH of the buffer. However, such devices require precise design and fabrication, and the size of particles separated is limited to the obstacle geometry per device.

1.3.4.3 The free-flow genre: continuous flow separation based on applied forces

As discussed earlier, forces have been used in combination with laminar flow to focus and manoeuvre particles in flow inside microchannels. In this section, the use of forces specifically for the continuous flow separation of particles or cells is explored. Many papers have been published over the last few years resulting in the development of a 'free-flow' or 'force-flow' genre of on-chip separation techniques.

Methods based on dielectrophoretic forces

Dielectrophoretic forces have been used quite extensively for the continuous flow separation of particles and cells and the following are only a handful of examples of literature published over the last ten years. Like continuous flow magnetic manipulation of particles, in order to move a particle a force must be exerted on it from field gradient by creating an inhomogeneous field. For electrical fields this is a little more complicated than magnetic fields but can be achieved by careful design of electrode geometries or by creating obstacles in the channel. In 1999, Schnelle *et.al.* described a microfluidic device in which curved electrode pairs were fabricated into a wide fluidic channel. Particle suspensions entering the channel were focussed into the centre plane between the two electrodes by nDEP and experienced repulsive forces from the electrodes. Hydrodynamic force pushed the particles against the force from the electrodes such that the particles followed the curvature of the electrode until the

dielectric forces became less than the hydrodynamic force and were ‘released’. Larger particles experienced greater nDEP forces and were held against the electrode for longer than smaller particles, thus separating them. A range of particles with diameters between 3 μm and 33 μm were investigated with flow rates up to 1 mm s^{-1} . The force acting on the particles was in the pN range.[97] The same group presented a similar device in which multiple 3D electrode structures were fabricated with different angled tilts. These were used to ‘guide’ different sized latex particles out of side channels. Investigations of flow velocity, applied field and electrode tilt were investigated with latex particles between 250 nm and 21 μm but no actual particle mixture separation was detailed.[98] The fabrication of 3D electrode structures is often complicated, in 2005 Choi and Park described the first planar electrode array using trapezoidal shaped electrodes. The electrodes created an inhomogeneous electric field perpendicular to flow such that particles with different dielectric velocities were separated spatially against flow as shown in figure 1.17. Particles between 6 and 15 μm were separated with 99 % efficiency, and were deflected by the nDEP up to 45 μm .[99]

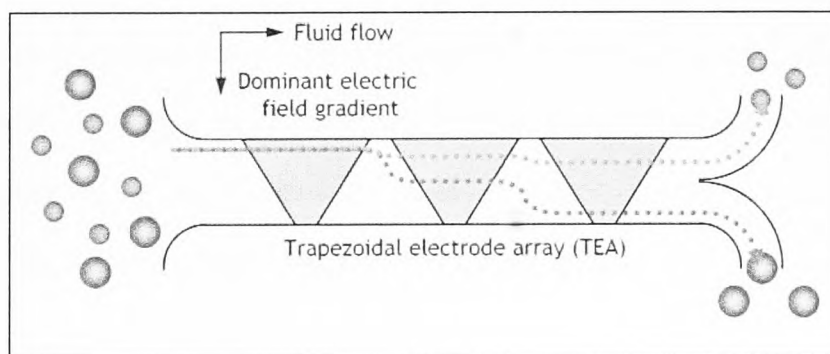


Figure 1.17. Dielectrophoretic separation. Trapezoidal shaped electrodes generate an electric field gradient across a channel. Particles with different dielectric velocities were separated into two fractions in flow.[99]

Similar to the H-design above, Narayanan *et al.* used electrical forces with a Split flow thin fractionation (SPLITT) device. Here, the device features two 'splitting' planes, called the inner splitting plane (ISP) and the outer splitting plane (OSP), created by having a faster flow rate for the sample stream than the collection. An electrical force was applied perpendicular to the flow via gold electrodes placed above and below the channel to push particles across the two planes. The system was used to sort 108 nm and 220 nm sized polystyrene particles from each other at a flow rate of 14 mm s^{-1} . [100]

Li *et al.* in 2007, used a rather complex electrode array fabricated into a wide flow channel. The electrodes ran parallel with flow but due to different resistors being placed on each electrode a bias could be applied between them, creating a field gradient to separate cells in flow. Viable and non-viable yeast cells were separated using this system. [101]

Another method for creating an inhomogeneous field is to fabricate obstacles inside the microchannel to 'squeeze' the field through a narrow gap. This has mostly been achieved by simple structures such as ridges [102] or blocks. [103] The presence of a droplet inside the channel has also been used to focus an electrical field. In this case, the field gradient can be easily adjusted by shrinking or expanding the dimensions of the droplet. This dynamic system was used to separate particles with $1 \text{ }\mu\text{m}$ and $5.7 \text{ }\mu\text{m}$ diameters.

A slightly different way of manipulating objects with DEP forces for separation was demonstrated in 1999 by Yang *et al.* who separated cancerous and normal blood cells by levitating them against gravity using DEP forces. Cells with different densities were

levitated at a different height in a parabolic flow profile such that when the applied flow rate was greater than the levitation force, the particles were separated into different flow streams velocities.

Inhomogeneous electric fields offer a contactless and label-free technique for manipulating both particles and cells in fluidic devices. However, to achieve the gradients required for separation, complex electrode and / or microstructure geometries are required. In addition, often high electric fields are required to exert the desired force required for moving a particle, the heating from which can be a disadvantage when working with biological samples.

Methods based on optical forces

Whilst there are only a couple examples of using optical forces for free-flow separation purposes, it is worth noting here the extensive literature that can be found on the use of optical forces for flow cytometry applications. However, this section will focus solely on the use of such forces to fractionate and separate particle populations. In 2003, MacDonald *et al.* reported a two inlet, two outlet device for the sorting of objects by size and refractive index (figure 1.18). The force field was generated by a single laser beam that was split into a five beam interference pattern to generate an 'optical lattice.' The device was used to sort a sample of 2 μm sized silica and polystyrene particles based on refractive index, and also protein capsules of 2 μm and 4 μm based on size.[104]

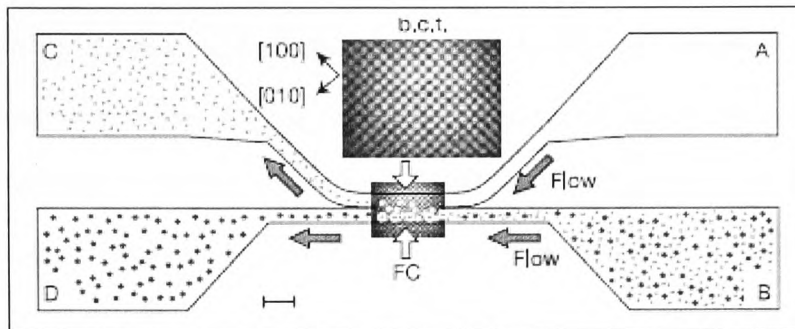


Figure 1.18. Continuous flow separation using optical forces. A mixture of two particle populations with differing refractive index were separated. System was also applied to protein capsules which were separated according to size. [104]

The same group used the device to later sort particle populations of 6.8 μm , 5.2 μm , 3 μm and 2.3 μm sized silica spheres with near 100 % efficiency.[105] The year after the group published another article on the use of a total internal reflection (TIRF) microscope to sort polystyrene particles. Here, a small beam of laser light was passed through a TIRF objective at an ‘off axis’ trajectory that created an elongated evanescent illumination of light at a water/glass interface, which formed a gradient. Using this, polystyrene particles 1 μm , 3 μm and 5 μm in diameter were injected into the device and the 5 μm particles were isolated from the mixture.[106]

Methods based on ultrasound

Acoustic forces from ultra sonic waves have also been used to continuously sort particles in flow. Hawkes and Croakley demonstrated in 2001 an acoustic standing wave generated at right angles to laminar flow to focus and separate particles from 1.5 μm to 25 μm in diameter and yeast cells from a sample stream and directed down a

separate outlet.[107] In 2004, Nilsson and Laurell reported a silicon chip across which the frequency of the wave was adjusted such that there were two pressure nodes present in a 750 μm wide channel. On injection of a suspension of 5 μm polyimide particles, two focussed lines of particles were formed and were collected by two outer outlets channels, with the depleted sample mixture exited via the middle outlet.[108] A slightly narrower channel of 350 μm was used later incorporating a half wavelength standing wave creating a single pressure node and two anti-nodes. This design was used to separate lipid particles from erythrocytes. Lipids were pushed to the outer walls of the channel whereas the erythrocytes were focussed towards the centre (figure 1.19). The two different fractions were then collected downstream via three outlets. This was demonstrated by separating milk and blood in the device.[109, 110]

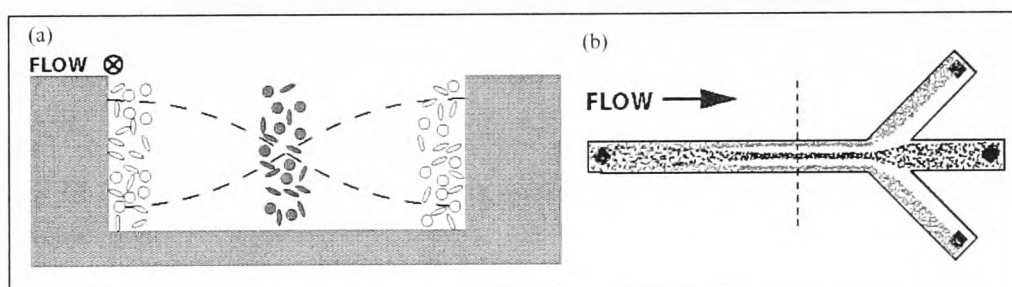


Figure 1.19. The sorting of different cell types using an acoustic standing wave. Lipid particles are focussed towards the anti-nodes at the channel edges, whereas erythrocytes are focussed towards the centre in the pressure node, thus separating them.[109, 110]

The group later went on to incorporate acoustic forces into a free-flow device, termed free-flow acoustophoresis. Here a chip design with four outlets and three inlets was used to separate a mixture of 2 μm , 5 μm , 8 μm and 10 μm polystyrene particles. Particles in flow were moved towards the centre of the channel according to their acoustic properties (figure 1.20), as they were all made of polystyrene the force

acting on them became exclusively size or volume dependent. In addition, the authors demonstrated that by varying the density of the carrier medium, by dissolving caesium chloride, previously unresolved particle types could be separated based on density. The device was also used to fractionate red blood cells, platelets and leukocytes.[111]

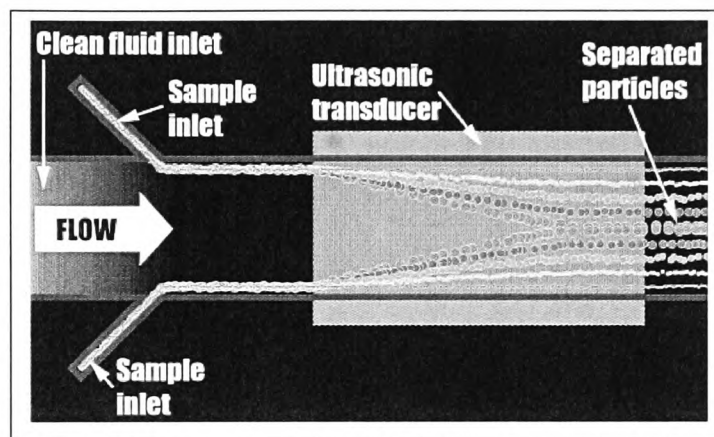


Figure 1.20. Free-flow Acoustophoresis. A mixed particle population is separated according to their size with larger particles been focused towards the centre of the chamber and smaller particles towards the edge.[111]

Acoustic forces offer a gentle, label free and contactless method of manipulating particles and cells in flow. However, trajectories of particles and cells inside the devices are limited by the frequency and so the shape of the standing wave, i.e. the number of nodes present in the channel. Like electrical forces, external transducers and power supplies are also required which can be bulky and complex.

Methods based on hydrodynamic effects

In 2003, Blom and van den Berg described an on-chip chromatography system for separating particles based on the hydrodynamic flow profile. A suspension of particles of differing size were driven through a microchannel under hydrodynamic pressure, smaller particles could flow closer to the channel wall in slower streamlines, whereas larger particles occupied fast streamlines further from the channel wall, thus eventually separating the two populations. The different particles sizes were detected optically without fractionation.[112] In 2005, Yamada and Seki *et al.* took the principles of hydrodynamic chromatography and applied it to a device in which particle fractions were collected separately; this was termed 'hydrodynamic filtration.' The different fractions of particles sizes were collected by using multiple side channels which bled a small amount of liquid from the main channel. Smaller particles travelling closer to the channel wall were collected by the side channel, whereas larger particles flowing towards the centre of the channel remained in the main channel (figure 1.21). This was used to separate and enrich particle populations of 1 μm , 2 μm and 3 μm and also applied to the separation of leukocytes from blood cells.[113, 114]

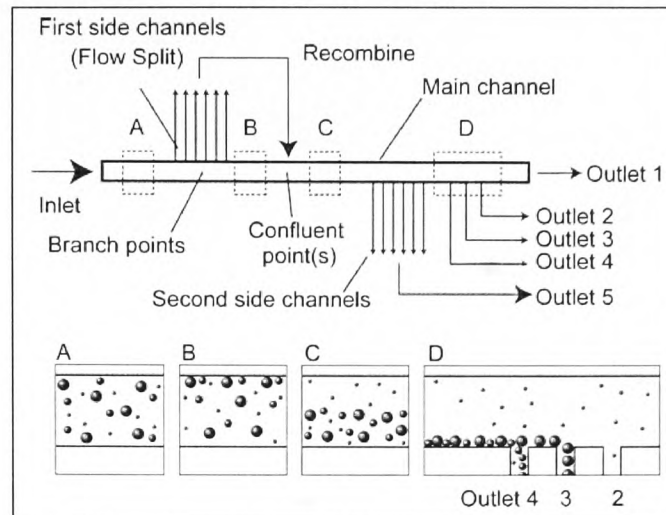


Figure 1.21. Hydrodynamic filtration. Particles are separated using the same principles as hydrodynamic chromatography, such that smaller particles flow closer to the channel wall than larger particles. Exhaustive side channels collect the separate particle fractions.[114]

Pinched flow fractionation is another method employing hydrodynamic forces to separate mixtures of microparticles based on size. Here, a particle mixture flowing along a microchannel is focused against the channel wall by the introduction of a second flow stream with a higher flow rate, the combined flow channel then enters a larger flow chamber such that the flow from the channel is widened across the chamber as shown in figure 1.22. Smaller particles flowing close to the wall in the channel and larger particles towards the centre of the channel are carried into separate flow streams in the wider chamber and thus separate from one another. This principle was first developed by Yamada and Seki *et al.* in 2004.[115, 116] Since then the same principles with slightly different fluidic designs have been used by other groups for the continuous separation of particles.[117-120]

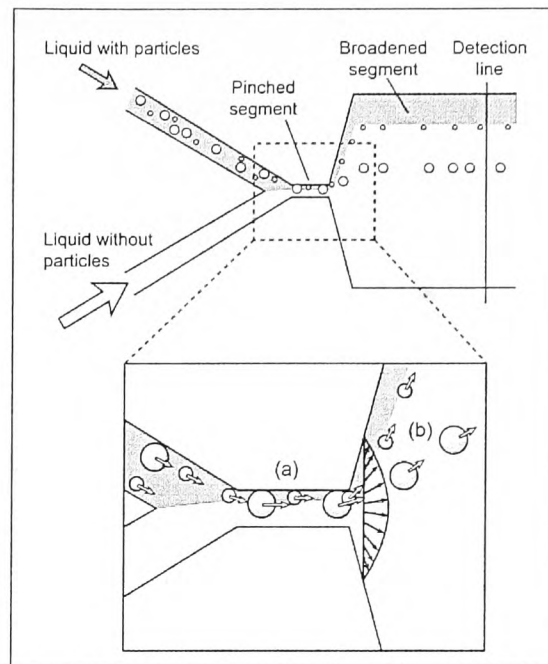


Figure 1.22. Pinched flow fractionation. A particle mix is focussed against a wall in a narrow channel. When this channel widens into a larger chamber the different sized particles are carried along different stream lines and separated. Separation is size dependent.[115]

Other techniques based on hydrodynamic effects include the inertial and drag forces created in spiral channel designs,[121, 122] and the cascade – squeeze effect similar to hydrodynamic filtration.[123] The Zweifach-Fung effect using bifurcation laws[124] and expansion – contraction induced separation have also been utilised.[125]

Hydrodynamic techniques in which channel design and flow rates are the key elements of the separation are passive and label free. Like using physical barriers to separate objects, hydrodynamic forces are independent of buffer conditions such as ionic strength and pH. However, they also often require carefully designed fluidic networks and optimised flow conditions.

Methods based on magnetic forces

Magnetic forces can be used to continuously sort magnetically susceptible objects from non-magnetic material, such as a sample flow, or other magnetic material differing in size and magnetic properties. Integral to exerting a force on a magnetic particle is the presence of an inhomogeneous magnetic field and a magnetic field gradient across the area of manipulation. As discussed later in section 2.2.1, magnets produce magnetic field gradients with increasing distance from their surface. When in close proximity to a microchannel (~ few mm), these gradients are sufficient to exercise a pN force on a particle. An immediately obvious advantage of magnetic force over other forces is its simplicity. Sorting of magnetic material can be easily achievable with a very basic fluidic and magnetic set-up. For example, Kim and Park presented a device with two inlets and a single channel and two outlets. Using a simple permanent magnet placed adjacent to the channel they were able to isolate fluorescent particles agglomerated with magnetic nanoparticles via an immunoassay procedure from a sample stream (figure 1.23). The magnetic field gradient across the channel could be varied by simply moving the magnet closer or further from the channel edge.[126]

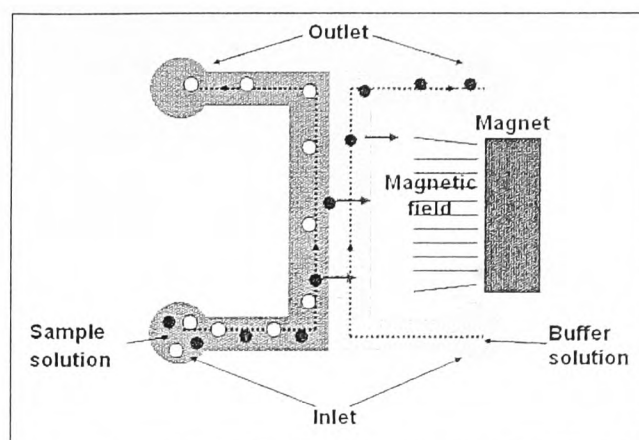


Figure 1.23. A simple magnetic separation device. Magnetic and non-magnetic particles are injected into an H-chip design. When a magnetic field is applied perpendicular to flow, the magnet particles are pulled towards the magnet and into a separate stream.[126]

The magnetic field gradient can be modified by embedding magnetically permeable metal features into the microfluidic devices that direct and concentrate magnetic field lines. Xia and Whitesides described a simple two outlet fluidic design on to which NiFe microstructures were deposited by soft lithography techniques. These were either a single needle or a 'comb' device and were magnetised by simply placing a permanent magnet onto the microstructures. The magnet alone produced a gradient of 15 T m^{-1} in the microchannel, but by incorporating the needle structure or the comb structure to the device the gradient was improved to 25 T m^{-1} and 50 T m^{-1} , respectively. The system was used to separate magnetic particles from non-magnetic particles and also magnetically labelled *E. Coli* cells from a sample flow.[127] Fabrication of magnetic structures can also be simple, Siegel *et al.* presented work on using a solder to fill two channels parallel to main microchannel with liquid metal. When this solidified, the result was two magnetically susceptible wires running alongside a channel but instead

of using a permanent magnet to magnetise the wires, they were used as electromagnets so they could be conveniently switched on and off by a power supply. The device was demonstrated by separating 6 μm sized magnetic particles from a sample flow with 90 % efficiency and a gradient in the channel of 40 T m^{-1} . By switching the two wires on or off the particles could be directed to either of the two exit channels.[128] In a similar technique, Lin *et al.* presented a device in which side channels next to a main separating channel were filled with nickel particles 20 μm in diameter. These were magnetised and used to concentrate magnetic field lines across the channel to separate 4.5 μm magnetic particles from flow.[129] Whilst electromagnets are advantageous in adding an extra feature of control to the magnetic field, they also remove some of the simplicity by requiring a power supply and can also cause localised heating around the electromagnet structure. However, some groups have been working towards utilising gentle Joule heating to improve biocompatibility of systems with the use of electromagnets.[130]

The above examples illustrate the simple designs required for separating magnetic material or magnetically labelled material from a sample flow. In order to fractionate out material according to magnetic properties, a chamber with multiple outlets is required. The development of free-flow magnetophoresis using a small permanent magnet was first developed by Pamme *et al.* in which a separation chamber was fabricated in glass with multiple exits. Magnetic particles were introduced and deflected from flow by the application of a magnetic field on the opposite side of the chamber, perpendicular to flow, as shown in figure 1.24.[131]

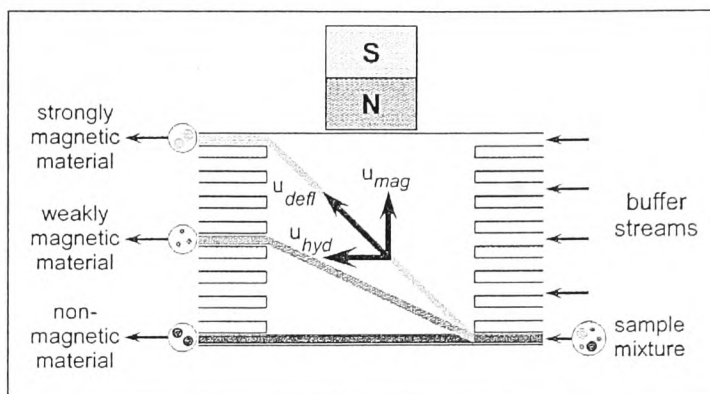


Figure 1.24. Free-Flow Magnetophoresis (FFM). Particles are injected continuously into a separation chamber in the x-direction. Perpendicular to flow, a magnetic field is generated in the y-direction. Magnetic particles are pulled away from the direction of laminar flow. System can be used to sort magnetic particles from non-magnetic particles, but also sort according to magnetic properties and to separate magnetically labelled cells from a sample stream.[131]

Free-flow magnetophoresis has been demonstrated for the separation of magnetic particles with different magnetic volumes and magnetically labelled cells.[132, 133] In a recent paper we have employed the technique to characterise a range of commercially available particles and also the effect of temperature on the magnetically induced velocity was also investigated using this system.[134]

Diamagnetic forces have also been employed for the continuous flow sorting of diamagnetic particles. Winkleman and Whitesides used diamagnetic levitation against gravitational forces to sort polymer particles of different densities and in 2009 Tarn and Pamme reported the continuous sorting of particles in a microfluidic device in the bore of a super-conducting magnet. Here, particles of different sizes, 5 μm and 10 μm polystyrene, were sorted in different concentrations of paramagnetic MnCl_2

solutions.[135]

Our group demonstrated recently, the use of small permanent magnets for the size-selective separation of particles in paramagnetic buffer termed free-flow diamagnetophoresis (FFD).[73]

1.3.4.4 Summary of continuous flow separation of particles

The use of continuous flow platforms for performing on-chip separations of particles and cells is an exciting advancement in microfluidics. Balancing externally applied forces against laminar flow is proving to be a simple and highly effective way of controlling and separating particles in fluidic channels. Table 1-3 summarises the different techniques reviewed here for continuous flow separations.

Table 1-3. Summary of continuous flow separation techniques including separation parameters and applications.

Separation technique	Separation parameters	Application / particle size	Reference
Obstacles	Size	Particles (0.8 – 1 μm) cells	[89 – 95]
Dielectrophoretic forces	Dielectric permittivity	Particles (108 nm – 45 μm)	[96 – 102]
Optical forces	Size Refractive index	Particles (2 – 7 μm) cells	[103 – 105]
Acoustic forces	Size Density Compressibility	Particles (1.5 – 25 μm) Cells	[106 – 110]
Hydrodynamic forces	Size	Particles (26 nm – 3 μm)	[111 – 124]
Magnetic forces	Size Magnetic properties	Particles (1 – 20 μm) cells	[125 – 133]
Diamagnetic forces	Size Magnetic properties	Particles (5 – 10 μm)	[135]

1.3.5 Continuous flow particle processing

Continuous flow techniques have mostly been used for the separation of particles and cells, with any preceding steps such as labelling or bioprocesses such as immunoassays or DNA hybridisation, still being performed off-chip prior to the on-chip separation. When Manz *et al.* first proposed the idea of micro-Total Analysis Systems in the 1990's, the intention was that for a true uTAS device, all steps in the analytical procedure, including sample pre-treatment, analyte capture, labelling, separation and detection would be performed on a single chip. However, few devices capable of this have been realised so far. These fully integrated devices[136] are hugely complicated and require several intricate microfabrication procedures with many mechanical and / or electrical components with specialised interfacing for control. There have, however, very recently been a few examples emerging of systems capable of performing all steps of a bioanalytical procedure on one device utilising the simplicity of force fields and laminar flow described for continuous flow separations. Many of the same advantages for continuous flow separations are true for continuous flow bioprocessing, such as the potential for on-line feedback and sample volumes can be continuously injected.

One approach towards achieving a fully integrated system has been to move particles between two adjacent streams, usually for the purpose of washing the particle with buffer. This has been achieved by trapping the object in the channel either by electrical or optical forces and either manually moving the microscope stage so that the object remains in the same position while the liquid streams are moved over its surface,[137] or by manipulating the flow rate of the two streams so that one can be focussed over the object surface.[138] In these cases, the methods are essentially still small batch procedures and are limited to the number of streams (two) and the number of particles

or cells that have been trapped, which is usually one at a time. In another example, Augustsson *et al.* used acoustic forces to move a particle between buffer streams with different concentrations. However, no reactions were performed on the particles as they moved between the streams.[139]

Very recently, Morton and Austin utilised an obstacle array for lateral displacement described earlier in section 1.3.4.2, but instead the array was used to manoeuvre cells across multi-laminar streams to label or lyse them.[140] Three laminar flow streams were generated along the asymmetric obstacle array, containing a sample stream, labelling or lysing stream and a final washing stream. In a first example, platelet cells whose diameter was greater than the critical size for the array were ‘bumped’ across the obstacles such that they crossed the different streams. A fluorescently labelled antibody in the labelling stream attached to the surface of the cell so they gave a fluorescent signal on leaving the stream (figure 1.25). In a second example, *E. Coli* cells were bumped across a tracer stream, which did not play any role in the cell processing, and into a stream containing 8 % SDS to lyse the cell. Cell particulates were less than the critical size of the array and so were carried away with laminar flow. The chromosome of the cell, which had been fluorescently stained previously, was observed to be bumped further along the array, thus separating it from the cell particulates. Whilst this work is a good example of label free continuous flow processing on-chip, it suffers from several limitations. The most obvious is the intricate design and fabrication required to create the asymmetric post array. The manipulation of particles and cells depends on the tilt angle of the array, the post spacing and the gap size. Once fabrication of the array is completed it is only suitable for use with particles or cells with diameters greater than the critical size. If the object of manipulation is smaller, then another array needs to be

designed and fabricated. The authors note that to avoid clogging in the array system the distance between the posts has to be suitably large, therefore the manipulation of smaller objects would become problematic.

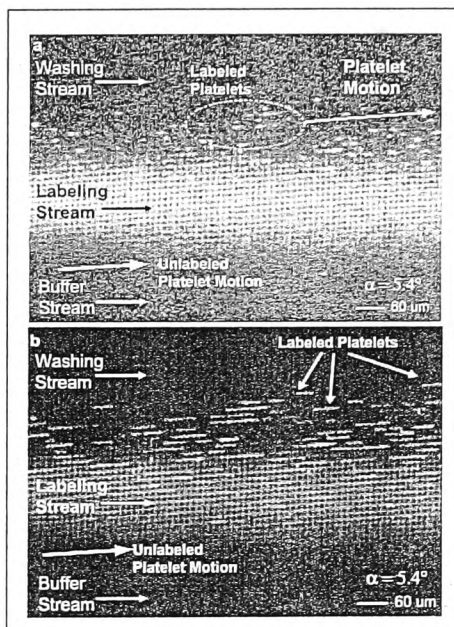


Figure 1.25. The continuous flow labelling of platelet cells using an obstacle array and multi-laminar flow. Image a) is in greyscale where as image b) Image with false colour. Images show platelets before and after labelling with a fluorescent antibody[140]

1.4 Summary of particle handling in microfluidic devices

In this chapter, the various methods for handling particles inside microfluidic devices have been explored. Initially, particles were often used as solid-supports in fixed plugs and beds over which reagents were pumped. Particles in this situation offer advantages such as increased surface to volume ratio and functional versatility. For many applications, it is necessary to separate particles from a solution in order to isolate a

surface bound antigen, or to fractionate different populations of particles. In these types of applications, batch procedures are inefficient and time consuming. In order to achieve high through-put and real time monitoring, continuous flow separations have been developed. The sorting of particles in flow has been achieved using obstacle arrays or by application of a force field, such as magnetic forces or dielectrophoretic forces. Particles are a good substitute for cells in prototype designs, and often these particle separation techniques have gone onto to be used for separating cells.

However, most continuous flow techniques to date have been limited to separation only, with reaction and washing steps still being performed in an off-chip, batch format prior to on-chip separation. For a true μ TAS application, up-stream and down-stream processing should be performed on a single device, yet little progression has been achieved towards fully integrated μ TAS devices in which all analytical procedures are performed on one microchip. In addition, to deliver on all the expectations of μ TAS, devices should be simple to operate and cheap to fabricate, and require little in terms of manual intervention, requirements that have not been realised to date.

1.5 Scope and aim of the thesis

The aim of this thesis is to describe work undertaken into utilising magnetic microparticles as mobile solid-supports in a simple microfluidic device for performing bioanalysis in continuous flow. Investigations were made into combining the magnetic deflection of functionalised particles with multiple laminar flow streams containing bioreagents to perform all steps of a bioreaction, including analyte capture, washing, labelling and detection, in one operation on a single device for the first time (figure 1.26).[141, 142] In addition, investigations into the use of diamagnetic repulsion forces

for microparticle handling are also described.[73]

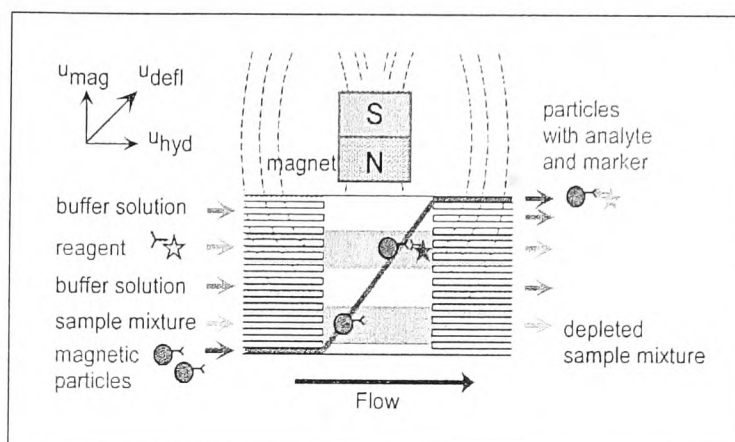


Figure 1.26. Principle of continuous flow bioprocessing combining a multi-laminar flow profile and mobile magnetic particles. Functionalised particles flowing in the x-direction are subjected a magnetic field gradient in the y-direction. Particles are subsequently pulled through multiple reagents such that an entire bioanalytical procedure, including washing steps, reaction steps and analyte detection, are performed on the particle surface in a single operation.

The structure of the thesis is as follows:

1. **Introduction:** To provide the reader with an overview of present literature involving the use of microparticles as solid-supports in microfluidic devices. In this chapter the use of different handling techniques for particle manipulation is discussed.
2. **Theory:** An introduction into the theory needed to understand the concepts behind the project, including particle suspensions and magnetic theory.
3. **Experimental:** A detailed description of the microparticles and reagents used along with the design and operation of the microfluidic devices. Details of data

acquisition and analysis are also included.

4. **Results:** In this chapter, the results obtained throughout the duration of this PhD are presented, discussed and summarised.
5. **Conclusions and Future Outlook:** Conclusions on the work presented are drawn and recommendations for the future outlook of the project.
6. **Appendix:** Contains journal publications of work described in this thesis.

2 Theory of on-chip magnetic particle handling

2.1 Stable particle suspensions

When using micro- or nano- particles in aqueous suspensions, a few factors need to be considered and understood in order to achieve the best performance from the particles. One of the most important aspects is the particle suspension stability. When performing continuous flow separations or particle by particle analysis, aggregation of particles is undesirable. In particular magnetic particles have a tendency under the influence of a magnetic field to form agglomerates and chains of two or more particles due to the lining up of individual magnetic dipoles. This can be controlled by keeping particle suspensions dilute and thus reducing the probability of a particle interacting with one another in the field. However, even in the absence of a magnetic field, particles can still aggregate due to non-specific interactions. In addition, particles can also stick to the surface of the microfluidic device under certain conditions and reduce particle throughput.

Particles and other solid surfaces, such as channel walls, can exhibit a surface charge depending on their chemical make-up or the charge of any molecules immobilised on their surface. In a buffer solution, this charge inevitably attracts ions of opposite charge to the surface, creating an electro-potential around the surface of the particle or against the channel wall (Figure 2.1).

The layer of opposing charges that gathers around the object surface is rigid and is known as the 'Stern Layer' and here the potential drops linearly with distance from the

object surface. After this rigid layer, a diffuse layer builds up in which oppositely charged ions are less firmly associated and this layer eventually extends into the bulk solution. The drop of potential in the diffuse layer is no longer linear and decreases exponentially. Between the rigid Stern layer and the diffuse layer is a boundary known as the slipping plane and the potential at this position is known as the Zeta potential of the particle.

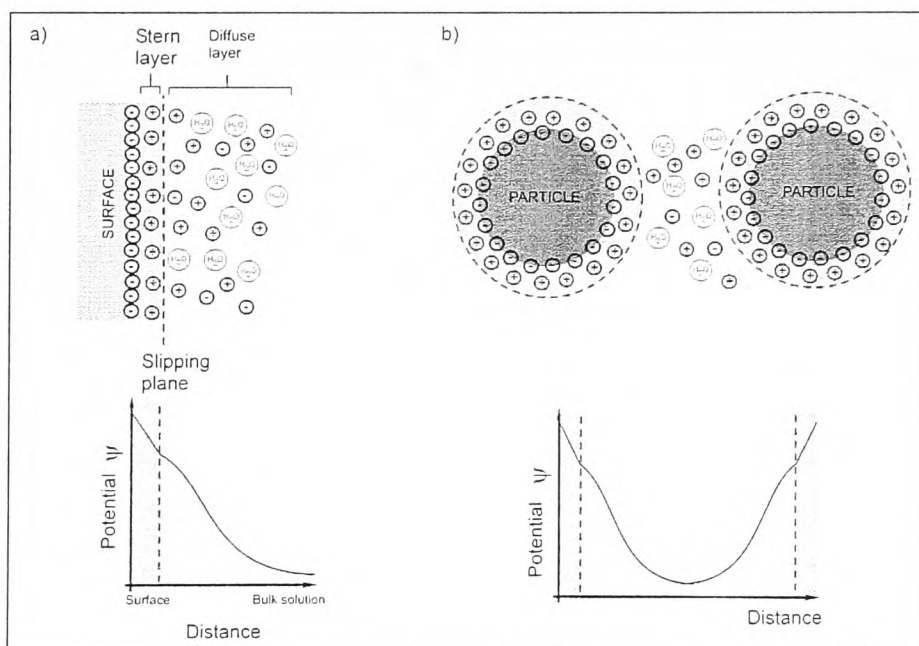


Figure 2.1a) Formation of an electrical double layer at a charged surface in solution. Potential decreases linearly with distance from the surface within the rigid Stern layer and then drops exponentially going into the diffuse layer. b) Formation of an electrical double layer in a particle suspension. There is electrostatic repulsion between the ionic atmospheres surrounding the particles.

As can be envisaged, when two particles come close together, or into close proximity to a channel surface with a similar charge, there is electrostatic repulsion. The level of

repulsion depends on the concentration of ions in solution and the thickness of the double layer. The thickness of the double layer, also referred to as the Debye layer, L_D , can be calculated using:[143]

$$L_D = \frac{0.304}{\sqrt{I}} \text{ nm} \quad \text{Equation 5}$$

Where I is the ionic strength of the buffer given by;

$$I = \frac{1}{2} \sum c_i \cdot z_i^2 \quad \text{Equation 6}$$

c_i is the molar concentration and z_i is the charge on the ions.[144]. For high salt concentrations, the double layer is thin and the potential falls to that of the bulk solution within a short distance. In this case, electrostatic repulsion between surfaces is low. In low ion concentrations, the opposite is true, the diffuse layer thicker and the potential extends further from the object surface. For example, in a 1 M solution of NaCl the Debye layer would be 0.4 nm thick, whereas at a molar concentration of 0.1 M NaCl the Debye layer would be 1.4 nm thick and in the latter case, repulsion between two surfaces is high. Therefore, low ionic concentrations are advantageous in achieving electrostatic repulsion between particles in a suspension.

Other forces are also present in colloidal suspension which are attractive and can cause agglomeration between particles and particle – surface interactions. Van der Waals forces result from dipole – dipole interactions and even though each one is relatively weak, the sum of all the interactions can cause large attractive forces. There are also other attractive forces with ranges up to 100 nm such as hydrophobic interactions. The DVLO theory, named after the scientists who developed it (Derjaguin Landau Verwey

Overbeek) demonstrates the relationship of these forces to one another (figure 2.2). The resultant curve contains an energy barrier close to the surface of the particles which repels particles from each other, however when a particle has enough energy to overcome this barrier it enters a trapping region and the particles will stick together.

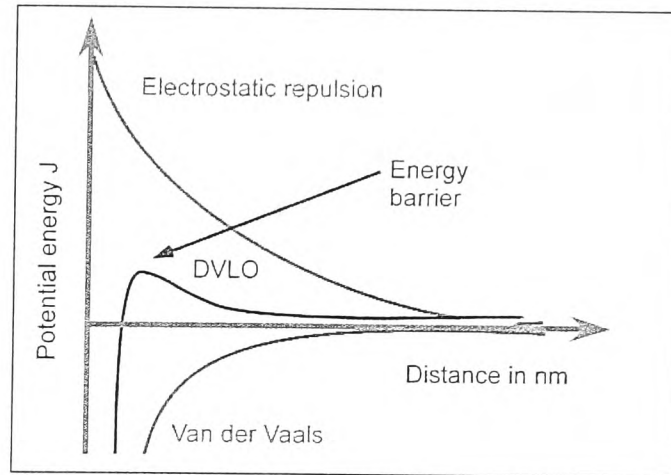


Figure 2.2. DVLO theory: sum of electrostatic forces and van der Waals forces of attraction. When a particle has enough energy to overcome the energy barrier, particles will stick together.

Another factor which affects the level of electrostatic repulsion in a suspension is the pH of the buffer. This is particularly relevant if the particle has a zwitterionic molecule on its surface. The change in charge at different pH depends on the chemical make-up of the material or molecule and the isoelectric point, or pI. At low pH, below the pI of the molecule, chemical groups become protonated, resulting in a predominantly positive charge whereas at high pH conditions, above the pI of the molecule, groups are deprotonated and exhibit a negative charge.

Therefore, in order to create a stable particle suspension, in which particles are repelled from one another and from the surface of the microfluidic device, the ion concentration of the buffer as well as the pH need to be carefully considered. For example, in a glass

microfluidic device, the surface is negatively charged over pH 4 and to repel particles from the surface of the glass, they also need to exhibit a negative charge, thus the pH needs to also be above the pI of the molecules on the surface of the particle.

2.2 Magnetic theory

The following section is intended to summarise the theory of magnetism and of magnetic materials required for the understanding of the concepts behind this thesis. Magnetic theory is a complex and extensive subject and readers interested in pursuing a more in depth understanding of its principles are directed to appropriate literature material.[145-147]

2.2.1 Magnets and units

If one considers a typical bar magnet, with north and south poles, the area around the magnet is occupied by its magnetic field which extends from its surface into the surrounding space, dispersing in strength with increasing distance. The field surrounding a magnet is often described in terms of field lines and these lines can be observed by using small magnetic objects such as iron filings which 'line up' along these field lines. The density of the magnetic field lines, defined as the magnetic flux density, B , can be measured in the units of Tesla (**T**). The closer the lines are together, the stronger the magnetic flux and the higher the value of B . The direction of the field lines is described in terms of magnet polarity, the lines run through the body of the magnet and then in the direction of the north pole to the south pole. Even though these poles do not technically exist and are under much debate, the idea of them helps to imagine the direction of magnetisation, i.e. the direction of the field lines and also

attraction and repulsion in arrays of two magnets or more. Another important point to consider is that the field lines of two magnets can never cross and this is why a repulsive force is felt if two opposing magnetic poles are pushed together, generating an area of magnetic field minima (figure 2.2a). In an attractive situation, the field lines redirect to penetrate both magnet bodies, creating an area of high magnetic flux density between the two magnets. This is also true if a material with a high magnetic permeability is placed within the magnetic field, magnetic field lines redirect through the material and are focused (figure 2.3b).

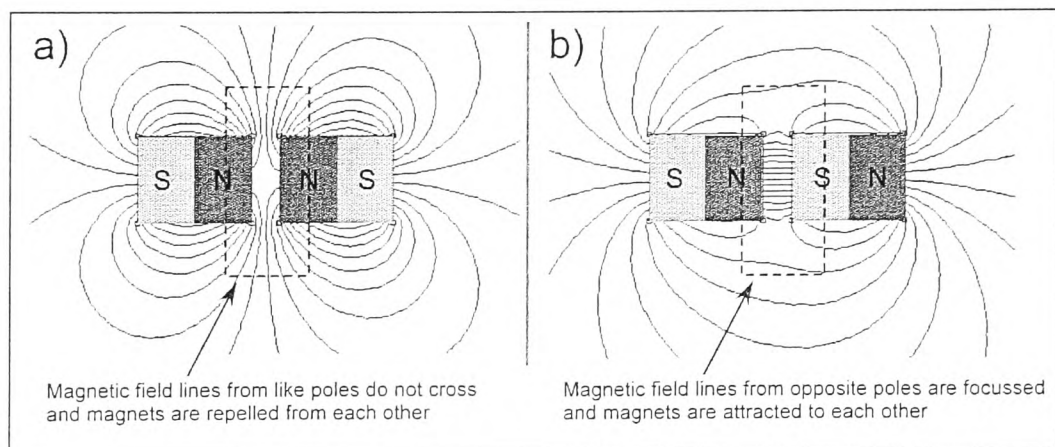


Figure 2.3a) Magnetic field lines from two like magnetic poles do not cross and the magnets are repelled from one another. b) Magnetic field lines from two opposing poles penetrate both magnets and they are attracted to each other.

The magnetic properties of a magnetic material can also be expressed in terms of magnetic field strength, or the magnetising field, H in the units of Amperes per meter ($A\ m^{-1}$). The magnetic induction, B is described as the materials' response to a magnetising field, H . The relationship between B and H is linked by the permeability of free space, μ_0 ($4\pi \times 10^{-7}\ V\ s\ A^{-1}\ m^{-1}$);

$$\mathbf{B} = \mu_0 \cdot \mathbf{H}$$

Equation 7

In most media, the relationship between B and H is linear and this is true for paramagnetic and diamagnetic materials. However, for ferromagnetic materials, μ_0 is no longer a constant and varies with H so the relationship is no longer linear. This becomes evident when considering the B - H curves of such materials and will be discussed in the following section 2.3.2.1.

Another very important property of magnetism is the material's magnetisation, M in $A\ m^2\ kg^{-1}$. The magnetisation can be described as the number of **magnetic moments**, m per unit volume of material (V), where the magnetic moment is defined as a material's tendency to align in an applied magnetic field. A materials magnetisation can be derived as:

$$M = \frac{m}{V} \quad \text{Equation 8}$$

When all the magnetic moments in a material are aligned with the applied magnetic field, the material behaves like a single magnetic domain and is said to have reached its **saturation magnetisation**, M_s . Even under a further increase of magnetic field there is no additional increase in magnetisation.

Magnetisation can be related to both the magnetic induction, B and the magnetic field H , by the following simple equation:

$$M = \frac{B}{\mu_0} - H \quad \text{Equation 9}$$

A value that is often used to quantify a material's bulk magnetic properties is the magnetic susceptibility, χ , which is dimensionless and derived from;

$$\chi = \frac{\mathbf{M}}{\mathbf{H}} \quad \text{Equation 10}$$

This can be described as a material's susceptibility to an external magnetising field.

Table 2-1. List of magnetic theory terms with symbols and SI units.

Term	Symbol	Units
Magnetic induction	B	Tesla ($V \text{ s m}^{-2}$)
Magnetic field strength	H	$A \text{ m}^{-1}$
Magnetisation	M	$A \text{ m}^{-1}$
Saturation magnetisation	M_s	$A \text{ m}^{-1}$
Magnetic permeability	μ_0	$V \text{ s A}^{-1} \text{ m}^{-1}$
Magnetic moment	m	$\text{m}^2 \text{ A}$
Magnetic susceptibility	χ	dimensionless

2.2.2 Magnetic materials

There are many types of magnetic materials that have different characteristics and

behave differently in an applied magnetic field. In this section, only the types of magnetic material that are directly relevant to the work presented in this thesis shall be discussed.

2.2.2.1 Ferro-, para- and dia- magnetic materials in bulk

Ferromagnetic materials

A ferromagnetic material, such as iron, contains areas within its structure called domains where all the atoms have their magnetic moments aligned in the same direction. When a magnetic field is applied to a ferromagnetic material, the magnetic moments in the material align with the magnetic field and domains with the same alignment expand, giving the material a net magnetic moment. In a hard ferromagnetic material, these domains are difficult to move so once the domains have been expanded by an external field, when it is removed they remain mostly where they are, leaving a magnetic memory or remanence. Removal of this field can only be achieved by applying a demagnetising field or by raising the temperature above a point called the Curie temperature, at which thermal energy is sufficient to overcome alignment and randomise the direction of magnetic moments so there is no net magnetisation. Ferromagnetic material has a high magnetisation, M and a large magnetic susceptibility, χ .

Paramagnetic material

For paramagnetic materials, which have some unpaired electrons, the thermal energy at room temperature is enough to randomise the magnetic moments of the atoms in the material so that there is no alignment of dipoles and no magnetic properties in the absence of

a magnetising field. The material does have a small susceptibility so that in the presence of an external field there is some alignment of moments and a small net magnetisation. However, there is no formation of magnetic domains like that of a ferromagnetic material and so this is lost in the removal of the magnetising field.

Diamagnetic material

Most day to day materials are diamagnetic in nature, including water, polymers, wood and glass. These materials have paired electrons spins and therefore no magnetic moment. Diamagnetic objects are repelled from high magnetic field gradients, the effect is so weak they are often more commonly known as ‘non-magnetic’ materials. Diamagnetic materials have a magnetic susceptibility of less than 0.

2.2.2.2 Magnetism on the microscale

Like many materials, the properties and behaviour of magnetic material can differ dramatically on the nano-scale compared to its bulk properties. Iron oxide, for instance, is a hard ferromagnetic material, with a large magnetisation. Many permanent magnets are made out of iron. However, the same material on the nano-scale behaves very differently. An understanding of the structure of bulk iron oxide is required to describe this.

Domain wall theory

Iron oxide, and other ferromagnetic materials, in the bulk form can be thought of as containing many magnetic ‘domains’. Within each domain all the magnetic moments of the atoms are aligned and point in the same direction as described above. Neighbouring domains have moments that are anti-aligned and are separated by a domain wall,

typically 100 – 150 atoms thick. The magnetic moments of the atoms inside the wall are in a constant transition state and their moments are a mix between those of the two adjacent domains (figure 2.4)

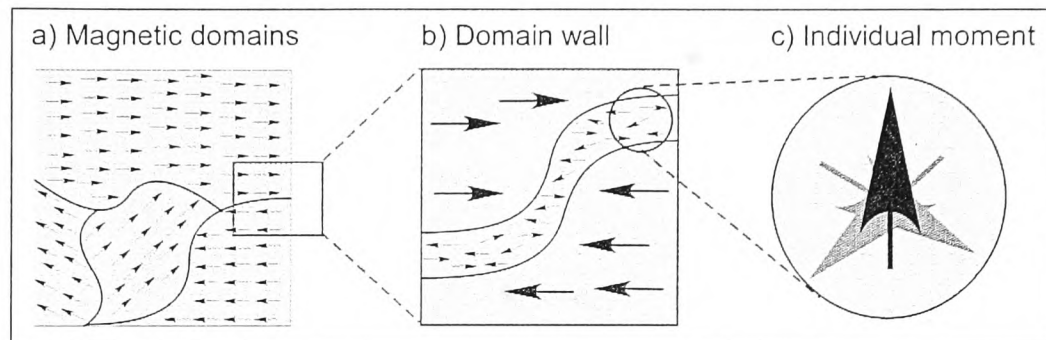


Figure 2.4. Domain wall theory. A ferromagnetic material is made up of many magnetic domains in which the magnetic moments of the atoms are all aligned (a). Between these domains are domain walls (b) in which the direction of the magnetic moments of the atoms are at a constant transition state between those of the adjacent domains (c).

Superparamagnetism

Superparamagnetism is a phenomenon that occurs when a magnetic material's dimensions are on the nano-scale. Iron oxide crystals or nanoparticles, below 50 nm in diameter are generally considered smaller than the width of an average domain wall. Like paramagnetism, the thermal energy is sufficient to keep the moments of the atoms randomised and so the material exhibits no net magnetic moment. However, when a magnetic field is applied this overrides the thermal energy and individual moments align with the field, so that the material displays a magnetic moment in response to the field. However, because there are no magnetic domains, once the field is removed then all the moments randomise again and the material retains no magnetic memory. The

susceptibility of the nanoparticles to the magnetising field is high compared to bulk paramagnetic material, giving a larger magnetisation and hence the phenomenon is termed **superparamagnetism** (figure 2.5).

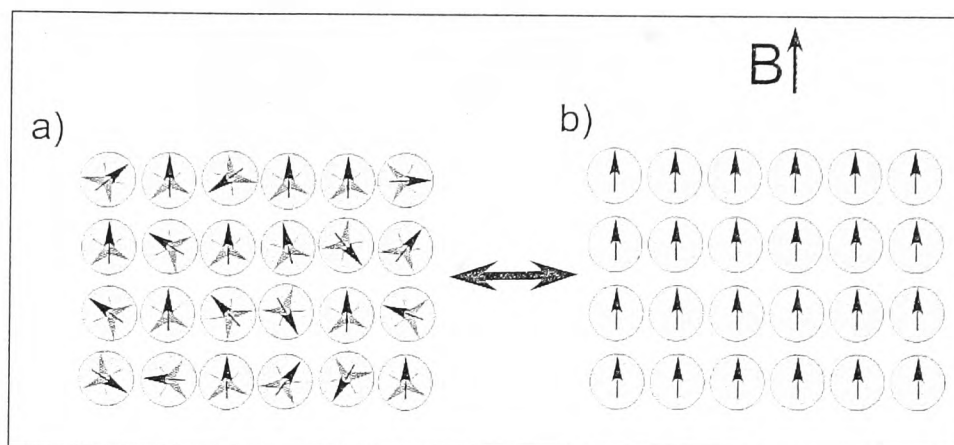


Figure 2.5. Superparamagnetism. a) In the absence of a magnetising field the magnetic dipoles of all the atoms are randomised so there is no net magnetic moment in the material. b) In the presence of a magnetising field the magnetic dipoles align with the field and the material has a net magnetic moment. With the removal of the magnetising field, thermal energy is enough to randomise the dipoles and there is no magnetic memory.

Magnetic microparticles

Most of the magnetic microparticles used in the described work have superparamagnetic properties. This is achieved by dispersing magnetic nanoparticles in a polymer matrix or by having a magnetic nanoparticle core surrounded by a polymer shell. The moments of the atoms are randomised in the absence of a magnetic field, but align to give a net magnetisation when a field is applied. This makes magnetic microparticles particularly convenient to manipulate in fluidic environments as they are easily redispersed into a

suspension when the magnetic field is removed (figure 2.6).

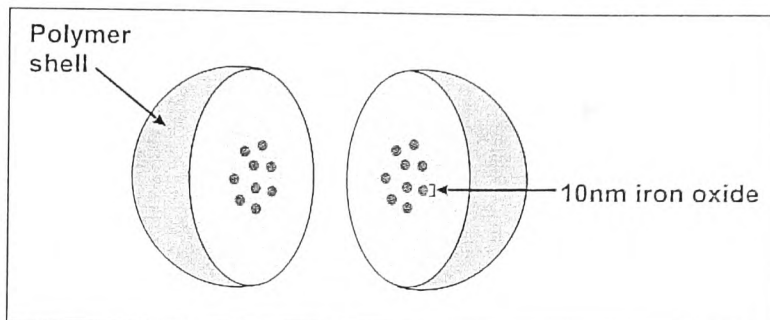


Figure 2.6. Magnetic microparticles usually consist of a polymer shell with a magnetic core. This can be a cluster of iron oxide nanoparticles dispersed in the polymer.

2.2.3 Measuring magnetism – the M/H curve

The relationship between an applied magnetic field, H and the resultant magnetisation of a material, M can be monitored by measuring an M/H curve. The shape of the curve, as well as values derived from it, indicates a good deal about the magnetic properties of a material. For instance, for a hard magnetic material such as iron oxide, the M/H curve has hysteric characteristics and is commonly referred to as a hysteresis loop.

For ferromagnetic materials such as iron oxide, there is a non-linear increase in magnetisation with increasing magnetic field until the material reaches its saturation magnetisation, when all individual magnetic moments are aligned. However, when the field is reduced to zero, the material retains a magnetic memory, known as the magnetic remanence, M_r . The coercivity, H_c , is the amount of demagnetising field required to bring the magnetic memory back to zero and ferromagnetic materials are described as

having high coercivity (figure 2.7).

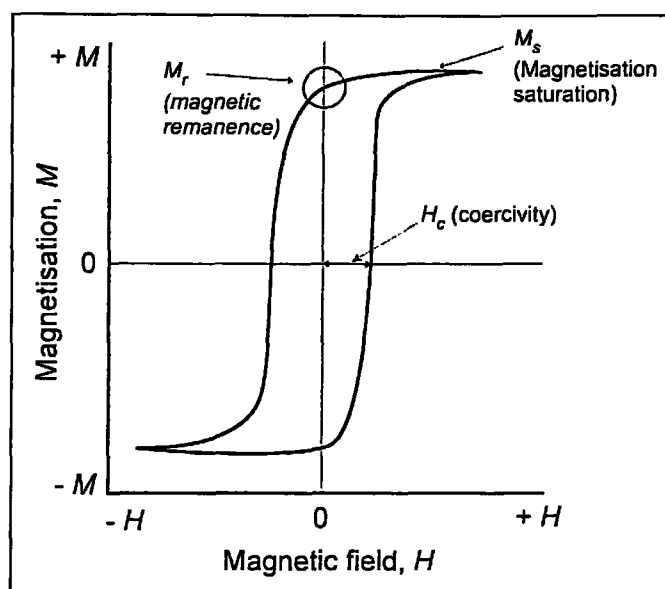


Figure 2.7. Typical M/H curve for a ferromagnetic material showing hysteresis and a high magnetic remanence.

The M/H curve for a paramagnetic material is different as the coercivity is much lower and for superparamagnetic material there is no magnetic memory and the curve is described as being anhysteretic (figure 2.8). In this example, there is little magnetic remanence or coercivity and thus the material behaves like a non-magnetic material in the absence of an applied magnetic field. This is a typical example of an M/H curve expected of a superparamagnetic microparticle.

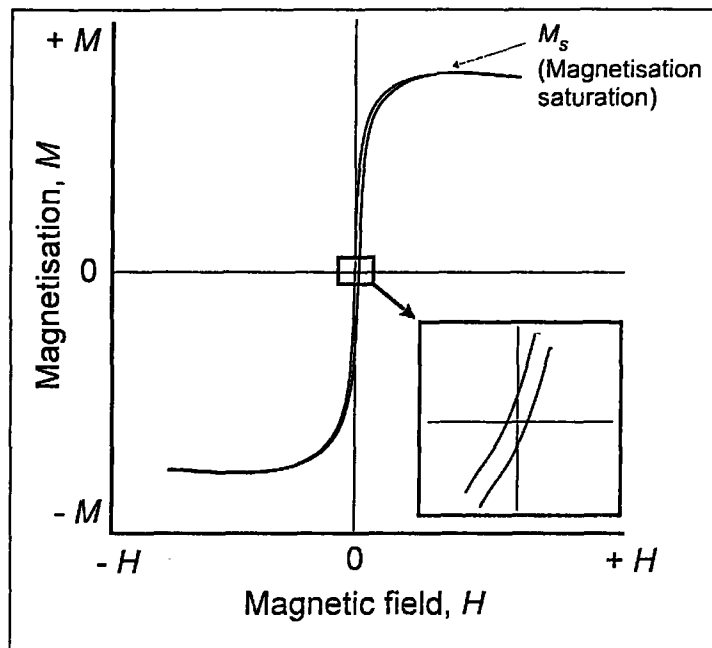


Figure 2.8 Typical M/H curve for a superparamagnetic material with anhysteretic characteristics and negligible magnetic remanence at zero magnetising field.

2.3 Deflecting magnetic particles in flow

The theory of free-flow magnetophoresis, which is integral to the working function of these devices discussed in this thesis, shares the same principles as other free-flow separation techniques; the balance and variation of a force field against laminar flow. In the case of FFM, laminar flow is generated across a chamber in the x-direction, and a magnetic field gradient is applied perpendicular to flow, in the y-direction (figure 2.9).

2.3.1 Magnetophoretic mobility

When a particle is deflected from laminar flow in an FFM device, it experiences two flow vectors; one from the hydrodynamic flow termed the hydrodynamic induced velocity, u_{hyd} , and the other from the magnetic field termed the magnetically induced

velocity, \mathbf{u}_{mag} .

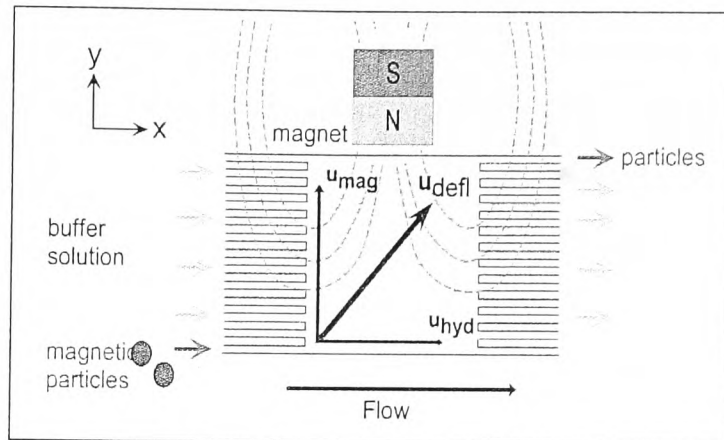


Figure 2.9. Principle of continuous flow magnetic deflection. Magnetic particles enter the chamber under the influence of the hydrodynamic flow vector, \mathbf{u}_{hyd} in the x-direction. A magnetic field is applied perpendicular to flow and the particles experiences a magnetically induced velocity, \mathbf{u}_{mag} in the y-direction. The resulting deflection from flow, \mathbf{u}_{defl} , is the sum of these two flow vectors.

The degree of deflection, \mathbf{u}_{defl} results from the sum of these two flow vectors;

$$\mathbf{u}_{defl} = \mathbf{u}_{hyd} + \mathbf{u}_{mag} \quad \text{Equation 11}$$

When a particle experiences a magnetically induced velocity, \mathbf{u}_{mag} , the magnetic force is opposed by another force, the viscous drag from the medium through which it is being pulled. It described as being equal to the magnetic force on the particle:

$$F_{mag} = F_{vis} \quad \text{Equation 12}$$

Where F_{vis} :

$$F_{vis} = 6 \cdot \pi \cdot r \cdot \eta \cdot \mathbf{u}_{mag} \cdot C_w$$

Equation 13

The viscous drag depends on the radius of the particle, r and the viscosity of the medium through which it is travelling, η . [131] The term C_w is the viscous drag coefficient due to the surface of the top and the bottom of the chamber walls [150] and is expressed as:

$$C_w = \frac{1}{1 - 1.004(r/h_z) + 0.418(r/h_z)^3 - 0.21(r/h_z)^4 - 0.169(r/h_z)^5}$$

Equation 14

To exert a force on a magnetic particle in solution in order to mobilise it, it must be in a magnetic field gradient produced by an inhomogeneous field. In a homogenous magnetic field, the particle would become magnetised but would not be moved. The force exerted on a particle can be described by equation 15.

$$F_{mag} = \mu_0 M_{s(\text{particle})} \text{grad}H$$

Equation 15

This equation, with the term $M_{s(\text{particle})}$, is only true for a situation in which the particle has reached its saturation magnetisation by the magnetic field. The particles used in these investigations saturate at approximately a few hundred mT, and therefore can be assumed to be saturated in the magnetic fields inside the chamber.

If one substitutes equation 15 into equation 13, we get an overall expression for the magnetically induced velocity [133];

$$\mathbf{u}_{\text{mag}} = \frac{\mu_0 M_{s(\text{particle})} \text{grad} \mathbf{H}}{6 \cdot \pi \cdot \eta \cdot r \cdot C_w} \quad \text{Equation 16}$$

In any one experiment, the gradient of the magnetic field remains constant, and therefore the magnetically induced velocity, and in turn the amount of deflection of the particle becomes dependent on the saturation magnetisation of the particle, M_s , over its radius, r .

$$\mathbf{u}_{\text{mag}} \propto \frac{M_s}{r} \quad \text{Equation 17}$$

Diamagnetic repulsion forces on diamagnetic particles in suspension can be described similarly to that of magnetic particles. It is more convenient to express the magnetic properties in this circumstance in terms of magnetic susceptibility, χ and the force on the diamagnetic particles can be expressed as;

$$\mathbf{F}_{\text{mag}} = \frac{\Delta\chi \cdot V_p}{\mu_0} (\mathbf{B} \cdot \nabla) \mathbf{B} \quad \text{Equation 18}$$

Where $\Delta\chi$ is the difference in susceptibility between the particle and the surrounding medium:

$$\Delta\chi = \chi_p - \chi_m \quad \text{Equation 19}$$

In magnetic attraction, the magnetic susceptibility of the particles, χ_p , is greater than 1 and that of the medium they are suspended in, χ_m . The result is a positive value for $\Delta\chi$

and thus an attraction to a magnetic field. For a diamagnetic particle suspended in a paramagnetic solution, such as manganese chloride, χ_p is less than 0 whilst the susceptibility for the solution, χ_m is greater than 1 and the result is a negative value for $\Delta\chi$ and a repulsion from a magnetic field (figure 2.10).

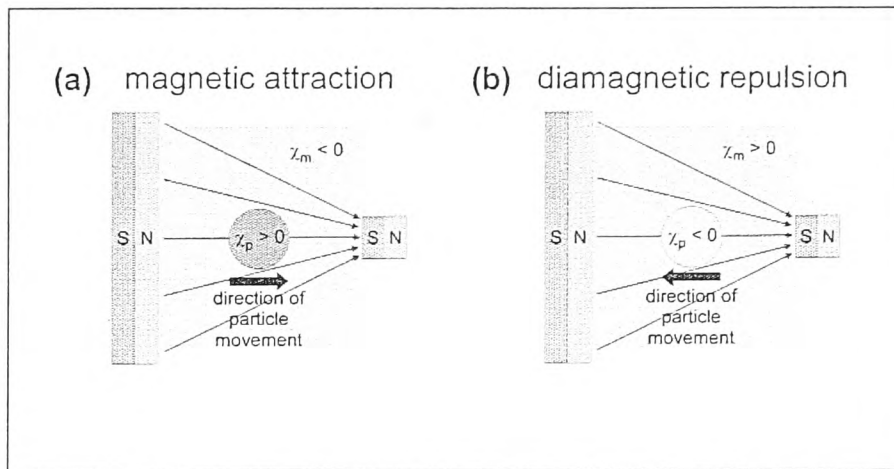


Figure 2.10. Principle of diamagnetic repulsion. a) for magnetic attraction the particle has a magnetic susceptibility > 1 , whereas the surrounding medium has a magnetic susceptibility < 1 and therefore the particle is attracted to a high magnetic field gradient. b) In diamagnetic repulsion, the particle has a magnetic susceptibility < 1 , whereas the surrounding medium has a susceptibility > 1 , the result is repulsion of the particle from areas of high magnetic field gradient.

The diamagnetic particle is pushed away to an area of magnetic field minima as it is displaced by the paramagnetic ions in solution. This effect can be used to manipulate diamagnetic objects in suspension.

Another force that is acting on the particles in solution is that of gravity. Due to their iron oxide cores, the magnetic particles have a slightly higher density than the solution

they are suspended in and over time they can be observed to settle. The gravitational force can be calculated using:

$$F_{grav} = \Delta\rho \cdot V_p \cdot g \quad \text{Equation 20}$$

Where $\Delta\rho$ is the difference in density between the particle and the medium, V_p is the volume of the particle and g is the acceleration due to gravity ($= 9.807 \text{ m s}^{-2}$).

3 Experimental

In this chapter the reagents, fundamental instrumentation, chip designs, magnets and procedures used throughout the work presented in this thesis is described.

3.1 Chemicals and solutions

All solutions were made up in purified water (18.2 M Ω at 25 °C, 0.05 μ m filtered) and filtered through a 0.2 μ m PTFE membrane syringe filter (Millipore, USA) prior to use inside the microchip.

Table 3.1 and table 3.2 list the commonly used chemicals and bioreagents used in this study and the corresponding suppliers.

Aqueous sodium hydroxide and potassium hydroxide in isopropanol

An aqueous 100 mM solution of sodium hydroxide was prepared by dissolving 0.04 g of NaOH pellets in 100 mL of purified water. Potassium hydroxide in isopropanol was prepared by dissolving two tablets of KOH (approximately 0.4 g) in 10 mL of isopropanol, giving a concentration of around 0.7 M. This was left for 1 hour on a magnetic stirring plate to fully dissolve the KOH tablets. Solutions were refreshed every couple of days due to the formation of crystals that would be transferred into the microchip. The microfluidic devices were pretreated with either of these basic solutions in order to de-protonate the silanol groups on the surface of the glass to render it negatively charged to repel negatively charged particles.

Table 3-1. Commonly used chemicals and suppliers.

Reagent	Company
Potassium hydroxide	BDH , VWR, Lutterworth, UK
Sodium hydroxide	Fisher Scientific, Loughborough, UK
Sodium chloride	Fluka, Sigma-Aldrich, Dorset, UK
Glycine	Fluka, Sigma-Aldrich Dorset, UK
Phosphate buffered saline	Gibco, Invitrogen, Paisley, UK
Bovine serum albumin	Sigma-Aldrich, Dorset, UK
Manganese chloride	Sigma-Aldrich, Dorset, UK
Tris-borate EDTA	Sigma-Aldrich, Dorset, UK
Tween20	Sigma-Aldrich, Dorset, UK

Table 3-2. Bioreagents employed and their suppliers.

Bioreagent	Company
Biotin-4-fluorescein	MolecularProbes, Invitrogen, Paisley, UK
Biotinylated mouse anti-human CD4 monoclonal antibody	AbD Serotec, Oxford, UK
FITC tagged goat anti-mouse antibody	AbD Serotec, Oxford, UK
Biotinylated mouse anti-human CRP monoclonal antibody	R&D systems, Abington, UK
Human recombinant c-reactive protein	R&D systems, Abington, UK
FITC tagged goat anti-human CRP polyclonal antibody	Abcam, Cambridge, UK

Glycine Saline Buffer

Glycine Saline Buffer (GSB) solutions were prepared by dissolving glycine powder and sodium chloride in water and adjusted to pH 8.3 with 100 mM sodium hydroxide. Three different concentrations of GSB were employed in these experiments and their uses and concentrations are summarised in table 3.3.

Table 3-3. Different procedures using glycine saline buffer and relative buffer concentrations.

Step	GSB	Concentration
Blocking of active sites on epoxy magnetic particles	10 x	150 NaCl mM 100 Glycine mM
Dilution of stock and general storage	1 x	15 NaCl mM 10 Glycine mM
Running buffer in chip	0.1 x	1.5 NaCl mM 1.0 Glycine mM

Phosphate Buffered Saline

Phosphate Buffered Saline (PBS) was prepared by dissolving one 5g tablet of PBS powder in 500 mL of purified water (pH 7.45, 0.14 M NaCl, 0.01 M PO₄, 0.003 M KCl).

Tris-Borate EDTA (TBE)

Tris-borate EDTA buffer (TBE) was purchased as a 5x concentrate solution (pH 8.4, 0.01 M EDTA.Na₂) and diluted to a 0.1x concentration for use in the microchip. TBE buffer was employed exclusively in the one-step binding assay between streptavidin and biotin.

Bovine Serum Albumin (BSA) and Tween20

Bovine serum albumin (BSA) is a standard blocking agent used in biochemical procedures. The role of BSA is to reduce non-specific binding of proteins to surfaces and other biological molecules by acting as a dynamic coating, blocking sites where other proteins involved in an assay may adhere.[148] For all work involving biological components presented in this thesis, BSA was used at a concentration of 0.01 % (w/v). Solutions were prepared by dissolving 100 mg of BSA crystals in 100 mL of purified water and then diluting again by 1 / 100 into the relevant reagent.

3.2 Magnetic particle Suspensions

3.2.1 Magnetic particle suspensions for particle comparison investigation

A variety of commercially available magnetic microparticles were compared in magnetophoresis experiments and they are listed in table 3.4 along with their respective manufacturers, sizes and relevant surface chemistries.

All magnetic particles were supplied by the manufacturer as aqueous particle suspensions with the exception of the Dynabead M-270 range which were supplied as dry particles.

Magnetic particles supplied as aqueous particle suspensions were prepared by vortexing the suspension to ensure particles were evenly dispersed and then diluting 10 μ L particle suspension in 990 μ L of 10 x GSB. The role of the 10x GSB was to deactivate any chemical active sites on the surface of the magnetic particles to reduce particle – particle interactions and particle – glass interactions inside the microchip (figure 2.1).

The sites were deactivated by blocking with a glycine molecule which at pH 7 is higher than the pI of glycine (5.97) resulting in a negative charge, thus repelling the particles from one another and the negatively charged surface of the glass microchip.

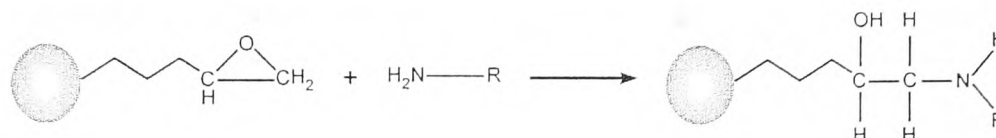


Figure 3.1. Deactivation of chemical active sites on the surface of the particles using glycine. At a pH > 6 glycine on the surface of the particle becomes negatively charged.

Solutions of particles in the blocking buffer were left to incubate overnight with agitation to keep particles evenly suspended. Solutions were then further diluted 1/100 using 1x GSB buffer prior to experiments, yielding concentrations between 4×10^6 and 6×10^9 particles per mL.

The Dynabead M-270 particles were prepared according to manufacturer's directions. 3 mg of the dry particles were washed by dispersing them in 1 mL of PBS buffer. The particles were vortexed and then collected using a magnet. The buffer supernatant was pipetted off and replaced with fresh buffer. This procedure was repeated twice before dispersing the particles into the 1x GSB and incubated as described above.

Table 3-4. List of magnetic particles employed along with respective manufacturers, diameters and surface chemistry.

Particle	Manufacturer	Diameter (μm)	Surface chemistry	Magnetic properties at saturation $\text{Am}^2/\text{particle}$
Dynabead MyOne	Invitrogen	1	Carboxylic Acid	2.1×10^{-14}
Dynabead M-270		2.8	Epoxy	2.2×10^{-13}
Dynabead M-450		4.5	Epoxy	1.3×10^{-12}
Dynabead Streptavidin		2.8	Streptavidin	2.2×10^{-13}
Compel 3 μm	Bangslabs	3	Carboxylic Acid	2.3×10^{-13}
Compel 8 μm		8	Carboxylic Acid	6.0×10^{-13}
Micromer 4 μm	Micromod	4	Carboxylic Acid	1.3×10^{-13}
Micromer 6 μm		6	Carboxylic Acid	4.5×10^{-13}
Micromer 10 μm		10	Carboxylic Acid	2.1×10^{-12}

3.2.2 Magnetic particle suspensions for bioassays

Dynabead M-270 magnetic particles coated with the protein streptavidin were used exclusively for multi-flow bioassay work. Streptavidin is a protein isolated from the

bacterium *Streptomyces avidinii* and exhibits an extraordinary binding affinity for biotin (also known as vitamin H) with the resultant complex having a dissociation constant in the order of 10^{-15} mol L⁻¹. [149] Due to this highly specific and strong interaction, the streptavidin – biotin binding characteristics are utilised throughout molecular biology as a method of biomolecule immobilisation. Molecules of interest can either be derivatised with biotin or streptavidin and the surface to which the molecule is to be immobilised is coated with the complementary molecule. The binding assay has also found its uses as an exemplary bioassay in proof-of-principle biological systems and methodologies. The M-270 magnetic particles are coated with streptavidin for both of these reasons in the work presented here; i.e. for a proof-of-principle assay in the one-step bioassay and as a method of immobilising the primary antibody in the two-step assay. M-270 streptavidin magnetic particle suspensions were prepared by diluting 10 μ L of particle stock into 990 μ L of buffer containing 0.01% BSA (w/v), yielding a particle concentration of 6×10^8 particles mL⁻¹. This was diluted further by a factor of 2 such that the final particle concentration used in the microchips was 3×10^8 particles mL⁻¹.

3.2.3 Vibrating Sample Magnetometer (VSM) for measuring magnetisation curves of magnetic particles

To measure and quantify the magnetic properties of the magnetic particles independently of manufacturers' data, a VSM (Lakeshore Scientific, USA) was utilised. The VSM comprised of two electromagnets between which the sample was inserted on the end of a probe. The probe in turn was fixed to a motor which vibrated in a vertical direction between the magnets at approximately 80 Hz (figure 3.2). The instrument measured the difference in magnetic induction between a region of space with and without the presence of the sample as it is vibrated up and down. The induction of the

sample was then detected by a pick-up coil and relayed back to a computer. The VSM controller swept over a range of magnetic fields, increasing to a preset strength in order to saturate the material and then decreasing again to produce a magnetisation versus magnetic field (M/H) curve. When taking measurements with a VSM it was important that the sample did not move in the sample holder, the only movement should be that of the vibration of the holder itself. Any external vibration would give rise to noise in the subsequent readings. Thus, the particles in suspension could not be loaded directly into the VSM. Instead, magnetic particle suspensions were dried in an oven at 60 °C. The dried particles were then weighed and packed into the sample holder. A typical sample weight between 1 and 10 mg was used. A wood resin was used to fix the particles in position to avoid movement.

The magnetisation response of the particles were scanned over a field range of 0 to 10 kOer (Oerstead) and the corresponding magnetisation curve or hysteresis was plotted in the non SI units of electromagnetic units per gram, emu g⁻¹. Such a high magnetic field strength was used to ensure the particles' magnetisation has reached saturation.

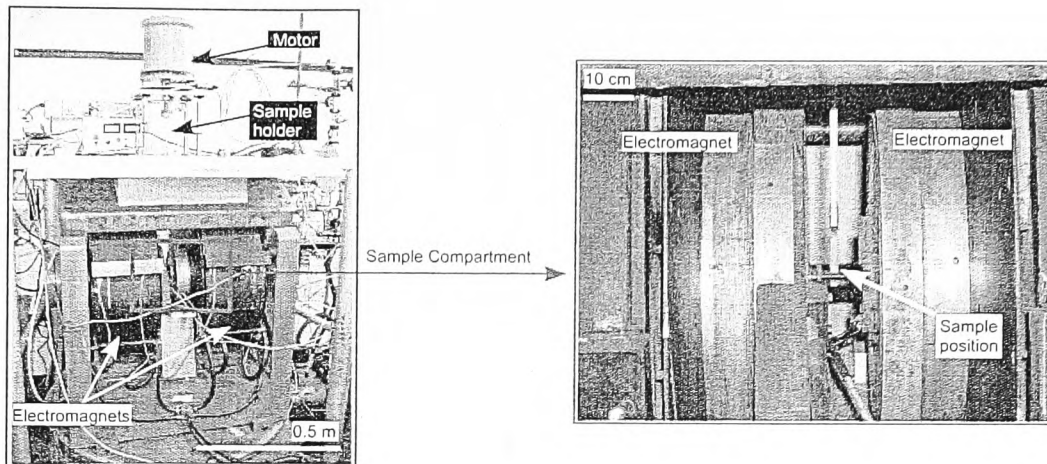


Figure 3.2. Photograph of the Vibrating Sample Magnetometer (VSM). A motor vibrates the sample between two electromagnets at varying magnetic fields. The change in induction between the sample and free space is measured by a pick-up coil.

When comparing the physical properties of the magnetic particles used in this project it was necessary to convert between different units of magnetism and values provided by the manufacturers. Two of the manufacturers reported magnetic properties of their particles as iron oxide ($\gamma\text{Fe}_2\text{O}_3$) content in wt %, with no values of magnetisation. In order to calculate the magnetisation of these particles it was necessary to first calculate the mass of an individual particle, m_p .

$$m_p = \rho \times V_p \quad \text{Equation 21}$$

Where ρ is the density (kg m^{-3}) and V_p is the volume (m^3) calculated by; $4/3\pi r^3$;

Once the mass of the particle was calculated it was then possible to determine the

amount of iron oxide in each particle by the per cent weight value provided by the manufacturer.

$$m_{Fe_3O_4} = \frac{m_p}{100} \cdot wt\% \quad \text{Equation 22}$$

The saturation magnetisation of iron oxide is approximately $85 \text{ A m}^2 \text{ kg}^{-1}$ and therefore the magnetisation of each particle was calculated theoretically (section 4.2.1.4, table 4.2).

$$M_{s(\text{particle})} = m_{Fe_3O_4} \cdot 85 \quad \text{Equation 23}$$

Magnetisation values provided by one of the manufactures were in the units of emu g^{-1} . These are also the units of magnetisation measured by the VSM machine. For comparison of the particles the units of A m^2 per particle were calculated from emu g^{-1} . It was necessary to first calculate the magnetisation of an individual particle using the volume and the density provided by the manufacturers. The number of particles per gram can then be calculated giving the magnetisation in emu per particle. A simple conversion factor of emu to A m^2 is then used, derived from equation 24 and the data is represented in Table 3-4:

$$\frac{\text{emu}}{\text{g}} = \frac{\text{Am}^2}{\text{kg}} \therefore 1000\text{emu} = 1\text{Am}^2 \quad \text{Equation 24}$$

3.3 Permanent magnets

A variety of magnetic set-ups were used throughout this work, the size and shape of the magnets used depended on the field requirements, such as for deflection or trapping magnetic particles and microfluidic set-up, whether it be a planar chip or a glass capillary. However, for all experiments the magnets used were permanent neodymium-iron-boron (NdFeB) and were purchased from MagnetSales, UK (figure 3.3). Specific magnetic set-ups for each experiment are discussed in the relevant experimental sections.

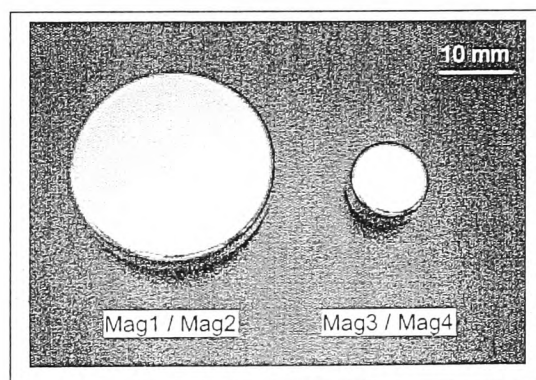


Figure 3.3. Two neodymium-iron-boron (NdFeB) disc magnets used for the particle deflection.

The magnetic fields generated by the magnets could be simulated in two dimensions using the freely downloadable software FEMM 4.0 (<http://femm.foster-miller.net>). The simulation was used to visualise the magnetic fields produced by the magnets and also to estimate magnetic field gradients.

3.3.1 Hall sensor for measuring magnetic flux

In order to measure the flux density of the various magnets a Hall sensor was used

(LOHET II, 244-3140, RS Components, Corby, UK). The sensor was capable of measuring fluxes up to 250 mT and was attached to a voltmeter and a 9 V battery (figure 3.4).

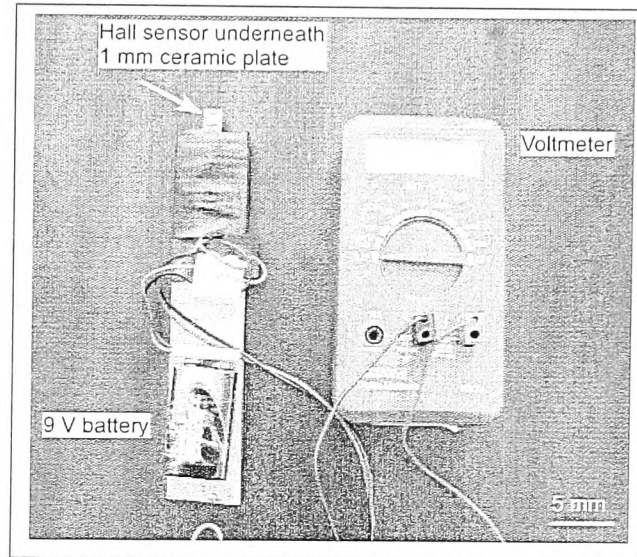


Figure 3.4. Hall sensor attached to a voltmeter with a 9 V battery.

When a magnetic field is brought into proximity with the Hall sensor, a change in the voltage output is observed, which is proportional to the strength of the magnetic field. The output on the voltmeter was converted to mT using the following steps:

Firstly, the sensitivity of the sensor must be:

$$S = \left(\frac{V_s}{8} \right) \times 1 \quad \text{Equation 25}$$

Where 1 is the specified sensitivity in mV / Gauss and V_s is the supply voltage which is taken from the battery using a voltmeter. The flux density B in Gauss can then be determined using:

$$B = \frac{V_{out} - V_{null}}{S \times 10^{-3}}$$

Equation 26

Where V_{out} is the voltage taken in the proximity of the magnet and V_{null} can be calculated by $0.5 \times V_s$. The units of $V \text{ gauss}^{-1}$ can then be converted to mT by dividing B by 10. The sensor saturates above 250 mT, therefore values for magnets with a higher flux density than 250 mT are an approximation by observing a trend.

3.4 Microchip fabrication

All microchips used in this thesis were fabricated in glass via photolithography and wet etching with hydrofluoric acid (figure 3.5). Microchips were fabricated in-house but not by the author and **all glass chips were etched to a depth of $20 \pm 1 \mu\text{m}$** . The following is a brief description of the fabrication process:

A 1 mm thick glass wafer, coated with a chromium layer and a photoresist layer (B270 glass, Telic, Valencia, CA, USA), was exposed to ultraviolet light for 60 s through a photomask featuring the chip design (JD Photo-Tools, Oldham, Lancashire, UK) drawn previously using Computer Aided Design (CAD). The photomask ensured that only the desired chip design was exposed onto the photoresist. The photoresist was subsequently developed for 60 s in Microposit Developer (Chestech Ltd., Rugby, Warwickshire, UK) to remove the exposed pattern, and the chromium layer was then removed by immersing the glass plate in Microposit Chrome Etch 18 (Chestech Ltd.) for 60 s, leaving the chip design visible on the glass itself. Access holes of $368 \mu\text{m}$ diameter were drilled into the glass wafer for the inlets and outlets. The plate was then immersed in a glass etching solution consisting of 1.3 % hydrofluoric acid, 13.3 % phosphoric acid and 85.3 %

water. Once etching was complete the remaining photoresist was removed using acetone, and the chromium layer removed by further use of Microposit Chrome Etch 18. The plates were thermally bonded in a furnace at 590 °C for 3 h, with weight applied.

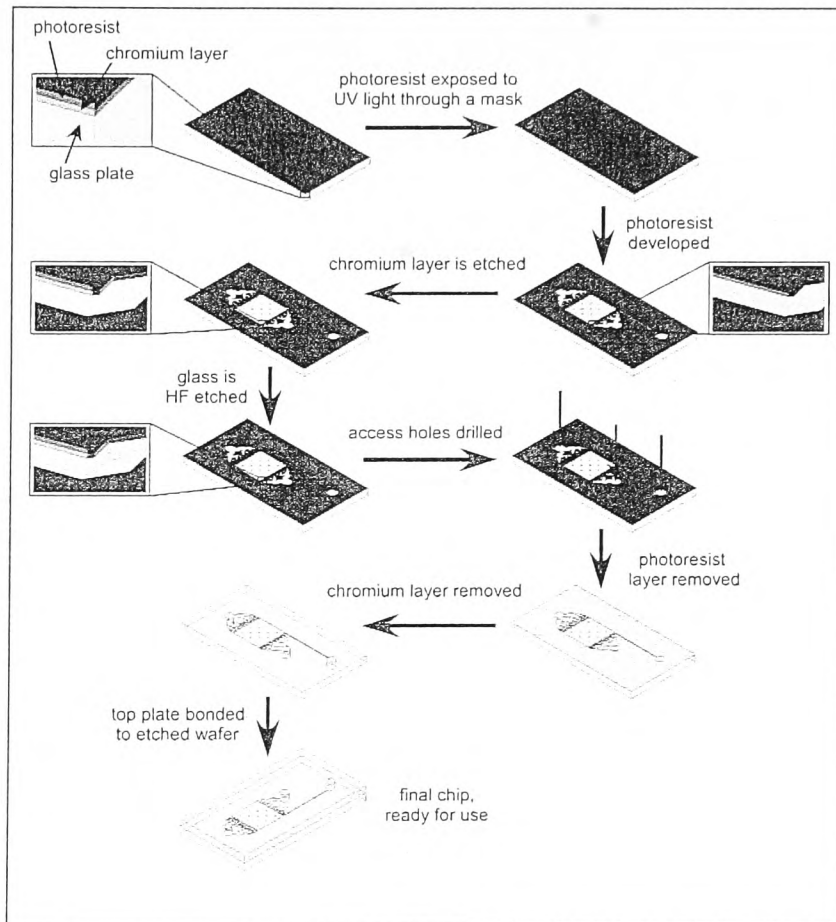


Figure 3.5. Schematic of the fabrication process showing the steps of photolithography, wet etching and thermal bonding. Figure courtesy of M. D. Tarn.

3.5 Particle comparison investigation

The following section describes the chip design, experimental set-up, magnets and

protocols used for the magnetic particle comparison investigation (figure 3.6).

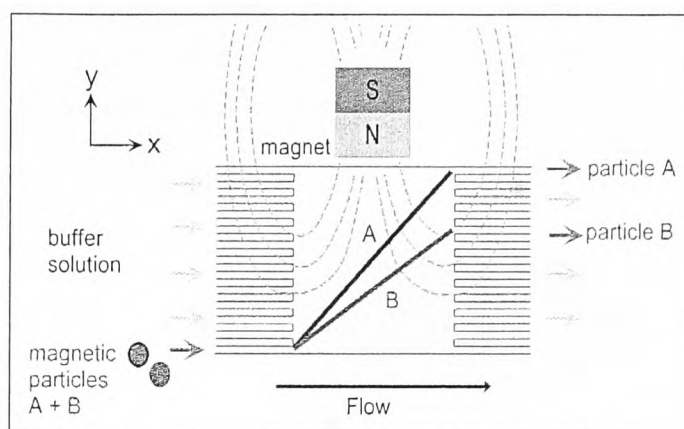


Figure 3.6. Principle of magnetic particle comparison via free-flow magnetophoresis. Particles A and B are deflected to different degrees depending on their size and magnetic content.

3.5.1 Microchip design

The microchip design used in these experiments was used previously for free-flow magnetophoresis (FFM) experiments.[131, 132] The design will therefore be referred to as FFM in this thesis and a CAD schematic is shown in figure 3.7. The microchip design featured a single square deflection chamber 6 mm x 6 mm which was supported by 13 diamond shaped pillars and with two inlet systems and a depth of 20 μm . The larger inlet was for buffer alone and was that branched from a single source into 16 inlet channels of equal size to help spread fluid evenly across the separation chamber. The other inlet channel was a single 10 mm long straight channel that entered the cell at one corner and was used for the introduction of the magnetic particles from the particle reservoir. At the opposite end of the flow cell there were 16 branched outlet channels that merged into a single outlet port, again these were branched to facilitate the application of pressure evenly over the width of the chamber. The outlet channels

were also numbered, to facilitate the recording of particle positions as they exit the chamber. All inlets and outlet channels were 100 μm in width and evenly spaced.

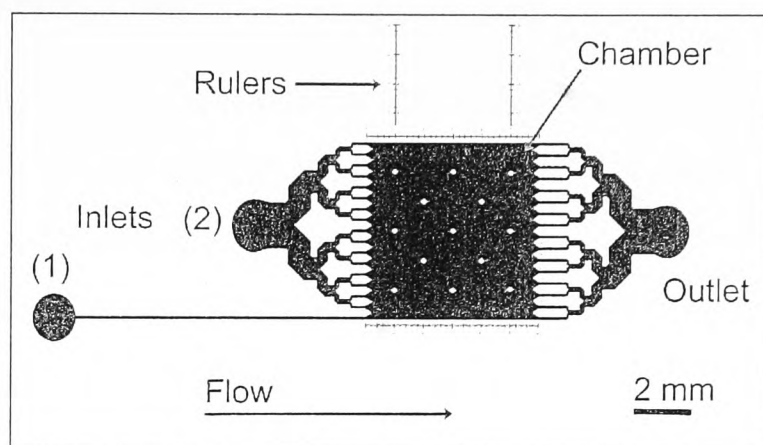


Figure 3.7. CAD schematic of the free-flow magnetophoresis chip design.

3.5.2 Microchip set-up

The microchip was interfaced with fittings by gluing with Araldite Rapid (RS Components, UK). Pipette tips were glued to the buffer and inlet ports to create reservoirs for the buffer solution and particle suspensions. A piece of PEEK tubing 2 cm in length (i.d. 0.51 Mm, o.d. 1.6 mm, Cole-Parmer, UK) was glued to the outlet and was connected to a piece of Tygon tubing, (i.d., 1.3 mm and o.d., 2.3 mm, Coleparmer, UK) typically 4 to 5 cm in length. A 20 gauge syringe needle was then carefully inserted into the tubing and attached to a plastic 5 mL syringe which was placed securely into a syringe pump (Harvard Apparatus 2000 PHD infuse / withdraw, USA). The set-up was such that negative pressure could be applied to the outlet and liquid drawn through the chamber from both reservoirs (figure 3.8). The chip was then mounted onto the stage of an upright microscope (Laborlux 12, Leitz, Leitz Microscope.com). In order to view

as many of the exits as possible at any one time the chamber was viewed with the smallest objective available, which was a 4x.

3.5.3 Magnetic set-up

A variety of magnets were used for the particle comparison investigation in order to optimise the deflection of the particles inside the chamber. The magnets varied in size, geometry and placement in relation to the deflection chamber. The magnet sizes, geometries and relative positions are summarised in table 3.5. Details of the magnetic fields produced by these magnets are discussed in section 4.2.

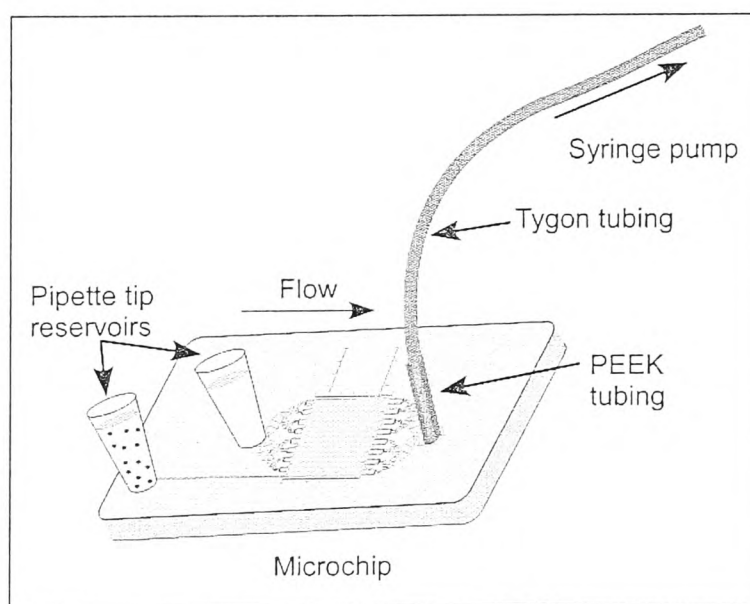


Figure 3.8. The FFM chip was interfaced to the syringe pump via Tygon tubing. Pipette tips were glued onto the access holes to act as reservoirs. Not drawn to scale.

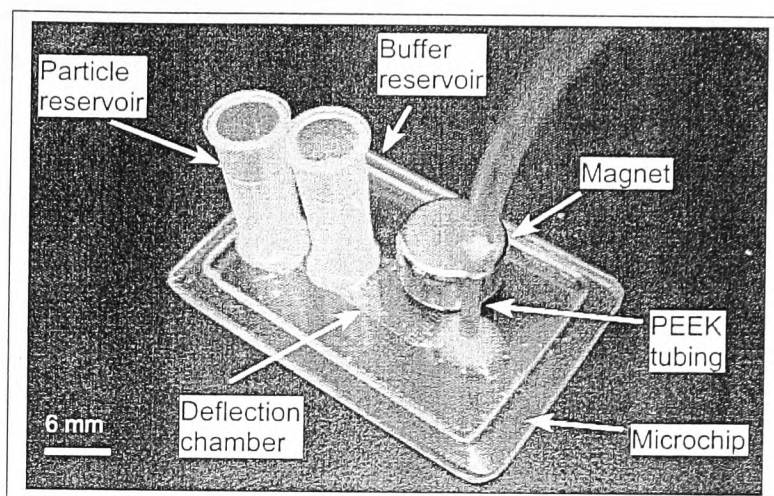
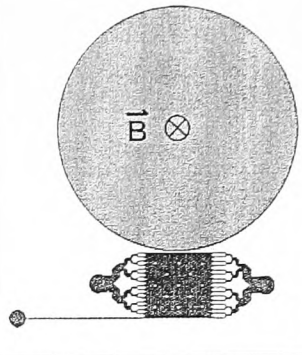
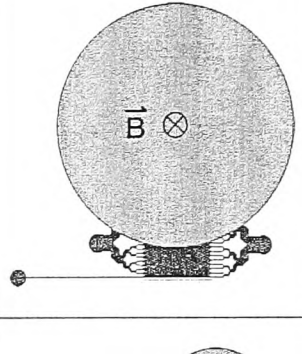
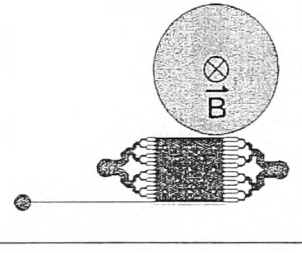
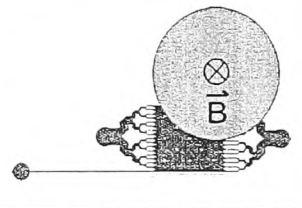


Figure 3.9. Photograph of the FFM chip with pipette tip reservoirs, magnet and PEEK tubing.

The magnet was placed on top of the microchip and positioned using the etched rulers. A small amount of BlueTac was used to secure the magnets so no movement was observed during the experiment (figure 3.9).

Table 3-5. Magnets used in the particle selection differed in size and position in relation to the separation chamber.

Magnet set-up	Shape	Geometries Diameter x depth [mm]	Position of magnet relative to chamber
Mag 1	Disc	20 x 5	
Mag 2	Disc	20 x 5	
Mag 3	Disc	10 x 5	
Mag 4	Disc	10 x 5	

3.5.4 Experimental procedures

Microchip pre-treatment

Before each experiment, the microchip was flushed with water to remove any air from the chamber and the channels by manual pumping. The microchip was then flushed with 100 mM NaOH using the syringe pump at a rate of $100 \mu\text{L h}^{-1}$ for 15 min. The NaOH was flushed out of the microchip with water and finally buffer was pumped through for 10 min.

Typical running conditions

Particle suspension was pipetted into the particle reservoir. The buffer reservoir was filled with buffer and then negative pressure was applied to the outlet by setting the syringe pump to the withdrawal mode. Care had to be taken that the reservoirs were filled to the same height with liquid. If the buffer reservoir was filled considerably lower than the particle reservoir the difference in hydrostatic pressure caused particles to flow towards the centre of the chamber. Flow rates between 50 and $500 \mu\text{L h}^{-1}$ were used which corresponded to flow velocities of 0.1 to 1 mm s^{-1} in the chamber. The magnetic particles with their core of iron oxide, featured a density of 1.1 to 1.6 g cm^{-3} , making them denser than the aqueous buffer they were suspended in. Thus the particles would settle to the bottom of the vessel over a certain length of time. In addition, the effect of the magnetic field, especially from the larger magnets reached the particle reservoir and pulled particles against the side of the pipette tip. This reduced the flow of particles into the chamber and in order to keep them suspended evenly the reservoir had to be agitated gently using a Pasteur pipette, without causing the introduction of air

bubbles.

3.5.5 Data acquisition and analysis

A Laborlux 12 microscope (Lietz, leitzmicroscopes.com) was used for the first year of experiments into magnetic particle comparison by free-flow magnetophoresis. The laborlux 12 was a simple, upright light microscope with a 4x objective. For all experiments during this period the 4x objective was utilised as this had a suitable working distance and was sufficient to see magnetic particles with diameters between 1 and 10 μm inside the microfluidic device.

In these early experiments a CCD camera was not available so all particle counting was carried out manually by watching the particle trajectories down the microscope and marking down the exits taken over a five minute period. From this data it was possible to make an estimation of u_{mag} and F_{mag} values (section 2.3.1. equation 12) for each particle population.

3.6 One-step bioassays

In the following, the first generation of the multi-laminar flow device, the experimental and magnetic set-ups along with reagents and protocols used for a single-step bioassay is described (figure 3.10).

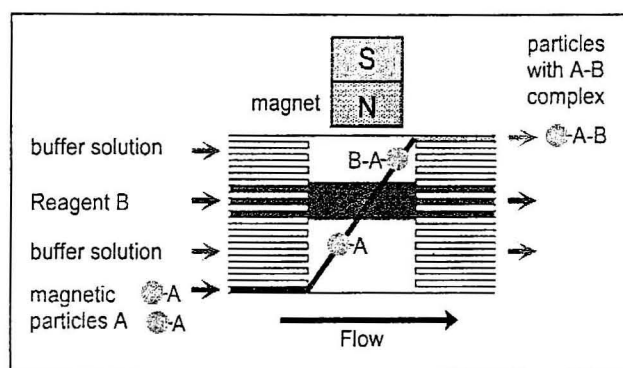


Figure 3.10. Principle of the one-step bioassays. Functionalised magnetic particles are deflected across two washing streams and a reagent stream.

3.6.1 Microchip design (MLF1)

The initial generation of microchip for the continuous flow bioassays was termed Multi-Laminar Flow 1 (MLF1) and was designed with several considerations in mind. Firstly, the deflection behaviour of magnetic particles in previous deflection experiments was considered and secondly, in order to realise the concept of performing multiple procedures on the surface of magnetic particles as they were deflected across the entire width of a flow chamber, the chip design needed to support several independent flow streams in one area. The chip featured a rectangular reaction chamber, 6 mm long and 3 mm wide. The width of the chamber in comparison to the first chip design was

reduced from 6 mm to 3 mm because particles were generally not deflected any further than 3 mm. The chip also featured four independent inlets, each capable of supplying a separate liquid stream to the chamber. Inlets 2, 3 and 4 were equal in size and branched to each form eight 60 μm wide channels (post etching) into the chamber. Inlet 1, which was intended for the introduction of a particle suspension, was unbranched and narrowed from 410 μm to 60 μm in width. The reason for this channel design was to try and focus the particles into a narrow flow stream along the wall of the chamber each particle being pulled across the chamber started at a similar position. The chip design featured a single branched outlet with 32 channels of 25 μm in width leading off from the chamber. This allowed for the initial investigation of both positive and negative pressure as a means of pumping liquid through the chip. Although particles would ultimately recombine with reagents as they flowed out of the chip, detection could be performed in real time within the chamber (figure 3.11).

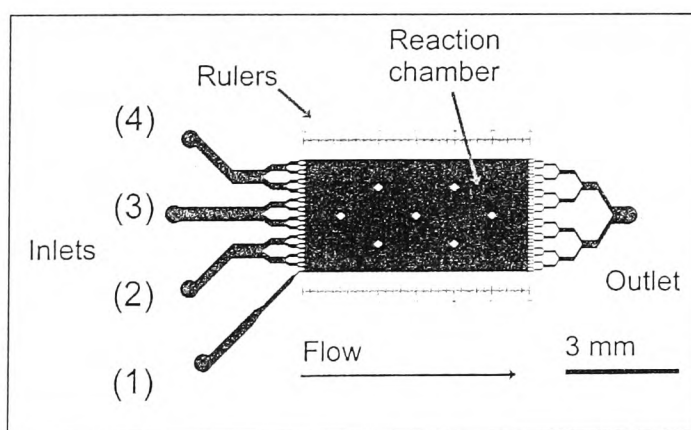


Figure 3.11. CAD schematic of the MLF1 chip design featuring four independent inlets, a reaction chamber 3 mm by 6 mm and a single outlet.

3.6.2 Magnetic set-up

The magnet utilised for the continuous flow bioassays was a small rectangular NdFeB magnet 5 mm x 4 mm x 4 mm. Initially, Mag4 was utilised, which had induced the greatest particle deflection. However, the particle inlet channel on the MLF1 design was 4 mm long, much shorter than the 10 mm particle inlet channel of the FFM design. When Mag4 was placed on to the MLF1 design, the magnetic particles in the inlet channel formed chains and were pulled against the wall of the channel. After a short period of time no particles entered the chamber, having been trapped inside the capillary. This was caused by the close proximity of the magnet to the particle inlet channel, approximately 6 mm away (figure 3.12). Therefore, it was concluded that Mag4 was too strong for the MLF1 chip design and a smaller magnet needed to be employed. The particles were observed to enter the chip consistently and without agglomerating when the magnetic field was generated using the small rectangular NdFeB magnet (5 x 4 x 4 mm³), shown in figure 3.13. The optimal position of this magnet and the optimal flow rate for the maximum degree of particle deflection is discussed in section 5.2.

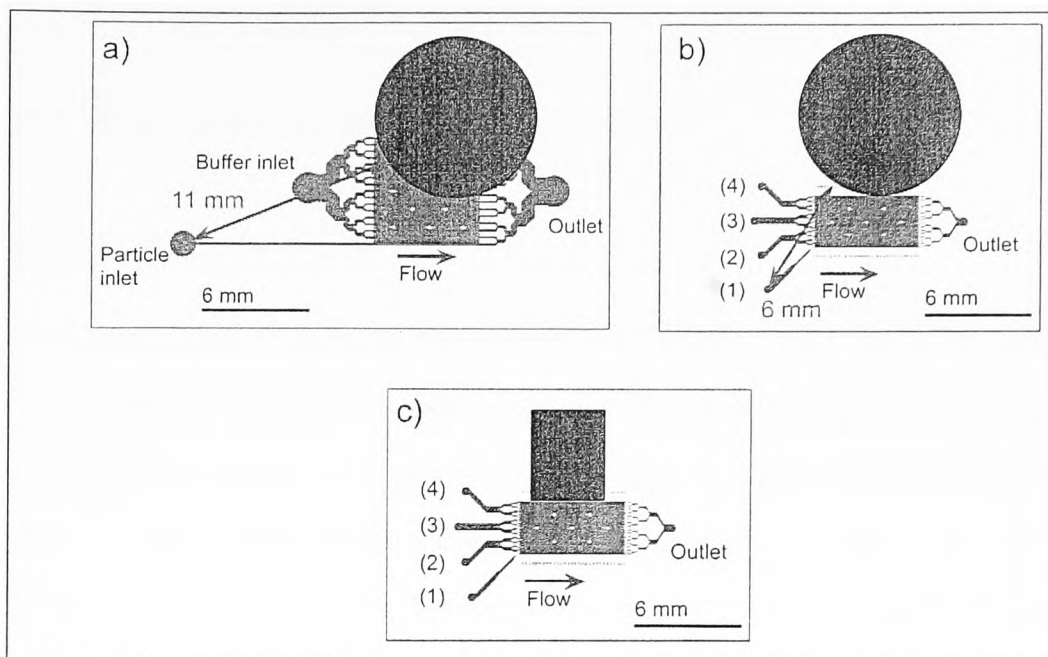


Figure 3.12. The position of Mag4 and smaller, rectangular magnet in relation to the particle inlet on a) the FFM chip design and b) the MLF1 chip design. c) The position shows the position of rectangular magnet ($5 \times 4 \times 4 \text{ mm}^3$) on MLF1.

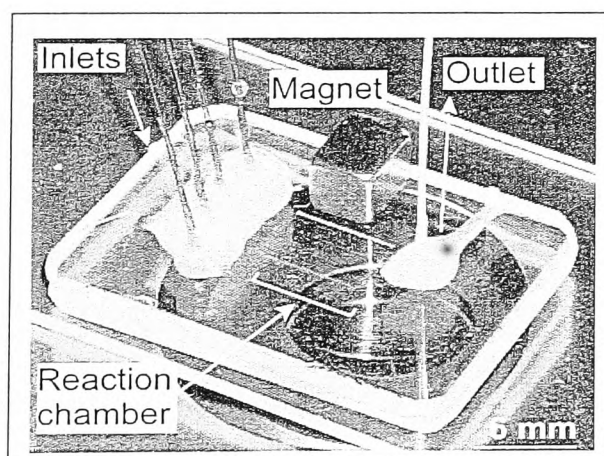


Figure 3.13. Photograph of the position of the rectangular magnet relative to the inlets, deflection chamber and the outlet.

3.6.3 Experimental set-up for one step bioassays

Pumping via negative pressure

Initial experiments to generate multi-laminar flow streams were performed using negative pressure. Firstly, the microchip was sonicated in purified water and the drill holes were vacuumed out to remove any debris from previous experiments. Small pipette tips were glued into the access holes of the device and a single fused silica capillary (o.d. 375 μm , i.d. 150 μm , Polymicro Technologies, USA) was glued into the outlet access hole. The capillary was interfaced to a plastic syringe via a plastic luer lock (Anachem, UK). The set up of the luer lock can be seen in figure 3.14, the capillary was inserted into a short piece of PTFE tubing (i.d. 0.3 mm, o.d. 1.6 mm, Supelco, UK) about 2 – 3 cm long. The PTFE tubing then fitted into a small ferrule which in turn sealed the PTFE tightly into a nut. This nut was then screwed firmly into the luer adapter and connected to the syringe.

Pumping via positive pressure

The chip was interfaced to a four port syringe pump using fused silica capillaries (o.d. 375 μm , i.d. 100 μm) typically between 4 and 5 cm long. Figure 3.15 is a schematic of this set-up. The capillaries were glued directly into the inlet and outlet drill holes using epoxy glue (Araldite Rapid, RS components, UK) and then connected to four 1 mL glass gas tight syringes (SGE Analytical Science, Australia) via luer lock adaptors. The single outlet capillary was placed directly into a waste reservoir via a small piece of

Tygon tubing (i.d. 254 μm , o.d.762 μm , Cole-Parmer, London, UK).

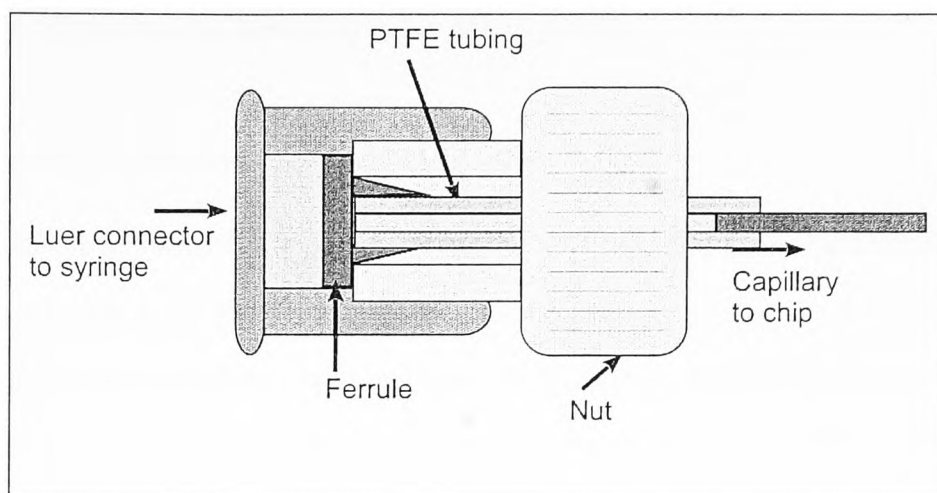


Figure 3.14. Schematic of the luer lock assembly with fused silica capillary.

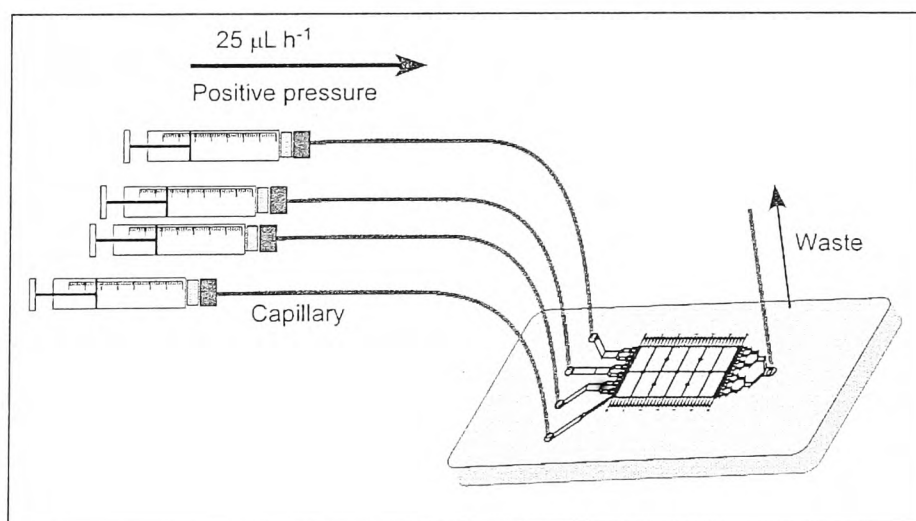


Figure 3.15. Schematic of the set-up for MLF1. Microchip is interfaced to syringes via fused silica capillaries.

3.6.4 Experimental procedures for MLF1 design

Microchip pre-treatment

The microchip was first flushed with purified water by applying manual pressure from a syringe on the single outlet. After all the air had been removed from the device, it was mounted on the microscope and a solution of KOH in isopropanol (IPA) was pumped via positive pressure into the chip from four 1 mL plastic syringes. The KOH / IPA was pumped for 10 min and care was taken not to exceed this time as after long periods of time the KOH / IPA would strip the rubber plunger of the syringe and leave deposits inside the chamber. After 10 min at a flow rate of $50 \mu\text{L h}^{-1}$ the KOH / IPA was changed for purified water which was flushed through for another 10 min at $100 \mu\text{L h}^{-1}$ to remove any KOH / IPA from the system. PBS with 0.01 % (w/v) BSA was pumped through the chip for a further 10 min to allow the BSA to dynamically coat the surface of the glass.

Typical running conditions

Unless otherwise stated, four 1 mL glass syringes were filled with $200 \mu\text{L}$ of liquid and secured on the multi-port syringe pump. The luer locks were then attached to the syringes and laminar flow streams were generated in the chamber by applying equal positive pressure to each of the four syringes to produce a combined flow rate of $100 \mu\text{L h}^{-1}$ ($25 \mu\text{L h}^{-1}$ from each syringe), leading to a flow velocity of $500 \mu\text{m s}^{-1}$ in the chamber. When liquids in the syringes required changing, such as replacing buffer with reagents, the flow was stopped and the pressure in the system was allowed to equilibrate

before the removal of syringes. When removing the syringes from the chip, care was taken to fill the end of the luer lock with a small amount of liquid before removing the syringe entirely. If there had been a tiny difference in pressure that would cause liquid to move back into the microchip then the small amount of liquid in the end of the lock would prevent air from being sucked in (figure 3.16.). The magnetic particles settled in the syringes much like they did in the particle reservoirs of the FFM chip and this would lead to particles being unable to enter the chip. In order to reduce this effect, the syringe containing the particle suspension was rotated by approximately 45° every 2 to 3 min. This had to be done very gently as any sharp movement of the syringe or the capillary would disrupt the laminar flow inside the chamber.

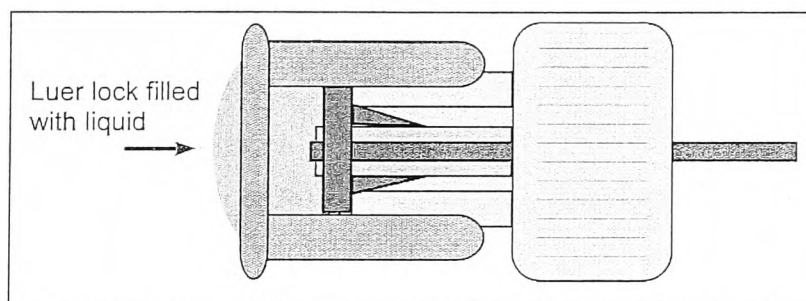


Figure 3.16. The luer lock was filled with a small amount of liquid by depressing the plunger of the syringe before changing to another syringe to stop air entering the system.

On-chip bioassay procedure

A suspension of streptavidin coated magnetic particles (3×10^6 particles mL^{-1}) was pumped into the microchip via inlet (1) as shown in figure 3.17, 0.1x TBE buffer was

pumped in via inlets (2) and (4). These formed two washing streams inside the chamber to remove any unbound material from the particle surface and to allow for optical detection in the final stream. Biotin which had been tagged with the fluorophore fluorescein was pumped through inlet (3). The magnet was then placed in the correct position on top of the microchip and videos were recorded of particles before entering the biotin stream and after reaching the opposite side of the chamber (figure 2.15.). A negative control was also performed in which plain epoxy M-270 particles were deflected through the chip instead of the streptavidin coated particles and videos taken before and after the biotin stream.

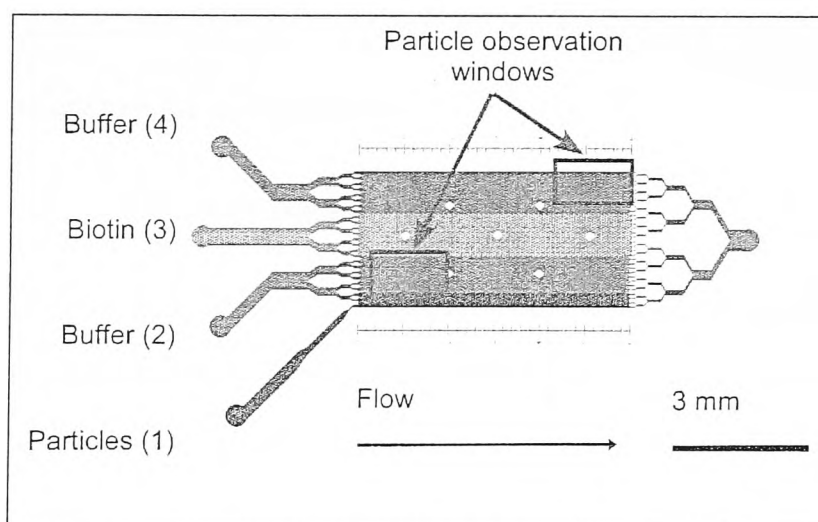


Figure 3.17. On-chip procedure for streptavidin – biotin binding assay. Magnetic particles introduced via inlet (1) were deflected through a stream of fluorescent biotin (3) and videos were taken of the particles before and after the stream.

Off-chip bioassay procedure

10 μL of streptavidin-coated magnetic particles ($6 - 7 \times 10^8$ particles mL^{-1}) were mixed with 200 μL of fluorescently labelled biotin at a concentration of 20 $\mu\text{g mL}^{-1}$ in an Eppendorf tube. The mixture was allowed to incubate at room temperature for 10 min with protection from light to avoid photo-bleaching of the fluorescent tag. Particles were then collected on the side of the tube using an external magnet and the supernatant was carefully pipetted off. This was followed by three washing steps in which particles were resuspended in 200 μL of 0.1x TBE, collected and resuspended again. A drop of particle suspension was then placed on a microscope slide, sealed with a cover slide and observed on the fluorescence microscope. A negative control was also performed in which the streptavidin coated M-270 particles were replaced with epoxy M-270 particles and the procedure above was repeated.

3.6.5 Data acquisition and analysis

3.6.5.1 Microscopy and data acquisition

The majority of the work, from the second year of study onwards, was performed with an inverted fluorescence microscope (Nikon, TE2000u, Japan) utilising five objectives; 2x, 4x, 10x, 20x and 40x. Fluorescent microscopy was performed using a mercury arc lamp (103 W/2, Osram GmbH, Germany) and for all bioassay work requiring fluorescence detection, the fluorophore fluorescein or fluorescein isothiocyanate (FITC) was used and therefore the B-2A filter cube (Ex 450-490, DM 505, BA 520) was utilised. The microscope was housed in a metal cage over which a black curtain was positioned to block out external light.

Initially, a small, colour CCD camera was used to video and take images of the particle. The Watec 221S camera (Watec, Japan), featured a 1 / 2" colour CCD element with a

resolution of 811 (H) by 508 (V). The camera had various parameters that could be controlled by moving switches on the camera casing, such as the shutter speed and the automatic gain control (AGC). For all experiments, the shutter speed was kept constant (1/4000 s) and the AGC was disabled. This was to avoid any artificial enhancement of low signals by the camera.

The Watec camera was later replaced by an MTV Mintron (Mintron, Taiwan) CCD camera which featured a 1 / 3" colour CCD with 795 (H) by 596 (V) resolution. The camera had an on-screen menu on which various parameters could be selected, such as the sensitivity and the AGC. The sensitivity could be adjusted from between 0 to 128x which altered the exposure time of the camera. At higher sensitivities the camera had a slower frame rate and took longer to take an image such that moving particles appeared as 'streaks'. The resolution of the camera was quite low so if the sensitivity was set too high and the streaks very long then the particles could not be detected against the background. Hence, a balance had to be struck between sensitivity and frame rate. For all experiments the sensitivity on the Mintron camera was thus set to 24x and the AGC was disabled to avoid any artificial brightening of the image.

When using the Watec 221S, the Mintron MTV and the Zoom CCD cameras, PVR Plus capture software (KWorld Computer Co. Ltd, Taiwan) was used for the observation and capture of videos as well as still images. These were then saved on the PC as MPEG or JPEG files respectively.

3.6.5.2 Data analysis software

The freely downloadable software *ImageJ* (<http://rsbweb.nih.gov/ij/>) was utilised for the analysis of all video footage taken by all video capture packages. *ImageJ* was used to

measure the fluorescence intensity of magnetic particles videoed during bioassay experiments. The greyscale intensity of the particle and the surrounding area in the image was measured using either the 'measure' option or the 'plot profile' option. The choice between using the 'measure,' which gave maximum pixel greyscale intensity or the 'plot profile' option, which measured greyscale intensity of pixels over a specified distance, depended entirely on the type of image being captured. For high levels of fluorescence signals, the camera exposure time was short and particles appeared spherical as they moved through the chip. In this case the maximum fluorescent intensity was sufficient for analysis (figure 3.18.). The same also applied on for the analysis of off-chip particle based procedures. However, with low levels of the fluorescence signals, the camera had to be adjusted in order to detect light emitted by lengthening the exposure time. In doing this, the frame rate of the camera was reduced and particles appeared as 'streaks' rather than single dots and thus the fluorescent signal from the particle was stretched over the distance of the particle trace. In order to measure the fluorescence signal for each streak, a line was drawn along the axis of the streak and a 'plot profile' measured. This could then be imported into *Origin7* and the area underneath the peak was integrated. This took into account the signal spread across distance, which in turn varied depending on the speed of the particle; faster particles giving shorter streaks than slower particles. In both cases, the background intensity of the images was deducted from the fluorescence signal of the particles.

Origin 7 was a software package used for the graphical representation of data and for the integration of particle trace peaks in the analysis of particle bioassays. For the integration of peak areas, data was imported directly from *ImageJ* into *Origin7* and a peak plotted using the software. As the background had already been taken away from

the particle trace signal the baseline was defined as $y = 0$. From this a peak was identified automatically by the software and the peak area was calculated (figure 3.19).

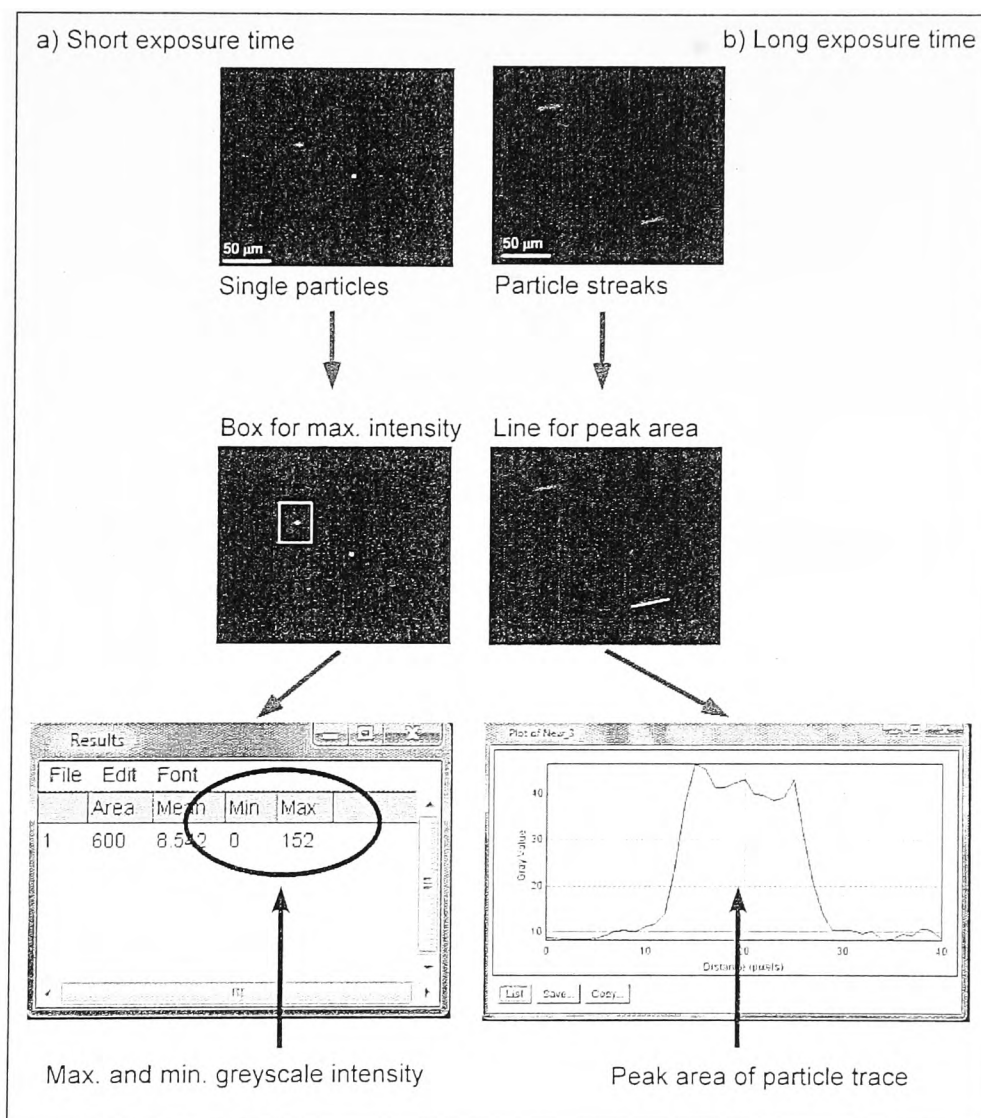


Figure 3.18. Data analysis at different camera exposure times. a) At short exposure times, maximum fluorescence intensity was measured from an area. b) At long exposure times, the area under the curve was measured using 'plot profile' giving a peak.

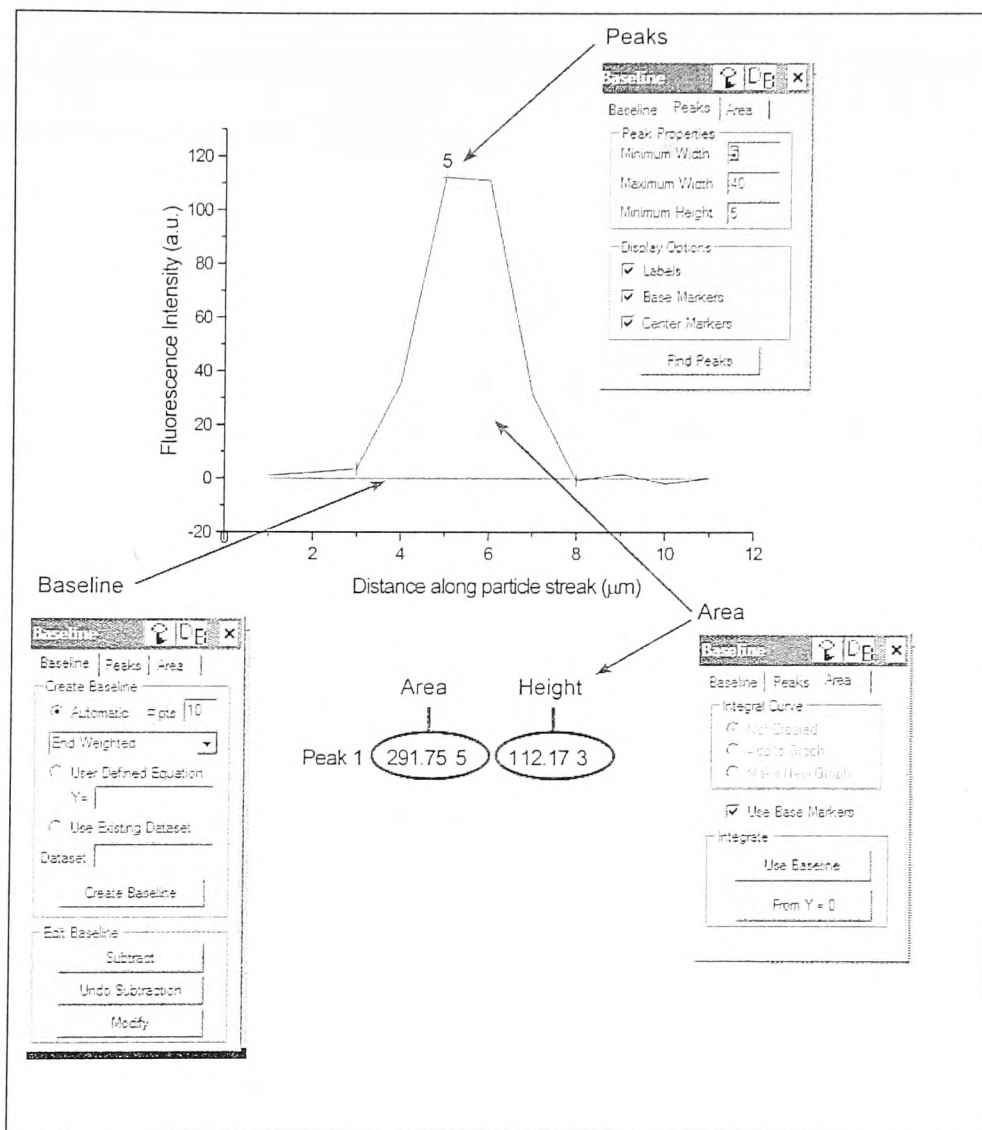


Figure 3.19. Peak areas from data analysis of particle streaks at long exposure times were integrated in Origin7.

3.7 Two-step bioassays

The following sections describe the design of the second generation of the multi-laminar flow micro-device, its experimental and magnetic set-ups and the protocols for two sandwich immunoassays (figure 3.20).

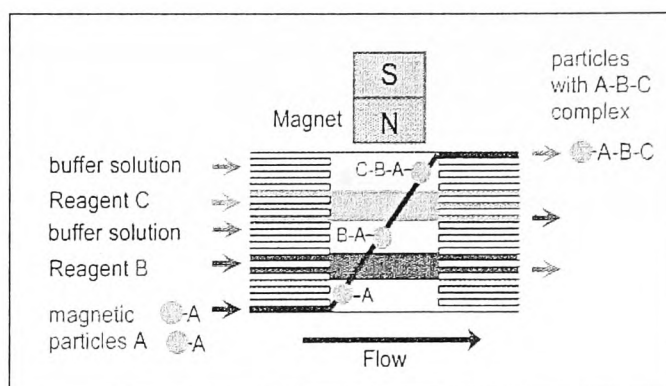


Figure 3.20. Principle of the two-step bioassays. Particles a deflected across two washing streams and two reagent streams.

3.7.1 Microchip design (MLF2)

The design of the second generation of microchips for the continuous flow bioassays was termed Multi-Laminar Flow 2 and the CAD schematic is shown in figure 3.21. The design was modified in several ways to take into account problems with the MLF1 microchip and also to accommodate a two-step bioassay. The chamber of the microchip was 3 mm wide by 8 mm long by 20 μm deep and supported by 10 diamond shaped pillars. The chamber was lengthened so that particles would take longer to reach the exits and thus incubation time in each liquid stream could be extended if needed. The design featured five 200 μm wide branched inlets instead of four to accommodate an extra reagent stream. The inlets branched to form two channels 120 μm wide at the

chamber edge and the design featured two outlets, a larger branched outlet (100 μm wide) branching into one outlet (400 μm wide) for waste reagents. The smaller, single outlet channel was for the collection of particles post-reaction and was 100 μm in width. The outlet channels were all wider by 75 μm than the previous chip design (MFL1) to facilitate the removal of bubbles and crystals from the chamber.

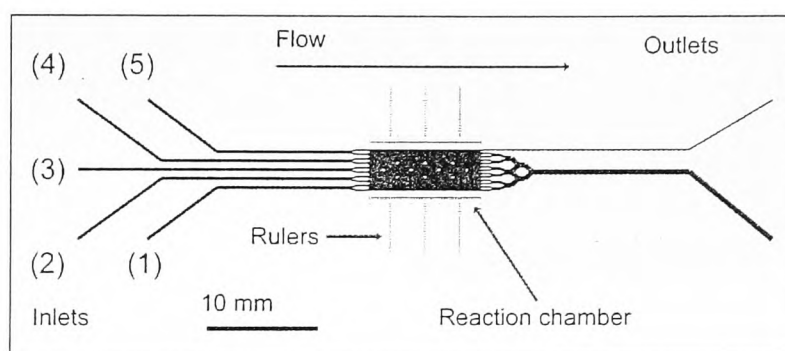


Figure 3.22. CAD schematic of the MLF2 device featuring five inlets, a 8 mm long reaction chamber and two outlets.

3.7.2 Experimental set-up of two step bioassays

The microchip was interfaced with the syringe pump in a similar way to the first generation device (section 3.6.3). Fused silica capillaries 100 μm in internal diameter were glued into the inlet access holes and attached to five 1 mL glass syringes via luer locks (figure 3.23). A short piece of 150 μm internal diameter capillary, typically 2 cm in length was glued into the branched outlet access hole and a longer piece of 100 μm internal diameter capillary, around 9 cm, was used for the single outlet. The difference in capillary length and internal diameter was optimised to even out the pressure at the outlets as discussed in detail in section 6.1.

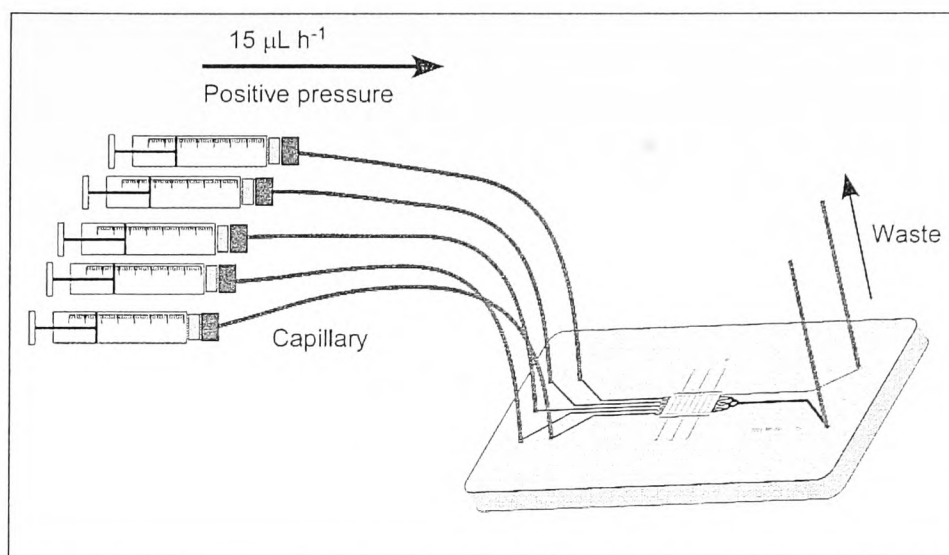


Figure 3.23. Drawing of MLF2 microchip interfaced to five glass syringes via fused silica capillaries. Two outlet capillaries were used in this chip design. Drawing is not to scale.

3.7.3 Magnetic set-up of two step bioassays

The same rectangular NdFeB ($5 \times 4 \times 4 \text{ mm}^3$) magnet used for the MLF1 chip design was also utilised for the MLF2 design. The magnet was placed on top of the chip, using the rulers for guidance and slightly towards the inlet side of the reaction chamber, approximately 1.4 mm from the inlet edge of the chamber. The edge of the magnet was also flush with the ruler running horizontal to the chamber (figure 3.24).

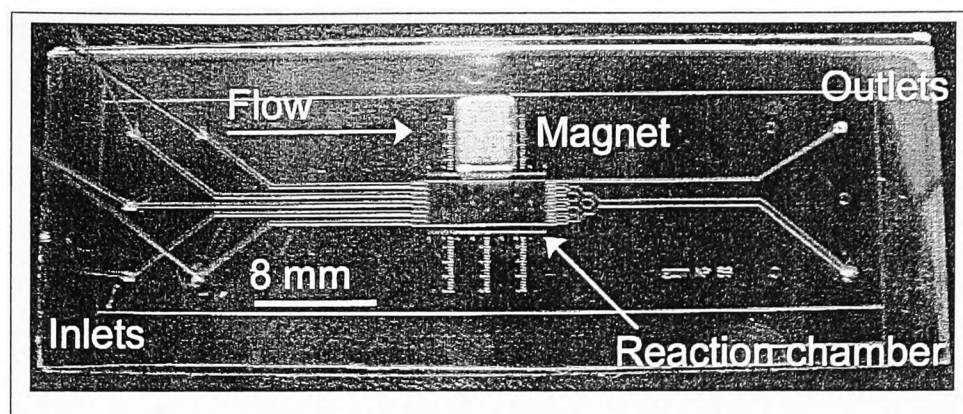


Figure 3.24. Photograph of microfluidic MLF2 device interfaced with the capillaries and with the magnet in position.

3.7.4 Experimental procedures

Microchip pre-treatment

Prior to experiments, the microchip was pre-treated with KOH in isopropanol and then flushed with purified water in the same procedure described as for the MFL1 microchip (Section 3.6.4.).

Typical running conditions

Unless otherwise stated, five 1 mL glass syringes were filled with 200 μL of liquid and secured on the multi-port syringe pump. The luer locks were then attached to the syringes and multi-laminar flow was generated in the chamber by applying equal positive pressure to each of the five syringes to produce a combined flow rate of 75 $\mu\text{L h}^{-1}$ (15 $\mu\text{L h}^{-1}$ from each of the five syringes), a flow velocity of 345 $\mu\text{m s}^{-1}$ in the chamber. The typical running conditions were as described in section 3.6.4.

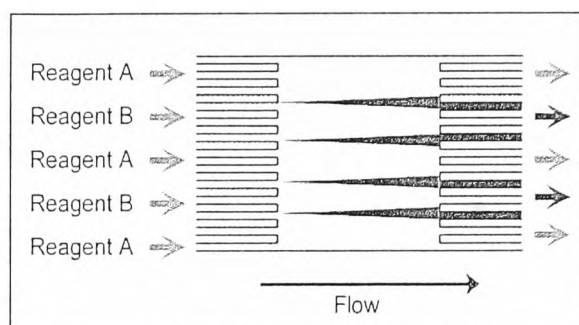
Inter-diffusional mixing investigation

Figure 3.25. Schematic of the interdiffusional mixing between reagents streams flowing adjacent to one another. Diffusion was investigated using iron thiocyanate.

The inter-diffusional mixing between adjacent streams was investigated by pumping alternate streams of 0.5 M iron (III) sulphate and 0.75 M potassium thiocyanate through the chamber at a flow rate of $15 \mu\text{L h}^{-1}$ ($350 \mu\text{m s}^{-1}$). The diffusion between the streams was observed on the 2x objective.

On-chip bioassay procedure for mouse IgG immunoassay

A suspension of streptavidin-coated magnetic particles (3×10^6 particles mL^{-1}) was pumped into the microchip via inlet (1), a solution of biotinylated mouse anti-CD4 IgG was introduced via inlet (2) and goat anti-mouse IgG tagged with FITC was pumped through inlet (4). PBS buffer was pumped through inlets (3) and (5), as shown in figure 3.26. These two streams acted as an initial washing stream after the primary (1°) antibody stream and as a washing / detect stream after the secondary (2°) antibody stream. For discussion on the two-step mouse immunoassay, the biotinylated mouse anti-CD4 antibody shall be referred to as the 1° antibody and the fluorescently tagged

anti-mouse IgG as the 2° antibody.

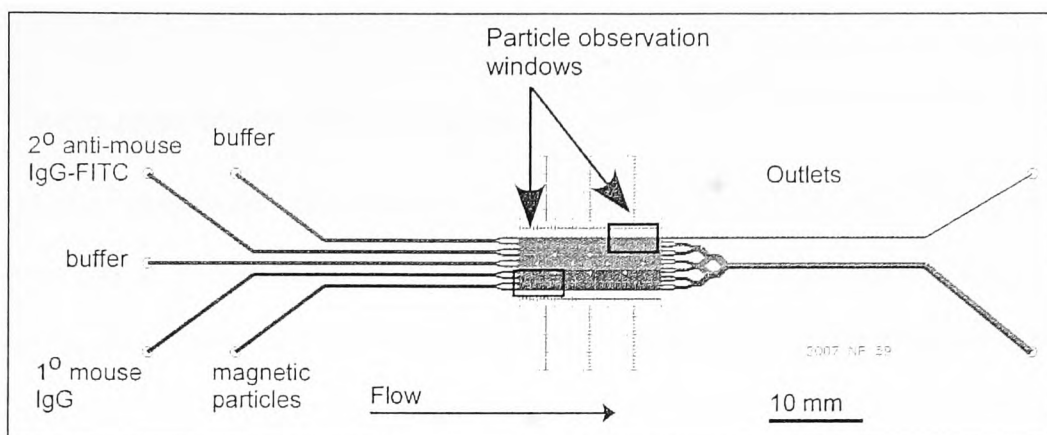


Figure 3.26. On-chip procedure for mouse IgG immunoassay. Magnetic particles pumped through inlet (1) were deflected through a stream of biotinylated mouse IgG and then a stream of fluorescently labelled anti-mouse IgG. Videos of particles were taken before and after these two streams.

The magnet was then placed in the correct position on top of the microchip and videos were recorded of particles before entering the 1° antibody stream and after reaching the opposite side of the chamber. A negative control was also performed in which the 1° antibody stream was left away and particles were deflected across the 2° antibody stream only and videos taken before and after.

Off-chip bioassay procedure for mouse IgG immunoassay

10 μL of streptavidin coated magnetic particles ($6 - 7 \times 10^8$ particles mL^{-1}) were mixed with 200 μL of biotinylated mouse IgG at a concentration of $10 \mu\text{g mL}^{-1}$ and allowed to incubate for 30 min. Particles were collected and washed three times with PBS and resuspended in 200 μL of fluorescently labelled goat anti-mouse IgG. The suspension was allowed to incubate for 30 min (and protected from light). The particles were

washed a further three times, resuspended in 100 μL of PBS and observed on the microscope.

On-chip procedure for CRP immunoassay

10 μL of streptavidin coated magnetic particles ($6 - 7 \times 10^8$ particles mL^{-1}) were mixed with 200 μL of the 1^o antibody; biotinylated monoclonal mouse anti-human C-reactive protein and allowed to incubate for 30 min with agitation. The particles functionalised with the 1^o antibody were then washed three times in PBS and resuspended into 990 μL of PBS. This suspension was pumped into the chip via inlet (1). Recombinant human CRP was pumped via inlet (2) and the complementary or 2^o antibody, a polyclonal goat anti-human CRP conjugated to FITC was pumped through inlet (4). PBS buffer was pumped through inlets (3) and (5), as shown in figure 3.27. The magnet was then placed in the correct position using the microchip rulers and videos were taken before and after traversing the chamber. A negative control was also performed in which plain M-270 particles were deflected across the reagents streams and videos recorded before and after.

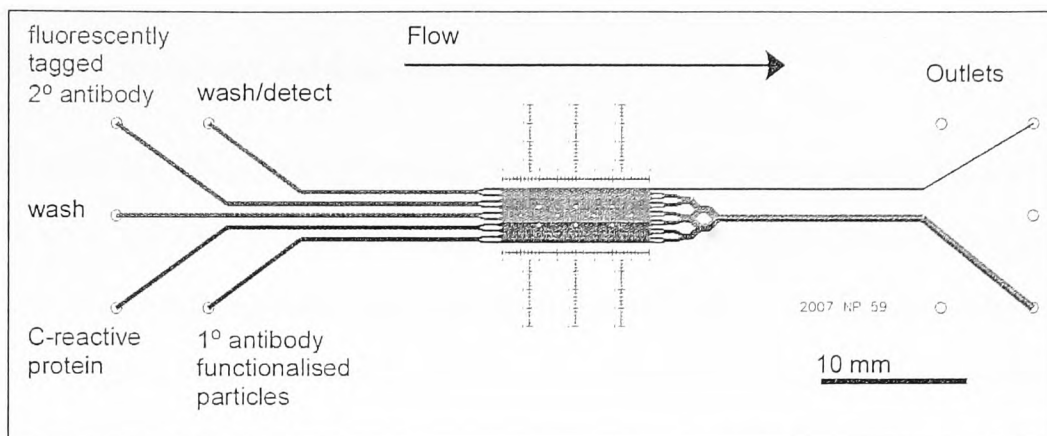


Figure 3.27. On-chip procedure for CRP assay. Magnetic particles functionalised with 1° antibody are introduced via inlet (1) and deflected across a stream containing CRP protein. Particles were then deflected across a 2nd stream containing the fluorescently tagged 2° antibody.

Off-chip bioassay procedure for CRP immunoassay

10 μL of streptavidin coated magnetic particles ($6 - 7 \times 10^8$ particles mL^{-1}) were mixed with 200 μL of the 1° antibody; biotinylated monoclonal mouse anti-human C-reactive protein and allowed to incubate for 30 min with agitation. The particles functionalised with the 1° antibody were then washed three times in PBS and resuspended in 200 μL of CRP solution for an incubation time of 30 min. The particles were then washed again in PBS and suspended for a last time in 200 μL of the 2° antibody for 30 min. After a final washing procedure, the particles were observed on the inverted fluorescence microscope.

3.7.5 Data acquisition and analysis

3.7.5.1 Microscopy and data acquisition

The Retiga – EXL camera (QImaging, Surrey, Canada) featured a peltier cooled 2 / 3” monochrome CCD element. The larger CCD allowed for a larger field of view than previous cameras but more importantly, the cooling of the CCD and the high resolution allowed for greater sensitivity when performing quantitative experiments by detecting much lower levels of fluorescence signals. The camera was bought with accompanying software (See following section 3.7.5.2, *ImagePro*) that allowed parameters such as exposure time, frame rate and binning to be controlled via a user interface.

Images of the inter-diffusional mixing and videos of the particles before and after immunoassay binding events were taken with the Regita - EXL cooled CCD camera using ImagePro capture software. For all experiments on the MLF2 chip design the exposure time of the camera was optimised and kept constant at 100 ms 340 μ s with the 4 x 4 binning activated. Activating the binning on the camera groups together information from collected from individual pixels, whilst this can lose quality in terms of resolution, it helps to increase the frame rate of the camera by reducing the amount of information being processed at any one time. This exposure time setting allowed particles to be seen even with low fluorescent signals but also the binning allowed the frame rate to be high enough to catch the particles in motion.

3.7.5.2 Data analysis software

ImagePro 6.2 (Qimaging, Surrey, Canada) was the user interface software supplied by QImaging for the Retiga – EXL CCD camera. The software was used to control the

camera and to capture images and videos. Data could either be recorded as a still capture image or a video by means of a sequence of images. The software also featured an automatic system calibration function. Images and videos could be saved either as TIFF files or as SEQ files, both of which could be imported directly into *ImageJ* for data analysis. Peak intensities of particles before and after then immunoassay were plotted using *Origin 7* as described previously in section 3.6.5.2.

3.8 Diamagnetic manipulation of particles

The following sections describe the micro-devices, experimental set-ups and the magnetic set-ups of two different investigations into using diamagnetic repulsive forces (section 2.3) for handling polystyrene particles, as shown in figure 3.28.

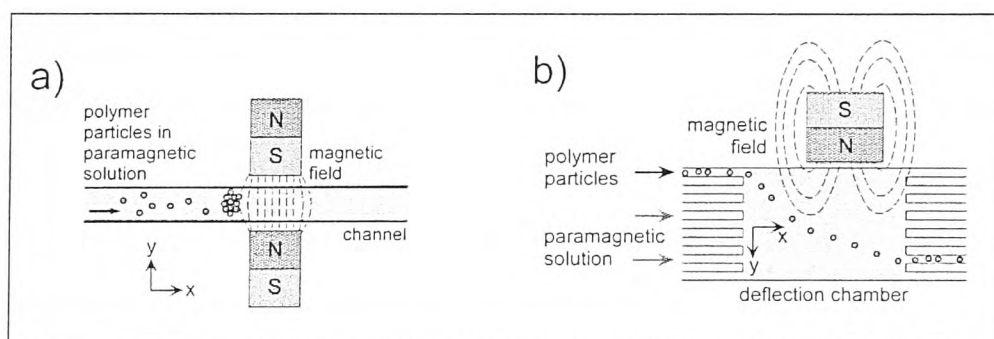


Figure 3.28. Principle of particle handling using diamagnetic repulsion forces. Particles are repelled by areas of high magnetic field gradient.

3.8.1 Chemicals and polystyrene particle suspensions for diamagnetic repulsion

Manganese Chloride

Aqueous solutions of manganese chloride salts were used for all diamagnetic repulsion experiments. Manganese (II) chloride tetrahydrate was purchased as a powder and solutions of 10 wt% (0.79 M) were prepared by dissolving 10 g salts in 100 mL of purified water.

Tween20 is a common non-ionic surfactant used in biological systems and in microfluidic applications involving microparticles. Tween20 was used in all diamagnetic repulsion work at a concentration of 0.01 % (w/v) by dispersing 100 mg of Tween20 liquid in 100 mL of purified water and diluting 1/100 into the MnCl_2 solution.

Diamagnetic plain polystyrene particles ($\chi_p = - 8.21 \times 10^{-6}$) were purchased in two particle diameters from Polysciences Europe GmbH (Eppenheim, Germany). For trapping, 10 μm diameter particles (Megabead NIST traceable standard) were used. For diamagnetophoresis experiments a mix of 10 μm and 5 μm (Microbead NIST traceable standard) was used. For the particle-based assay, 10 μm streptavidin-coated polystyrene particles were purchased from Partikeltechnologie GmbH (Micromod, Germany). Table 3.6 summarises the particles, their surface chemistry and the concentration in which they were used for each experiment by suspending particles in MnCl_2 solution.

Table 3-6. List of diamagnetic polystyrene particles used for the diamagnetic repulsion experiments detailing particle diameters, surface chemistries and concentrations.

Experiment	Particle diameter (μm)	Surface chemistry	Concentration particles / mL
Trapping, plug based assay	10	Plain	1.9×10^5
	10	Streptavidin	4.6×10^5
Diamagnetophoresis	10	Plain	6.0×10^5
	5	Plain	3.7×10^5

3.8.2 Microfluidic set-up

The particle trapping experiments were carried out using fused silica capillaries with an internal diameter of 100 μm and cut to a length between 13 and 15 cm. The polyimide coating was partly removed using a flame to create a window approximately 3 cm in length for optical viewing and the capillary was fixed to a glass slide for support. Tygon tubing (i.d. 254 μm , o.d. 762 μm) was used to interface the capillary to a syringe on one end while the other end was dipped into a sample tube. Particle suspensions were pulled into the capillary by applying negative pressure to the syringe with a pump (figure 3.29).

For the diamagnetic deflection investigations, the FFM chip design discussed in section 2.51 was used and set-up in the same procedure described earlier.

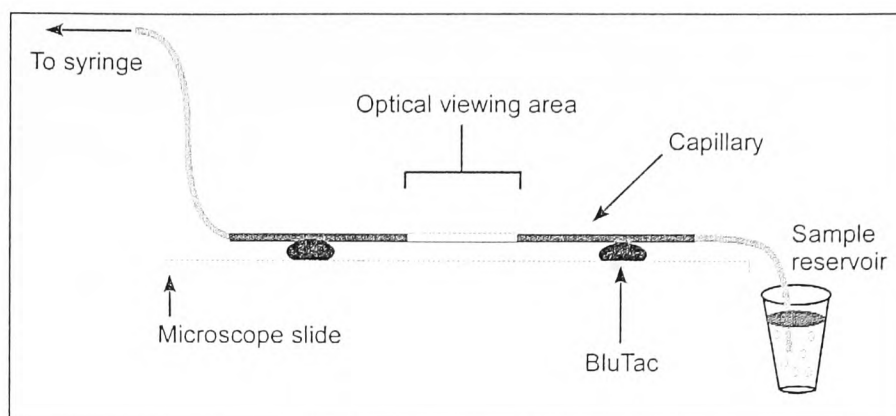


Figure 3.29. Drawing of capillary set-up for diamagnetic repulsion experiments for. Drawing not to scale.

3.8.3 Particle trapping investigation

Typical running conditions

The capillary was first manually flushed with MnCl_2 to remove any air from the system. The capillary was then interfaced to the syringe pump and the sample tube as outlined above. Negative pressure was applied to the syringe to draw up the particle suspension from the sample tube. The density of the polystyrene particles (1.03 g cm^{-3}) was less than that of MnCl_2 (1.08 g cm^{-3}) so in these experiments the particles experienced a buoyancy effect and floated to the top of the solution of MnCl_2 . In order to keep particles entering the chip in a consistent through-put the Tygon tubing linking the sample tube to the capillary was placed at the top of the solution, just below the liquid line. When the particle solution required changing, the system was stopped and left for 10 min to allow the pressure to equilibrate. This was to prevent the introduction of air

bubbles into the capillary. When forming plugs of particles the presence of an air bubble moving in the capillary would destroy the plug by pushing the particles out of the magnetic field area.

Magnetic set-up for particle trapping

Two cylindrical magnets with opposite poles facing were fixed to a small 1 mm by 2 mm section of glass by nipping several short pieces of capillary between the two magnets and gluing them with Araldite 2014 (RS Components, UK) to the slide (figure 3.30). When the glue had dried the pieces of capillary were removed such that the faces of the magnets were the width of the capillary apart every time. The magnets were then positioned across the capillary by gently lowering the glass side so that the capillary fitted between the two magnets.

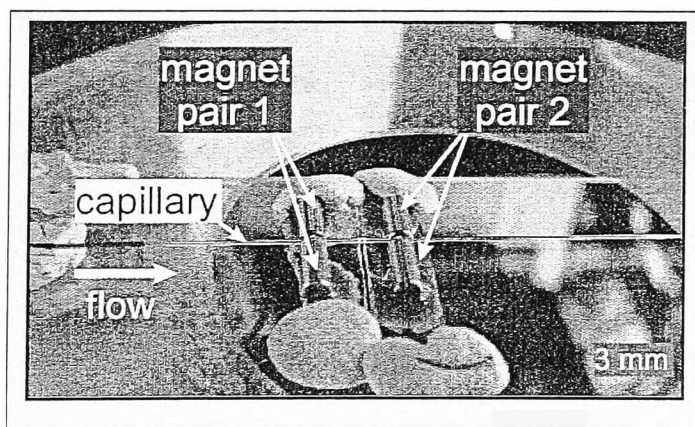


Figure 3.30. Photograph of trapping set-up with capillary and magnetic set-up.

Off-capillary bioassay procedure

A 200 μL aliquot of the streptavidin coated polystyrene particles was mixed with 200 μL of 1 $\mu\text{g mL}^{-1}$ fluorescently labelled biotin (biotin-4-fluorescein) in MnCl_2 in an Eppendorf tube. The tube was allowed to incubate for 30 min with protection from light and then centrifuged at 5000 rpm for 5 min to collect the particles. The supernatant was removed and the particles resuspended in MnCl_2 . This was repeated three times to ensure all of the free biotin was removed before a 10 μL aliquot of particles was placed on a microscope slide for viewing on the fluorescence microscope.

On-capillary procedure for streptavidin – biotin assay

The capillary was first flushed with MnCl_2 to remove any air bubbles from the system. A pair of magnets was then placed across the capillary and a suspension of streptavidin-coated polystyrene particles was pulled into the capillary to form a plug before the first magnet set. The system was then washed again with MnCl_2 before a second pair of magnets was placed upstream from the first. A suspension of plain polystyrene particles was then pulled into the capillary such that a second plug formed upstream from the first. The capillary was washed again with MnCl_2 before a solution of fluorescently tagged biotin in MnCl_2 was pumped through the capillary at a flow velocity of 210 $\mu\text{m s}^{-1}$ for approximately 13 min. The plug of streptavidin coated particles and the plug of plain polystyrene particles acted as positive and control tests, respectively.

Simultaneous trapping of diamagnetic and paramagnetic particles

A mixture of 10 μm polystyrene particles and 10 μm magnetic particles (Micromer, Micromod GmbH, Germany) in MnCl_2 , with particle concentrations of 1.9×10^5 and 8.7

$\times 10^5$ particles mL^{-1} , respectively was pulled through the capillary at $8 \mu\text{L h}^{-1}$ (0.28 mm s^{-1}) and a pair of magnets placed across the width of the capillary. Cross contamination between plugs was also investigated by pumping $10 \mu\text{m}$ polystyrene particles and $8 \mu\text{m}$ fluorescent particles (DragonGreen, Compel, Bangslabs) through the capillary and observing plug formation in fluorescence mode.

3.8.4 Diamagnetophoresis

Typical running conditions

The FFM microchip was first flushed with MnCl_2 using manual positive pressure to remove any bubbles from the microchip. The buffer reservoir supplying the majority of the separation chamber was filled with MnCl_2 and the particle inlet reservoir was filled to the same level with a particle suspension in MnCl_2 . A mixed particle suspension of $10 \mu\text{m}$ and $5 \mu\text{m}$ particles was used with concentrations of 6×10^5 and 3.7×10^5 particles mL^{-1} , respectively. Negative pressure was applied to the outlet between flow rates of $20 \mu\text{L h}^{-1}$ to $100 \mu\text{L h}^{-1}$, which corresponded to flow velocities of $45 \mu\text{m s}^{-1}$ to $230 \mu\text{m s}^{-1}$ in the chamber. The flow paths of the particles and the exits they took from the chamber were videoed with and without the magnet present.

Magnetic set-up of diamagnetophoresis experiments

A cylindrical magnet 20 mm in diameter and 5 mm deep was initially placed in various positions on top of the chip, at the same side of the chamber as the particle inlet. The maximum deflection distance of $10 \mu\text{m}$ particles was observed in the different positions until an optimum position was determined. Figure 3.31 shows the optimal position of the magnet, with the edge of the magnet being flush with the edge of the chamber

and lying slightly to the right of the chip, near the particle inlet such that the curve of the magnet crosses over the 3.4 mm point on the ruler. A photograph of the set-up is also shown in figure 3.32, showing the position of the magnet relative to the pipette reservoirs.

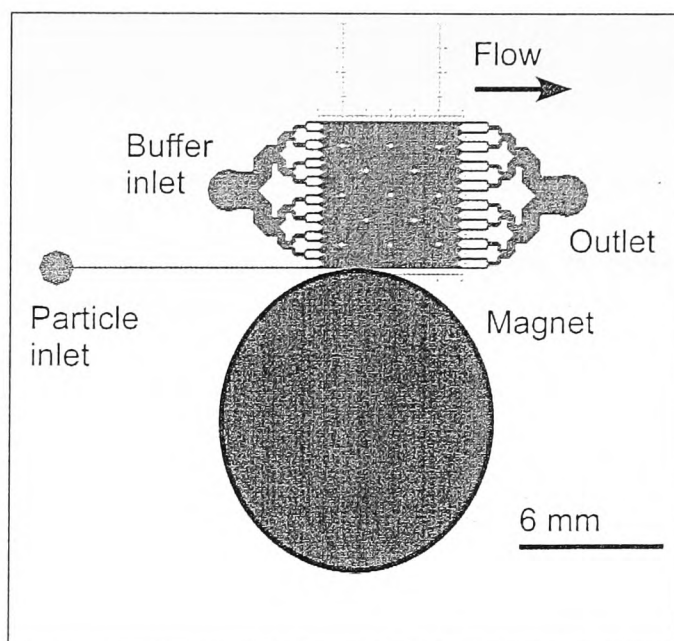


Figure 3.31. Schematic of FFM chip design with the position of the cylindrical magnet (20 mm in diameter, 5 mm deep).

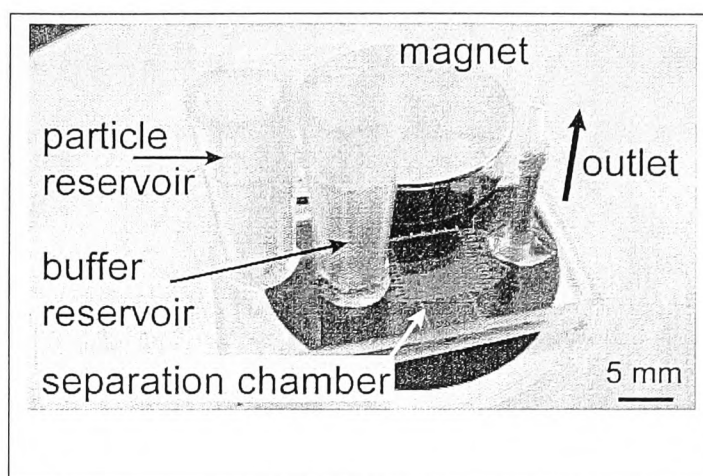


Figure 3.32. Photograph of the diamagnetophoresis set-up showing the position of the magnet relative to the chamber and the pipette reservoirs.

Flow rate investigation

To investigate the effect of flow rate on the deflection of the two particle populations negative pressure was applied to the chip, starting at a higher flow rate of $100 \mu\text{L h}^{-1}$ ($230 \mu\text{m s}^{-1}$) and slowly lowered to 80, 60, 40 and finally $20 \mu\text{L h}^{-1}$ ($45 \mu\text{m s}^{-1}$). After each change of flow rate the set-up was left for 5 min to allow the flow rate in the chamber to slow before videos were taken. The particle reservoir was also agitated in this time and the buffer reservoir replenished to the same level as the particle reservoir.

Temperature investigations

The effect of temperature on the deflection of the two particle populations was also investigated by mounting the chip on top of a microscope heating plate attached to a control box. The temperature was controlled by the box and calibrated using a

thermocouple. Negative pressure was applied to the outlet at a flow rate of $65 \mu\text{L h}^{-1}$ and the temperature was increased in stages of $5 \text{ }^{\circ}\text{C}$ from room temperature (approximately $20 - 25 \text{ }^{\circ}\text{C}$) up to $50 \text{ }^{\circ}\text{C}$ on the controller. The thermocouple was placed on top of the chip, next to the chamber and the temperature recorded. Table 3-7 shows the temperature of the controller and the corresponding temperature of the chip surface taken by the thermocouple. Figure 3.33 shows how measured temperatures on the heating plate surface and the microchip surface differ from that set on the controller. Again, the system was left for five minutes to allow the temperature of the chip to reach that of the controller before the videos were taken. The particle reservoir was agitated in this time and the buffer reservoir replenished.

Table 3-7. Comparison of heating plate controller temperature with the temperature taken by a thermocouple.

Controller ($^{\circ}\text{C}$)	Plate ($^{\circ}\text{C}$)	Chip surface ($^{\circ}\text{C}$)
No heating (19.1)	19.6	19.5
30	26.5	25.0
35	28.7	26.3
40	31.2	29.5
45	33.7	33.9
50	35.3	34.9

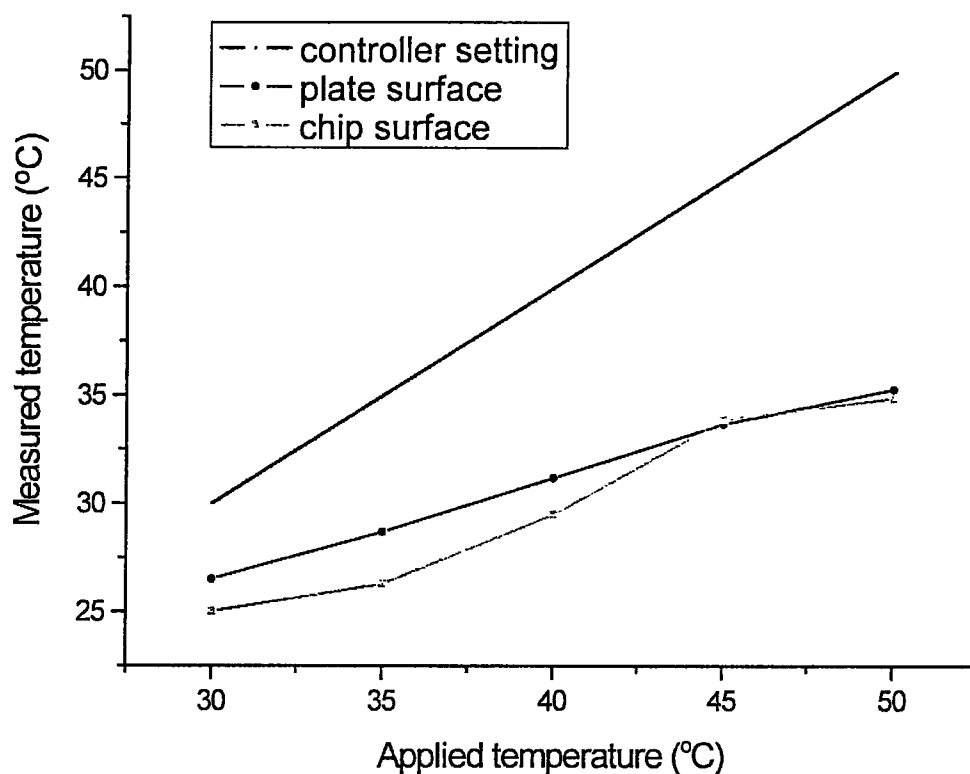


Figure 3.33. Temperature measured on the surface of the heating plate and the surface of the microchip, compared to the temperature specified by the heating plate controller.

Magnetic field investigation

To investigate the magnetic field gradient generated inside the chamber, the chip was filled with Compel 3 μm magnetic particles (Bangslabs, Park Scientific, Northampton, UK) in non-flow conditions such that the entire chamber was filled with particles. The magnet was then quickly placed into the correction position and videos were taken of the particles at 12 specific areas of the chip. The magnet was then removed and the particles redispersed by applying a small amount of pressure to the outlet. The procedure was repeated until videos of the entire area of the chamber were obtained.

Data acquisition and analysis

For all the investigations on the diamagnetophoresis work the Regita - EXL camera was used and videos captured by *ImagePro 6.2*. were imported directly into *ImageJ*. Particle trajectories and velocities were measured from the videos.

For the magnetic field investigation, *ImageJ* was used to draw a 0.6 by 0.6 mm grid over the video and the velocity along with the angle of the particle trajectory was measured (figure 3.34) using 'measure' and 'angle' functions. The values per grid were then averaged and normalised against the grid with the highest velocity values.

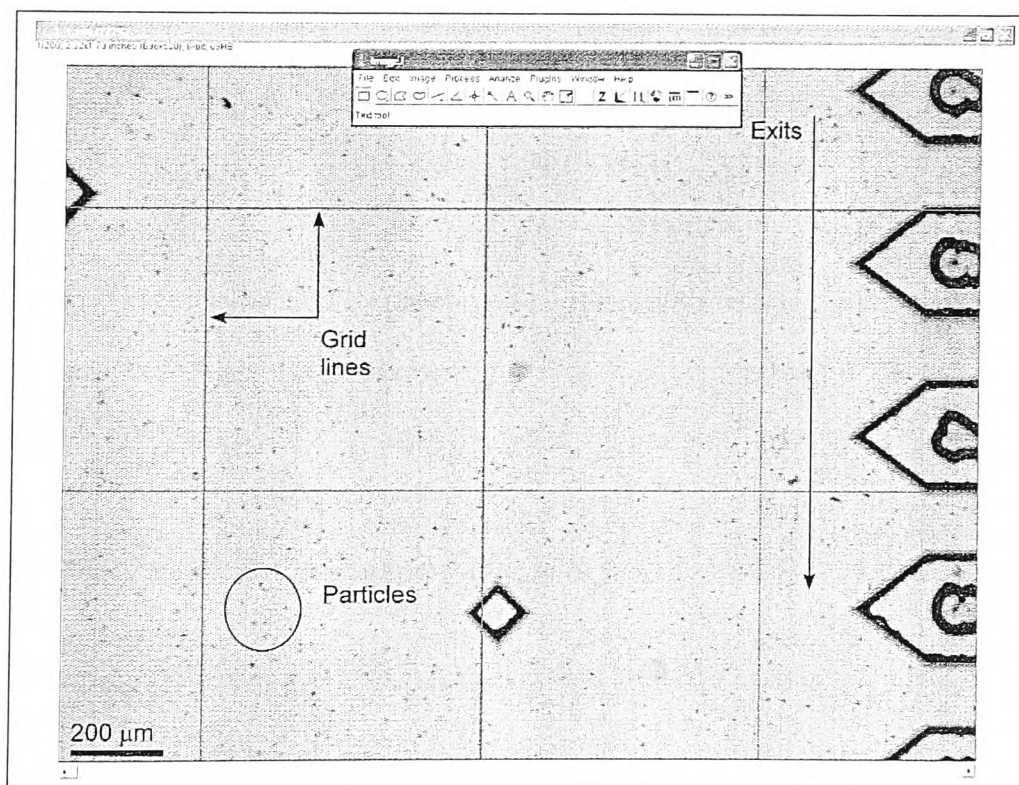


Figure 3.34. Data analysis of magnetic field investigation. The chamber was split into sections using a grid the velocity and trajectory angle of each particle measured in *ImageJ*.

4 Magnetic particle selection

The use of magnetic microparticles as mobile solid-supports inside the microfluidic devices was a fundamental aspect of this project. Therefore initial investigations into the suitability of various commercially available magnetic particles as manoeuvrable solid-supports in fluidic environments were made. The key factor that had to be considered and explored was how far a single particle could be deflected from laminar flow inside a chamber using an external magnetic field. The magnetophoretic mobilities of different particles were compared using the same principles and chip design as used for free-flow magnetophoresis (Section 3.5.1).

In total, eight types of magnetic particles with diameters between 1 and 10 μm were investigated at a range of flow rates between 50 and 500 $\mu\text{L h}^{-1}$ with different magnetic set-ups. The results of these experiments were compared with information provided by the manufacturers of the particles. In addition, a Vibrating Sample Magnetometer (Section 3.2.3) was utilised to further investigate their magnetic properties.

4.1 Comparison of permanent magnets used for particle deflection

Four magnetic set-ups were investigated, termed Mag1 to Mag4, for producing the optimal particle deflection inside the FFM microfluidic device. These set-ups utilised two differently sized disc magnets at two different positions relative to the chamber (Table 3.5). The magnets were all made from an alloy of neodymium, iron and boron. Permanent magnets were chosen over the use of electromagnets for this study because magnets such as NdFeB produce very high magnetic field gradients for their size. To

produce such fields using an electromagnet would require a much larger assembly and would generate a considerable amount of heat, which was not desirable. In addition, small permanent magnets are cheap, readily available and simple to use. Electromagnets are more difficult to assemble and require a power supply to generate a magnetic field.

For any magnetic material, the flux density or strength of the magnetic field diminishes with increasing distances from the magnet surface as the field lines disperse. Figure 4.1a shows field lines around a typical rectangular permanent magnet and how they disperse with increasing distance from the surface. Figure 4.1b shows this as a plot of flux density, B in Tesla against distance from the magnet surface.

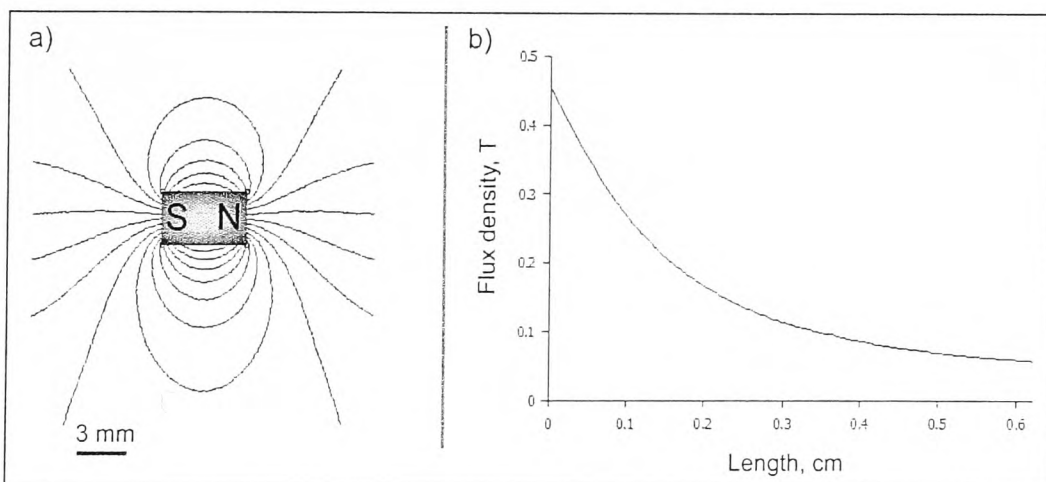


Figure 4.1a) Magnetic field lines around a typical bar magnet. b) Magnetic flux density with increasing distance from the magnet surface.

When each magnet set-up was placed on top of the microchip an inhomogeneous magnetic field was produced across the deflection chamber, with the highest flux density at the end adjacent to the magnet surface. This created the necessary magnetic

field gradient across the chamber, which was required to exert a force on the magnetic particles (equation 13, section 2.3.1). It should be noted that the decrease in flux density with increasing distance from the magnetic surface is not a linear relationship and that the gradient of the magnetic field across the separation chamber is different in both magnitude and direction, depending on the position inside the chamber in relation to the magnet. Figure 4.2 shows the magnetic field gradient produced by Mag1 across the deflection chamber. The length and thickness of the arrows indicates the normalised strength of the field in that position in the chamber, whereas the angle of the arrows indicates the direction of the magnetic field.

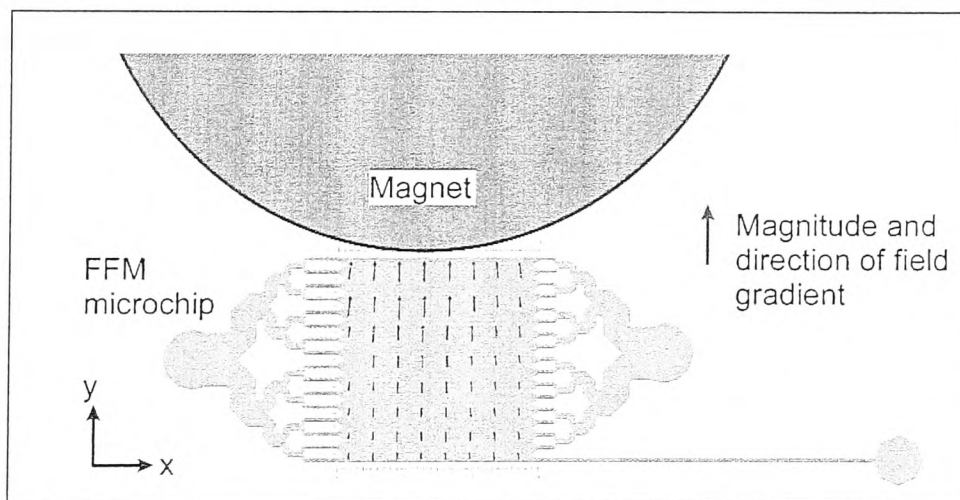


Figure 4.2. The magnetic field gradient produced by magnetic set-up 1 over the chamber. The size and direction of the arrows indicate the magnitude and direction of the gradient.

The plot shows how the direction and strength of the magnetic field differed at different locations over the deflection chamber and hence the force acting on a magnetic particle

within this chamber will be dependent on the particles' position relevant to the magnet. In addition, it can be seen that due to the curvature of the magnet, the direction of force is not always perpendicular to the direction of flow. These aspects make the accurate calculation of the magnetic force within the chamber very difficult and therefore any theoretical magnetic force calculations in this thesis have been based on an average value for the magnetic field strength and field gradient over the deflection chamber.

In order to compare the four magnetic set-ups with each other, the magnetic flux density at the magnet surface and at the position of the particle inlet was measured using a Hall sensor (Section 3.31) by placing the magnet adjacent to the sensor in the same plane as would be occupied by the microchip (figure 4.3). The disc magnets' directions of magnetisation were orientated through the depth of the disc.

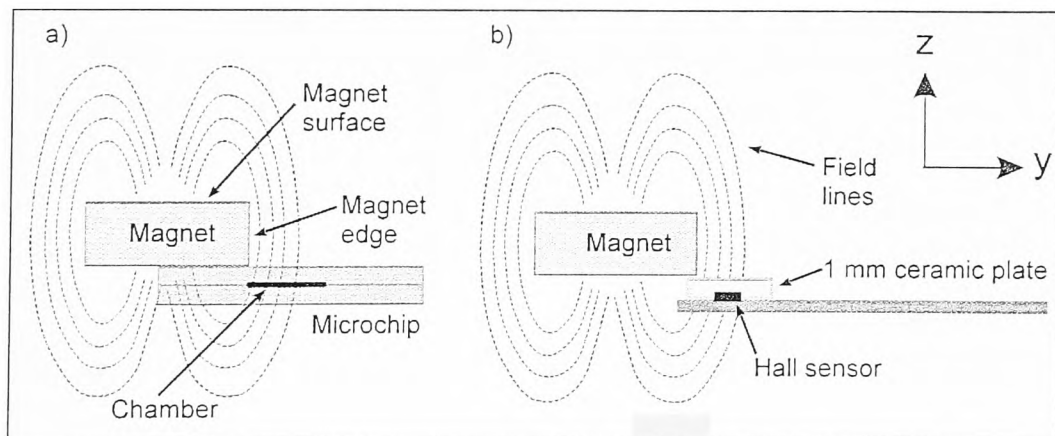


Figure 4.3a) Drawing of the magnetic field lines produced by a disc magnet in relation to the microchip. 4.3b) The position of the Hall sensor in relation to the magnetic field lines of a disc magnet, occupying the same plane as the chip.

The magnetic flux densities of each of the magnetic set-ups were measured by the Hall sensor and calculated in mT according to Section 3.31. In table 4.1 the flux density values are summarised together with the distance between magnet surface and particle inlet for each magnetic set-up.

Table 4-1. The distance of each magnetic set-up from the particle inlet along with the magnetic flux density at the particle inlet.

Magnetic set-up (see table 3.5)	Distance from magnet edge and particle inlet (mm)	Flux density at particle inlet (mT)
Mag1	6.6	41
Mag2	3.4	68
Mag3	7.7	20
Mag4	4.3	41

The values in table 4.1 show that as the magnet is moved closer to the particle inlet, the magnetic flux density increases at the particle inlet. Mag2, with the largest diameter and closest proximity to the particle inlet, produced the highest field with a value of 68 mT. The same sized magnet in position Mag1 produced a field of 41 mT at the particle inlet, a similar field produced by the smaller magnet Mag4, situated 4.3 mm from the particle inlet.

Femm 4.0 software (Section 3.3) was used to model the magnetic field produced by

permanent magnets. Unfortunately, this software can only generate 2D magnetic models and therefore, the disc magnets would not be accurately modelled, since the direction of their magnetisation was in the plane perpendicular to the software model.

4.2 Particle selection

4.2.1 Comparison by free-flow magnetophoresis

Once the different magnet positions had been characterised, they were used to deflect magnetic particles inside the FFM microchip in order to compare their deflection behaviour and u_{mag} values. The different gradients produced by each of the magnets were used to determine an optimal magnetic field to produce the furthest deflection of magnetic particles. The effect of flow rate on the deflection behaviour of particles at each setting was also investigated.

4.2.1.1 Initial deflection of M-270 magnetic particles

Stock solutions of particles were prepared according to section 3.2.1 and initially, magnets were used to trap the particles in the suspensions into plugs against the side of the Eppendorf tube. The large disc magnet used for mag1 and mag2 set-ups pulled most of the particles to the side of the tube in less than 1 minute. The smaller disc magnet used for mag3 and mag4 pulled most of the particles to the wall in under 2 minutes. This gave initial indications of how the strength of the magnets affected particles over a distance of 1 cm, i.e; diameter of the eppendorf tube, with the largest of the magnets having the greatest effect. The superparamagnetism of the particles was then demonstrated by resuspending the particles by use of a vortex. In the absence of any

field the particles were evenly suspended in the solution, with no visible clumps.

The comparison of deflection behaviour of magnetic particles was performed in the microchip termed FMM (Section 3.5). To visualise the flow inside this device the microchip was set-up according to section 3.5.2 and the buffer inlet was filled with an aqueous blue ink, while red ink was pipetted into the particle inlet. Negative pressure was applied to the outlet at $500 \mu\text{L h}^{-1}$. Figure 4.4 is a photograph of the flow inside the chamber showing the contrast between the flows in the particle inlet against the flow from the buffer inlet.

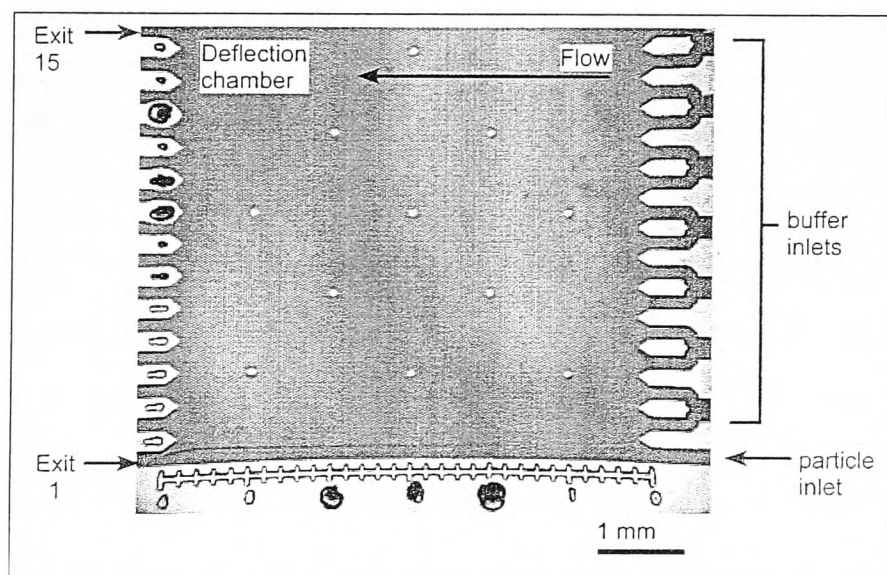


Figure 4.4. Flow inside FFM chip. The buffer reservoir was filled with blue ink while the particle inlet was filled with red ink. Any liquid that entered via the particle inlet flowed through the chamber and left via exit 1, directly opposite. The slight bend in the image was caused by the optics of the observation system.

In microfluidic systems, fluid flow is described as being predominantly laminar, that is

all the fluid molecules are travelling in the same direction and therefore there is no turbulent observed. The flow regime can be calculated by determining the dimensionless Reynolds number, Re , which is described as the ratio of inertial forces over viscous forces;[151, 152]

$$Re = \frac{\textit{inertial}}{\textit{viscous}} = \frac{\rho \cdot r_h \cdot v}{\eta} \quad \text{Equation 27}$$

Where ρ is the density of the fluid, v is the average fluid velocity and η is the fluid viscosity. r_h is the hydraulic diameter, calculated using;

$$r_h = \frac{4A}{U} \quad \text{Equation 28}$$

A is the cross sectional area of the chamber and U is the wetted perimeter. For Reynolds numbers below 2300, flow is predicted to be laminar and for microfluidic systems, the Reynolds number is typically less than 1.[153]

The Reynolds number for the chamber at this flow velocity was calculated to be 9.9×10^{-6} , which is considerably less than 1 and as expected, laminar flow was observed. As a consequence of this, the liquid in the chamber flowed straight through such that the red ink entering the chamber from the particle inlet exited the chamber from the exit channel directly opposite without turbulent mixing with the blue ink. The flow rate was reduced to $50 \mu\text{L h}^{-1}$, the slowest flow rate to be used in the experiments with the same flow observations for which the Reynolds number was calculated to be 9.9×10^{-7} .

Once the flow had been characterised inside the microfluidic device, particle

suspensions were introduced according to the experimental procedure (section 3.5.4). Initial experiments were performed with the Dynabeads M-270. Negative pressure was applied to the outlet and particles could be seen entering the chamber via the particle inlet. In the absence of a magnetic field the particles were observed to exit only via the opposite exit channel, exit 1. This was because particles were under the influence of the hydrodynamic force alone, u_{hyd} , (equation 9, section 2.3.1) and followed the laminar flow. One early observation made was the difference in particle velocities as they travelled through the chamber. Some particles were observed to move more slowly than others. This can be accounted for by the parabolic flow profile associated with hydrodynamic pressure pumping.

When a liquid is pumped under pressure through a channel or tube a gradient in fluid velocity develops with liquid in the centre of the channel flowing faster than the fluid at the edges. Here, fluid interacts with the solid walls and a 'non-slip' boundary develops in which fluid does not flow.[154] In a shallow microchip chamber, this effect is quite pronounced. Hence, flow would be expected to be significantly slower at the top of the chamber and the bottom, than the flow at the centre height within the chamber. In the FFM microchip, the chamber was 20 μm deep and the particles utilised were 2.8 μm in diameter, therefore the particles could occupy different flow velocity streams within the chamber. A particle flowing through the centre of the chamber would be moving in a faster flow stream than a particle flowing along the top or bottom of the chamber (figure 4.5).

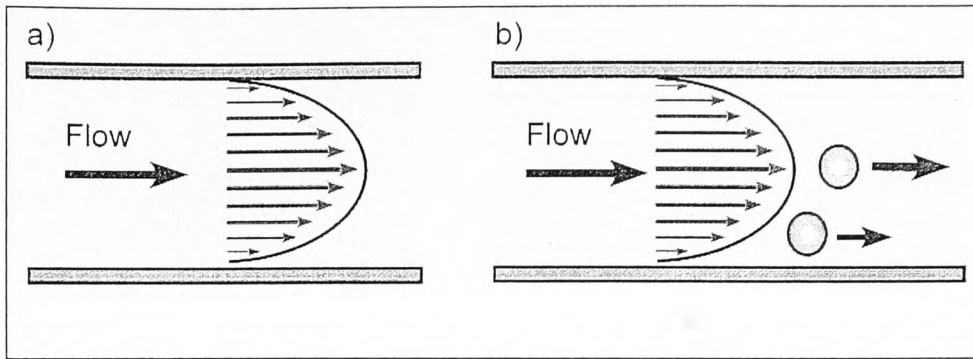


Figure 4.5a) Schematic of the parabolic flow profile. Liquid in the centre of the channel flows at a greater velocity than liquid at the sides of the channel. b) Particles flowing in centre streams will have a greater velocity than particles flowing along the edges of the channel.

The velocity of the flow at various depths in the chamber can be calculated using equation 30, where the velocity of the fluid, v , depends on the distance from the centre height of the chamber, x , the depth of the chamber, d and the length, l . It also depends on the pressure drop in the system, Δp , and the dynamic viscosity of the liquid, η .

$$v = \frac{\Delta p}{4 \cdot l \cdot \eta} \cdot \left[\left(\frac{d}{2} \right)^2 - x^2 \right] \quad \text{Equation 29}$$

The pressure drop, Δp , can be calculated as the product of the flow rate ϕ and the flow resistance, R_ϕ , according to equation 31. Flow resistance in turn can be determined using equation 32, where w is the width of the chamber, l is the length and d is the depth. fRe is the friction coefficient for the shape of the chamber, classed as a narrow slit and can be assumed to be 24 for a narrow slit such as the cross-section of the deflection chamber and δ is the hydrodynamic cross section.[153]

$$\Delta p = \phi \cdot R_\phi \quad \text{Equation 30}$$

$$R\phi = \frac{2 \cdot f \text{Re} l \cdot \eta}{w \cdot d \cdot \delta^2}$$

Equation 31

The hydrodynamic cross section, δ can be calculated by equation 33.

$$\delta = \frac{2 \cdot w \cdot d}{w + d}$$

Equation 32

The flow resistance, $R\phi$, in the chamber at a flow rate of $500 \mu\text{L h}^{-1}$ was calculated to be $1.5 \times 10^{12} \text{ kg m}^{-4} \text{ s}^{-1}$ and the corresponding pressure drop $\Delta p = 212 \text{ Pa}$. Using these values the flow velocity of liquid inside the chamber was calculated, in increments of $2 \mu\text{m}$ from the centre line of the chamber. Figure 4.6 shows the parabolic flow profile of the fluid in the chamber at $500 \mu\text{L h}^{-1}$.

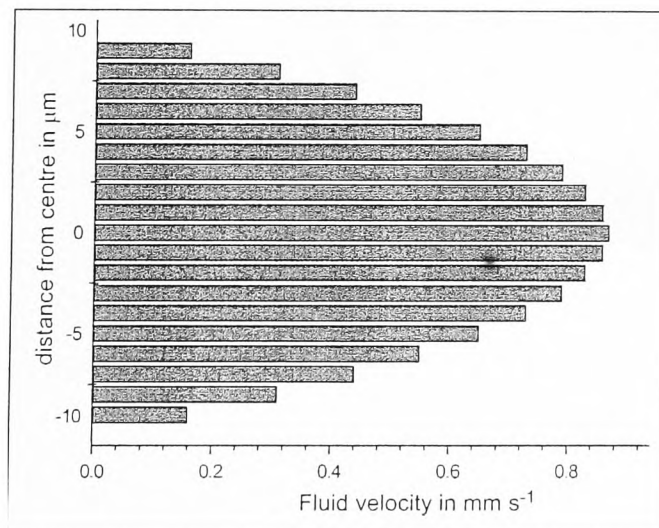
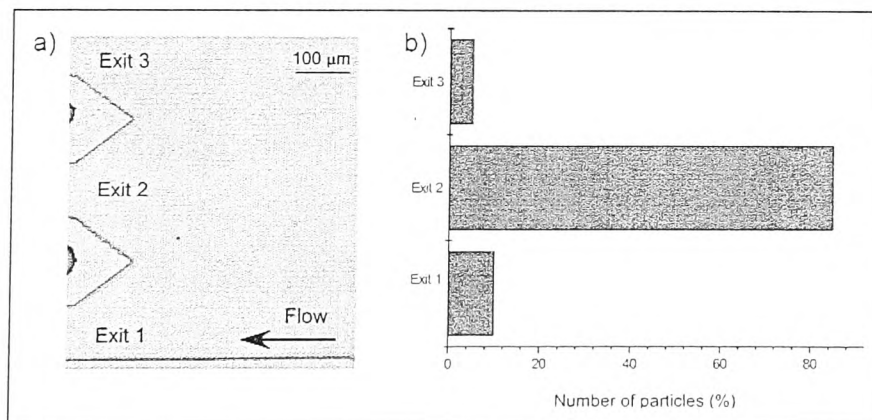


Figure 4.6. Velocity profile of fluid as a function of channel height flowing through the chamber at a volume flow rate of $500 \mu\text{L h}^{-1}$.

In the centre of the chamber the flow velocity was calculated to be 0.87 mm s^{-1} whereas the flow velocity of liquid just $1 \mu\text{m}$ from the chamber roof or floor would be 0.16 mm s^{-1} , a reduction in velocity of nearly 80 %. Therefore a particle occupying a position in the centre of the chamber, would be travelling at five times the speed of a particle at the edge of the chamber. The average flow velocity was calculated to be 0.6 mm s^{-1} which is almost 40 % lower than the applied flow rate on the syringe pump.

For initial deflection experiments, the Mag1 set-up was utilised by placing it on top of the deflection chamber, with its edge tangential with the edge of the chamber on the opposite side to the particle inlet (table 3.5, section 3.5.3). The M-270 particles were pulled into the magnetic field and deflected from flow as far as exit 2 (figure 4.7), a displacement in the y-direction of approximately 150 to $750 \mu\text{m}$. From these initial deflection experiments, two observations were made: 1) particle deflection was not uniform and a ‘spread’ of particles between exit 1, exit 2 and exit 3 was observed; 2) particle agglomerates of two or more were deflected further than single particles.

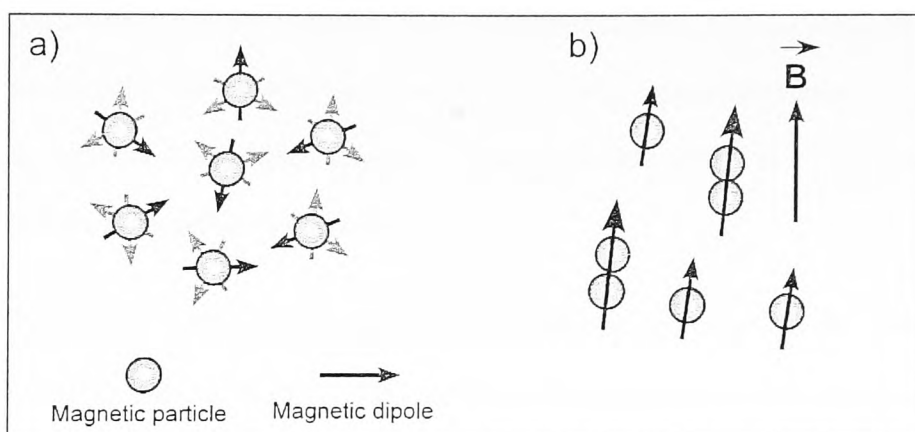


4.7a) Photograph of the exits in the FFM chip with exit 1 being directly opposite the particle inlet.
 b) Distribution of particles exiting the chamber under the influence of the Mag1. The majority of particles left via exit 2.

The spread in particles across more than one exit can be attributed to two factors. The first being the initial position of the particle as it entered the chamber. The particle inlet and the particle stream were 150 μm wide, and so particles would occupy any position within that width. As discussed previously, the magnetic field gradient in the chamber was inhomogeneous and particles at the edge of the stream, closest to the magnet would inevitably experience a larger force from the magnet than particles slightly further away and hence be deflected further. The closer the magnetic particles were pulled towards the magnet, the greater the force exerted on them from the field. Particles entering from the other side of the inlet were further away from the magnet and would experience a lower deflection force, consequently this led to a variation in the magnetically induced velocity, u_{mag} of the particles. In addition, particles moved at different velocities due to the parabolic flow profile as discussed above, which caused variation in the flow vector, u_{hyd} . A particle moving in the central height of the chamber, at 0.87 mm s^{-1} would be influenced by the magnetic field for approximately 6.9 seconds as it passed through the chamber. A particle occupying a stream with a lower fluid velocity, such as $5 \mu\text{m}$ from the chamber roof, would have a velocity of 0.65 mm s^{-1} and would take approximately 9.2 s to pass through the chamber. This particle would therefore be influenced by the magnetic field for a longer period of time and hence be deflected further than a particle with greater velocity. This combination of variation in both flow vectors, u_{mag} and u_{hyd} , resulted in a large variation in u_{defl} and an observed spread of particles across three exits. A way to avoid this effect in future experiments would be to focus particles into a narrow flow stream, both in starting position and depth or to reduce the height of the chamber.

When the magnetic field was applied, some agglomerates of particles were observed. As

a particle enters a magnetic field, the iron oxide nanoparticles in its core become magnetised and a magnetic dipole is created. The presence of the dipole makes the particle act like a tiny bar magnet and when another particle moves within close proximity, the two dipoles align and the particles are attracted to each other, causing agglomeration (figure 4.8)



4.8a) In the absence of a magnetic field the magnetic dipoles of each particle are randomly orientated and there is no net magnetic field. b) In the presence of a magnetic field particle dipoles line up with the field. If two particles are in close proximity, their dipoles will align together causing agglomeration.

In addition to this, when the two dipoles of the particles align together they have a greater magnetic moment, and have a greater attraction to the field produced by the magnet, causing them to be deflected further. To reduce the occurrence of agglomerates it was necessary to keep particle concentrations sufficiently low to avoid close proximity with each other. However, this has to be balanced with an acceptable through-put of particles into the chamber to produce statistically relevant data. The average particle throughput at $500 \mu\text{L h}^{-1}$ for the M-270 Dynabeads at a concentration of 6×10^6 particles mL^{-1} was approximately 10 particles min^{-1} which gave an average

of 50 particles over a five minute experiment.

4.2.1.2 Effect of flow rate

For any given particle at a fixed magnetic set-up, the deflection in the x-direction, u_{def} is affected by the velocity of hydrodynamic flow in the y-direction, u_{hyd} (equation 9). At high flow rates the particles spend less time in the chamber and therefore less time under the influence of the magnetic field. At too high a flow rate u_{hyd} dominates and particles are not deflected whereas at too low flow rates, u_{mag} is dominant which can result in particles being pulled toward the magnet surface where they often became trapped in the field against the chamber sides.

The effect of flow rate was investigated for two different particle types, the Dynabead M-270 particles and the Micromer 6 μm particles, using magnetic set-up 4 (Mag4, table 3.5, section 3.5.3). Figure 4.9 shows the deflection of Micromer 6 μm particles at flow rates between 50 $\mu\text{L h}^{-1}$ and 500 $\mu\text{L h}^{-1}$.

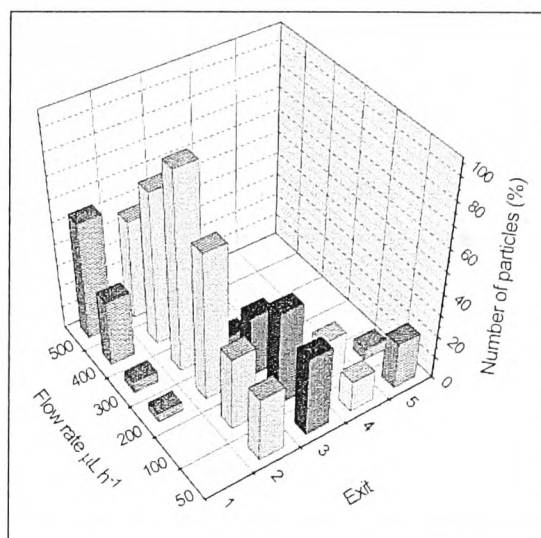


Figure 4.9. Deflection behaviour of Micromer 6 μm particles with varying flow rate.

At $500 \mu\text{L h}^{-1}$, u_{hyd} was relatively high and over half of the particles were not deflected beyond exit 1 and just under half reached exit 2. At this flow rate the particles would only have spent 6 s in the chamber under the influence of the magnetic field. At a flow rate of $400 \mu\text{L h}^{-1}$ more of the particles were deflected to exit 2. At $300 \mu\text{L h}^{-1}$, particles were deflected as far as exit 3, having spent 8.5 s in the chamber. As the flow rate was decreased further, particles were deflected to exits 4 and 5, with none leaving via exit 1. At these lower flow rates, u_{mag} became more prevalent as particles spent longer in the chamber under the influence of the magnetic field. However, at these low flow rates, particles sticking to the sides of the chamber due to the magnetic field became problematic, especially at $50 \mu\text{L h}^{-1}$. In addition, at low flow rates the number of particles entering the chamber per minute decreased due to the reduction in volume of particle suspension being pulled into the chamber. Figure 4.10 shows the particle through-put in a typical experiment, in which particles were counted at each flow rate

for five minutes.

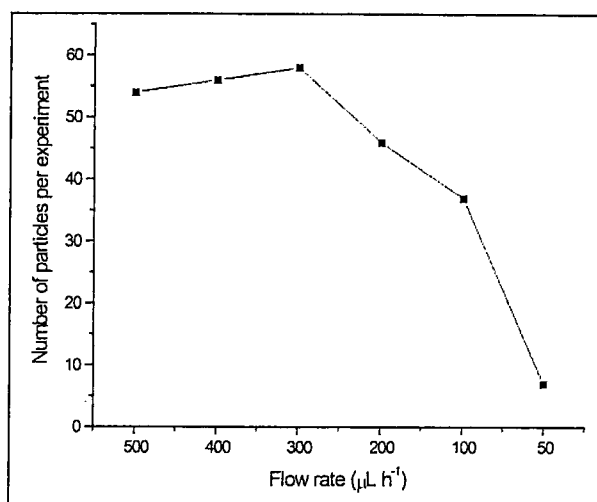
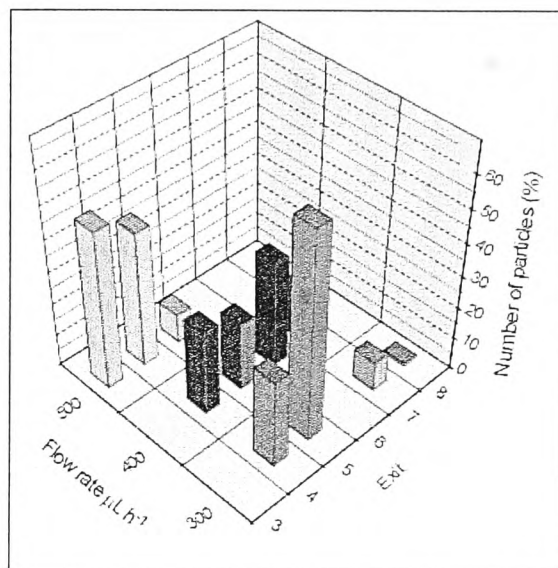


Figure 4.10. Particle through-put in the chip at flow rates between 500 and 50 $\mu\text{L h}^{-1}$.

Each experiment was always started at 500 $\mu\text{L h}^{-1}$ and then the flow rate was decreased and once stabilised, particles were observed at each flow rate for five minutes. Initially particle through-put would increase slightly, which could be explained by the settling of the particles in the reservoir. As they accumulated at the bottom they became more concentrated at the drill hole and more were pulled into the chamber. However, as the flow rate was decreased to 200 $\mu\text{L h}^{-1}$ and below, particle through-put rapidly dropped off, with only 7 particles observed at 50 $\mu\text{L h}^{-1}$. Again, this is undesirable as a high through-put of particles is required to obtain meaningful data, both for the deflection experiments and any subsequent bioanalysis in future experiments. For the Micromer 6 μm particles, the optimum flow rate was 200 $\mu\text{L h}^{-1}$ which gave the best combination of deflection and particle through-put.

Figure 4.11 shows the deflection behaviour of Dynabead M-270 particles with decreasing flow rate.



4.11. Effect of flow rate on the deflection behaviour of Dynabead M-270 particles.

Again, a similar trend was observed, with increasing deflection distance as the flow rate was decreased. Data for 50, 100 and 200 $\mu\text{L h}^{-1}$ was not plotted because almost all of the particles became stuck in the chamber at these flow rates and those that did pass through the entire chamber were agglomerates of two or more particles. An optimum flow rate for maximum deflection of the M270 particles was 300 $\mu\text{L h}^{-1}$, with particles reaching as far as exit 8.

4.2.1.3 Effect of magnetic set-up on particle deflection

Another parameter that affects the force acting on a magnetic particle is the strength and

gradient of the magnetic field (equation 13, section 2.3.1). The four different magnetic set-ups described in section 3.5.3 all produced different flux densities and different gradients at the particle inlet and over the deflection chamber. For example, for a single particle type such as the Compel 8 μm range, at a fixed flow rate of $400 \mu\text{L h}^{-1}$, each magnetic set-up resulted in a different deflection behaviour. Figures 4.12 show particle deflection at magnetic set-ups 1 and 2.

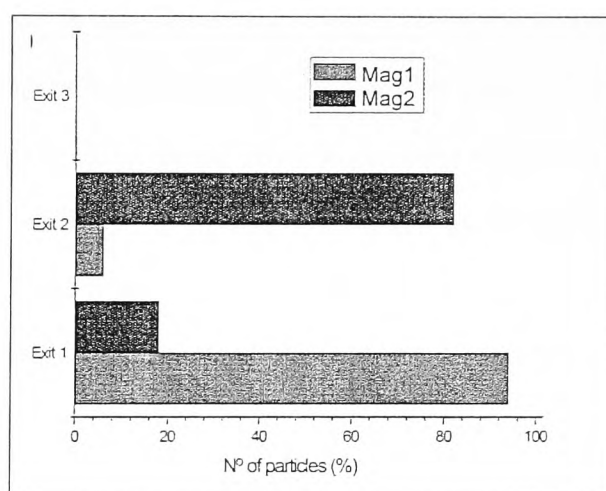


Figure 4.12. Deflection behaviour of Compel 8 μm particles with magnetic set-ups 1 and 2.

In figure 4.12, for magnetic set-ups 1 and 2, the same magnet was utilised. For Mag2 the magnet was placed 3 mm closer to the particle inlet than with Mag1, with respective magnetic flux densities of 41 and 68 mT at the particle inlet. As discussed earlier, the magnetic flux density is higher nearer the surface of the magnet and therefore particles at magnetic set-up 2 were deflected further than at magnetic set-up 1. This clearly shows how the position of the magnet in relation to the chamber can greatly affect the deflection behaviour of the particles. A similar effect was observed with magnetic set-ups 3 and 4, with flux densities of 20 and 41 mT, respectively, with particles generally

being deflected further by Mag4 than for Mag3.

The average force exerted on the particles by the magnetic field gradient can be calculated according to equation 12 (section 2.3.1). The u_{mag} values were calculated from the distance the particle was deflected in the y-direction over the time the particle took to flow through the chamber. For example, the Compel 8 μm particles were travelling at a flow velocity of $400 \mu\text{m s}^{-1}$ and took 6.7 s to cross the deflection chamber. In this time, for magnetic set-up 4, the particles were deflected predominantly to exit 3, corresponding to a distance of 1150 μm . This yields an average u_{mag} value of $172 \mu\text{m s}^{-1}$. It should be noted that for these experiments, calculating the u_{mag} values in this way is an approximation, as videoing equipment was not available at that time, the distance deflected in the y-direction was taken from the centre of the exit the particle took, rather than from a measured value. For example, the maximum force acting on the Compel 8 μm particles by magnetic set-up 4 was estimated to be 14 pN. This magnitude of force, which was estimated to be in the tens of pN for each particle, is in agreement with other free-flow magnetophoresis experiments.[52, 53]

Of the four magnetic set-ups, Mag2 and Mag4 produced the greatest deflection. However, the strength of the magnetic field from the Mag2 set-up often caused particles to become trapped in the chamber, which was not desirable. Mag4 produced good deflection behaviour but also the general through-put of particles in the chamber was not as affected as for Mag2. It was also noted that Mag1 and Mag4 had the same flux density at the particle inlet of 41 mT, however despite this the particles were deflected further at Mag4. This could have been a result of the shape of the magnetic field in the chamber from the curvature of the magnet as the magnetic field is also inhomogeneous

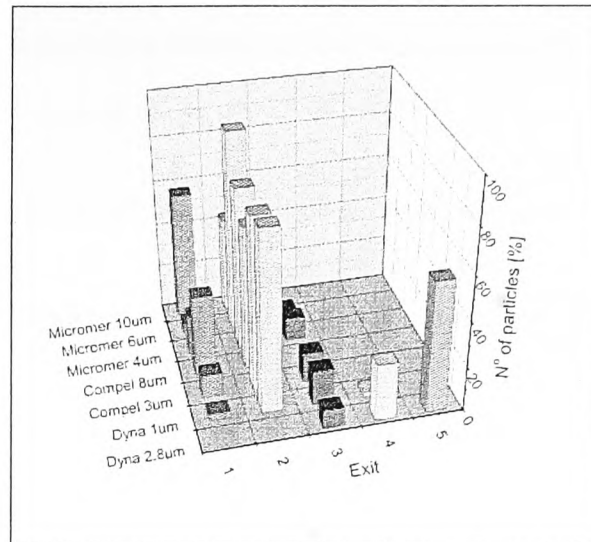
in the x-direction as discussed in section 4.1.

The gravitation force was also calculated for each particle type was calculated according to equation 18 (section 2.3.1) and was found to be in the order of tens of fN. Due to the short time the particles spent in the chamber this downward pull on the particles was found to be negligible.

4.2.1.4 Comparison of different particle types

The force acting on a magnetic particle depends on the magnetic properties of the particle, its volume and the strength and gradient of the magnet field (equation 13, section 2.3.1). If the magnet field is fixed, the force on the particle and therefore its deflection behaviour, will depend on its size and magnetic properties. The eight particles compared in this investigation ranged from 1 μm to 10 μm in diameter and had a range of magnetic properties as described in table 3.4, section 3.2.1.

To compare directly particles of different sizes and particles from different manufacturers it was necessary to keep both the flow rate and the magnetic set-up identical. In this case, only the size of the particle, r and its magnetic properties, M_s were varied. In order to observe the difference in deflection trends between particles, the most optimal conditions for deflection were utilised. In general, magnetic set-up 4 and a flow rate of 300 $\mu\text{L h}^{-1}$ (velocity of 700 $\mu\text{m s}^{-1}$) produced the furthest deflection for each particle type, without extensive particle sticking in the chamber and these conditions were utilised to compare their deflection behaviours. Figure 4.13 shows the deflection trends of each particle type.



4.13. Deflection behaviour of different particle types at magnetic set-up 4 and an applied flow rate of $300 \mu\text{L h}^{-1}$. Data for M-450 particles are missing as they became trapped in the magnetic field and did not exit the chamber.

The Dynabead M-270 particles exhibited the greatest deflection under these conditions, particles were deflected as far as exit 5 with none leaving via exits 1 and 2. The Dynabead MyOne particles were spread across exits 1 to 4, the second furthest deflection. The Compel $3 \mu\text{m}$ particles, Micromer $4 \mu\text{m}$ and $6 \mu\text{m}$ particles all showed similar deflection behaviour, reaching as far as exit 3. The Micromer $10 \mu\text{m}$ particles showed the least deflection, with the majority of particles still exiting via exit 1 and some reaching exit 2. Data for the Dynabead M-450 range are missing from this figure as under these conditions the particles interacted very strongly with the magnetic field. \mathbf{u}_{mag} dominated in this system and the particles were dragged toward the magnet edge and became stuck in the chamber.

Table 3.4 (Section 3.2.1) shows the physical properties of the particles, including the saturation magnetisation, M_s , of the particles calculated from the information provided by the manufacturers. To compare this data to the on-chip observations, values were

divided by the radius of the particle (equation 15, section 2.3.1). Table 4.2 summarises the M_s/r values of the particles.

4-2. Table of M_s/r values calculated from manufacturer's information.

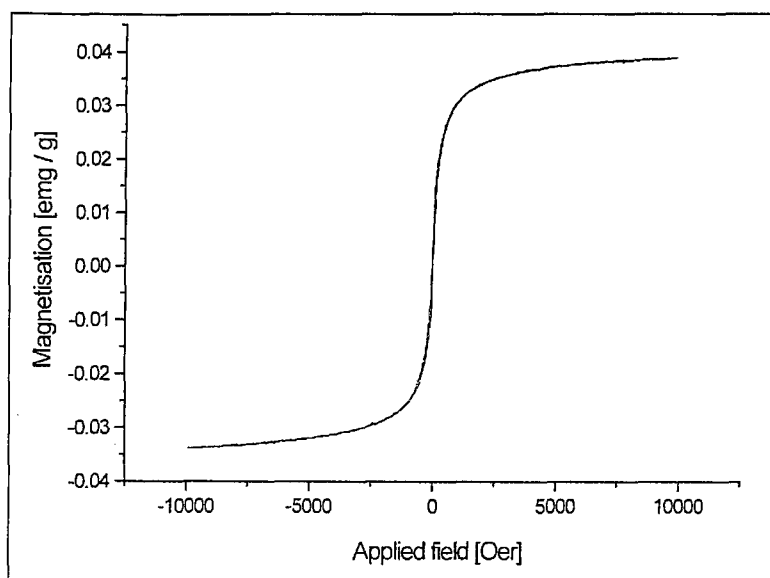
Particle type	M_s/r per particle (A m)
Dynabead MyOne	4×10^{-8}
Dynabead M-270	1.8×10^{-7}
Dynabead M-450	5.8×10^{-7}
Compel 3 μm	1.5×10^{-7}
Compel 8 μm	3×10^{-7}
Micromer 4 μm	6.5×10^{-8}
Micromer 6 μm	1.5×10^{-7}
Micromer 10 μm	4.2×10^{-7}

There is generally a good correlation between the expected deflection from the manufacturers' information and the on-chip observations. The M-450 range from Dynabead has the highest M_s/r and these particles were observed to interact with the magnetic field the most out of all the particle types. However, the deflection behaviour of some of the particles in the FFM experiments was surprising, when considering the magnetic properties of the particles as stated by the manufacturers. For instance, the Micromer 10 μm particles were calculated to have a similar M_s/r value to the M-450

particle, having the second highest M_s/r value of all the particles but were only observed to be deflected as far as exit 2 on-chip, one of the poorest deflection trends. In another example, the Dynabead MyOne particles have the lowest calculated M_s/r value of all the particles, yet on-chip they showed the second furthest deflection behind the M-270 range. To help explain these discrepancies it was necessary to further characterise the particles by measuring their magnetic properties independently of the manufacturers.

4.2.2 Comparison by VSM measurements

Following the unexpected results of the deflection experiments, it was necessary to investigate the magnetic properties of the particles independently. A VSM machine was used to measure the magnetisation vs applied magnetic field, or M/H curve, of the particles, from which the saturation magnetisation of an individual particle could be calculated. The shape of the M/H curve can give a wealth of information regarding the properties of a magnetic material as discussed earlier in section 2.2.3. Figure 4.14 shows a typical hysteresis curve for the Dynabead M-270 particles.



4.14. M/H curve for Dynabead M-270 particles showing anhysteretic characteristics consistent with superparamagnetic properties.

The M/H curve would be described as anhysteretic, meaning there is no hysteresis present in the curve. This indicates that the material is superparamagnetic, as there is no magnetic memory left in the sample when the applied field is reduced to zero. As the field increases the corresponding magnetisation also increases, until a point where all the dipoles in the nanoparticles are aligned and the signal plateaus. As discussed in section 2.2, the particle is described as being at its saturation magnetisation and any further increase in magnetic field has little effect on the magnetisation. The saturation magnetisation per particle can be calculated accurately from the M/H curve using equations 22 (section 3.2.3). If the magnetic field gradient, $gradH$, remains constant then the magnetically induced velocity, u_{mag} , is proportional to the saturation magnetisation, M_s , of the particle over its radius, r . (equation 17, 2.3.1) Table 4.3 summarises the M_s/r values in A m for each particle type.

Table 4-3. Table of M_s/r values calculated from VSM measurements.

Particle type	M_s/r per particle (A m)
Dynabead MyOne	5.2×10^{-8}
Dynabead M-270	1.4×10^{-7}
Dynabead M-450	6.7×10^{-7}
Compel 3 μm	1.2×10^{-7}
Compel 8 μm	1.2×10^{-7}
Micromer 4 μm	1.2×10^{-7}
Micromer 6 μm	1.2×10^{-7}
Micromer 10 μm	5.7×10^{-8}

The VSM data suggests that the Dynabead M-450 have the highest M_s/r radius and should show the largest u_{mag} , whereas the Micromer 10 μm particles have the smallest M_s/r value. However, the M/H plots for larger particles, such as Micromer 10 μm and Compel 8 μm , showed a lot of noise in the magnetisation values at high magnetising field strength and hence the saturation magnetisation results were not as accurate (figure 4.15).

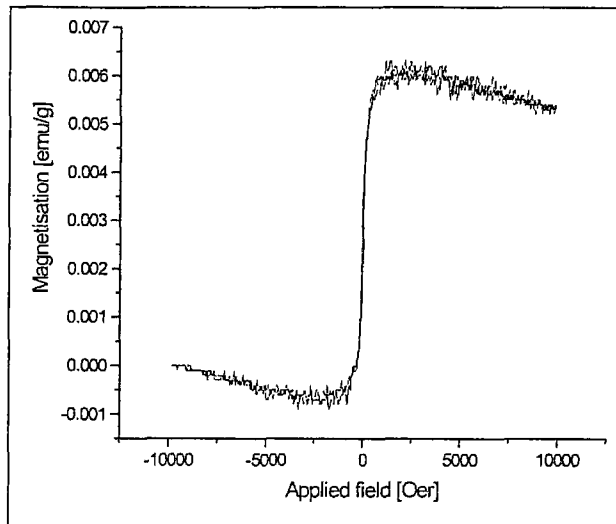


Figure 4.15. M/H curve for Micromer 10 μm particles with noise associated with slight movement of particles in VSM holder.

This could be attributed to the packing of larger particles in the VSM sample tubes. Particles with larger diameters would not pack as closely or tightly as smaller particles and therefore some movement of particles was likely, giving rise to the noise observed. However, each reading was repeated three times and an average of the saturation magnetisation was taken to reduce any variation from the noise.

The measured M_s/r values from the VSM machine correlate well with the manufacturers' data for the Dynabead particles and for the two Compel particles. However, the values differ for the Micromer 4 μm particles and the Micromer 10 μm particles. The Micromer 4 μm particles had a much higher M_s/r value measured by the VSM machine than the value calculated from manufacturers' data. In a similar case, the Micromer 10 μm particles had a much lower M_s/r value than the calculated value. The value measured for the Micromer 10 μm particle, $5.7 \times 10^{-8} \text{ A m}$ was the second lowest value of all the particles.

4.2.3 Comparison of free-flow magnetophoresis and VSM results

To compare the results from the VSM instrument to the deflection behaviour of the particles on-chip, the u_{mag} value for each particle type was calculated. These values are shown in table 4.4 along with their corresponding normalised values, with the normalised VSM results alongside for easy comparison. Both sets of data were normalised with respect to the Dynabead MyOne particles.

Table 4-4. Table showing u_{mag} values for each particle type. u_{mag} values and M_s/r values have been normalised with respect to Dynabead MyOne particles for easy comparison.

Particle	From experiments		From VSM
	$U_{\text{mag}} (\mu\text{m s}^{-1})$	Relative U_{mag}	Relative M_s/r
Dynabead MyOne	59	1	1
Dynabead M-270	214	3.6	2.7
Dynabead M-450	-	-	12.9
Compel 3 μm	56	0.9	2.3
Compel 8 μm	44	0.7	2.3
Micromer 4 μm	44	0.7	2.3
Micromer 6 μm	44	0.7	2.3
Micromer 10 μm	31	0.5	1.1

When comparing the relative u_{mag} and M_s/r values taken from the VSM measurements, a good correlation was observed for different particles from the same manufacturer. For Dynabeads particles, the observed u_{mag} increases with increasing particle diameter. The M-450 had the highest value and the MyOne particles had the lowest. This trend was supported by M_s/r values from the VSM results. The observed u_{mag} values for the Compel and Micromer particles remained similar, despite changes in particle diameter, which is consistent with the magnetisation results. Interestingly, the VSM results for the Micromer 10 μm supported the observed u_{mag} values for this particle type in that they were the deflected the least, which was in contrast to the values obtained from the manufacturer's data. However this was not the case for the MyOne particles. The VSM measurements supported the manufacturer's data in that the MyOne particles had the lowest M_s/r value of all the particles. The M_s/r values for the Compel and Micromer particles from the VSM measurements were two times higher than for the MyOne particles. However, on-chip the MyOne particles had a higher observed u_{mag} than the Compel and Micromer particles. This discrepancy might partially be explained if we consider again the parabolic flow profile. The depth of the chamber was 20 μm and a particle can occupy any position in this depth from the centre to the roof or bottom of the chamber, which shall be referred to as walls. However, the particle can only get as close to the wall by a distance equivalent to its radius (figure 4.16)

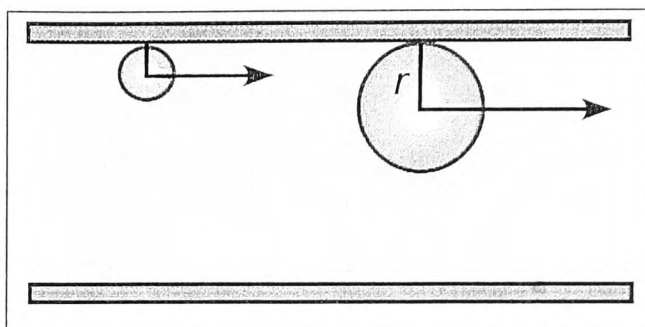


Figure 4.16. The nearest position to the channel wall a particle can occupy is at a distance equivalent to its radius. A smaller particle can occupy a flow stream closer to the channel wall than a larger particle.

Therefore the MyOne particles, with a radius of $0.5 \mu\text{m}$ could occupy a position $0.5 \mu\text{m}$ from the chamber walls whereas larger particles, such as the Micromer $4 \mu\text{m}$ particles, could only approach a position $2 \mu\text{m}$ from the walls. Due to the differences in liquid flow velocity in the parabolic flow profile, some of the MyOne particles would have a lower velocity than the Micromer $4 \mu\text{m}$ particles as they flow closer to the wall, resulting in a larger interaction with the magnetic field and a greater u_{mag} value. This would also account for the spread of MyOne particles across four exits in comparison to other particles, as they could occupy many more different velocity streams in the chamber than larger particles and hence have a variable residence time in the magnetic field. There is unlikely to be diffusion of the particles from one stream line to another as a result of Brownian motion due to the size of the particles. The diffusion coefficient of a spherical particle at low Reynolds numbers can be calculated using the Einstein – Stokes equation:

$$D = \frac{k_b T}{6 \cdot \pi \cdot r \cdot \eta}$$

Equation 33

Where k_b is the Boltzmann's constant ($1.380 \times 10^{-23} \text{ J K}^{-1}$) and T is the temperature in K (298 K). The diffusion coefficient, in $\text{m}^2 \text{ s}^{-1}$ can then be used to calculate the theoretically expected diffusion distance, x over time using equation 34[151].

$$x = \sqrt{2 \cdot D \cdot t}$$

Equation 34

The diffusion distance of a $2.8 \mu\text{m}$ particle due to Brownian motion was calculated for the length of time it is likely to spend in the chamber (approximately 6 s at $500 \mu\text{L h}^{-1}$) and was found to be $1 \mu\text{m}$. This indicates that particles are unlikely to diffuse significantly from one flow stream to another in the chamber due to Brownian motion alone and any movement in the x-direction is likely to be from the gradient of the magnetic field.

4.2.4 Summary of particle selection

In order to select a type of magnetic particle suitable for acting as a mobile solid-support for the proposed continuous-flow bioreactor, a total of eight differently sized magnetic particles from three different manufacturers were compared using the principle of free-flow magnetophoresis. In addition, the deflection behaviour of these particles was also compared at different flow rates and different magnetic arrangements to ascertain an optimal set-up for particle deflection. Discrepancies were observed between on-chip particle performance and what would be expected from the magnetic properties supplied by the manufacturers for certain particle types and hence independent measurements of particle magnetisation were obtained using a VSM

instrument. These measurements correlated well with u_{mag} values calculated from particle deflection for each manufacturer, however discrepancies were observed between particles from different manufacturers.

Overall, the Dynabead M-270 particles were observed to give the most useful deflection, with magnetic set-up 4 and with an applied flow rate of $300 \mu\text{L h}^{-1}$. Under these conditions, the M-270 particles were deflected up to 3 mm inside the deflection chamber.

4.2.5 Discussion

The Dynabead M-270 particles were shown to have the most useful deflection behaviour out of the eight magnetic particle types tested using the principles of free-flow magnetophoresis. The M-270 had the second highest saturation magnetisation of the eight particles, with the M-450 particles having higher still. This would suggest, theoretically, that the M-450 particles would be deflected further than the M-270 particles. However, a balance between the magnetically induced velocity, u_{mag} and the hydrodynamic flow velocity, u_{hyd} , needs to be struck to achieve the best deflection. In the case of the M-450 particles, their strong magnetic properties meant they interacted with the magnetic field so much so that u_{mag} dominated in the system and the particles were easily trapped in the chamber. This was unfavourable for particles which are to be used as a mobile solid-support.

The effect of flow rate on magnetic particle deflection was investigated and an optimal flow rate of $300 \mu\text{L h}^{-1}$ was determined. At higher flow rates particles were deflected less as they had less time to interact with the magnetic field. At lower flow rates particles were deflected further, but the particle through-put was reduced significantly

which in a bioassay, would reduce the number of particles available to obtain statistically relevant data within a reasonable time.

In addition, the magnetic set-up was also varied to achieve an optimal field. Four different magnetic set-ups were investigated; all exerted different magnetic flux densities on the particles as they entered the chip. The magnetic set-up which achieved the best deflection was mag4, with a flux density at the particle inlet of 41 mT. Stronger magnetic arrangements tended to cause agglomeration of particles and sticking within the chamber; whilst weaker fields did not deflect the particles far enough, even at low flow rates.

In general, the FFM chip was a simple and effective way of comparing the magnetic particles with each other. However, it was difficult to perform precise measurements of magnetically induced velocities due to the spread of particles across many exits. This was because of both the width of the particle stream, which caused variation in u_{mag} , and also the height of the particle inside the chamber, causing variation in u_{hyd} . One way to reduce these effects in future experiments would be to reduce the width or focus the particle inlet stream so that more particles started their deflection in the same position in the magnetic field. Experiments using a homogeneous gradient along the length of the chamber in the x-direction could also be investigated to decrease the variation in u_{mag} . In addition, the height of the chamber could also be reduced to lessen the difference in particle velocity for a more uniform u_{hyd} .

The work discussed in this chapter highlights the need for careful consideration when selecting a magnetic particle type for mobile applications. Differences in the magnetite content in relation to size play a hugely important part in on-chip manipulation.

Particles with high magnetite content may not necessarily be the best choice of particle, as shown by the M-450 particles. In addition, larger particles, such as the Micromer 10 μm particles, may not necessarily contain more magnetic material and rather than relying on information provided by the manufacturers an independent characterisation of magnetic properties should be performed.

5 Development of a one-step streptavidin – biotin continuous flow binding assay

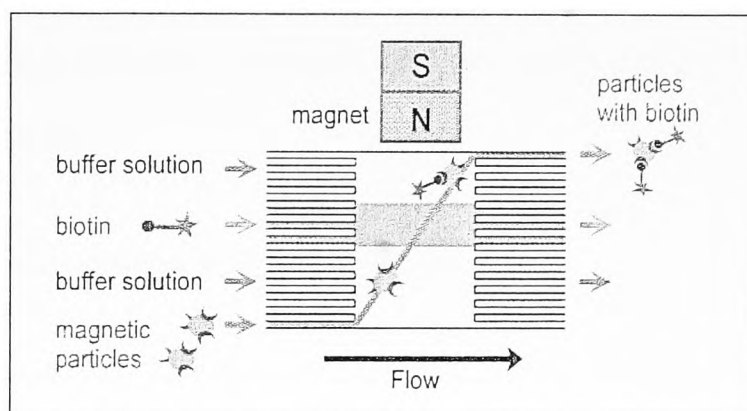


Figure 5.1. Principle of the one step streptavidin - biotin continuous flow bioassay. Magnetic particles, surface functionalised with streptavidin, were continuously deflected across a stream containing fluorescently tagged biotin.

Bioassays such as immunoassays have become integral methods in biological and chemical sensing. Their sensitivity and specificity make them ideal for the detection of analytes in clinical diagnostics, environmental analysis or forensic testing. However, a drawback of using these techniques are the laborious steps frequently associated with each test. These usually involve many washing and reaction steps, often taking several hours, to achieve the final result.

As outlined in the section 1.5, the aim of this project was to design and implement a microfluidic device capable of performing all the steps of a bioassay in one operation in continuous flow. To achieve this, the deflection of magnetic particles across a reaction chamber was required and within chapter 4, the optimisation process of this and the

selection of a suitable particle type is described.

This chapter details an initial proof-of-principle one-step bioassay (figure 5.1). The continuous flow device was developed from an initial concept. In this chapter microdevice interfacing, the generation and characterisation of multi-laminar flow streams, particle deflection optimisation and a one-step streptavidin – biotin binding assay are described.

5.1 Characterisation of flow in MLF1

The MLF1 microchip (Multi-Laminar Flow – 1), detailed in section 3.6 was designed such that four independent laminar flow streams could be generated inside the reaction chamber by utilising four separate fluid inlets. The Reynolds number (equation 26, section 4.2.1.1) for this chamber was calculated to be 4.6×10^{-6} for a typical flow rate of $500 \mu\text{m s}^{-1}$, indicating that fluid flow should be laminar and that the independent streams will flow side by side without turbulent mixing.

Positive pressure

The microchip was interfaced to a syringe pump as detailed in section 3.6.3 and to visualise the flow, alternating streams of blue and yellow aqueous coloured ink were generated (figure 5.2).

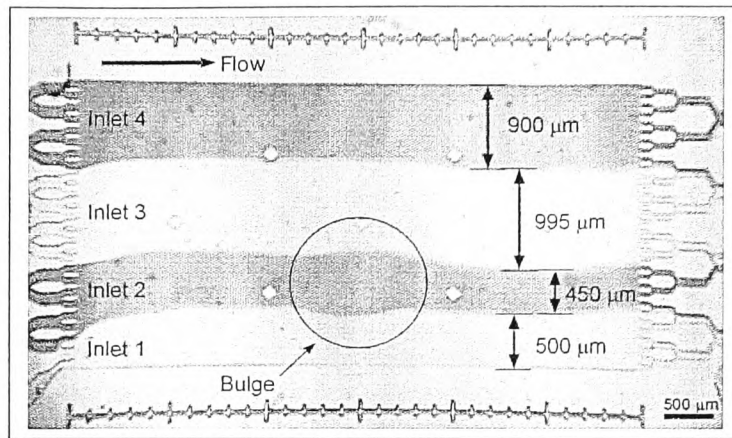


Figure 5.2. Multi-laminar flow streams in MLF1 chip design with alternating streams of blue and yellow ink. The slight bulge in the flow from inlet 2 was a result of uneven etching of the chamber roof.

In the photograph, the four flow streams were stable in the sense that the streams were flowing alongside one another and were not turbulently mixing. These flow streams did not change position, even after several hours of operation. The bulge evident in the photo is due to uneven etching of the roof of the chamber. However, the streams were irregular in width, which was unexpected as an equal flow rate was applied to the four syringes. If the pressure was equal on all four syringes then it would be expected that the width of the streams would be equal inside the chamber. Uneven streams could be attributed to many factors both in the set-up of the system and within the microchip. Firstly, the syringes must be held tightly in the syringe pump brackets, any looseness of a syringe fitting would lead to a lack of pressure in the corresponding inlet. Secondly, all four capillaries had to be the same in length. If for instance, capillary in inlet 2 was shorter by 1 cm than the capillary in inlet 3, this would cause an increase in back pressure, causing resistance to fluid flow and subsequently resulting in uneven flow in

the chamber. The flow resistance, R_{ϕ} , in a tube or pipe can be approximated using equation 32.

$$R_{\phi} = \frac{\Delta p}{v} \quad \text{Equation 35}$$

Where Δp is the pressure drop over the tube and v is the volume flow rate. The pressure drop can be calculated from Poiseuille's equation 33.

$$\Delta P = \frac{8 \cdot \eta \cdot L \cdot v}{\pi \cdot r^4} \quad \text{Equation 36}$$

Where η is the dynamic viscosity, L is the length of the tube, v is the volume flow rate and r the radius of the tube.

For example, a capillary of 6 cm long in inlet 2 would have a flow resistance of $2.4 \times 10^{12} \text{ kg m}^{-4} \text{ s}^{-1}$ where as a longer capillary of 7 cm would have a higher flow resistance of $2.9 \times 10^{12} \text{ kg m}^{-4} \text{ s}^{-1}$. The syringe pump used for the work operated by dispensing a volume flow rate, so the same amount of liquid was always pumped through the capillaries regardless of flow resistance. However, differences in capillary length did create instability in the flow in the chamber and this was sometimes observed as a narrower flow streams. In addition to these factors, a small blockage in the inlet caused by an air bubble or crystals, would have a similar effect by causing back pressure. So in order to achieve even flow streams it was essential that all the access holes in the chip were clean and when interfacing the chip to the syringe pump that all the syringes were securely fixed into position and that the capillaries were all cut to the same length.

Another observation made when the flow streams were generated in the MLF1 chip design was the spread of the fluid leaving inlet 1 (particle inlet) as it entered the chamber (figure 5.3).

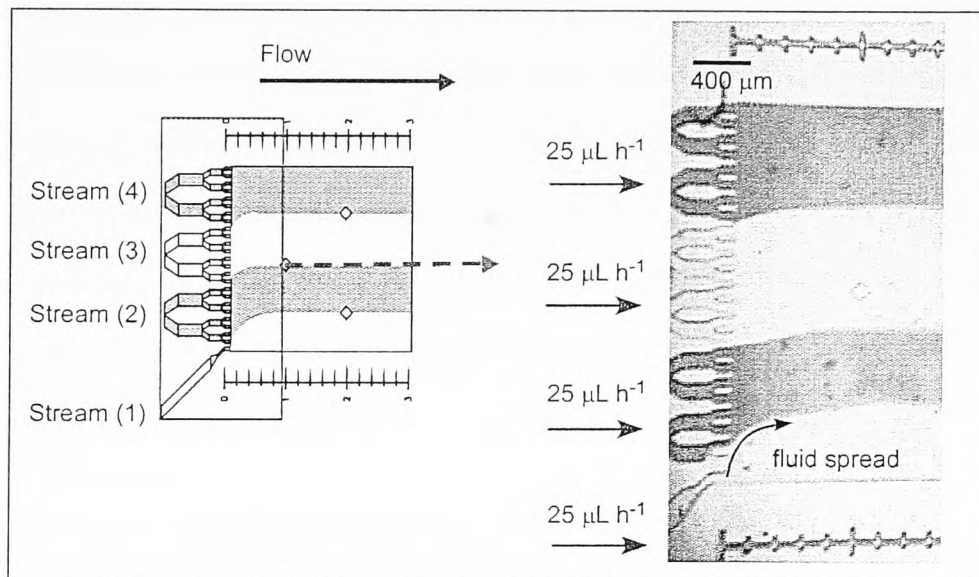


Figure 5.3. The effect of different inlet geometries on fluid flow in the chamber. A higher flow resistance in inlet 1 caused fluid to spread into a wide stream in the chamber.

This again was caused by differences in inlet design and therefore, in difference in flow resistance between inlet 1 and the other three inlets. Inlets 2 to 4 have identical designs and geometries whilst inlet 1 has a much narrower channel width. The syringe pump is programmed to deliver a set volume of liquid to each inlet and therefore the liquid going into inlet 1 had to squeeze down a narrower channel compared to the other three branched inlets, resulting in an increase in fluid velocity. When the liquid reaches the much wider chamber the fluid spreads in order to balance the velocity with the other streams. This effect was not ideal when deflecting magnetic particles since particles

entering the chamber from this inlet could occupy positions across the entire width of the inlet stream. When a magnetic field was applied, particles were deflected from different starting points in the chamber (as discussed in section 4.2.1.1), this was unfavourable for controlling particle trajectories across the width of the chamber. In order to reduce this effect the flow through inlet 1 needed to be reduced so that the pressure drop was similar to that of the other inlets. The Harvard syringe pump did not have the option of altering flow rates between different syringes, so in order to reduce the pressure in inlet 1 a smaller syringe was connected. A 100 μL syringe was available and was used to replace the 1 mL syringe used previously. The 100 μL syringe generated a lower fluid velocity and therefore less spread in the chamber. Figure 5.4 shows the flow through inlet 1 with the 100 μL syringe containing blue ink.

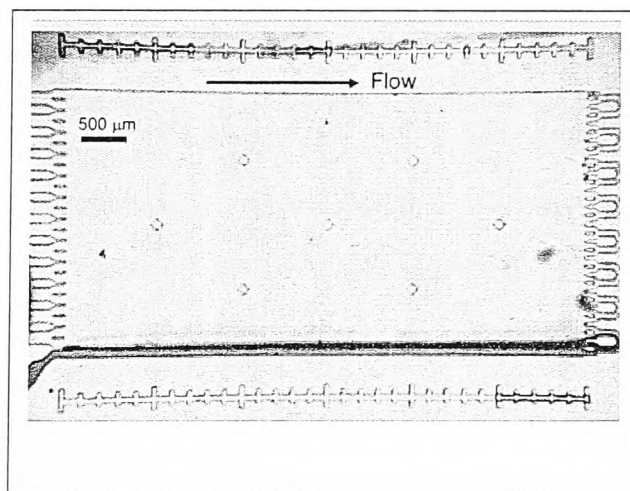


Figure 5.4. Fluid flow from inlet 1 when using a 100 μL syringe.

Whilst this set-up significantly reduced the width of the particle inlet stream to approximately 150 μm in width, it also caused other problems with the stability of the flow inside the chamber. If the 100 μL syringe was being used for the particle inlet in

combination with 1 mL syringes on the other three inlets, the dissimilar flow volumes sometimes resulted in unreliable flow streams in the chamber and liquid from the three wider inlets flowed back down the particle inlet. This was extremely undesirable for the final application of the device as it would cause the magnetic particles in the inlet 1 syringe to be contaminated with the reagent in inlet 3 before entering the chamber. This problem was intrinsic to the microchip design so it was decided to keep a 1 mL syringe on the particle inlet. The very narrow exit channels at the outlet also caused other problems when using the device, such as the build up of crystals at the outlet channels which exaggerated the unreliable flow problems by causing blockages. In addition, air bubbles entering the chamber from the inlets became trapped at the outlets, which in turn caused a build up of air and a disruption to flow.

Negative pressure

The application of negative pressure was also investigated for this chip design in order to overcome some of the problems associated with positive pressure pumping described above. The chip was interfaced as described in section 3.6.3 and negative pressure applied to the outlet at $500 \mu\text{L h}^{-1}$. The access holes in the MLF1 chip design were $370 \mu\text{m}$ in diameter and so smaller pipette tips had to be used than in experiments with the FFM chip. This initially caused problems when trying to fill the pipette tips with liquid as the hydrophobicity of the plastic resulted in trapped air at the very bottom of the pipette and because of their narrow size, this was then difficult to remove. When negative pressure was applied at the outlet, the fluid was pulled into the chip but because of trapped air and subsequently different volume levels, the flow was particularly unstable due to hydrostatic factors. In addition, a large amount of air was

pulled into the chamber, which was difficult to remove under negative pressure conditions. As a result, negative pressure was not used for bioassays in the MLF1 chip design.

5.2 Deflection of M-270 particles

Once the multi-laminar flow had been characterised inside the MLF1 chamber and a set-up optimised for stable multi-laminar flow streams, the deflection of Dynabead M-270 magnetic particles inside the MLF1 chamber was investigated.

Magnetic set-up

In order to act as mobile solid-supports in a continuous flow reactor, the particles must be deflected the full 3 mm width of the reaction chamber so that they pass through each of the reagents streams. Previously, the deflection of M-270 particles was optimised for use with magnetic set-up mag4 at a flow velocity of $700 \mu\text{m s}^{-1}$ (chapter 3). With these settings the particles could be deflected up to 3 mm, which would be adequate for their desired purpose in the MLF1 chip design. However, the choice of magnet had to be changed for this chip design as discussed in the experimental chapter (section 3.6.2). The rectangular magnet employed for the MLF1 chip was both smaller and of different dimensions to the magnet used in mag4, resulting in a different field strength and gradient across the chamber. As a result, the deflection of the M-270 particles was optimised again for the new magnetic set-up by varying the applied flow rate and position of the magnet. Figure 5.5 shows the Femm simulation of the magnetic field produced by the magnet in relation to the MLF1 chamber.

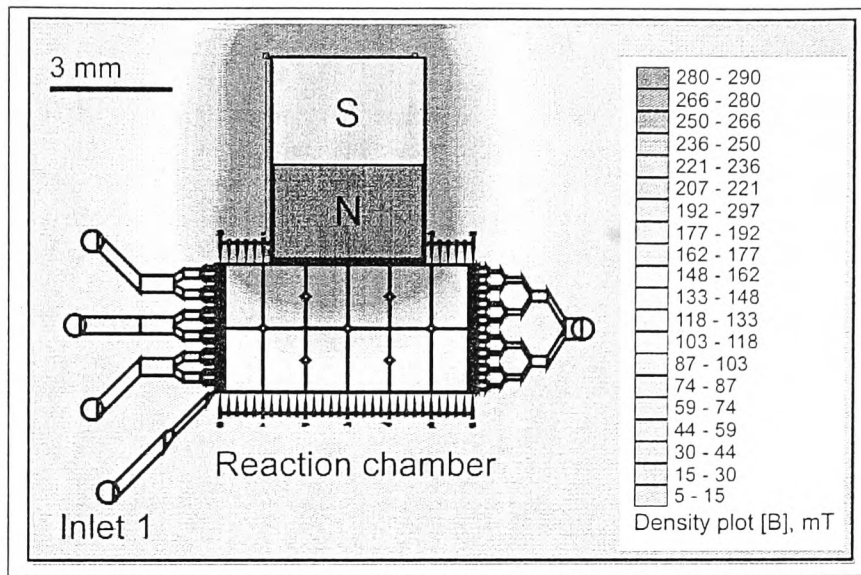


Figure 5.5. Femm simulation of the magnetic field generated by a $5 \times 4 \times 4 \text{ mm}^3$ magnet in relation to the deflection chamber.

The surface magnetic flux density of this magnet was measured to be 320 mT using by the Hall sensor. The magnetic flux density, B_x , of rectangular magnets can be calculated theoretically using equation 34 (www.magnetsales.com).

For a rectangular magnet;

$$B_x = \frac{B_r}{\pi} \cdot \left(\tan^{-1} \frac{AB}{2X\sqrt{4X^2 + A^2 + B^2}} - \tan^{-1} \frac{AB}{2(L+X)\sqrt{4(L+X)^2 + A^2 + B^2}} \right)$$

Equation 37

Where B_r is the residual flux density, L is the length, A and B are the widths and X is the distance from the surface of the magnet. The flux density at the magnet surface was

calculated to be approximately 580 mT and figure 5.6 shows the flux density with increasing distance from the magnet surface. The difference in measured flux density from the Hall sensor and the theoretical calculations could be attributed to the limitations of the Hall sensor, which was reported to saturate at 250 mT by the manufacturers. However, the flux density produced by the magnet, whether calculated or measured, was at several hundred mT, sufficient to exert a strong enough force on the particles to pull them across the entire width of the chamber.

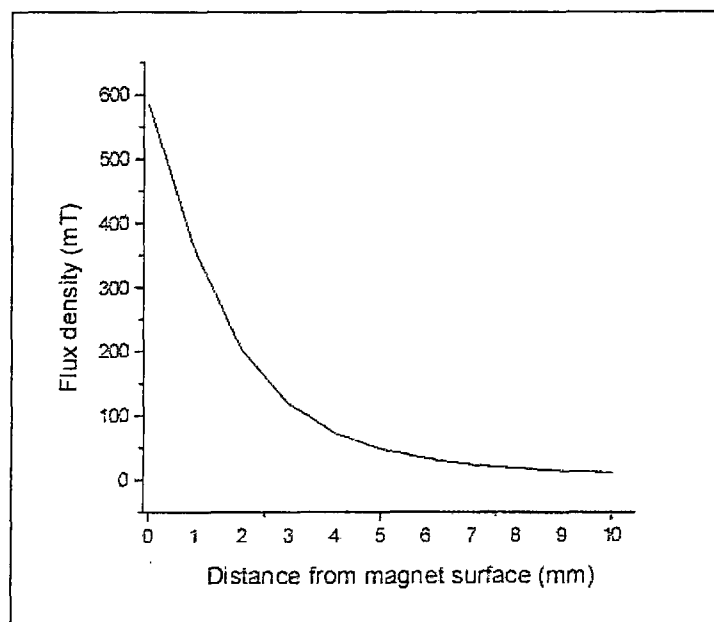


Figure 5.6. Theoretical flux density of rectangular magnet with increasing distance from the magnet surface.

Effect of flow rate on particle deflection in MLF1

Magnetic particles were pumped into the chamber via inlet 1 and the deflection of particles at a range of flow velocities between 370 and 900 $\mu\text{m s}^{-1}$ was investigated. Table 5 summarises the flow velocity, deflection distance achieved and general observations.

Table 5. Summary of M-270 particle deflection at different flow velocities.

Flow rate ($\mu\text{m s}^{-1}$)	Distance deflected in y-direction (mm)	Observations
900	<1.5	Particles moving very fast in x-direction. No deflection observed
830	1.5	Particles moving fast in x-direction. Little to no deflection observed
740	1.9	Small degree of deflection observed
650	2.0 – 2.2	Particle velocity reduced resulting in some deflection
560	2.3 – 2.5	Particle velocity reduced in x-direction, allowing deflection $\frac{3}{4}$ of chamber
460	2.6 – 3.00	Single particles deflected entire width of chamber. Some agglomerates
370	3.0	Particles pulled against chamber wall next to magnet

As discussed in section 4.2.1.2, when the magnetic field is fixed then \mathbf{u}_{mag} remains constant, and the degree of deflection, \mathbf{u}_{def} is influenced only by the flow rate in the x-direction, \mathbf{u}_{hyd} . For higher flow rates, between $740 \mu\text{m s}^{-1}$ and $900 \mu\text{m s}^{-1}$, \mathbf{u}_{hyd} dominated over \mathbf{u}_{mag} and little deflection was observed. At slower flow rates, $560 \mu\text{m s}^{-1}$ to $650 \mu\text{m s}^{-1}$, particles had more time to interact with the magnetic field and \mathbf{u}_{mag} became more influential. Particles at these flow rates were deflected from laminar flow up to 2.5 mm in the y-direction. At a flow velocity of $460 \mu\text{m s}^{-1}$, \mathbf{u}_{mag} and \mathbf{u}_{hyd} were balanced such that the particles were deflected the full 3 mm width of the chamber and exited at the top right hand side. For a flow velocity of $370 \mu\text{m s}^{-1}$, \mathbf{u}_{mag} was much greater than \mathbf{u}_{hyd} . In this situation, particles were pulled against the chamber wall and became stuck, which was undesirable for a continuous flow device. Figure 5.7 shows typical particle trajectories for flow velocities of 900, 460 and $370 \mu\text{m s}^{-1}$.

The force acting on the particles from the magnetic field can be estimated using equation 12, section 2.3.1. However, such a calculation can only be an approximation as each particle occupied a different starting position in the chamber due to the positional spread of the particles in the inlet stream, as discussed in section 4.2.1.1.

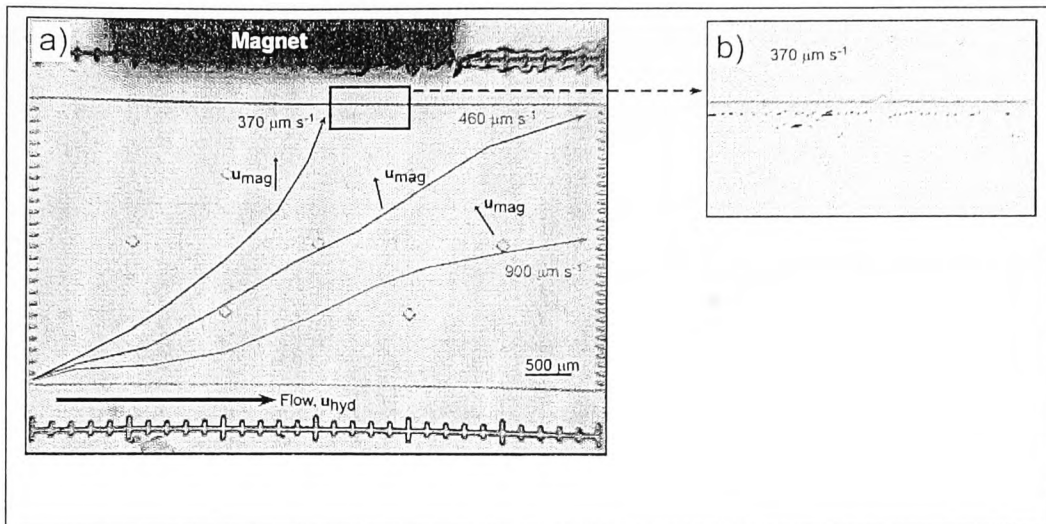


Figure 5.7. a) Particle trajectories at 900, 460 and 370 $\mu\text{m s}^{-1}$. b) At 370 $\mu\text{m s}^{-1}$ u_{mag} dominated and particles were pulled towards the magnet surface and became stuck in the chamber.

At a flow velocity of 460 $\mu\text{m s}^{-1}$ the particles took approximately 60 s to travel from one side of the reaction chamber to the other, giving an average u_{mag} value of 50 $\mu\text{m s}^{-1}$. Using this approximation the force on the magnetic particles can be estimated at around 1.3 pN.

5.3 Streptavidin – biotin binding assay

Once the multi-laminar flow streams inside the chamber and the deflection of the M-270 magnetic particles had been optimised, the system was ready to be applied to a proof-of-principle one-step bioassay. The molecular binding between the protein streptavidin and vitamin biotin has long been used as a model assay for demonstrating early bioanalytical sensors, either as a detection system and or as an affinity system for immobilising other biomolecules to solid-supports.[149] The popularity of the

streptavidin – biotin binding assay can be attributed to several advantages it holds over other molecular recognition systems, such as those involving antibodies.

- 1) Firstly and probably most prominently is the high affinity between streptavidin and biotin. It has been reported as one of the strongest non-covalent bonds known in biology with an affinity constant in the range of $10^{15} \text{ L mol}^{-1}$, which is around 10^5 times greater than that of ligand – antibody interactions.
- 2) Such a high affinity ensures that the streptavidin – biotin complex is largely unaffected by pH, temperature, ionic strength or shear forces, making it a robust binding assay capable of being used in otherwise biologically undesirable environments.
- 3) The binding between streptavidin and biotin is specific so binding only occurs with the target analyte in a detection or affinity system. This is also advantageous as little non-specific binding is observed.

Each streptavidin molecule has four biotin binding sites. However, it should be noted that when using a fluorescently labelled biotin molecule such as the type used in these experiments, and an immobilised streptavidin molecule on a solid-support, that not all four sites are always available for binding. After the initial binding of the first biotin molecule into an available pocket, this is followed by the insertion of the conjugated fluoroscein molecule into a second, resulting in steric hindrance to further biotin insertion and fluorophore quenching.[155]

This section details the suitability of the MLF1 design to performing a streptavidin – biotin binding assay in continuous flow, including optimisation and data analysis. The

applicability of the system to performing quantitative analysis was also investigated in the form of a dose – response curve with respect to biotin concentration.

5.3.1 Initial assay experiments and optimisation

Off-chip streptavidin – biotin binding assay

M-270 magnetic particles coated in streptavidin were purchased and initially the binding between the particles and fluorescently labelled biotin in free solution was investigated off-chip according to the procedure outlined in section 3.6.4. The reaction scheme between streptavidin and biotin is shown in figure 5.8. When mixed together the fluorescently labelled biotin binds to the streptavidin on the surface of the magnetic particle.

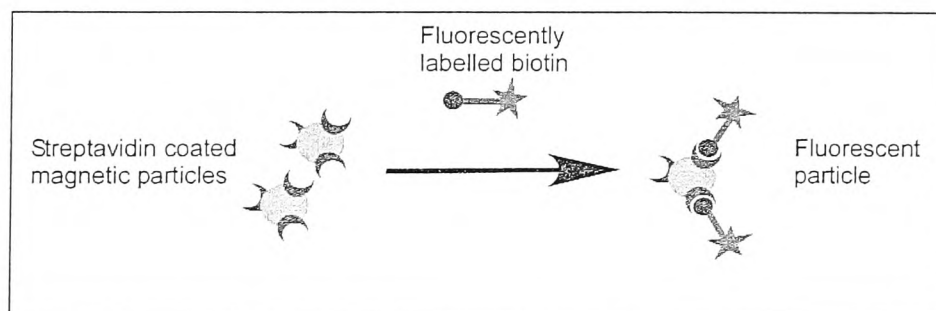


Figure 5.8. Reaction scheme for streptavidin coated magnetic particles and fluorescently labelled biotin in solution.

M-270 particles before the reaction and after were observed on the fluorescence microscope under blue light and compared. After incubation with the fluorescently labelled biotin, the magnetic particles appeared a very bright green in colour which was

easily distinguishable from the unreacted particles. As any unbound biotin had been removed by the three washing steps after the incubation, the fluorescent signal could be attributed to the fluorescent biotin binding to the streptavidin on the surface of the particle.

From suspending the particles in the biotin solution to observing the particles on the microscope, the off-chip procedure involved 11 different manual steps including a 10 minute incubation time. The entire procedure took around 25 minutes to complete.

On-chip streptavidin – biotin binding assay

Once the binding between streptavidin coated particles and fluorescently labelled biotin in free solution was investigated off-chip, the procedure was adapted for an on-chip, continuous flow procedure according to Section 3.6.4. Figure 5.9 shows a CAD schematic of the MLF1 design with reagents in the relevant inlets and a photograph taken of the fluorescent stream of biotin at a concentration of $1 \mu\text{g mL}^{-1}$ at a flow rate of $100 \mu\text{L h}^{-1}$.

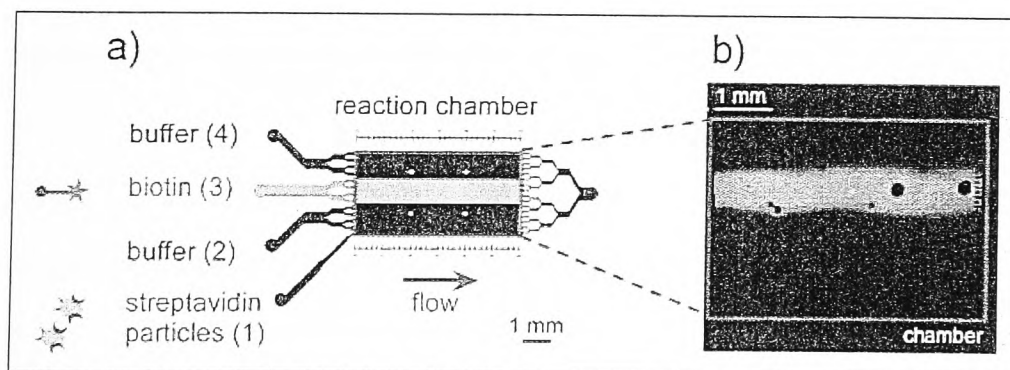


Figure 5.9. a) CAD schematic with streptavidin particles in inlet 1 and fluorescent biotin in inlet 3. b) Photograph of the fluorescent biotin stream at $25 \mu\text{L h}^{-1}$ ($460 \mu\text{m s}^{-1}$).

In this photograph, the stream appears slightly wavy. This effect was caused by the presence of small air bubbles inside the stream which were difficult to remove without upsetting the laminar flow. Small bubbles such as these were allowed to reside in the chamber whereas larger bubbles, that caused disruption to the multi-laminar flow streams, were forced out of the chamber by the application of manual pressure on the syringe rack. The biotin stream in this photograph, at a flow velocity of $460 \mu\text{m s}^{-1}$, was approximately $750 \mu\text{m}$ wide.

Once the flow of biotin had been established and particles were entering the chamber, the magnet was placed on top of the chip. The magnetic particles were deflected from flow but were observed to stick easily in the chamber. Most particles stuck before reaching the biotin stream and none were seen crossing the full chamber. As the conditions in the previous particle deflection optimisation had been identical, except for the streptavidin coating on the particles, the sticking was attributed to the presence of the protein. An online data base (ExpASY Proteomics Server. www.expasy.org) was used to calculate the theoretical pI of the protein from its amino acid sequence. This was done by entering its unique SwissProt protein identity code provided by the manufacturer into the server. Streptavidin has a pI of 7.9 and is generally considered as having a neutral state in physiological conditions (pH 7 – pH 7.5). As PBS is a biological buffer, with a pH of approximately 7.4 we can assume a net neutral charge on the streptavidin molecule. However, the reality of this is not that there is no charge at all on the molecule, but that there is an equal presence of NH_3^+ and COO^- and other charged groups, creating a neutral net charge over the protein and little electrostatic repulsion between particles. The presence of positively charged groups on the protein surface could account for some sticking in the chamber, as they interact with the

negative charge on the glass surface. The magnet lies above the chamber, so to some degree there will be a gradient pulling the particles up against the chamber roof similar to the gradient shown in figure 4.2 (section 4.1). Particles would not only experience a force in the y-direction towards the magnet, but also in the z-direction, which would facilitate the protein – glass interaction (figure 5.10).

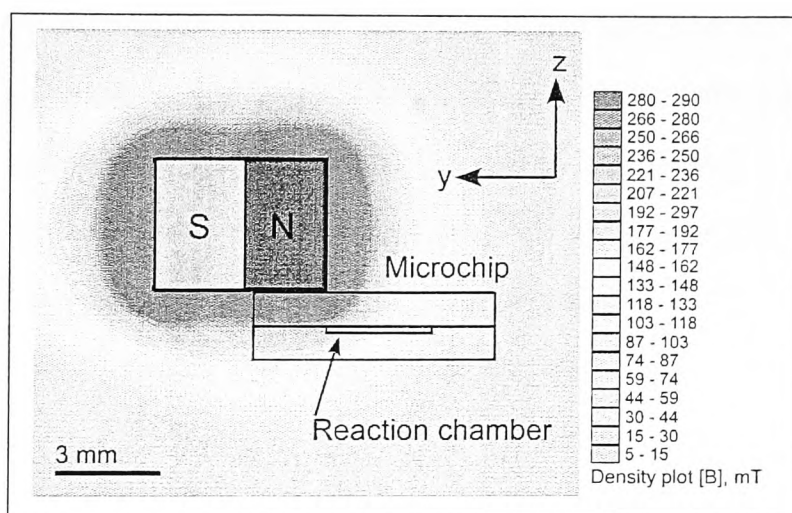


Figure 5.10. Femm simulation of the magnetic field gradient over a cross-sectional view of the microchip.

To reduce this effect, it was necessary to control the charge on the surface of the particles by altering the pH of the buffer. At a higher pH, the presence of negatively charged groups on the protein should dominate. TBE buffer has a higher pH than PBS, at pH 8.4 and is used primarily with nucleic acids, particularly in electrophoresis as it keeps DNA deprotonated. As the pH of TBE is higher than the pI of streptavidin it was expected to have a similar effect on the protein. Off-chip tests were repeated in TBE and

were successful. On-chip particle deflection experiments were also performed in TBE. Streptavidin particles entered the chip with an average particle through-put of 20 particles mL^{-1} and were successfully deflected the full width of the chamber. Some sticking was still observed, but the addition of 0.01% w/v BSA reduced this further. BSA is usually employed as a blocking agent to reduce non-specific binding between proteins, but it can also reduce protein adhesion to surfaces by dynamically coating the surface and blocking any sites the protein of interest may stick to. The on-chip streptavidin – biotin binding assay was then investigated in TBE buffer with 0.01% w/v BSA present. Particles were deflected from laminar flow and pulled by the magnetic field through the first washing stream, the fluorescently tagged biotin stream and finally into the last washing stream. Figure 5.11 shows images taken from a video with particles before, during and after passing through the biotin stream.

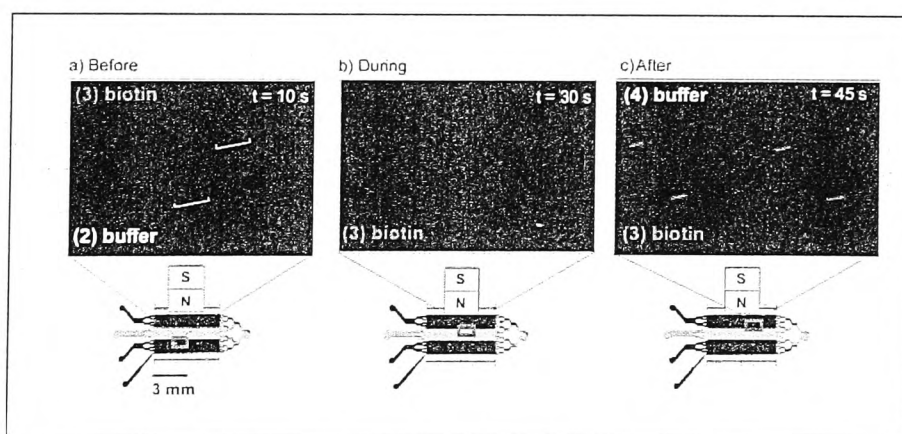


Figure 5.11. a) Particle traces before entering the biotin stream. b) particle traces as they are pulled through the biotin stream. c) Particle traces once they have passed out of the biotin stream and into the final washing stream. The particles appear as streaks due to the low frame rate of the camera.

Before entering the biotin stream the particles exhibited a slight background fluorescence, which appeared as a dull orange colour (figure 5.11a). This was probably due to the polystyrene shell of the particles and despite being undesirable for signal to noise ratio factors, it facilitated their tracking under fluorescence conditions. As the particles were pulled into the biotin stream, they began to fluoresce green instantaneously as the biotin bound to the streptavidin on the surface of the particles (figure 5.11b).

The particles were then pulled from the biotin stream into the final washing stream where any unbound biotin could be washed away (figure 5.11c). In this final stream the particles retained their fluorescent signal, indicating that the biotin had successfully formed a complex with the streptavidin as the particles traversed the stream. The residence time of the particles inside the biotin stream was approximately 16 s, which was a huge reduction in the time compared to the 10 minutes required to perform the same procedure in an Eppendorf tube. As the particle traversed the biotin stream, the continuous flow of biotin from inlet 3 delivered the molecules directly to the particle surface, rather than relying on diffusion. In addition, the particle was free-flowing through the reagent stream, ensuring maximum exposure of available streptavidin sites over the entire particle surface to the biotin stream in contrast to an immobilised particle such as one trapped in a plug in a channel, which would have part of its surface interacting with the vessel wall or other particles in the bed.

Negative control

In biological procedures, it is routine to perform negative controls in which the entire procedure is repeated with the omission of a reagent integral to the test, such as the target antigen or in this case, streptavidin on the surface of the particle. This was to confirm that the positive result observed is not a result of non-specific binding between proteins. Another concern is the presence of a potential ‘boundary layer’ of liquid around the particle that may be carried between two adjacent streams. If particles carry a layer of fluorescent biotin into the final washing stream, this could be mistaken for a positive result. A negative test was thus performed to ensure the signal seen from the particles after the biotin stream was not a product of non-specific binding. Uncoated epoxy M-270 particles were deflected across a stream of biotin and their fluorescence intensity before and after were recorded. There was no detectable increase in fluorescence, intensity indicating little or no non-specific binding of biotin to their surface, or movement of a boundary layer.

Analysis of particles using fluorescence microscopy

Once the streptavidin – biotin system had been demonstrated, quantitative analysis of the particles was developed using fluorescence microscopy and image analysis software. Still photographs were taken from videos of the particles and these were imported into *ImageJ* as discussed in section 3.6.5.2. Before analysing the particles in the image it was necessary to omit particle agglomerates from measurements, as the signal produced by agglomerates of two or more particles would cause large variance in quantitative measurements. For qualitative measurements this was not necessary. Under UV conditions particle agglomerates of three or more particles were easily discernible

as they were noticeably brighter and the streaks wider than single particles. However, distinguishing between single and double agglomerate particle streaks was less obvious and after investigating several videos a small difference in the particle trace length of single and double agglomerates was recorded (figure 2.12). Single particle streaks averaged around $14\ \mu\text{m}$ in length using the 20x objective on the microscope. Doublets averaged around $24\ \mu\text{m}$, which made it possible to remove these data sets from the analysis. The length of the fluorescent streaks could be confirmed as single particles or doublets by quickly switching to brightfield.

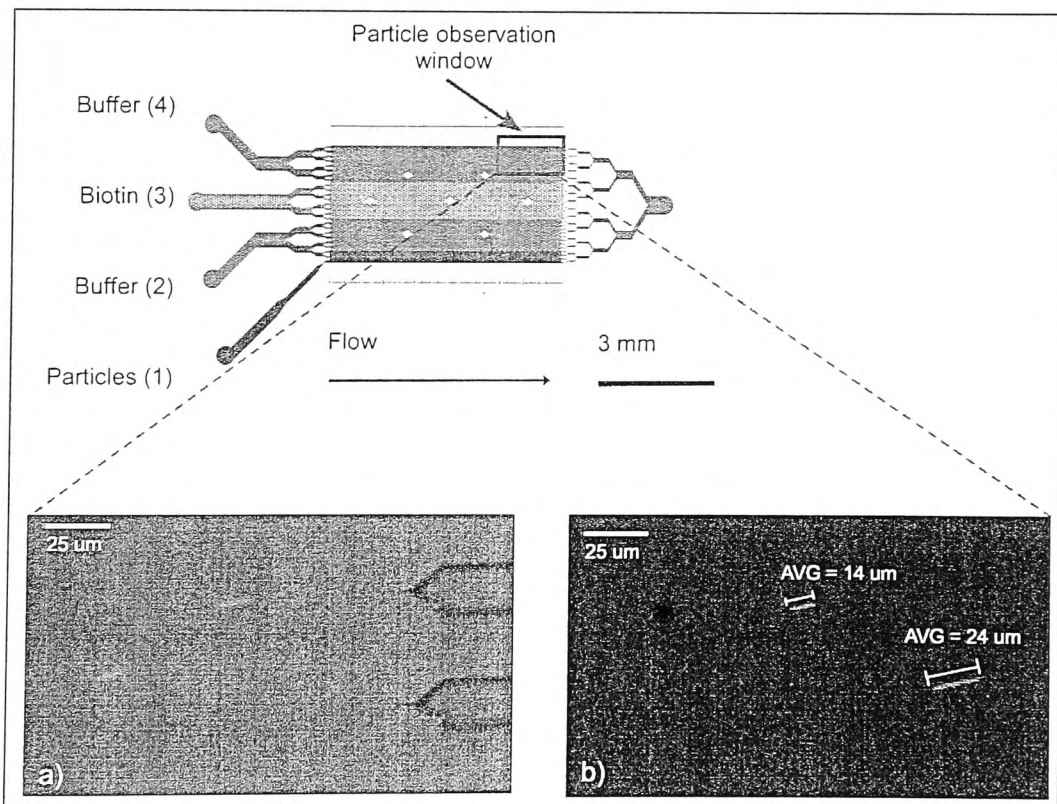


Figure 5.12.a) Particle traces under combined UV and brightlight conditions. b) Measurement of particle traces showed that doublets were on average $24\ \mu\text{m}$ in length and singlets were $14\ \mu\text{m}$.

When taking videos that would later be used for data analysis, care had to be taken at all times to not over-expose the fluorophore to light. Fluorescein is notoriously easy to photobleach, resulting in a significant reduction in fluorescent signal. An investigation into the photobleaching of fluorescein on the surface of the particles was conducted with particles that had been incubated off chip and placed on a microscope slide. Particles were observed under blue light and an immediate measurement taken, then the light source was shut off for five seconds before exposing the particles again and a second measurement taken. The average initial fluorescent signal was 65 a.u. and for the second exposure this was 45 a.u., a signal reduction of 30 %. To help avoid photobleaching, particles entering the area of the chip being videoed were observed first using brightfield, before being quickly changed over to blue light as they passed through the observation window. When the videos were analysed, the fluorescent signal was measured from all the particles within the first few frames of the particle entering the window to avoid loss of signal over longer periods of time.

5.3.2 Effect of biotin concentration

Once the system had been optimised, and the method developed for the magnetic particle detection, the effect of varying the concentration of biotin was investigated.

Limit of detection

In a first investigation, the limit of detection (LOD) of the system was determined by lowering the concentration of biotin until the fluorescent signal from the particles was indistinguishable from the background. For this experimental set-up the LOD was found to be 20 ng mL⁻¹ of free biotin. A concentration of 2 ng mL⁻¹ was attempted but the signal-to-noise ratio between the particles and the background was so low, that the

particles could not be measured with confidence. This LOD for free biotin was comparable with LOD values of other methods. Table 5.6 shows the limit of detection for other streptavidin – biotin binding assays in microfluidic devices.

Table 5-6. Other reported limits of detection for on-chip streptavidin - biotin binding assays.

Solid - support	LOD (M)	Assay time (minutes)	Reference
Single magnetic particles	30 nM	< 1	[141]
Single particles	50 nM	6.7	[49]
Microchannels	1 nM	Not specified	[156]
CD disk microchannels	0.2 μ M	> 60	[157]

However, when considering the procedural time, the continuous flow approach described here had the shortest procedural time and the least manual intervention. In addition, detection of the particles was performed with a basic CCD camera. As discussed in section 3.6.5.1, the Mintron camera had various sensitivities that could be selected and the option of 24x sensitivity was selected which was a good balance between sensitivity and frame rate. However, the sensitivity of the detection system was also limited by the resolution of the camera. At very low levels of light, the particle streaks were very pixelated and not easily distinguishable from the background, and any change in the sensitivity option did not alter this. In addition, the camera's CCD was not cooled, which caused light noise in the images over prolonged use. If we consider the

binding capacity of the particles, which is stated by the manufacturers as 9.7×10^{-18} mol per particle, or 5.8×10^6 molecules of biotin and then the number of molecules each particle may interact with as it passes through the biotin stream, there is potential for the system to detect a significantly lower limit of biotin. The model used for this calculation was very basic, and considered the amount of reagent displaced by the particle as it travelled through the stream over a 16 s period and the diffusion of biotin molecules to the surface of the particle. Liquid displacement occurred in the direction of two axes, the liquid the particle displaces in the y-direction as it travels towards the magnet, V_y , and the displacement of liquid flowing over its surface from the applied flow in the x-direction V_x . The total volume displaced, V_t , is then the sum of these two values.

The volume, V_y , can be calculated from the volume of a cylinder (figure 5.13a) using equation 35, where $(r_1+r_2)^2$ is the cross-section of the radius of the particle plus the radial diffusion distance of the reagent in solution calculated using equation 3.4 ($D_{\text{biotin}} = 3.5 \times 10^{-10} \text{ m}^2 \text{ s}^{-1}$) and l is the width of the biotin stream.

$$V_y = \pi \cdot (r_1 + r_2)^2 \cdot l \quad \text{Equation 38}$$

V_y was calculated to be 8.5×10^{-14} L. The second displacement, V_x , is a result of the amount of time the particle spends in the stream and the applied flow rate. If the particle were stationary in the stream at a flow rate of $25 \mu\text{L h}^{-1}$, it would take 6 ms to displace its own volume in liquid. Therefore in a 16 s residence time, the particle would displace 4.8×10^{-10} L of liquid flowing in the x-direction as it passed through the stream, a total volume displacement, V_t of 4.8×10^{-10} L. At a concentration of 20 ng mL^{-1} the total number of molecules during the particle's passage through the biotin stream at 8.8×10^6

molecules giving a 1:1.5 ratio of available binding sites to number of molecules encountered.

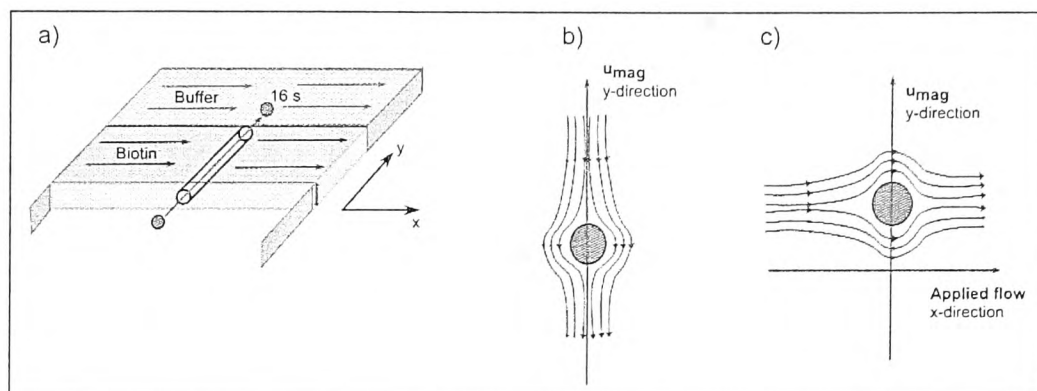


Figure 5.13. a) The particle took 16 s to traverse the biotin stream. b) The particle displaces fluid in the y-direction as it is pulled towards the magnet surface. b) The particle also displaces liquid in the x-direction as flow passes over it.

In reality, it is unlikely that every molecule the particle encountered would bind, however this is a basic calculation and with a more sophisticated camera for detection a lower LOD might be achieved.

Dose – response curve

In biochemical procedures, it is common practice to investigate the detected signal variance (the response) against change in analyte concentration (the dose), known as a dose-response curve.

Molecular recognition assays, such as immunoassays, are often categorised into four

common formats: homogeneous or heterogeneous, and competitive or non-competitive. For the streptavidin – biotin assay described here, it would be categorised as a heterogeneous, non-competitive assay with the streptavidin being the immobilised antigen on the surface of the particle and the biotin being the detector molecule in excess in solution.[148, 158] For this type of assay format, the response of the signal would be expected to increase with increasing concentration of biotin, until all the streptavidin binding sites were occupied on the particle's surface and the dose – response curve would reach saturation. Figure 5.14 shows a typical dose – response curve for a non-competitive immunoassay.

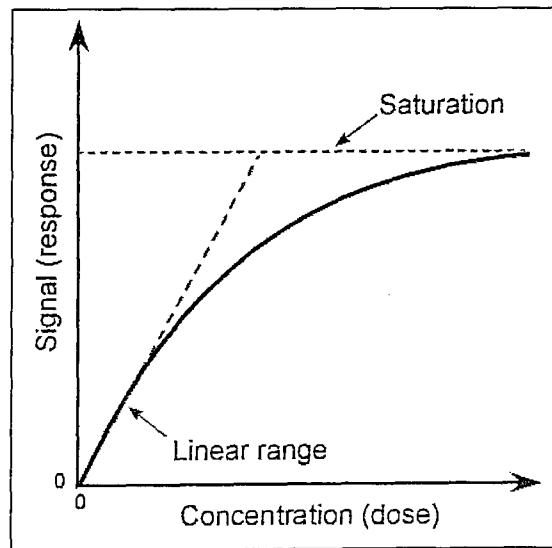


Figure 5.14. Typical dose - response curve for a non-competitive molecular binding assay.

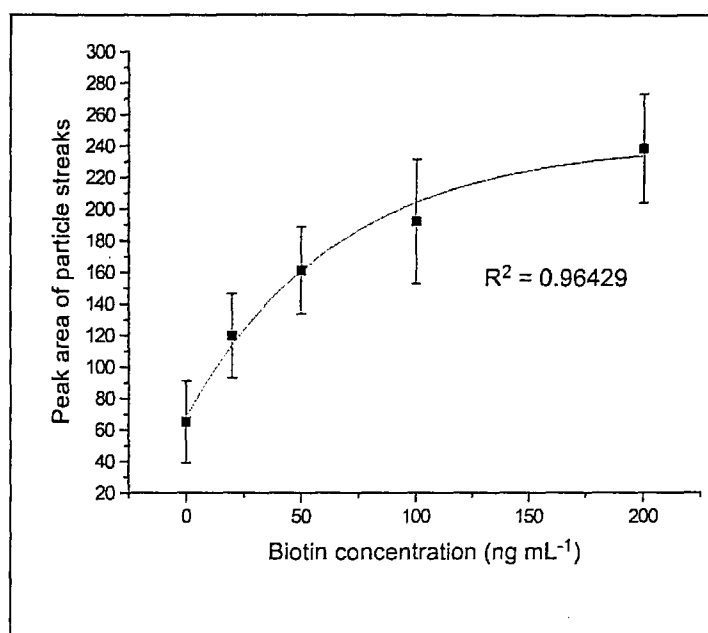


Figure 5.15. Dose - response curve for the peak area of the particle streaks (response) at varying concentrations of biotin (dose). A sigmoidal curve has been fitted to the data. The error bars represent +/- the standard deviation of the measurements.

Particles were analysed at the LOD concentration of 20 ng mL⁻¹ of biotin in free solution. The concentration of biotin was then increased in steps up to 200 ng mL⁻¹. Figure 5.15 shows the response of 16 particle streak areas against biotin concentration, with 0 ng mL⁻¹ being the particles before entering the biotin stream. A sigmoidal curve was fitted to the data with an R² value of 0.96429. The shape of the curve corresponds well to the expected trend of a non-competitive molecular recognition assay. At low concentrations not all the binding sites were occupied on the particle surface and the peak area was small. As the concentration increased, between 20 and 100 ng mL⁻¹, the signal also increased as more biotin became bound. At concentrations above 100 ng mL⁻¹ the particles became saturated. At this point no more biotin could bind to the particles and the signal reached a plateau.

A notable point from the dose – response curve is the relatively large error at each data point. This variance in fluorescence signal and subsequent peak areas could be attributed to several factors including 1) differences in particle velocities, 2) sticking of particles in the biotin stream and 3) focal plane of the microscope.

As described in section 4.2.1.1, under hydrodynamic pressure pumping, liquid adopts a parabolic flow profile. A 2.8 μm diameter particle in a 20 μm deep chamber could potentially occupy several different positions in that depth, each with its own flow velocity. As the particles were pulled through the biotin stream they would not all have had the same velocity, so there would have been a variance in biotin stream residence time. Even if this difference was only a fraction of a second, the particles would still have been exposed to a different number of biotin molecules. In addition, not all M-270 particles were pulled through the chamber in free-flow. There were a few particles that stuck momentarily to the chamber walls and again, even when these particles only stuck for a few milliseconds, they would have been exposed to more biotin molecules than, say, particles pulled straight through the biotin stream without sticking.

Another factor affecting the variance in fluorescence signal was the depth of the chamber. As mentioned above, a 2.8 μm particle could occupy numerous depths in a 20 μm deep chamber and because of this not all the particles were in the same focal plane of the microscope when videos were taken. This resulted in some particles being slightly blurred and lower in fluorescence intensity than a particle that was sharply in focus. During data analysis it was not possible to distinguish between these subtle differences in focal depth by eye and so all the data was included in statistical calculations.

5.3.3 Summary and discussion of the one-step bioassay

To summarise, it was shown, that a continuous flow reactor combining multi-laminar flow streams and magnetic particles as mobile solid-supports can be employed to perform the multiple steps required for performing bioassays in a single operation in one area of a microfluidic device. The device was developed from scratch, which included the interfacing of the microchip, characterisation of the flow, optimisation of magnetic particle deflection and then application to a one-step molecular recognition assay. A streptavidin – biotin binding assay was used as a proof-of-principle assay and an LOD of 20 ng mL^{-1} was achieved with an incubation time of 16 s in the biotin stream, and an overall procedure time of less than 1 min. A dose – response curve was also determined for concentrations between 20 ng mL^{-1} and 200 ng mL^{-1} of free biotin and found to fit the trend expected for a non-competitive binding assay.

The continuous flow microfluidic reactor developed in this work has been shown to be capable of performing single – step molecular recognition assays in less than 1 min without any manual intervention. While the achieved sensitivity did not improve on current on-chip streptavidin – biotin sensitivities, it was comparable and more notably, it was performed within a fraction of the time. The sensitivity of the system was limited by the quality of the CCD camera used, which did not have sufficient resolution at low light levels and was prone to heating, which gave rise to higher noise levels. In order to improve the sensitivity a higher resolution, cooled CCD would need to be employed in which particle streaks would appear sharper and with less background noise.

Another area for improvement would be the variation in fluorescence signals between particles in a single run. One way would be to narrow the particle inlet stream without

reducing the pressure. This could be achieved by improving the microchip design by incorporating a flow focussing design to inlet 1 to focus particles against the chamber wall as they enter. In doing this the particles would start deflection from a similar position in the chamber and be subjected to a more uniform u_{mag} and therefore biotin residence time. To reduce variance from focal depth, a confocal microscope could be employed so that the signal from each particle would be analysed in focus, and any out of focus signal would not be detected.

Once the one – step proof – of – principle assay had been performed and optimised, the next step was to move onto an assay format that was more likely to be used in a real clinical diagnostics situation. Sandwich immunoassays are a common technique for detecting target antigens and a two – step binding assay was investigated next. This included a new chip design to incorporate an extra reaction step and an examination of the diffusion of molecules inside the device.

6 Two – step sandwich immunoassay

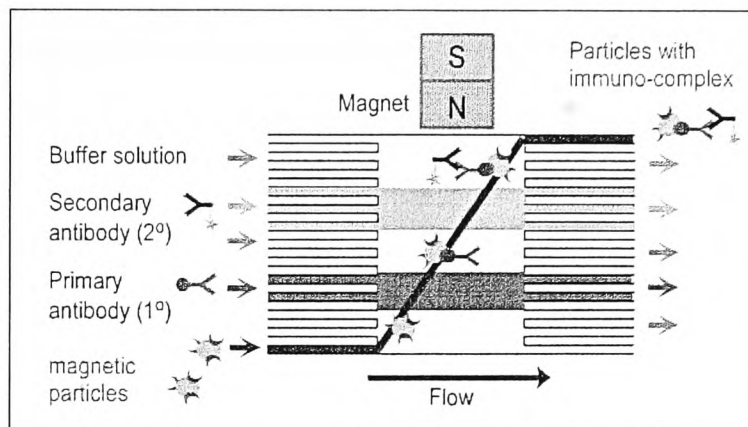


Figure 6.1. Principle of the two-step sandwich immunoassay. Functionalised particles are deflected through a stream containing the target antigen, washing buffer, a stream fluorescently labelled secondary antibody and a final washing stream.

In the previous chapter, a proof-of-principle streptavidin – biotin binding assay was used to demonstrate the use of magnetic particles as mobile solid-supports in a continuous flow microfluidic reactor. The one-step binding assay showed the system was capable of performing such procedures in reduced time scales and with a sensitivity comparable to other on-chip methods for a streptavidin – biotin binding assay.

As discussed in the previous chapter, the streptavidin – biotin binding assay is a popular procedure for proof-of-principle experiments because of its specificity combined with its high affinity constant. Biotin is a small molecule ($RMM = 244 \text{ g mol}^{-1}$) and binding kinetics are quick, making it an ideal example assay for newly developed systems.

However, most biochemical procedures are not as simple nor are the kinetics as quick as the streptavidin – biotin binding assay and to really test the system's applicability to

bioanalysis, a more relevant type of assay needed to be investigated. Commonly, bioassays such as those used in clinical diagnostics, require more than one binding step. An example is the sandwich immunoassay, which in its most basic form usually requires the binding of a primary antibody (1^o) to an antigen followed by the binding of a secondary (2^o) antibody, known as the tracer to label the presence of the antigen. Each binding step requiring several washing steps to remove unbound biomolecules. In addition, biomolecules such as antibodies are relatively large molecules, usually tens of kDa in size. Inevitably, their kinetics are slower and more complex, and often feature lower affinity constants, usually between 10^6 and 10^{12} L mol⁻¹(www.biocore.com), much lower than that of streptavidin – biotin. Therefore, to really test the system's applicability to the type of assay commonly used in laboratories, a sandwich immunoassay with two binding steps involving immune-recognition between complementary antibodies was chosen (figure 6.1).

In this chapter, the development of a device capable of performing two binding steps and two washing steps, including flow characterisation, an investigation into diffusion inside the reaction chamber and finally its applicability to two different sandwich immunoassays, is described.

6.1 Characterisation of flow in the chip design MLF2 (Multi-Laminar-Flow-2)

In the previous chapter investigations into a one-step binding assay involving one reagent step and two washing steps were described. In order to carry out a sandwich immunoassay involving two reagent steps and two washing steps, a new microchip was

designed to incorporate the extra step and was named Multi-Laminar Flow 2 (MLF2), as described in section 3.7. Several design considerations were taken into account in light of problems encountered using the MLF1 chip design. Firstly, the access holes were situated much further away from the chamber than in the MLF1 design (Section 2.8.1). The purpose of this was to reduce the effect of the magnetic field on the particles before they entered the chamber and to minimise particle agglomeration and sticking. The width of the inlets and outlets was also increased to help reduce the pressure drop inside the chamber and facilitate the expulsion of bubbles and crystals from the chip.

To characterise the multi-laminar flow streams inside the chamber, alternate streams of red and blue ink were pumped through the chip at $350 \mu\text{m s}^{-1}$. Figure 6.2 shows the ink streams in the MLF2 microchip. It was observed that as the ink streams flowed through the chamber they became uneven in width and the ink coming through inlets 4 and 5 both exited through the particle outlet, as circled in the figure, whilst the ink in 3, 2 and 1 widened and exited through the wide branched exit. This was not ideal as the widening of streams 1, 2 and 3 caused narrowing of the other two streams, particularly stream 5. In an assay experiment this would cause the particles to be exposed to less reagent in stream 4, and leave very little room for the detection window in stream 5.

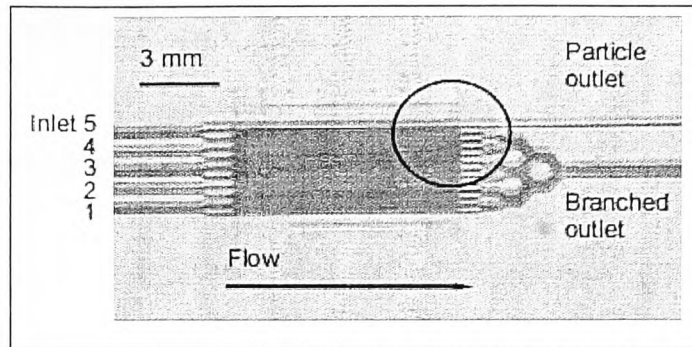


Figure 6.2. Multi-laminar flow streams in MLF2 chip visualised using alternating blue and red ink. Circled area highlights where flow is distorted by flow resistance in capillary outlets.

The reason for this unexpected flow could have been a result of two different factors 1) The chip design, having one large branched outlet and one narrower outlet or 2) The presence of narrow tubing glued into the exit drill holes. In order to test the chip design experimentally, ink was pumped through the device without any exit tubing glued into the drill holes and under these conditions no disruption to flow was observed. This indicated that the uneven flow was due to the capillaries glued into the exit holes. The capillaries had the same internal diameter and had been cut to the same length and so a larger volume of liquid flowing down the wider outlet still had to fit down the same dimensions of tubing as that of the smaller outlet, resulting in a greater flow resistance. In an ideal situation, only liquid flowing through inlet 5 should flow down the narrow particle outlet, and inlets 1 to 4 should flow down the branched outlet. Due to this resistance to flow in the wider outlet capillary, the streams were distorted as seen in figure 6.2. After some experimental investigations it was found that by lengthening the capillary on the narrow exit, and shortening the capillary in the wider exit, the differences in flow resistance could be balanced out so streams would flow evenly

through the device. Optimal lengths for the capillaries were approximately 9 cm for the narrow stream, and 2 cm for the wider exit.

6.2 Diffusion investigations

When performing biochemical procedures such as immunoassays, it is crucial there is no cross-contamination between reagents. For bench top procedures this is usually ensured by repeatedly washing the solid-support after every reagent step with assay buffer to remove any unbound material and to ensure the complete isolation of the target analyte. For on-chip procedures in the MLF2 chip design, these essential washing steps were addressed by having a stream of washing buffer between the two reagent streams and another washing stream after the second reagent stream (figure 6.1). As the particles travelled through the chamber any unbound material from the first and second reagent streams was washed away as the particle passed through the washing streams. However, because all the reagent were together in one area of the chip it was also necessary to consider any cross-contamination that might arise from diffusion mixing between reagent streams. The first washing step separated the two reagent streams from each other. Over time as the molecules travel through the chamber in the x-direction there will be a certain amount of molecular diffusion in the y-direction, as shown in figure 6.3.

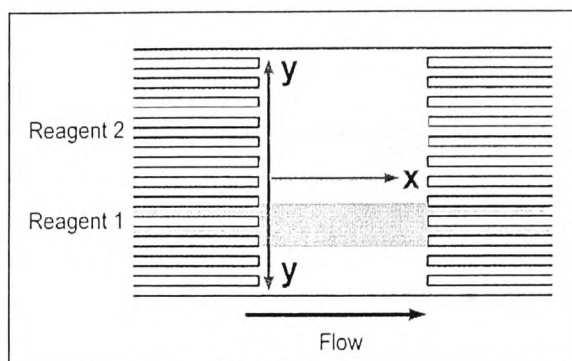


Figure 6.3. As reagents flow through the chamber in the x-direction, there will be molecular diffusion in the y-direction over time.

In order to investigate diffusion within the MLF2 chamber, the inter-diffusion between adjacent streams was visualised by pumping alternating streams of iron (III) sulphate and potassium thiocyanate through the chamber at $350 \mu\text{m s}^{-1}$, a velocity typically employed for assay experiments. Iron (III) sulphate and potassium thiocyanate are both colourless solutions. However, when the two are mixed together the product, iron (IV) thiocyanate, exhibits a very dark red colour which was easily distinguishable by eye.

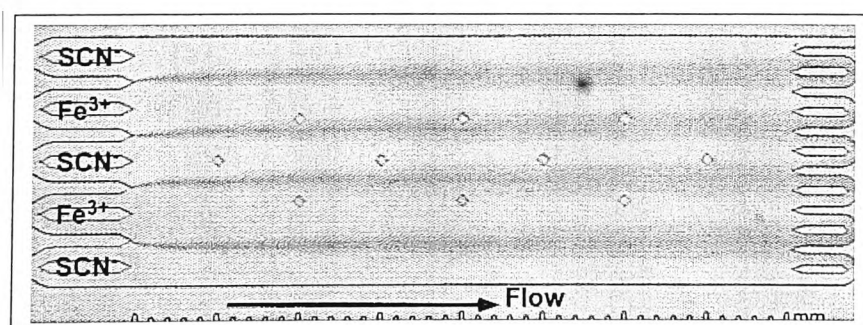
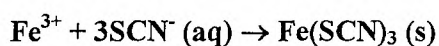


Figure 6.4. Diffusion in the chamber was investigated by pumping alternating streams of iron sulphate and potassium thiocyanate. The formation of the red reaction product, $\text{Fe}(\text{SCN})_3$, enabled visualisation of the diffusion process.

Figure 6.4 shows the diffusion between alternating streams of iron (III) sulphate and potassium thiocyanate at a flow rate of $350 \mu\text{m s}^{-1}$. Mixing between the two streams was observed immediately in the chamber by a narrow band of red at the inlets as the Fe^{3+} and SCN^- ions diffused into each other to form the iron(II) thiocyanate complex. As the reagents flowed through the chamber, over approximately 23 s, this band of red expanded in the y-direction, indicating the diffusion of Fe^{3+} and SCN^- ions during this time. In these experiments, the Fe^{3+} was pumped through inlets 2 and 4 in place of reagents streams, and the SCN^- was pumped through inlets 1, 2 and 5 in place of washing streams. From figure 6.4 it is clear to that reagents diffused into washing stream 3 but there was no mixing between the reagents in streams 2 and 4. The extent of diffusion at the inlets and the outlets of the chamber were determined by using image analysis software (section 3.7.5.1) to measure the greyscale intensity of the image across the width of the chamber. The darker area of diffusion gave lower greyscale intensities than the areas of the colourless, lighter solutions. Greyscale intensities were plotted at two positions, A and B; position A being $600 \mu\text{m}$ downstream from the point of confluence (figure 6.5) and position B being $7800 \mu\text{m}$.

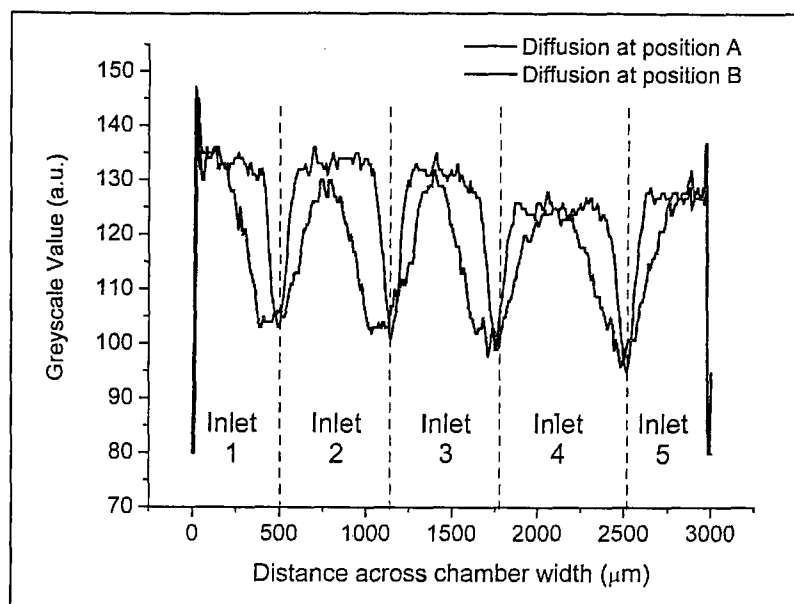


Figure 6.5. The extent of diffusion between adjacent streams was measured using *ImageJ* at position A (black) and position B (red) in the chamber.

A small band of diffusion was already observed at position A, measuring approximately $160\ \mu\text{m}$ in width. At a flow velocity of $350\ \mu\text{m s}^{-1}$ it took approximately 20.6 seconds for the reagents to flow from position A to position B, where the width of diffusion was measured at $500\ \mu\text{m}$. This gave an overall diffusion width over this time of $340\ \mu\text{m}$. The diffusion coefficients of Fe^{3+} and SCN^- ions are, $0.604 \times 10^{-9}\ \text{m}^2\ \text{s}^{-1}$ and $1.758 \times 10^{-9}\ \text{m}^2\ \text{s}^{-1}$, respectively, hence the theoretical diffusion over 20.6 seconds was calculated using equation 34 and found to be $420\ \mu\text{m}$. [159] This correlated reasonably well with the observed results. The discrepancy between theoretical and observed diffusion distances could be attributed to the temperature of the laboratory when the measurements were taken. The laboratory temperature was low, between $20 - 21^\circ\text{C}$, whereas the diffusion coefficients used for the calculation were quoted at room temperature, 25°C . The lower temperature for experimental results would lead to a reduction in kinetic energy of the molecules and an increase in solution viscosity, both of which would result in a lower

diffusivity.

The Fe^{3+} ion, with an RMM of 55.9 g mol^{-1} is a significantly smaller molecule than an antibody, which has a mass of approximately 50 kDa ($50,000 \text{ g mol}^{-1}$) and therefore features a much lower diffusion coefficient, in the order of $10^{-11} \text{ m}^2 \text{ s}^{-1}$ (www.biocore.com). Therefore the diffusion observed for the Fe^{3+} and SCN^- ions is likely to be much less than what the bioreagents in the system would diffuse in reality, hence these experiments showed that reagents in the streams do not mix inside the chamber and that the multi-laminar flow concept is feasible.

6.3 Optimisation of magnetic particle deflection

Having shown that there was no diffusion between reagent streams in the chamber the next step was to optimise the deflection of the magnetic particles. The MLF2 microchip design featured a reaction chamber with the same width as the MLF1 design and was etched to the same depth, therefore having the same cross-section in m^2 . Due to this, initial experiments into the deflection of the M-270 particles were performed at the same flow rate as the MLF1 design, which was $100 \mu\text{L h}^{-1}$ ($460 \mu\text{m s}^{-1}$) in the chamber or $25 \mu\text{L h}^{-1}$ applied flow rate on each syringe. MLF2 has five inlets, so to achieve an overall flow rate in the chamber of $100 \mu\text{L h}^{-1}$, $20 \mu\text{L h}^{-1}$ was applied to each of the five syringes. However, the M-270 particles were not deflected as well at this flow velocity as they were in the MLF1 microchip with some only being deflected as far as 1.5 mm (half the chamber width). The reason for this could have been the multi-port syringe pump; in order to fit five syringes onto the pump a rack that had spaces for ten syringes had to be used which did not have a bracket to hold the syringes down as the four syringe rack. When using ink to visualise the flow it became apparent that the syringes

all had to be held tight in the holder or the pump did not apply pressure to them evenly. When using ink this was easy to spot, but when the system was used for the assay it was much harder to tell if the pressure in the streams was equal. Differences in fluid velocity in each of the streams could explain a difference in deflection behaviour of the particles inside the chamber. It was found by lowering the flow rate to $15 \mu\text{L h}^{-1}$ on each syringe, corresponding to $350 \mu\text{m s}^{-1}$ combined velocity in the chamber, the particles were deflected the full width of the chamber. The degree of particle deflection could differ slightly from day to day, with some particles being dragged towards the magnet surface one day and on another they were deflected towards the particle outlet. Again this could be explained by the slight differences in liquid flow velocity in the streams from uneven pumping and temperature fluctuations. However, it was generally observed at $350 \mu\text{m s}^{-1}$ that the majority of the particles were deflected to the detection window (figure 6.6).

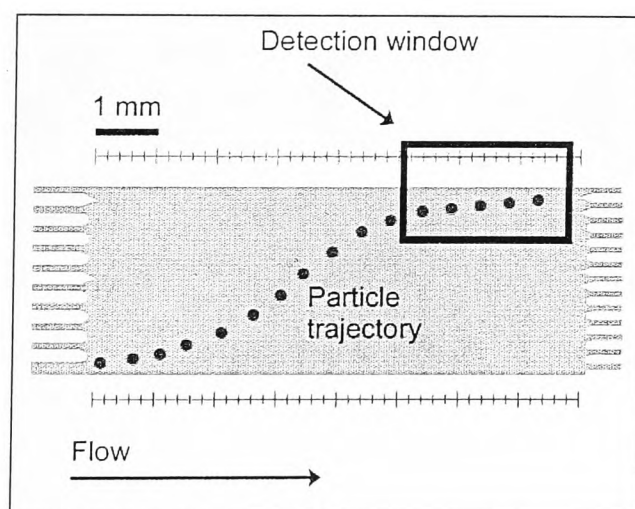


Figure 6.6. Drawing of a typical particle trajectory into the particle detection window.

6.4 Mouse IgG sandwich immunoassay

In chapter 5, a biochemical system involving a single reaction step and two washing steps was discussed. Now a reaction scheme was chosen with two binding steps and two washing steps. One reaction step being the streptavidin – biotin binding step as demonstrated previously and the second being an immune-recognition step between two complimentary antibodies, biotinylated mouse IgG, referred to as the 1^o antibody, and goat anti-mouse IgG tagged with FITC, referred to as the 2^o antibody, as shown in figure 6.7.

In the following section the progression of the multi-flow system on to performing biochemical procedures involving two reaction steps and two washing steps is described.

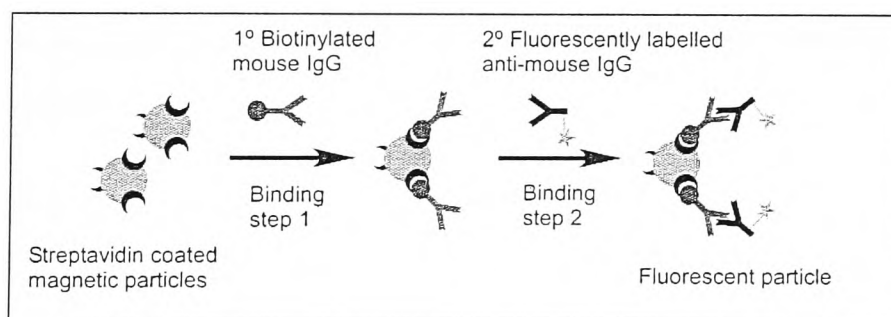


Figure 6.7. Schematic of the two-step mouse IgG immunoassay with streptavidin coated particles and 1^o and 2^o antibodies.

6.4.1 Initial investigations into two-step binding assay

6.4.1.1 Off – chip mouse IgG sandwich immunoassay

Initially, the reagents were tested off-chip firstly in TBE buffer, which had been used previously for the streptavidin – biotin binding assay. However, when the particles were observed under UV conditions after incubation with both 1^o and 2^o antibodies, there appeared no detectable increase in fluorescence signal. The test was still unsuccessful after several repetitions with the TBE buffer, so the buffer was swapped to PBS according to section 3.7.4. The streptavidin coated particles were first incubated with the 1^o antibody. The particles were observed on the microscope slide and no observable fluorescence signal could be seen. The particles were then incubated with the 2^o antibody and when observed again under the microscope they appeared a very bright green in colour. This indicated that the particles would only give off a fluorescence signal after the completion of both steps with successful binding of the 2^o, fluorescently tagged, antibody.

A negative test was also performed in which the first step involving the 1^o antibody was left away so the streptavidin coated particles were incubated with the 2^o antibody alone. Under observation on the microscope the particles did not exhibit any detectable increase in fluorescence signal, indicating a positive signal would only be obtained by the successful binding of the 1^o antibody first. This also suggested little non-specific binding of the antibody to the particle surface.

6.4.1.2 On – chip sandwich immunoassay

Once the biochemical process had been tested off chip, it was adapted for an on-chip

procedure as described in section 3.7.4. Figure 3.26, section 3.7.4 shows the on-chip method, with streptavidin particles introduced through inlet 1, the 1° antibody through inlet 2 and the 2° antibody via inlet 4, with washing buffer via inlets 3 and 5. The initial investigation into the two step immunoassay in continuous flow was performed at reagent dilutions recommended by the manufacturers for ELISA applications, with 1° and 2° antibodies having concentrations of 10 µg mL⁻¹ each.

Particle sticking to glass in PBS

The first problem encountered was somewhat predicated by the change of buffer: the sticking of particles inside the chamber. As discussed earlier, the pH plays an important role in the control of surface charge on the particles. In the chamber, the sticking of particles was most prominent at the interface between a reagent stream and a buffer stream, most notably the edge of the 1° antibody reagent stream. Particles were deflected as far as this point before they began to stick, either being totally immobilised or moving in a stop – start manner. The most obvious explanation was a change in surface charge as the particle was exposed to and coated with 1° antibody molecules. The theoretical pI of the 1° antibody was calculated to be 9.64 using the ExpASY Proteomics Server described in section 5.3.1 and so in PBS, with a pH of 7.4, the antibody molecule was expected to be predominantly positively charged. This would explain the sticking of the particles to the negatively charged surface of the glass chip as the molecules bound to the streptavidin on its surface.

Another interesting observation was that those particles that did pass through the 1° antibody stream did not experience as much sticking towards the opposite side of the chamber. This could again be explained by the surface charge of the particle as the

theoretical pI of the 2^o antibody was much lower at 6.02, which meant it was predominantly negatively charged. Also, as the particle traversed the chamber the gradient of the magnetic field was higher (section 4.1), and therefore more force was exerted on the particle, pulling it more strongly towards the magnet. The effect of the particle sticking was a reduction in the number of particles that successfully crossed the entire reaction chamber and therefore a reduction in statistically relevant data points. However, the sticking of particles was not detrimental to the completion of the bioassay and to maximise the number of particles successfully crossing the chamber, the particle concentration in the syringe was raised from 3×10^6 particles mL⁻¹ to 6×10^6 mL⁻¹. Care had to be taken not to increase the particle concentration too much, as this would facilitate the formation of agglomerates due to particles being closer to each other.

Residence time limitations

Once the particle concentration had been adjusted to increase the number of particles crossing the chamber, videos of the particles were taken. Almost immediately it was noted there was no obvious increase in fluorescence intensity, either by observation down the objective or monitoring the particle streaks by eye in the videos. Particles in the final washing stream (5) appeared a similar colour and intensity as the particles before the reagent streams. However, on analysis with *ImageJ* the particles showed a slight increase in fluorescence intensity after deflection through both reagent streams. Figure 6.8 shows the average particle intensities before and after both reagent streams.

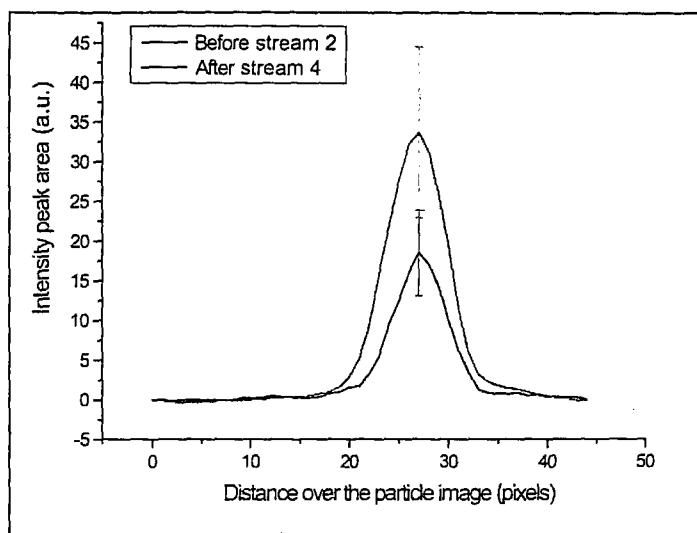


Figure 6.8. Average fluorescence intensity of 15 particles before and after traversing the stream of biotinylated 1° antibody and fluorescently labelled 2° antibody. The concentration of the 1° antibody was 10 $\mu\text{g mL}^{-1}$.

The small increase in fluorescence intensity could be attributed primarily to the short incubation time experienced by the biomolecules inside the reaction chamber. The MLF2 microdevice has a 3 mm wide chamber, the same as the MLF1 design but in the case of the former, there are five inlets feeding the chamber as opposed to four. When equal pressure was applied to the syringes the width of each stream inside the chamber was approximately 600 μm . The only stream visible under the microscope was the stream of fluorescently labelled 2° antibody and particles traversing this stream were timed. The particles took approximately 12 s to cross the 2° antibody stream and as each stream was similar in width, it was assumed the particles would take a similar length of time to traverse the 1° antibody stream. If we consider the first step, involving a

biotinylated antibody, there is already a reduction in the residence time of the particles in the reagent stream in comparison to the 16 s the particles spend in the biotin stream in the one-step assays, which would lead to a decrease in the number of fluorescent molecules being picked up by the particle. However, in addition to this, the binding of biotin to the streptavidin on the surface of the particle was likely to be hindered by the steric effects of being conjugated to such a large protein. The second step in the process involved the immuno-recognition between two complimentary antibodies, a reaction with a lower binding affinity than streptavidin – biotin as discussed earlier. Also, antibodies are likely to have a slower diffusion than biotin and not as many antibody molecules encountered by the particle. These three factors, the residence time, slower kinetics and diffusivity, would result in the significantly lower signal observed in the two-step process. Initially, the exposure time of the camera was set to 500 ms. To try to maximise the signal the exposure time was lengthened to 700 ms. However, by lengthening the exposure time the response of the camera slowed down such that the particles appeared as very long, faint streaks in the videos and were very difficult to see, which made analysis virtually impossible. Therefore an exposure time longer than 500 ms was not ideal.

Another factor that needed to be considered was the effect of photobleaching on the fluorescent tag. When such a low signal was being observed from the two step binding assay, it was necessary to preserve as much of the signal as possible. So far in the experiments the aperture on the microscope, which controls the area of the sample exposed by the excitation light, had been fully opened. Thus the beam of light illuminated around a third of the chamber during the experiments. The CCD on the camera only viewed a small area on the chip through the 20 x objective which resulted

in the particles being exposed to the excitation light before being captured by the CCD camera, giving time for the fluorescent tag to experience some photobleaching before analysis could be performed. The effect of photobleaching on particles incubated with reagents off-chip and unreacted streptavidin particles were investigated. Figure 6.9 shows the fluorescence intensity of the particles before and after a 5 s exposure to the excitation light.

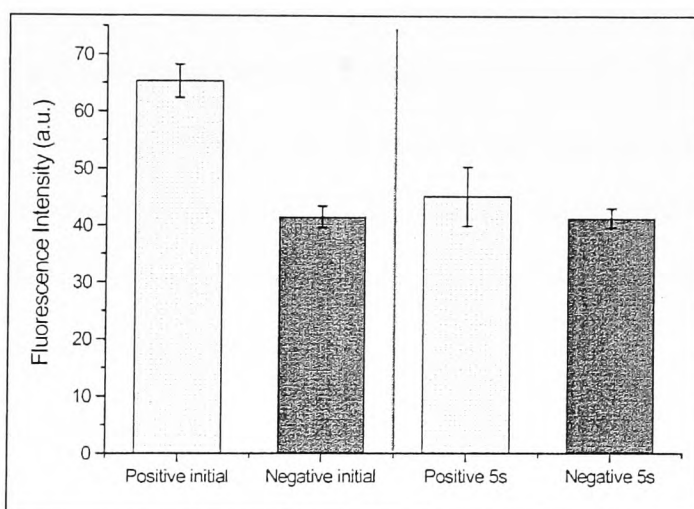


Figure 6.9. Investigation into photobleaching of the particles. The fluorescence intensity of reacted (positive) and unreacted (negative) particles was measured at 0 s and after a 5 s exposure to the excitation light.

Before the 5 s exposure, the fluorescence intensity of the positive particles and the unreacted particles was an average of 65 a.u. and 41.5 a.u., respectively. After exposure to the excitation light for 5 s, by leaving the aperture open, the intensity of the positive particles dropped significantly. However, compared to the unreacted particles, whose signal was not bleached by the excitation light, after 5 s the positive particles gave

almost the same signal as the unreacted particles. Therefore, we can calculate that the loss of signal from bleaching of the fluorophore on positively reacted particles over 5 s was around 84 %. In the case of the on-chip experiments, where low light levels are being observed, loss of this amount of signal before analysis was going to be detrimental to the sensitivity of the system.

In order to reduce the amount of time the particles were spending in the excitation light before being captured on video, the set-up on the microscope had to be changed. The aperture was closed right down until only a small spot of excitation light was visible in the chamber by eye. This was further optimised by focusing the light on the fluorescent stream and narrowing it further such that by observing the intensity on the capture software the diameter of the excitation light was adjusted to within the dimensions of the CCD detection window (figure 6.10).

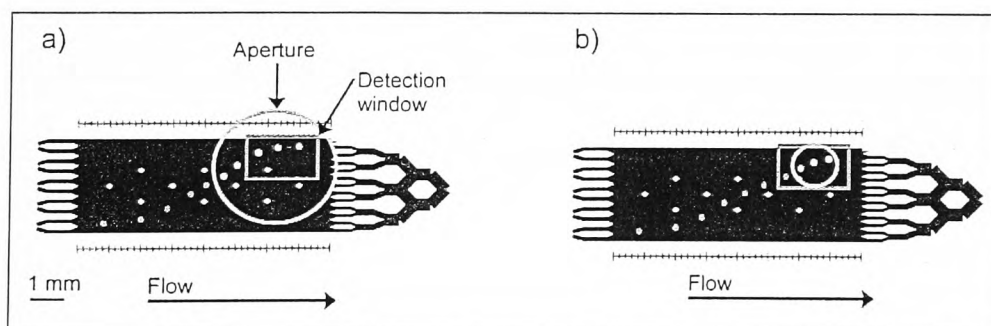


Figure 6.10. Optimisation of the detection set-up. a) With the aperture fully opened the particles were exposed to the excitation light before passing into the detection window. b) By narrowing the aperture to within the dimensions of the detection window the fluorescence intensity was recorded as soon as the particles entered the excitation light and photobleaching was reduced.

By doing this, the particles were not excited by the illumination until they were already being videoed. Therefore, when particles were analysed as soon as they entered the excitation light, the maximum intensity prior to photobleaching was recorded. Using this illumination set-up it was also possible to reduce the exposure time of the camera to 100 ms 340 μ s, which resulted in a faster response from the camera and better particle images for analysis. Figure 6.11 shows the same experiment conducted previously (figure 6.8) with the new illumination set-up. An improvement in the signal and the signal to noise ratio can clearly be seen from the two graphs. The width of the negative peak is wider than that of the positive peak. The particles are videoed before entering the reagent streams as they enter the chamber (figure 3.26, section 3.7.4) and are flowing quickly, giving a long particle trace in the videos. In the second observation window, the positively reacted particles flowed away from the magnet towards the chamber exits and thus experienced a retardation effect from being pulled back towards the magnet, against flow. Due to this the particles are moving more slowly and were observed as a shorter streak in the videos and thus gave a narrower peak. The speed of the particles would affect the intensity recorded from their traces and so the peak area, rather than the height, was used to compare particles before and after the reaction.

On-chip negative control

An on-chip negative control was performed by removing the 1^o antibody stream and replacing it with buffer. Particles were deflected across the chamber under the same conditions as the positive experiments. Figure 6.12 shows the fluorescence intensity of particles before and after crossing the 2^o antibody stream.

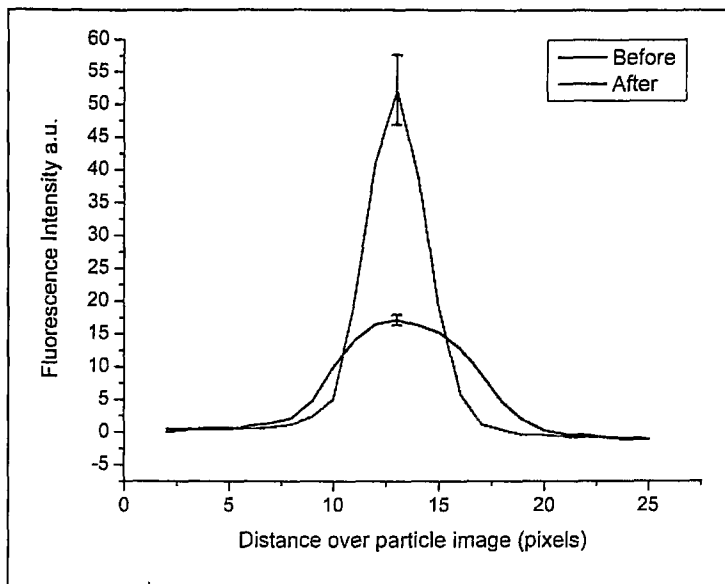


Figure 6.11. Fluorescence intensity of particles before and after traversing the reagent streams after detection optimisation. Concentration of 1° antibody was $10 \mu\text{g mL}^{-1}$.

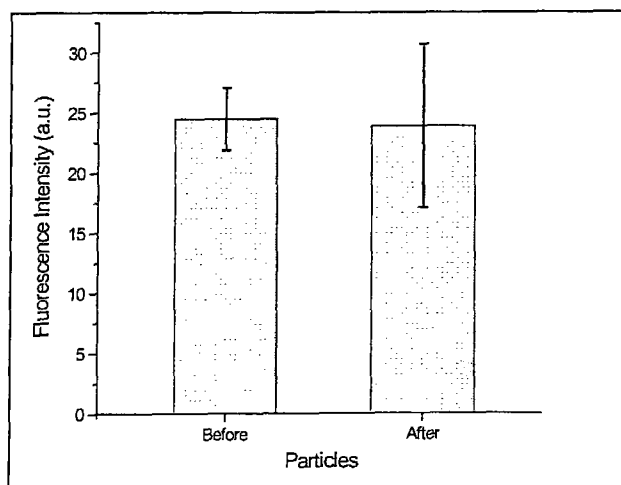


Figure 6.12. Negative control. Fluorescence intensity of particles before and after traversing a 2° antibody stream only.

There was no significant difference between the fluorescence intensity of the particles before and after traversing the reaction chamber indicating that for a positive result on-chip, the 1^o antibody stream had to be present. This also shows that there is little non-specific binding of proteins to the particle surface.

6.4.2 Effect of 1^o antibody concentration

Once the detection of the magnetic particles has been optimised in the MLF2 chamber, the system was tested further by performing a quantitative investigation, i.e. varying the concentration of 1^o antibody. Since the 2^o antibody was used as a detection label, its concentration was kept constant at 10 $\mu\text{g mL}^{-1}$ throughout.

Limit of detection

As an initial investigation, the limit of detection of the system was tested by lowering the concentration of the 1^o antibody until the fluorescence intensity of the reacted particles was no longer distinguishable from the background signal of unreacted particles. The limit of detection for this experimental set-up was determined as 0.1 $\mu\text{g mL}^{-1}$. If considering the binding capacity of an individual particle, which was stated by the manufacturers as 10 μg of biotinylated antibody per mg of particles or the equivalent of 3.2×10^6 molecules of 1^o antibody per particle, it is possible to calculate the number of molecules the particle is likely to encounter by using the simple model described in section 5.3.2. At the LOD of 0.1 $\mu\text{g mL}^{-1}$, a single particle would encounter approximately 1.4×10^5 molecules of 1^o antibody as it traverses the reagent stream. Even if every antibody molecule the particle encountered had bound to the surface of the particle only around 5 % of the streptavidin binding sites would be occupied. However, the actual occupancy is likely to be less due to reason such as steric

hindrance from the binding of such large molecules as antibodies and hence the experimentally observed LOD is plausible.

Dose – response curve

Once the limit of detection had been established for the two-step system a dose – response curve was investigated by varying the concentration of the 1^o antibody between 0.1 $\mu\text{g mL}^{-1}$ and 10 $\mu\text{g mL}^{-1}$ with increments of 1 μg , 2.5 μg and 5 $\mu\text{g mL}^{-1}$. Figure 6.13. Shows the curve for this range including the blank particle signal which was the signal from the particles before the reaction.

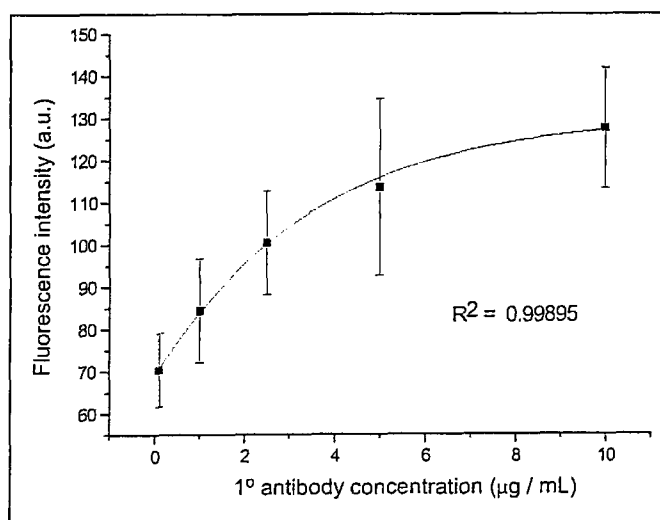


Figure 6.13. Dose - response curve of two-step mouse IgG immunoassay. 1^o antibody concentration was between 0.1 and 5 $\mu\text{g mL}^{-1}$. Signal of the blank particles is also included.

The results of the two step immunoassay fit the trend expected for a non-competitive binding assay dose – response curve. An increase in signal was observed between the

concentrations of $0.1 \mu\text{g mL}^{-1}$ and $5 \mu\text{g mL}^{-1}$ as more 1° antibody molecules bind to the surface of the particle, with the curve reaching plateau at the $10 \mu\text{g mL}^{-1}$ mark. At this higher concentration the number of molecules encountered by the particle is approximately 4.2×10^7 , which gives an excess ratio to streptavidin binding sites of 13:1 and therefore the particle is likely to be near saturation. The concentration of the 2° antibody does not affect the signal output of the system as long as the 2° antibody is always in excess of the primary. In these experiments a particle would encounter approximately 2.5×10^7 2° antibody molecules as it traverses the labelling stream, which is an excess ratio of 8:1 of 2° antibodies to binding sites on the particle surface

The dose – response curve showed relatively large variation for each data point the reasons for which, regarding particle velocity and chamber depth, were discussed in section 4.3.2. The errors seen in the two step immunoassay were slightly larger than those in the one step binding assay, which could be explained by the addition of a second step and the higher extent of particle sticking observed in the PBS buffer. It was not possible to track the particles as they crossed the chamber because the exposure time on the camera was too long and it took too much time updating each frame. However, it was likely that some of the particles that were deflected across the chamber to the detection window had at some point stuck briefly in the chamber. If a particle became temporarily stuck in the first reagent stream it would have been exposed to slightly more 1° antibody than a particle that had passed through without sticking at all. This, in addition to variation in particle velocity and variation in focal depth, would contribute to the slightly higher error observed in the two-step reaction.

6.4.3 Summary of mouse IgG immunoassay

In summary, the principles of the continuous flow reactor described in section 4 were adapted to perform a two-step sandwich immunoassay. A new chip design was utilised to incorporate another reaction step and subsequently the multi-laminar flow and particle deflection was further optimised. In addition, because two reagents were in close proximity within the chamber, experiments were performed to exclude any cross-contamination due to diffusional mixing. Initial experiments showed a poor fluorescence signal but after some optimisation of the detection method the signal was improved. The system was used to perform the two step sandwich assay with a limit of detection of $0.1 \mu\text{g mL}^{-1}$ within one minute, with on-chip incubation times of approximately 12 s in each reagent stream. Quantitative data was also obtained and a dose- response curve for 1° antibody concentrations between 0.1 and $10 \mu\text{g mL}^{-1}$ was produced. This was a good fit with the sigmoidal curve expected of a non-competitive sandwich assay.

Whilst the LOD for this system is fairly high it is still within the clinical range for certain types of immunoassay.[148] Other microfluidic techniques based on magnetic particles have reported much lower LOD in the order of pg or ng mL^{-1} . However, it should be noted that procedural times for these techniques were also much greater than for our system. [160]

6.5 C-reactive protein sandwich immunoassay

Once the system had been optimised to perform a two-step binding assay it was necessary to consider a clinically relevant biochemical procedure used in laboratories in

real clinical diagnostics tests. An immunoassay was chosen with a clinical range suitable to the range that was achievable with the device.

The inflammation marker, C-reactive protein (CRP), is produced in the body as a response to inflammation caused by acute and chronic infections. Disease states such as cardiovascular disease, can also be detected by fluctuations in CRP levels. Clinical tests involve the detection of elevated levels of CRP as an indicator of infection or coronary disease. The test for CRP was subsequently chosen as its clinical range is between $0.1 - 1 \mu\text{g mL}^{-1}$, which falls within the detection range achieved by the system in the previous chapter.[148]

6.5.1 Proof of concept for CRP sandwich immunoassay

6.5.1.1 Off-chip CRP immunoassay

The reagents for the CRP immunoassay were first tested off chip in PBS buffer according to section 3.7.4 and the schematic for the reaction is shown in figure 6.14.

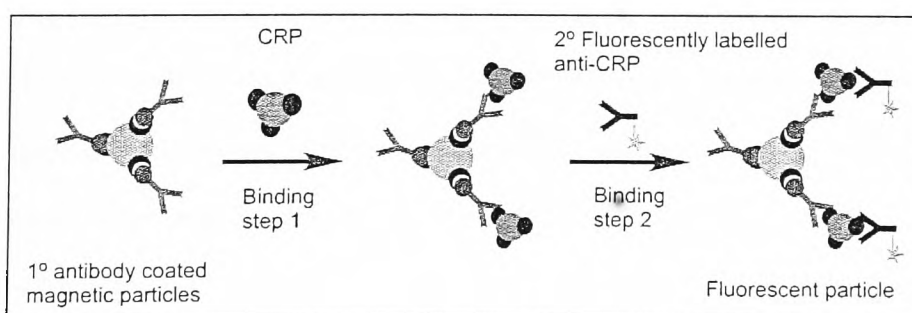


Figure 6.14. Schematic of the CRP immunoassay. In the first binding step, CRP binds to the 1° antibody on the surface of the magnetic particles. In the second binding step, the CRP is labelled with a fluorescently tagged 2° antibody.

The magnetic particles were coated with the 1^o antibody before incubation with the CRP protein. The particles were checked on the microscope at this stage and there was no detectable increase in fluorescence signal. The particles were then incubated with the 2^o labelling antibody and observed on the microscope again. The particles appeared a very bright green indicating that an increase in fluorescence signal would only be observed after the successful completion of the second step.

A negative test was also performed in which the incubation step with the CRP protein was left away so that the 1^o antibody coated particles were incubated with the 2^o antibody only. Under observation on the microscope there was no detectable increase in fluorescence signal indicating little to no non-specific binding of proteins to the particle surface and also, that there was no cross-recognition between the two anti-CRP antibodies.

6.5.1.2 On-chip CRP immunoassay

Once the reagents had been tested off-chip and found to work well in the PBS buffer conditions, the method was adapted for an on-chip procedure according to section 3.7.4. The magnetic particles were surface functionalised with the 1^o antibody first and then introduced to the chip via inlet 1, with the CRP protein antigen in inlet 2 and the 2^o antibody in inlet 4. The same chip design (MLF2) was used for these experiments and the same flow rate and magnetic set-up was used as in section 3.3.

Effect of temperature on particle deflection

As soon as the on-chip assay was started, it was observed that the particle trajectory in

the presence of the magnetic field was steeper, and particles were dragged towards the magnet rather than flowing to the chamber exits. This increase in magnetically induced velocity (u_{mag}) was surprising as the magnetic particles, the magnet position and flow rate were kept the same as the previous immunoassay. In addition, more particle sticking problems were encountered. However, unlike the sticking previously that had occurred at the edge of the 1^o antibody stream due to surface charge, the sticking observed in the CRP assay occurred as soon as the particles entered the chamber. Initially, the surface charge of the particles with the 1^o antibody attached was considered to be the problem, as the particles enter the chamber with this antibody already present on its surface. However the theoretical pI of the antibody was 5.45, much lower than the buffer pH (7.4) and so the particles were expected to be negatively charged and thus be repelled from the glass surface. Another explanation could be the particles becoming trapped in the magnetic field, even though this was thought to be unlikely as the magnetic field was exactly the same as for the previous experiment. To test whether the particles were adhered to the surface of the glass by electro-static effects or trapped in the magnetic field, the magnet was removed from the chip. Many of the particles that had become stuck in the chamber were almost immediately dislodged with the removal of the field and continued with the laminar flow towards the exits, indicating they had become trapped against the glass ceiling of the chamber by the field. As discussed in section 3.3.1 the placement of the magnet on-top of the glass chip creates a slight vertical gradient that exerts an upwards force on the particles. One factor that affects the magnetically induced velocity is the viscosity of the medium, which is a function of the viscous drag force (equation 14, section 2.3.1). Viscosity in turn is affected by temperature, as the temperature of the medium increases, its viscosity decreases

(equation 39), resulting in less viscous drag and a greater magnetically induced velocity.[134]

$$\eta = A \exp\left(\frac{\Delta E_{vis}}{RT}\right) \quad \text{Equation 39}$$

Where η is the viscosity, A is a constant, E_{vis} is the activation energy for viscous flow, R is the gas constant and T is the temperature.

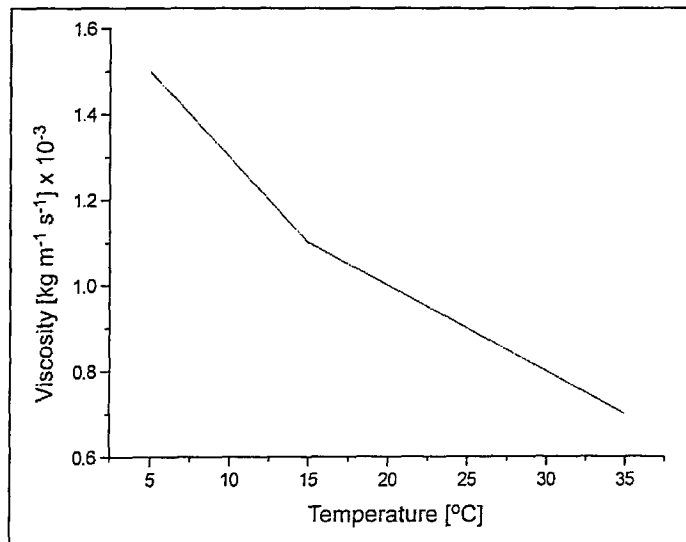


Figure 6.15. The change in the viscosity of water as temperature increases.

Figure 6.15 shows the decrease of the viscosity of water against increasing temperature. It was noted that the temperature in the laboratory during the CRP experiments was much higher at 24 – 27 °C than the temperature when the mouse IgG immunoassay was experiments had been performed, 19 – 21 °C. The effect of this was that the particles

experienced an increase in u_{mag} and in addition, they were also pulled to the ceiling quicker by the magnet than previous experiments at lower temperatures, which in turn would facilitate particle sticking by Van der Waals and hydrophobic interactions. For example, by using equation 12 (section 2.3.1) we can calculate the expected u_{mag} of particles at different temperatures if all other variables, such as magnetic field and particle diameter, are kept constant. At a temperature of 20 °C a M-270 particle experiencing a force of 1.5 pN will have u_{mag} value of $5.8 \mu\text{m s}^{-1}$. The same particle at 25 °C will experience u_{mag} at $98 \mu\text{m s}^{-1}$.

In order to reduce these effects two changes were made to the experimental set-up. Firstly, the flow rate was increased from $15 \mu\text{L h}^{-1}$ on each syringe to $20 \mu\text{L h}^{-1}$ in order to increase the hydrodynamic induced velocity, u_{hyd} , on the particles and push them towards the exits. Secondly, a small hole was drilled into the top of the microchip, by the side of the reaction chamber so that a magnet could be placed inside and the magnetic field gradient was in the same plane as the chamber, reducing the upwards pull (figure 6.16).

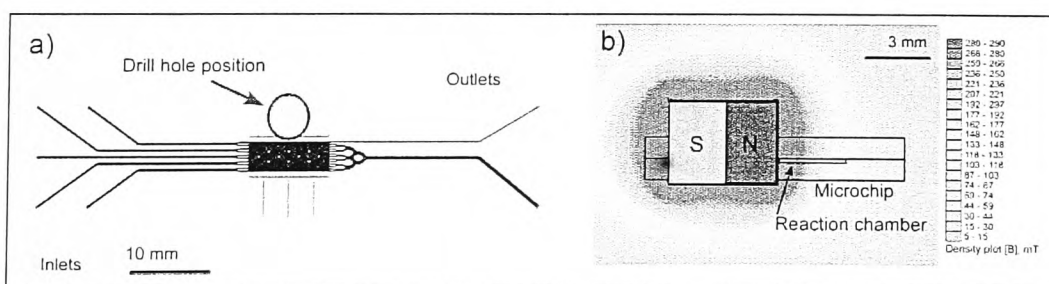


Figure 6.16a) Approximate position of the drill hole against the chamber. **b)** Model of the magnetic field in relation to the chamber when placed in the same plane via a hole drilled into the glass device.

These two changes went some way to improving the situation. Particles were deflected towards the exit and also particle sticking was reduced enough so that experiments could be performed. However, there was still a relatively high level of particle sticking in the chamber.

Qualitative CRP assay

Using this set-up it was possible to deflect some single particles across the entire chamber and preliminary analysis was performed on particles that crossed into the detection window. Figure 6.17 shows the fluorescence intensity of particles before the CRP and labelling streams, a positive control using $10 \mu\text{g mL}^{-1}$ of CRP protein and a negative control using plain epoxy coated M-270 particles.

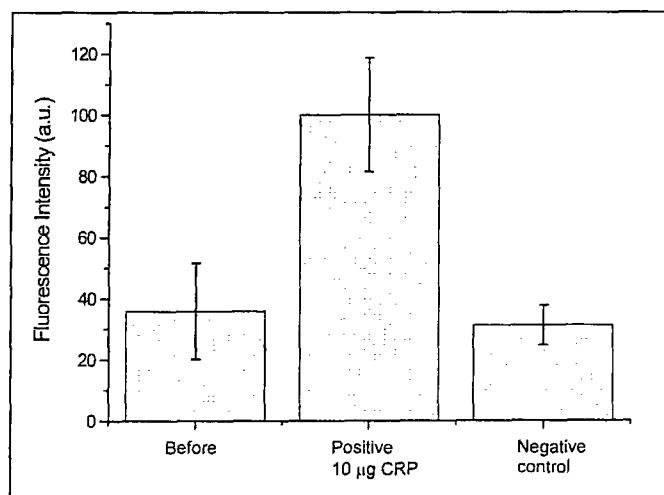


Figure 6.17. Qualitative results for CRP immunoassay with average intensity before and after traversing the reagent streams including a negative control. Concentration of the CRP protein was $10 \mu\text{g mL}^{-1}$.

The increase in fluorescence intensity from before the particles that traversed the reagents to the intensity afterwards clearly indicates the successful binding of the CRP

protein to the 1^o antibody on the surface of the particle and then the labelling of the protein by the 2^o antibody. There error bars on the graph again can be attributed to the sticking of the particles in the chamber causing variable residence times from particle to particle. However, even with the relatively large error bars it can be seen from the graph that it may be possible in future experiments to lower the concentration of CRP further.

The negative control performed with the M-270 epoxy particles showed little increase in fluorescence signal, signifying the signal observed in the positive test was a product of the immuno-recognition between the 1^o antibody on the surface of the particle, CRP protein in solution and the 2^o antibody in solution and not a result of non-specific binding or boundary layer transfer of reagents around the particle surface.

6.5.2 Summary of CRP immunoassay

To summarise, the MFL2 microdevice was used to perform a sandwich immunoassay for the qualitative detection of the inflammatory marker C-reactive protein. Due to a change in laboratory temperature, which affected the behaviour of the magnetic particles inside the reaction chamber, the chip set-up had to be changed in order to optimise the magnetic field. A hole was drilled into the side of the microdevice so the magnet could be lowered into the plane of the chamber. The system could qualitatively detect CRP at a concentration of $10 \mu\text{g mL}^{-1}$ within 1 minute in continuous flow.

6.6 Discussion of two-step immunoassays

The 2nd generation of continuous flow microfluidic reactor developed, as outlined in this chapter, has been shown to be capable of performing two – step molecular binding assays in less than 1 minute without any manual intervention. As a first example,

biotinylated mouse IgG antibody was detected by streptavidin coated particles and labelled with fluorescently labelled anti-mouse IgG antibody. Detection of the biotinylated mouse IgG was achieved down to $0.1 \mu\text{g mL}^{-1}$ and demonstrated over a range of concentrations from $0.1 \mu\text{g mL}^{-1}$ to $10 \mu\text{g mL}^{-1}$. The system showed a significant reduction in procedural time, both in comparison to bench-top methods and other on-chip binding assays. The entire two – step procedure, involving two binding steps and two washing steps was less than one minute, whereas the same assay off-chip took approximately 90 min including two 30 minute incubation periods. In a further example, the system was used to qualitatively detect the inflammatory marker C-reactive protein at a concentration of $10 \mu\text{g mL}^{-1}$ using a sandwich immunoassay procedure in continuous flow. Again, the procedural time for this immunoassay was less than one minute with no manual intervention.

Both binding assays described here were limited by two main problems. First, the short on-chip incubation times compromised the sensitivity of the system. Whilst having such short incubation times inevitably kept the procedural time very fast, the limit of detection for the two – step system was not as low as other on-chip examples.[160] In order to improve the sensitivity it would be necessary to lengthen the incubation time. This could be achieved in various ways such as modifying the magnetic field and the flow to slow the particles down, or using magnetic elements inside the chamber to ‘trap’ the particle in a reagent stream and then releasing it. Another method would be to widen the reagent streams by widening the chamber, however this would also mean the magnetic deflection and perhaps the magnetic particles would need to be optimised again to deflect the particles across a wider chamber. However, the real advantage of the current system is the speed of analysis, and for certain bioanalytical procedures this is more

desirable than sensitivity. To go down the route of lengthening incubation time to improve sensitivity would inevitably lengthen the current procedural time, which for some applications, would not be as desirable.

The second area for improvement would be the particle sticking. Whilst this didn't affect the system's ability to perform the two – step assays, it reduced the number of particles that could be analysed and in addition it caused a relatively high variance in the measurements taken. Particle sticking was caused either by the surface charge of the particle or by the direction of the magnetic force. The former could be improved by careful consideration of the protein pI and thus the choice of buffer for the system. In the case of the latter, modification of the magnetic field set-up would be advantageous. In addition, control over the temperature of the device by using a control system such as a Peltier element that could heat or cool the chip to a desired temperature.

Despite these complications, the multi-flow system has been able to perform whole sandwich immunoassay procedures on a single device in continuous flow in less than one minute, something that has not been achieved elsewhere to date. The combination of multiple laminar flow streams and functionalised mobile magnetic particles has produced a simple and effective device for performing reaction, washing and labelling steps in one operation. The speed of the procedure, coupled with an adequate limit of detection should prove to be desirable to an analyst requiring fast, preliminary clinical results.

7 Diamagnetic repulsion for on-chip manipulation

In the previous chapter, magnetic particles were manipulated via magnetic attraction forces. Another interesting phenomenon that has been used to manipulate objects using magnetic forces is that of diamagnetic repulsion. In the same way that magnetic objects are attracted to a magnetic field, diamagnetic objects such as plastic, wood and water are repelled from a magnetic field. The stronger the magnetic field, the greater the repulsion. Diamagnetic repulsion is an alternative to other forces for the manipulation of objects because it relies on the intrinsic diamagnetic properties of the object, so there is no need for labelling or complex instrumentation.

In this chapter, diamagnetic repulsion forces are explored as an alternative to magnetic attraction for on-chip microparticle manipulation. Diamagnetic repulsion forces were used for the trapping of diamagnetic polymer particles in a glass capillary for a surface based bioreaction and also as a method for separating a mixture of two different sized polymer particles.

7.1 Diamagnetic plugs for simultaneous bioanalysis

As discussed in the introduction (Section 1), microparticles are most commonly used as packing materials in microfluidic devices, acting as a high surface area solid-support for reactions. Magnetic particles can be elegantly trapped into plugs of particles using simple magnetic set-ups and this has already been demonstrated many times for bioanalytical applications.[59, 64] However, in order to make the particles magnetic they have to contain an iron oxide core or be doped with iron oxide nanoparticles. As

discussed in the theory section 2.3.1, diamagnetic particles are repelled from areas of high magnetic field gradient, a phenomenon that is greatly enhanced when suspended in a paramagnetic buffer. In this section is described an alternative method for the trapping of polymer particles utilising diamagnetic repulsion forces in a simple capillary set-up and its applicability to surface-based bioanalysis (figure 7.2).

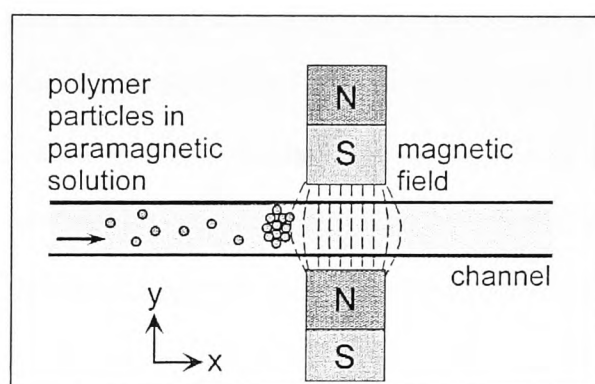


Figure 7.2. Principle of particle trapping using diamagnetic repulsion forces. Particles flowing in the x-direction are repelled from the high magnetic field gradient between the two magnet poles in the y-direction. The particles form a plug upstream of the magnet assembly.

7.1.1 Diamagnetic forces for trapping polymer particles

Magnetic set-up for trapping experiments

The magnetic set-up used for the particle trapping investigation is described in section 3.8.3 and consisted of two cylindrical magnets glued together such that opposite poles were facing across the width of the capillary (figure 7.2). The magnets were positioned in this way to create an area of high magnetic field gradient across the capillary, along the direction of flow.

Initial trapping of a single plug

The aim of this work was to form several plugs of polystyrene particles along one capillary, each with a different surface functionality for bioanalysis and so it was imperative that a plug was formed in the capillary with 100 % trapping efficiency. If particles escaped from one plug to become trapped in another downstream, this would cause cross-contamination in the system. A suspension of 10 μm polymer particles in 10 % w/v MnCl_2 was pulled into the capillary using negative pressure at an initial flow rate of 12 $\mu\text{L h}^{-1}$ (424 $\mu\text{m s}^{-1}$). In the absence of a magnetic field the particles flowed through the capillary without stopping or sticking. When the magnetic set-up was placed across the capillary the particles were observed to slow down in velocity as they approached the gap between the magnets. The polystyrene particles have a magnetic susceptibility of -8.21×10^{-6} and the MnCl_2 solution has a magnetic susceptibility of 1.46×10^{-4} . [135] As the particles have a negative susceptibility that is lower than the susceptibility of the surrounding medium, then $\Delta\chi$ in equation 16 (section 2.3.1) becomes a negative value and the particles experience a repulsive force exerted on them from the magnetic field. The particles are repelled from an area of high magnetic gradient to an area of field minima. This was observed in the capillary as the particles lost velocity on approaching the gap between the magnets due to the repulsive force from the area of high magnetic field between the magnet poles. However, at 12 $\mu\text{L h}^{-1}$ flow rate the force acting on the particles from the hydrodynamic flow was too great, and the particles were forced through the gap between the magnets. In order to trap the particles into a plug the flow rate was reduced until the particles slowed to a stop upstream from the magnet set-up. Figure 7.3 shows the formation of a plug of polystyrene particles in the capillary over a 10 minute time frame. The flow rate was 10

$\mu\text{L h}^{-1}$ ($350 \mu\text{m s}^{-1}$), which was found to be optimum for 100 % trapping efficiency.

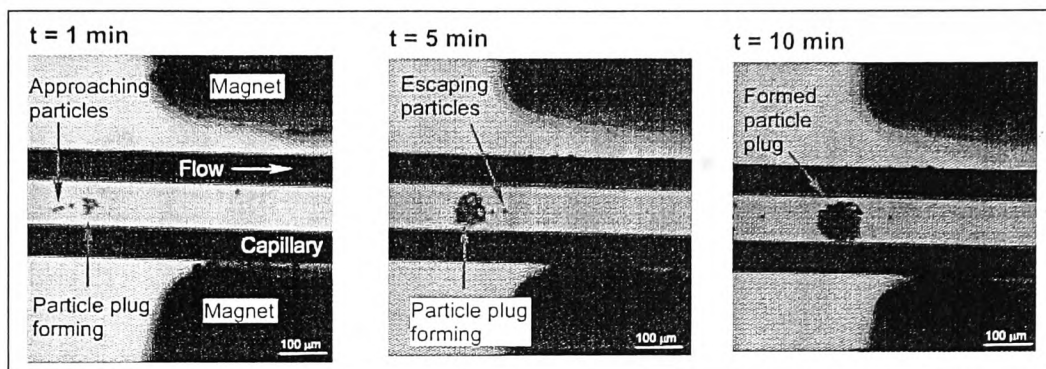


Figure 7.3. Formation of a diamagnetic plug. Polymer particles flowing through the capillary were repelled by the field produced by the magnets and slowed down in velocity. After 5 minutes a plug of particles began to form upstream of the magnet assembly. After 10 minutes the particles had formed a plug as wide as the capillary. Escaping particles were pushed back into the plug by the magnetic field.

The figure shows some particles escaping the plug at $T = 5$ and $T = 10$ minutes, however these particles did not pass through the gap between the magnets but were pushed back into the plug. Figure 7.4 shows a model of the magnetic field in the x -direction between the two magnets. An area of field minima is observable just before the magnet set-up and it is here that the diamagnetic particles were trapped.

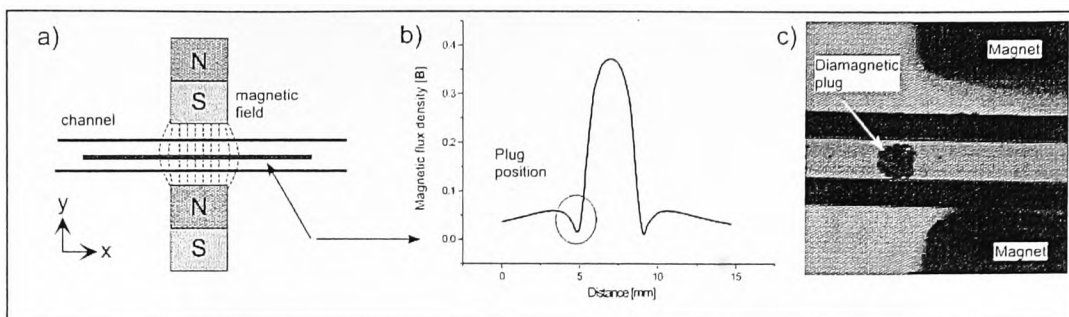


Figure 7.4a) The magnet field gradient was modelled between the two magnet poles in the x -direction. **b)** The model showed a dip in the magnetic flux density just before the magnetic set-up. **c)** Diamagnetic particles were trapped in this area of field minima.

An interesting phenomenon observed was the rotation of the plug as it formed. As the particles built up over time the plug appeared to rotate in the capillary, but on a closer inspection of the footage it became obvious that it was movement of the particles within the plug which was being observed. The particles in the plug nearest the magnet set-up were constantly being repelled by the high magnetic field gradient and pushed back upstream along the side of the capillary where the hydrodynamic force was least. The particles immediately behind were pushed into their place by the hydrodynamic force in the centre of the capillary pushing in the opposite direction, which were in turn repelled so that particles in the plug were constantly moving (figure 7.5).

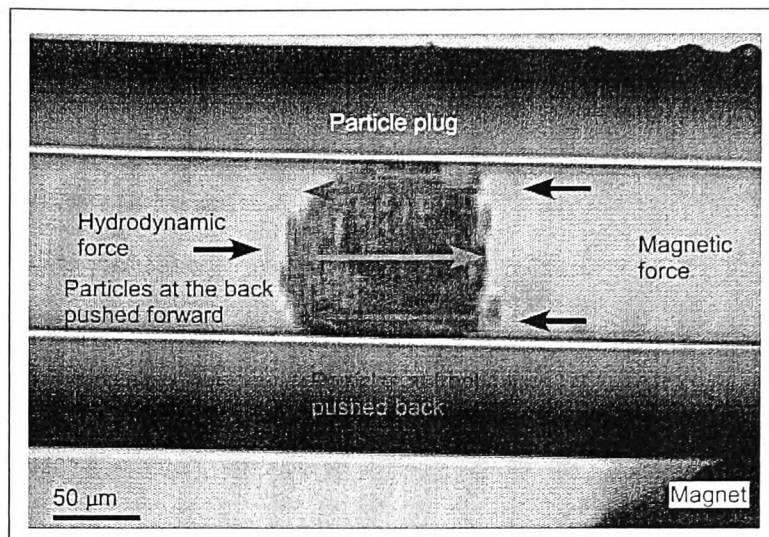


Figure 7.5. Rotation of the diamagnetic particle plug. Particles were shuffled through to the right of the plug by the hydrodynamic force. As they moved closer to the opposing magnetic force they were pushed back to the left side of the plug.

The rotation of the particles facilitated the expulsion of some particles from the plug towards the field, but at a flow rate of $10 \mu\text{L h}^{-1}$ these expelled particles were always pushed back into the plug by the magnetic field. The constant movement of particles could also be viewed as advantageous when performing surface-based bioanalysis, as rotation of the plug would constantly mix the particles with the reagent and expose all areas of the particle for reaction.

Trapping of two particle plugs

After the flow rate had been optimised for the trapping of a single plug in the capillary, the same flow rate was used to trap a second plug in an upstream position to the first. The procedure for which is outlined in section 3.8.3.

The exact same procedure for the formation of the first plug was used for the formation of the second, however at a flow rate of $10 \mu\text{L h}^{-1}$ there was not 100 % trapping

efficiency and some particles escaped into the first plug. The flow rate was lowered until 100 % trapping efficiency was achieved and this was found to be at $7 \mu\text{L h}^{-1}$ ($250 \mu\text{m s}^{-1}$). The differences in flow rate needed for 100 % trapping efficiency in each plug was not entirely clear. It could be attributed to the assembly of the magnetic set-up, which is described in section 3.8.3. The magnets were left to dry after the glue had been applied and for some time they were vulnerable to movement so that the different magnetic set-ups were not all identical. In addition, the placement of the magnets over the top of the capillary had to be performed with extreme care as to not break the glass capillary and especially for the placement of the second set as any rough movement could dislodge the first plug. This often meant that if the magnets were slightly off-centre it was difficult to straighten them up again. These two factors may have meant the magnetic field gradients of the two set-ups were not identical and if the particles felt less repulsive force from the second set of magnets, it would explain a lower flow rate required for 100 % trapping efficiency.

A negative control was also investigated in which polymer particles were suspended in water with no MnCl_2 present. Under the same conditions the particles were unaffected by the magnetic field and passed straight through the gap between the magnet poles. This indicated that the trapping observed in the paramagnetic buffer was a result of diamagnetic repulsive forces.

7.1.2 Diamagnetic particle plugs for simultaneous streptavidin – biotin binding assay

Once the system had been optimised for the formation of two polymer particle plugs a proof-of-principle binding assay was selected to test the system. Again, the streptavidin

– biotin binding assay was chosen for the same reasons discussed in chapter 3 and also because the reagents were readily available. The system was utilised to perform the streptavidin – biotin binding assay with both positive and negative control plugs on the same capillary simultaneously.

Off-chip streptavidin – biotin binding assay

To start, the binding of fluorescently labelled biotin to streptavidin coated polymer particles, similar to the reaction scheme described in section 5.3.1 was tested off-chip in the 10 % MnCl_2 buffer. The MnCl_2 solution is not a biological buffer and the Mn^{2+} is widely considered toxic so it was necessary to test that the biological reagents would still work in the solution. The procedure is outlined in section 3.8.3. After incubation with the fluorescently labelled biotin in MnCl_2 , the streptavidin coated particles were observed on the microscope and gave a very bright green colour. This indicated that the binding between streptavidin and biotin had been successful in the MnCl_2 , and also that the fluorescent signal was still observable as the Cl^- ion is a known quencher of fluorescein and other fluorescein based fluorophores.

On-capillary streptavidin – biotin binding assay

Once the reagents had been tested off-capillary successfully in the MnCl_2 , the system was set-up to perform a simultaneous bioassay as described in section 3.8.3. Two plugs were loaded into the capillary, the first plug to be loaded (plug 1) contained plain polystyrene particles with no surface functionality to act as a negative control in the assay and the second plug (plug 2) contained the streptavidin coated polymer particles as the positive control (figure 7.6).

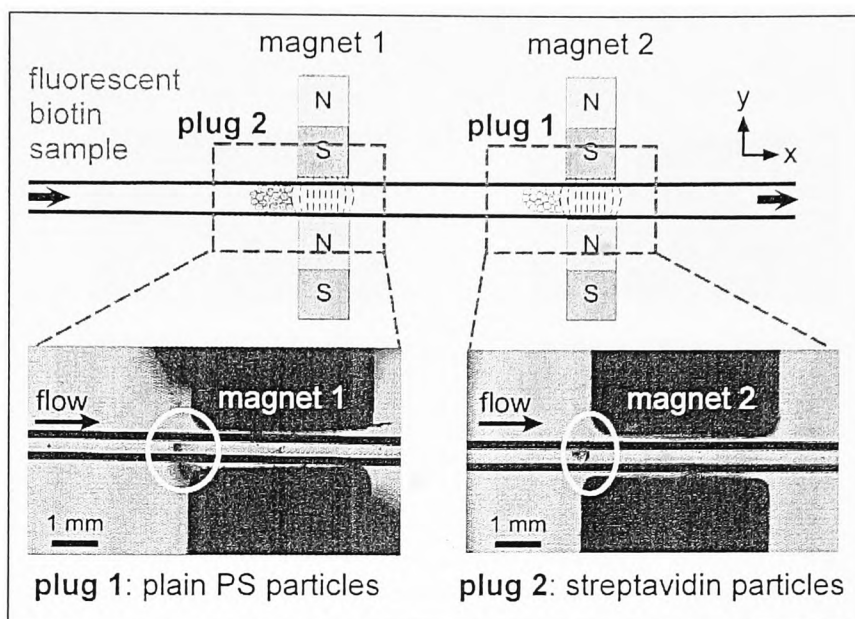


Figure 7.6. Formation of two diamagnetic particle plugs using two magnet assemblies. The first upstream plug contained plain polystyrene particles whereas the second downstream plug contained streptavidin coated particles. For 100 % trapping efficiency of both plugs, plug 2 was formed at $10 \mu\text{L h}^{-1}$ and plug 1 was formed at $7 \mu\text{L h}^{-1}$.

Initial observations showed that the particles coated with streptavidin did not show the rotation of particles previously observed with the plain polymer particles. This could be attributed to the presence of the protein streptavidin on the surface of the particles. As discussed earlier proteins have a complex structure with many charged areas. Thus particles in the plug may have become stuck to each other through electrostatic effects, and were not free to rotate.

The fluorescently labelled biotin was then pumped through the system at a flow rate of $6 \mu\text{L h}^{-1}$ to avoid any disruption of the plugs and observed on the microscope after washing. Figure 7.7 shows the two plugs under bright field conditions and under

illumination with the excitation light.

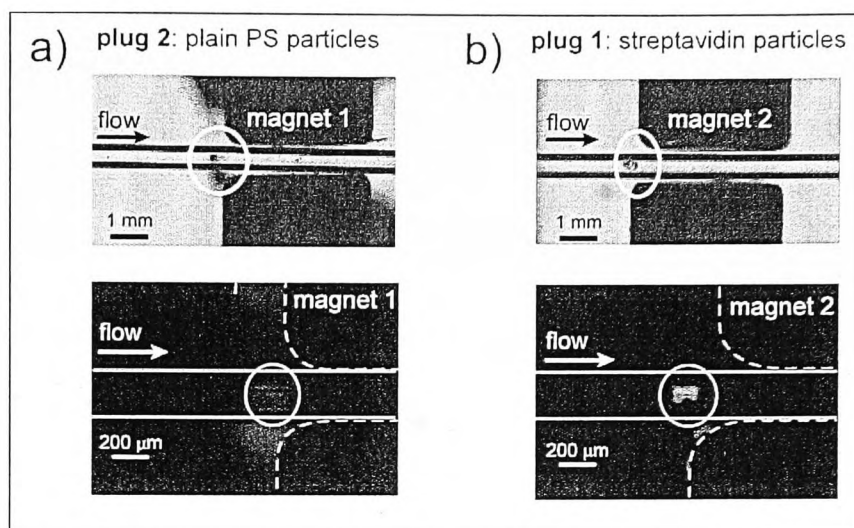


Figure 7.7. Streptavidin - biotin binding assay result a) Plug 2 contained the negative control which showed no detectable increase in fluorescence intensity b) Plug 1 contained the positive control which appeared a very bright green indicating the fluorescently labelled biotin had bound to the streptavidin on the surface of the particles.

Plug 2 contained plain polystyrene particles and showed very little increase in fluorescence intensity. A slight background fluorescence was observed from the polystyrene of the particles. Plug 1 contained the streptavidin coated particles and under observation the plug appeared a very bright green in colour indicating the fluorescently labelled biotin had selectively bound the streptavidin on the particles in plug 2 but not to the plain polystyrene in plug 1. The concentration of biotin was $1.6 \mu\text{M}$ and was pumped through the plug for 13 minutes, corresponding to 22 nL of reagent. Therefore the plug of particles was exposed to 35 fmol of biotin. The 22 nL of reagent represented a very small sample volume and because of the two particle plugs in the one device, the small sample was probed by a positive and negative control simultaneously.

One of the disadvantages of this system was the loading of the plugs. It was both time consuming, taking up to 10 minutes to load one plug but also the placement of the magnets across the capillary was quite precarious and often the slightest nudge of the capillary would dislodge a formed plug.

7.1.3 Formation of simultaneous diamagnetic and paramagnetic plugs

In order to decrease the loading time of the plugs, and to reduce the number of magnet set-ups needing to be placed across the capillary, an alternative system was investigated utilising a mixture of diamagnetic polymer particles and superparamagnetic particles. In this section the simultaneous loading of diamagnetic and paramagnetic plugs into a capillary is described.

Initial investigation into simultaneous loading

A mixture of 10 μm polymer particles and 10 μm superparamagnetic particles were pulled into the capillary as described in section 3.8.3. As the volume of the particles affects the amount of force acting on them the two particles populations were kept the same size so that their magnetic properties were the only difference. In the absence of a magnetic field, the two particle populations flowed through the capillary without stopping and were mixed together. When a magnet assembly was placed across the capillary, the two particle populations began to separate, with the diamagnetic particles stopping before the gap between the magnets, and the paramagnetic particle becoming trapped between the two magnet surfaces. Figure 7.8 shows the formation of two plugs using a single magnet assembly.

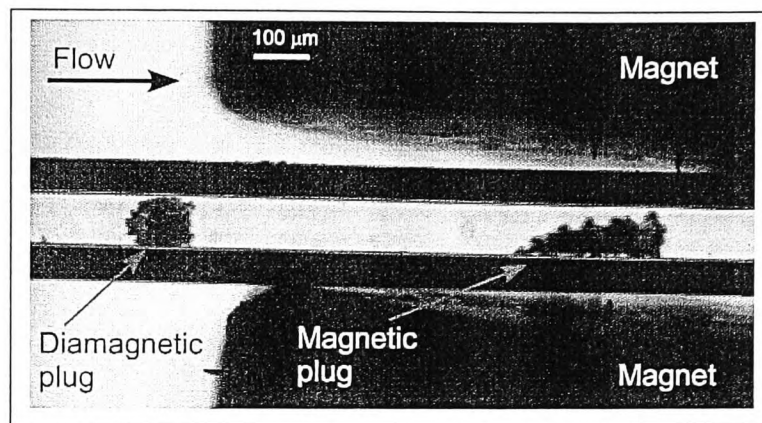


Figure 7.8. The simultaneous formation of a diamagnetic plug and a paramagnetic plug from a mixture of diamagnetic and paramagnetic particles using a single magnet assembly.

The first observation was that like previously, the diamagnetic particles began to slow in velocity as they approached the magnet assembly before eventually stopping before the gap between the magnets. In contrast the paramagnetic particles accelerated towards the magnet assembly as the particles experienced an attractive force into the magnetic field gradient before they then stopped and became trapped between the two magnet surfaces. Again, like previous experiments, the diamagnetic plug that was formed was quite spherical and sat in the centre of the capillary. The superparamagnetic plug however, formed to one side of the capillary, the particles appeared to be trapped against the capillary wall (figure 7.8). This was probably due to the magnet assembly not being placed with the capillary directly through the centre. If one of the magnet surfaces is closer to the capillary than the other, the particles will be pulled to that side of the capillary. The two plugs were loaded for 10 minutes, which gave diamagnetic and paramagnetic plug lengths of approximately 130 μm and 260 μm , respectively.

As both particle populations were of the same diameter it was difficult to distinguish between the two by eye, the superparamagnetic particles were slightly darker in colour than the polystyrene particles. However, it was impossible to tell if the trapping efficiency of both plugs was 100 % because once trapped in the plugs this subtle difference in colour was not so evident and further investigations were required.

Plug cross – contamination investigation

In order to investigate the trapping efficiency of the system the 10 μm magnetic particles were replaced with fluorescent 8 μm magnetic particles so the two particle populations could be distinguished on the fluorescence microscope. The two plugs were formed as before and monitored both under brightfield conditions and under blue light. Figure 7.9 shows the two plugs under these conditions. Under the blue light the diamagnetic plug appeared a dark grey colour due to a slight background fluorescence from the polystyrene. The magnetic plug is coated with the Dragon Green fluorophore and appeared a very bright green. In the figure this was white as the camera used for these experiments was monochrome. At 10 $\mu\text{L h}^{-1}$, over 10 minutes, there was 100 % trapping efficiency of the two plugs and no cross-over contamination of particles between plugs as can be seen from the fluorescence image.

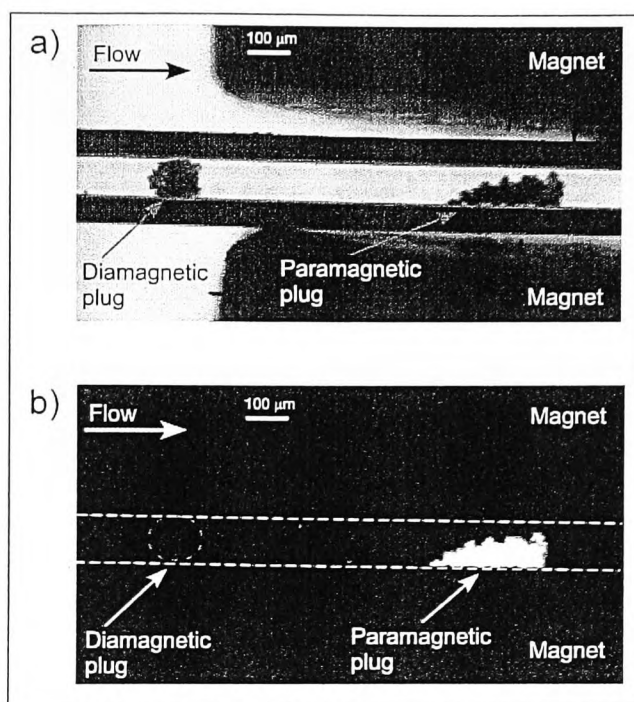


Figure 7.9. Trapping efficiency investigation a) a diamagnetic and fluorescently labelled paramagnetic plug were formed simultaneously b) fluorescence image of the particle plugs showing no cross contamination.

As the diamagnetic plug became larger over time, and filled more of the capillary some of the magnetic particles flowing down the capillary inevitably became stuck in the diamagnetic plug. However, due to the shuffling of the diamagnetic particles described earlier, the magnetic particles were shuffled along the plug and eventually expelled at the other side. Due to their attraction to the magnetic field they were then pulled into the magnetic plug (figure 7.10).

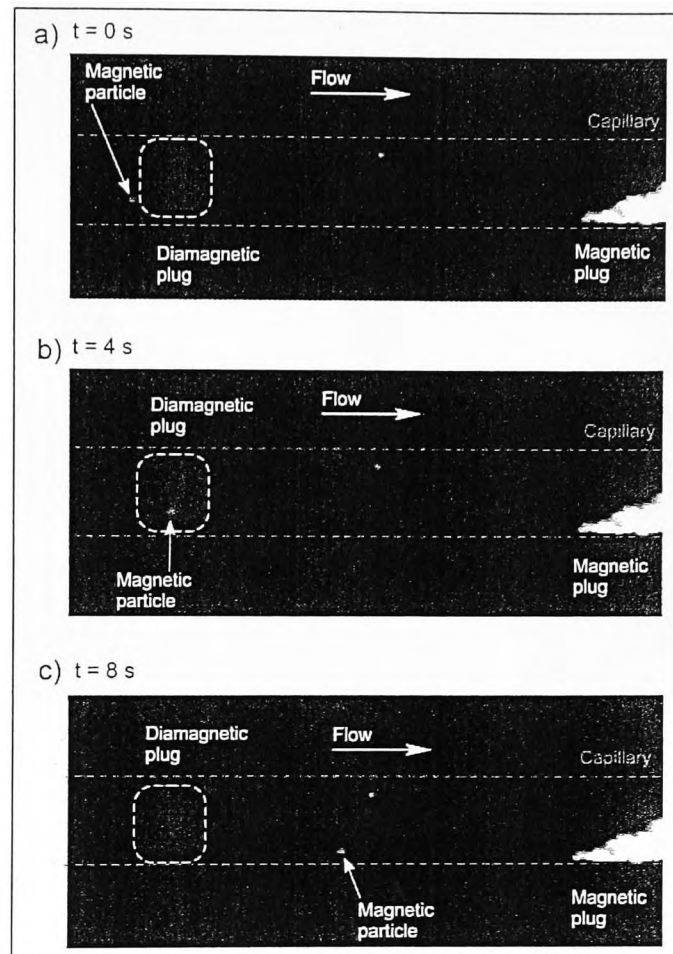


Figure 7.10. Expulsion of magnetic particle from the diamagnetic plug a) A magnetic particle approached and became stuck in the diamagnetic plug b) As the diamagnetic particles shuffled to the right, the magnetic particle was pulled along c) The magnetic particle was eventually expelled from the diamagnetic plug and pulled into the magnetic field.

Loading of with more than one magnet assembly

Once the trapping efficiency of the particles was determined, an investigation into the how many plugs could be loaded into one capillary was undertaken. As each particle plug could have a different surface functionalisation, this effectively was how many ‘probes’ could potentially be used in the system. Figure 7.11 shows the formation of six

plugs, three paramagnetic and three diamagnetic, using three magnet assemblies.

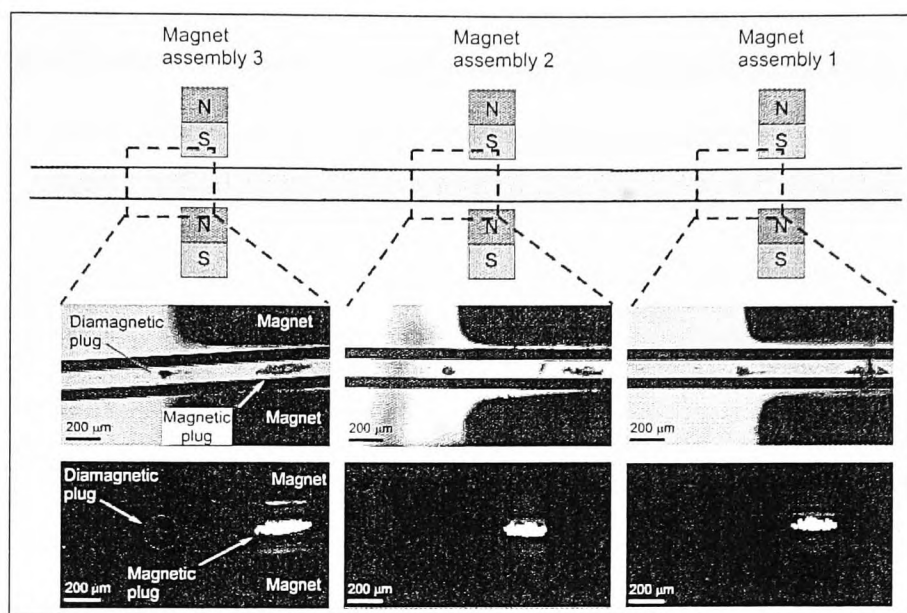


Figure 7.11. Loading of six particle plugs, 3 diamagnetic and 3 paramagnetic, using 3 magnet assemblies. The flow rate for the simultaneous assembly was $8 \mu\text{L h}^{-1}$.

All six plugs were formed at a flow rate of $8 \mu\text{L h}^{-1}$ to ensure there was 100 % trapping efficiency. The plugs were allowed to form at each magnet assembly for 10 minutes before placing the next, so the formation of all six plugs took approximately 40 minutes and the distance between the diamagnetic plug of one magnet assembly and paramagnetic plug of the next upstream magnet assembly was approximately 3 mm.

7.1.4 Summary of diamagnetic repulsion forces for trapping particles

As an alternative to using magnetic microparticles, diamagnetic repulsion forces were explored by exploiting the intrinsic diamagnetic properties of polystyrene particles. The polymer particles were suspended in paramagnetic MnCl_2 buffer and manipulated using

assemblies of small, permanent magnets. The particles were trapped into plugs inside a capillary by placing a magnet either side of the capillary with opposite poles facing. The trapping efficiency of the plugs was investigated and an optimum flow rate of $10 \mu\text{L h}^{-1}$ was established, when a second plug was loaded this was reduced to $7 \mu\text{L h}^{-1}$. Two plugs were loaded into the capillary, one containing plain polystyrene particles and the second containing streptavidin coated particles. The system was used for a surface based binding assay in which fluorescently labelled biotin selectively bound to the plug of streptavidin coated polystyrene particles. In order to reduce the loading time of plugs and the number of magnet assemblies required, the formation of alternate diamagnetic and paramagnetic plugs from a mix of particles was investigated. Up to 6 plugs were loaded with 3 magnet assemblies in 40 minutes.

7.2 Size - selective diamagnetophoresis

In another example of the potential of diamagnetic repulsion forces for particle manipulation, the same principles of particle deflection discussed in section 3 were investigated using repulsion instead of magnetic attraction (figure 7.12). The latter has been used before to deflect and separate magnetic particles of different sizes using free-flow magnetophoresis[132] as discussed in chapter 3. Similar to free-flow magnetophoresis the amount of repulsive force acting on a diamagnetic particle is proportional to the volume of diamagnetic material (equation 16, section 2.3.1) and therefore the applicability of diamagnetic repulsion to deflecting and separating two particle size populations was investigated.

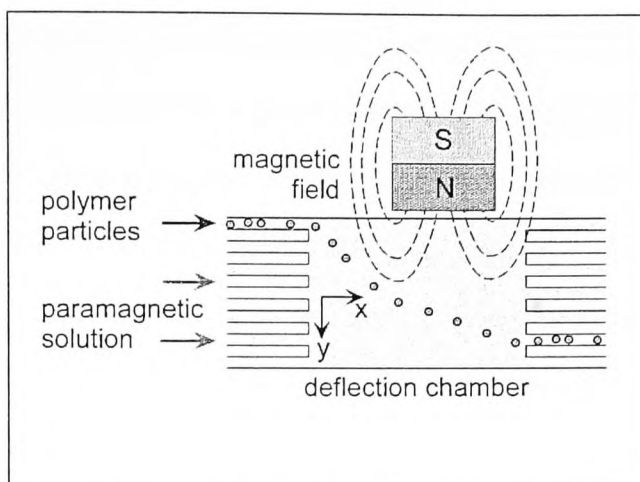


Figure 7.12. Principle of free-flow diamagnetophoresis. Polymer particles suspended in paramagnetic MnCl_2 solution enter a chamber flowing in the x-direction. A magnetic field gradient is applied perpendicular to flow in the y-direction. The particles experience a repulsive force from the magnetic field and are deflected from flow.

7.2.1 Diamagnetic repulsion for deflecting particles

7.2.1.1 Magnetic set-up optimisation

Initially, experiments were undertaken to optimise the magnetic field set-up for the deflection of polymer particles. The experiment was set up as described in section 3.8.4 using the FFM chip utilised in the magnetic particle comparison experiments (chapter 3). In the previous section, the $10\ \mu\text{m}$ polymer particles were manipulated in a relatively narrow ($100\ \mu\text{m}$) glass capillary and the repulsive effect on the particles was observed quite clearly. However, the chamber of the FFM chip was $6\ \text{mm}$ by $6\ \text{mm}$ and to observe deflection from the $150\ \mu\text{m}$ wide particle inlet stream, a relatively large amount of deflection would need to be achieved. A variety of magnets were placed at the same side of the chamber as the particle inlet to bring the surface of the magnet where the

field gradient is highest as close as possible to the particles (figure 3.31, section 3.8.4). However, the only magnet that appeared to have a strong enough field gradient to exert a clear repulsive force on the particles was a large disc magnet 20 mm in diameter and 5 mm thick. Whilst conducting these initial experiments it became apparent that the position of the magnet against the side of the chamber was also very important for optimising the deflection. The flow rate in these experiments was $65 \mu\text{L h}^{-1}$ and was chosen after a brief optimisation in which the flow rate was lowered from $100 \mu\text{L h}^{-1}$ until deflection was observed whilst still maintaining a reasonable particle through-put of approximately $10 \text{ particles min}^{-1}$. Figure 7.13 shows three different magnet positions investigated.

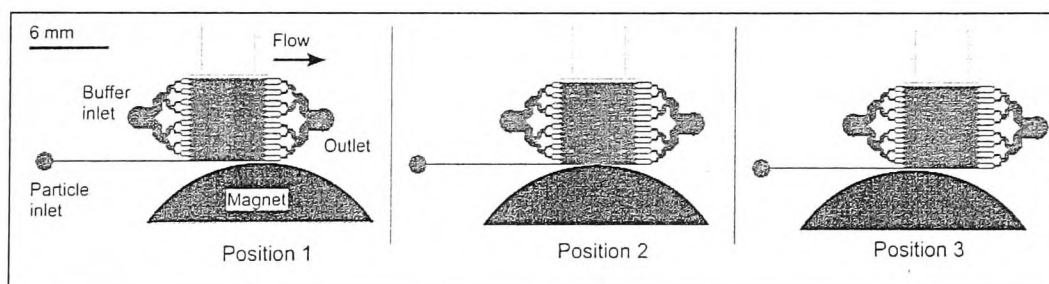


Figure 7.13. Three different magnet positions investigated for diamagnetic repulsion for particle deflection. Position 1 was in line with the outlets, position 2 was central to the chamber and position 3 was in line with the inlets.

In the absence of a magnetic field, the $10 \mu\text{m}$ polymer particles followed laminar flow and exited the chamber via exit 1, directly opposite the particle inlet. When the magnet was placed in position 1, the curve of the magnet was directly in line with the outlets and was placed here with the expectation that particles would be repelled by the

increasing field gradient as they flow from left to right and be deflected from laminar flow. In position 1, particles were deflected very little with particles already flowing furthest from the channel wall (up to 300 μm) only just being deflected to inlet 2. In position 2, the curve of the magnet is central to the chamber and this position improved the deflection slightly with particles being exposed to the high field gradient at the curve of the magnet sooner in the chamber and for longer before the outlets than in position 1. However, it was position 3 that produced the best deflection. In this position the curve of the magnet is directly in line with the particle inlet so the particles experienced the highest field gradient as soon as they entered the chamber. With position 3, particles were deflected towards the centre of exit 2

A negative control was also performed with the particles suspended in water instead of the MnCl_2 buffer. In the presence of the magnetic field the particles were not deflected at all from laminar flow indicating that the deflection observed in the MnCl_2 buffer was from diamagnetic repulsion forces.

7.2.3 Diamagnetic repulsive forces for the size-selective separation of two particle populations.

Once the magnetic set-up had been optimised for the deflection of one size of polymer particles, the system was applied to a mixture of 10 μm and 5 μm polymer particles according to section 2.9.4. In the absence of a magnetic field both the 10 μm and 5 μm particles followed laminar flow and exited the chamber via exit 1 at a flow rate of 100 $\mu\text{L h}^{-1}$. Both particle populations were randomly distributed over the particle stream and were mixed together (figure 7.14a).

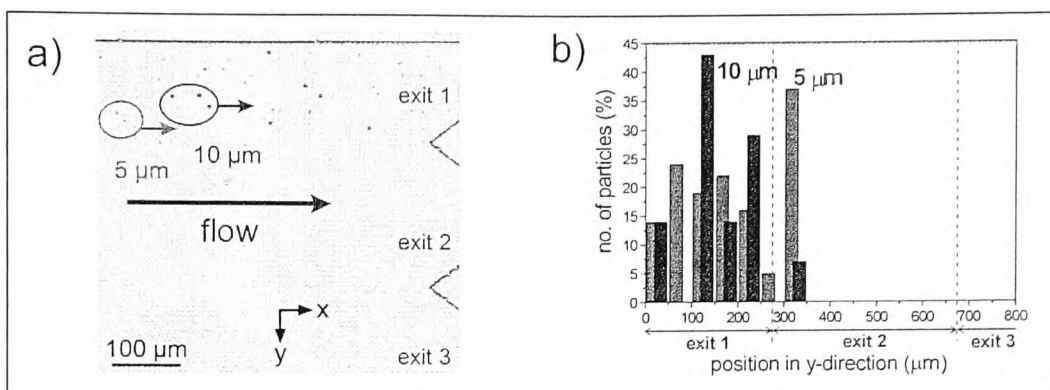


Figure 7.14 a) Photograph of particles in flow. In the absence of a magnetic field both particle populations left the chamber via exit 1. b) Histogram showing position of 60 particles in the y-direction.

The histogram in figure 7.14b indicates the position of the particles for both populations in the y-position. Particles were analysed approximately 300 μm upstream of the exits. The particles were not analysed any closer to the exits because as the liquid flowed around the exit posts, particles close enough to the posts followed laminar flow and therefore would give an inaccurate y-position through diamagnetic deflection alone.

When the magnet was placed against the side of the chamber in position 3 (figure 7.13), both particle sizes were deflected slightly from the direction of laminar flow. Figure 7.15a shows that both particle populations were deflected and left the chamber via exits 1 and 2.

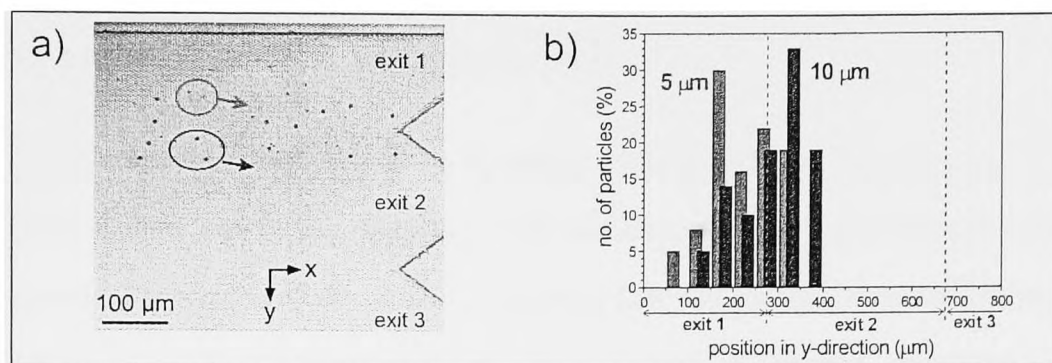


Figure 7.15 a) Photograph of particles being deflected towards exit 2. b) Histogram of the particle positions in the presence of a magnetic field for around 60 particles.

Figure 7.15b shows the particle positions in the y-direction and whilst the two populations were still mixed, the histogram shows that the 10 μm particles were deflected the furthest. This can be explained by equation 16 in section 2.3.1. The repulsive force acting on the particles depends on the difference in magnetic susceptibility between the particles and the MnCl_2 but also on the volume of diamagnetic material. The 10 μm particles have an eight times larger volume than the 5 μm particles and therefore experience a greater repulsive force from the magnetic field, deflecting them further, up to 400 μm. The histogram also shows that the 5 μm and 10 μm particles were depleted entirely from the chamber wall, with no particles observed in the first 50 μm. According to equation 9, section 2.3.1. The degree of deflection, \mathbf{u}_{def} , depends on the magnetically induced velocity, \mathbf{u}_{mag} and the hydrodynamically induced velocity, \mathbf{u}_{hyd} . \mathbf{u}_{mag} is dependent on the repulsive force acting on the particles from the magnetic field gradient, whilst \mathbf{u}_{hyd} can be varied by changing the flow rate. Therefore to improve the deflection of the two particle populations and optimise the separation,

the effect of flow rate on the deflection behaviour of the particles was investigated.

7.2.3.1 The effect of flow rate on particle separation

After the initial investigation into the separation of the two particle size populations, the effect of flow rate on the behaviour of the particles was investigated following the procedure outlined in section 2.9.4. The range of flow rates investigated were between $100 \mu\text{L h}^{-1}$ and $20 \mu\text{L h}^{-1}$, corresponding to flow velocities of $230 \mu\text{m s}^{-1}$ and $45 \mu\text{m s}^{-1}$. Figure 7.16 shows the deflection of both particle size populations in the y-direction against varying flow rate.

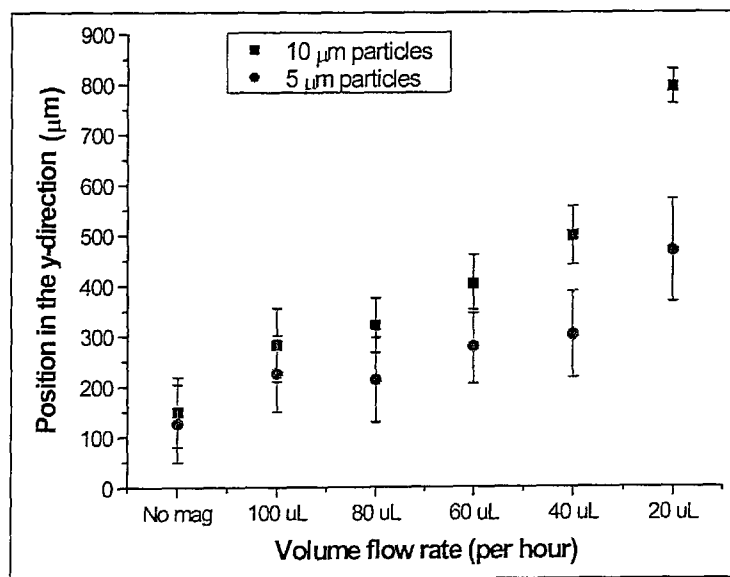


Figure 7.16. Effect of decreasing flow rate on particle separation. As the flow rate decreased, the two particle populations began to separate with the $10 \mu\text{m}$ particles being deflected further than the $5 \mu\text{m}$ particles. At $40 \mu\text{L h}^{-1}$ and $20 \mu\text{L h}^{-1}$ the two populations were separated.

As the flow rate was decreased, both particle sizes were deflected further due to the

smaller contribution of u_{hyd} to the particle deflection. As the particles were moving more slowly, they had more time in the chamber to be repelled by the magnetic field and were deflected further. The error bars show the distribution of the particles at each flow rate. The spread can be attributed to different flow velocities due to the hydrodynamic flow profile and the width of the particle stream, both of which were discussed earlier in section 3. As the flow rate decreased the two particle size populations could be separated from each other. At $60 \mu\text{L h}^{-1}$ the particles spend approximately 43 s in the chamber under the influence of the magnetic field. Under these conditions, the majority of the $10 \mu\text{m}$ particles took a different flow trajectory to the $5 \mu\text{m}$ particles with maximum y-deflection of up to $420 \mu\text{m}$ and $500 \mu\text{m}$, respectively. However there was still some overlap in the distribution.

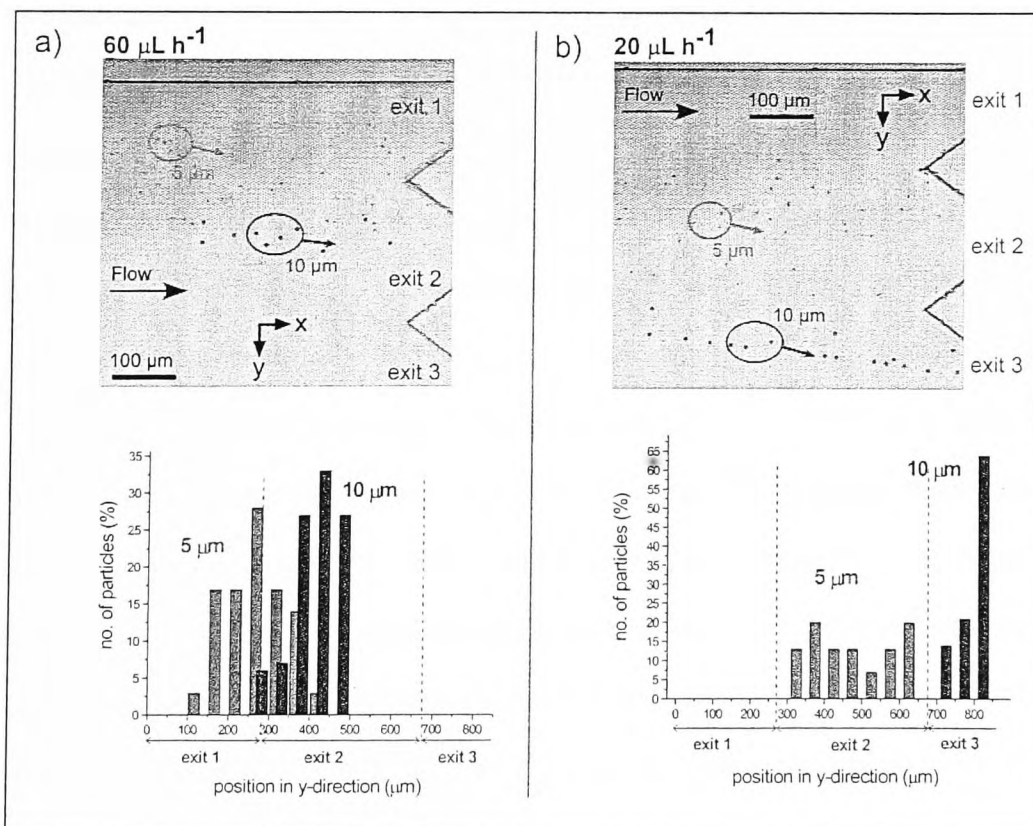


Figure 7.17 a) Photograph and y-position histogram of particles at 60 $\mu\text{L h}^{-1}$. B) Photograph and y-position of particles at 20 $\mu\text{L h}^{-1}$ showing separation of the two particle populations.

At 40 $\mu\text{L h}^{-1}$ (figure 7.16) the two populations were separated spatially, with the maximum deflection of the 5 μm particles being 380 μm and the least deflection of the 10 μm particles being 420 μm , a separation of approximately 40 μm . Despite this resolution, on-chip the particles overlapped across exit 2. It wasn't until the flow rate was decreased to 20 $\mu\text{L h}^{-1}$ that the particle populations were fully separated via exits (figure 7.17b). At this flow rate the particles spent approximately 130 s in the chamber, the 5 μm particles were deflected between 300 μm and 650 μm corresponding to exit 2 and the 10 μm particles were deflected 700 μm or more, corresponding to exit 3. Despite the spatial separation being only 10 μm more than at 40 $\mu\text{L h}^{-1}$ flow rate, the two population sizes were fully resolved and were not spread across more than one exit. The flow rate was not lowered further than 20 $\mu\text{L h}^{-1}$ as the particle through-put for both populations was greatly reduced as less liquid from the particle reservoir was pulled into the chamber. In addition, particle sticking in the deflection chamber was also a problem at low flow rates. The density of the polymer particles was 1.03 g cm^{-3} , which is lower than that of the 10% MnCl_2 at 1.08 g cm^{-3} . The buoyancy effect as a result of this caused particles to float to the top of the MnCl_2 solution. At low flow rates when the particles were moving very slowly through the chamber, this buoyancy effect caused particles to stick to the ceiling of the chamber before they reached the exits, reducing the number of particles available for analysis. In addition, 10 μm particles that stuck at the particle inlet also had a 'blocking' effect on other particles entering the chamber. The 10 μm diameter particles would occupy half the depth of the chamber and when they became immobilised they formed a barrier in the deflection path of other particles

entering the chamber which reduced the amount of observed deflection (figure 7.18).

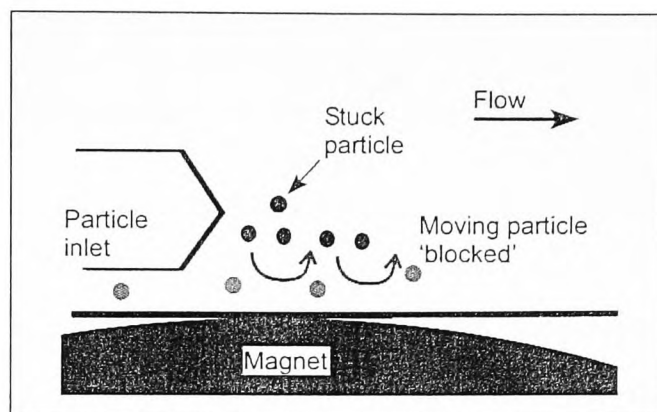


Figure 7.18. The sticking of particles at the particle inlet reduced the amount of deflection of moving particles by blocking their trajectory.

7.2.3.2 Calculation of F_{mag} values

In order to compare the on-chip results to what was expected theoretically, the repulsive forces acting on the particles was calculated. The theoretical force acting on the polymer particles, F_{mag} was calculated using equation 16, section 2.3.1. The observed F_{mag} values was calculated from the experiments using equation 12 and the measured u_{mag} values. Table 7-1 shows the theoretical and observed F_{mag} values for the 10 μm and 5 μm particles at 20 $\mu\text{L h}^{-1}$.

Table 7-1. Theoretically calculated F_{mag} values and observed F_{mag} values for the 5 μm and 10 μm particles.

Particle size (μm)	Theoretical F_{mag} (N)	Observed F_{mag} (N)
5	-6.2×10^{-13}	$-2 (\pm 0.06) \times 10^{-13}$
10	-5×10^{-12}	$-1.2 (\pm 0.07) \times 10^{-12}$

The theoretical F_{mag} values indicate that the repulsive force acting on the 10 μm particles is eight times greater than the force acting on the 5 μm . The observed F_{mag} values at 20 $\mu\text{L h}^{-1}$ show good correlation with the theoretical results with the repulsive force on the 10 μm being eight times larger than the force on the 5 μm particles.

The effect of temperature on separation

The effect of temperature on the separation of two particle populations by free-flow magnetophoresis has been investigated previously in our group[134] and was found to improve the resolution of particles with 2.8 μm and 4.5 μm diameters. The effect of temperature on the separation of particles in the diamagnetic system was also investigated according to the method outlined in section 3.8.4. Figure 7.19 shows the deflection of the two particle sizes at 65 $\mu\text{L h}^{-1}$ and at a temperature range between 20 and 50 $^{\circ}\text{C}$. This flow rate was chosen to ensure a high through-put of particles.

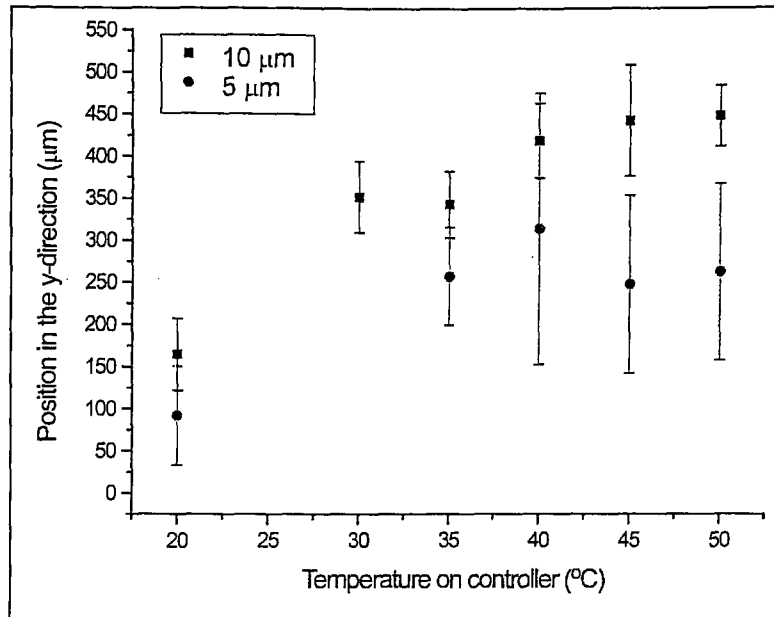


Figure 7.19. The effect of increasing the temperature on the separation of 5 μm and 10 μm particles.

As the temperature increases the deflection of the 10 μm particles and the 5 μm particles also increases. An increase in the temperature reduced the viscosity of the surrounding medium so that the particles being repelled from the magnetic field gradient experienced less opposing viscous drag force and were deflected further. At the higher temperatures of 45 $^{\circ}\text{C}$ and 50 $^{\circ}\text{C}$ the two particle populations were separated from each other, however the deflection of the 5 μm particles appeared to be reduced at the higher temperatures. The 5 μm particles were observed to stick in the chamber at the higher temperatures more than the 10 μm particles, which would affect the amount of deflection. However, the reason for the 5 μm particles sticking so much was not entirely clear as both the buoyancy effect and the downwards repulsion from the field, which would cause sticking, should affect the 10 μm particles more than the 5 μm .

The effect of temperature did improve the separation of the two particle populations at $65 \mu\text{L h}^{-1}$, however the response of the deflection to the change in temperature did not follow a clear trend. The heating stage used in this set-up was very basic and calibration of the stage was quite poor as described in section 2.9.4, figure 2.24. Therefore the temperature of the chip was not the same as the temperature displayed on the controller. This meant that the increase of temperature on the chip was not very reliable and therefore not an ideal set-up to use to improve the separation resolution. The use of a Peltier system, with greater control over temperature, would be more advantageous.

7.2.4 Summary of size-selective diamagnetophoresis

In a second application, diamagnetic repulsion forces were used to deflect polystyrene particles from laminar flow similar to the magnetic particle deflection described in chapter 3. The principles were then applied to a mix of $5 \mu\text{m}$ and $10 \mu\text{m}$ particles and the separation of the two particle populations based on size was investigated. The $10 \mu\text{m}$ particles were deflected further than the $5 \mu\text{m}$ particles due to a larger volume of diamagnetic material. The effect of varying the flow rate was on the separation of the two particle populations was also investigated and the two populations were completely resolved at $20 \mu\text{L h}^{-1}$. In addition, the effect of temperature on the separation was explored and found to improve the separation at a fixed flow rate.

7.3 Discussion of diamagnetic repulsion forces for manipulating particles

The use of diamagnetic repulsion forces, as a label-free technique for particle manipulation, has been described in this chapter and shown to be a viable alternative to

magnetic attraction forces.

As a first example, diamagnetic polymer particles were trapped into plugs for a surface-based bioreaction. The system was used to probe a small sample volume of fluorescently labelled biotin with a negative and a positive plug simultaneously. In a second example, diamagnetic forces were used to separate a mix of 5 μm and 10 μm polystyrene particles based on volume of diamagnetic material and termed free-flow diamagnetophoresis.

The use of diamagnetic repulsion forces for these two examples of common particle handling techniques only required plain commercially available polystyrene particles and a simple magnetic set-up. By suspending the particles in paramagnetic MnCl_2 solution and bringing the surface of the magnets close to the particles in the device, it was possible to see a diamagnetic repulsion effect without the need for the high magnetic fields produced by specialist superconducting magnets. However, in both cases the diamagnetic repulsion effect was still relatively weak, especially in comparison to magnetic attraction forces. For instance, with the current deflection set-up it would not be possible to deflect the polystyrene particles far enough for use in the multi-laminar flow devices. Possible ways to improve the repulsion effect on the particles would be to optimise the magnetic set-up. An array of magnets could be used, such as a Halbach array to produce a higher magnetic field gradient or the patterning of magnetic elements into the chips, such as nickel, to focus direct the field lines. In addition, a more paramagnetic ion such as Gadolinium could be used to increase the magnetic susceptibility of the medium. The gadolinium ion, when complexed to molecules such as DPTA, is considered non-toxic and would be more suitable to

biological samples than the manganese ion.[161]

Despite the relatively weak effect, diamagnetic repulsion forces show an interesting potential for handling objects in microfluidic devices not only because of the simplicity of the set-up but also because of its versatility. Many substances and compounds are intrinsically diamagnetic, such as wood, air and water and so there is a large potential for the diamagnetic handling of a variety of objects. For instance, cell handling plays an extremely important role in clinical diagnostics and cells consist mostly of water, a diamagnetic substance. Therefore the handling of cells using diamagnetic repulsion forces, without the need for labelling which can affect or damage a cell, would be of great interest.

8 Conclusions and future outlook

The aim of this work was to develop and characterise a microfluidic platform for continuous flow bioprocessing on the surface of single magnetic particles. In order to achieve this, the research was separated into three sections 1) the selection of a magnetic particle suitable for a mobile solid support, 2) characterisation of laminar flow and performance of a proof – of – principle one step bioreaction and 3) the application of the optimised system to a multiple step sandwich immunoassays. In addition, the applicability of diamagnetic repulsion forces to on-chip particle handling was also investigated. In this chapter the achievements of the work will be summarised and discussed, along with considerations for future work on the project.

8.1 Particle selection

A study concerned with the selection of a suitable magnetic particle type to be ultimately used as a mobile solid support inside a microfluidic system was performed. The comparison of eight different magnetic particles, ranging in size and magnetic content, by free-flow magnetophoresis was presented. The different particle types were pumped through a square deflection chamber and a magnetic field applied perpendicular to flow. Particles were characterised by the degree of deflection induced by the magnetic field. The effect of flow rate and the magnetic set-up on the deflection behaviour was investigated.

Four different magnetic set-ups were tested utilising to different sized NdFeB disc magnets, 20 mm for magnetic set-up 1 and 4, and 10 mm in diameter for magnetic set-

up 3 and 4. Each magnetic set-up produced a different magnetic flux density at the particle stream, Mag2 produced the highest flux at 61 mT and Mag 3 the lowest at 20 mT. The best deflection behaviour was achieved with magnetic set-up 4, which produced a flux density of 41 mT at the particle inlet. This was because high flux densities caused particles to agglomerate and particles to become trapped in the chamber. Magnetic set-ups with lower flux densities did not induce as good particle deflection.

The effect of flow rate on the deflection behaviour of particles was investigated. Particles were not deflected at flow rates between $500 \mu\text{L h}^{-1}$ and $50 \mu\text{L h}^{-1}$. It was observed at higher flow rates the particles were not deflected as far as particles at lower rates due to the strong influence of \mathbf{u}_{hyd} and the short time the particles spent in the deflection chamber. However, at lower flow rates the particle through-put was very low and therefore also undesirable. An optimal flow rate of $300 \mu\text{L h}^{-1}$ was determined with particles being deflected up to 3 mm with an average particle through-put of 60 particles per five min experiment.

The on-chip magnetically induced velocity, \mathbf{u}_{mag} , of the different particles was compared with what was expected from manufacturers' data. Particles with a higher magnetisation were expected to be deflected further than a particle with a lower magnetisation. Despite good correlation between expected deflection behaviour and what was observed on-chip within each particle brand, there were discrepancies discovered between particles from different manufacturers. For example, the Micromer $10 \mu\text{m}$ particles were expected to be deflected further than Dynabead MyOne particles based on magnetisation values calculated from manufacturer's data, however on-chip the MyOne particles were deflected the most. Further characterisation was performed

using a VSM machine to measure the saturation magnetisation of the particles independently of the manufacturers' data. The magnetisation values measured by the VSM machine were in good agreement with the observed on-chip deflection behaviour suggesting that larger particles, such as the Micromer 10 μm particles, may not necessarily contain as much magnetic material and independent measurements of magnetic properties should be performed.

The eight magnetic particle types were characterised and compared in order to find an a particle that would later be used as a mobile solid support. Ideally the particle type would be deflected the furthest and with minimum agglomeration and sticking. The Dynabead M-270 particles were deflected the furthest at 3 mm with an optimum flow rate of 300 $\mu\text{L h}^{-1}$ at magnetic set-up 4 and thus were chosen as the solid support for the rest of the project.

Although free-flow magnetophoresis is primarily a separation technique, it has also proved a simple and effective way of characterising magnetic particles with different magnetic properties and sizes. This work has emphasised that careful consideration is needed when choosing a magnetic particle type as a solid support as theoretical expectations of particle behaviour in a magnetic field based on manufacturer's data maybe not be observed experimentally and independent characterisation should be performed.

8.2 One step bioassays

A method for performing continuous flow bioprocessing on the surface of single magnetic particles was presented. Functionalised magnetic particles were pumped into a

rectangular reaction chamber along which multiple laminar flow streams were generated containing bioreagents for an assay. As the particles were deflected across the streams, washing steps and a reaction step were performed on the particle surface in continuous flow. The particles were detected in real time using fluorescence microscopy and signals analysed using data analysis software.

A microfluidic device (MLF1), featuring four fluid inlets, a rectangular reaction chamber 3 mm wide and a single outlet was investigated. Multi-laminar flow streams were generated along the chamber under positive pressure and were found to be stable over long periods of time without mixing. The magnetic set-up of the device was optimised using a small rectangular magnet and balanced against the applied flow rate to achieve the deflection of Dynabead M-270 particles across the 3 mm wide chamber. The optimal flow rate was found to be $100 \mu\text{L h}^{-1}$ ($460 \mu\text{m s}^{-1}$).

The molecular recognition between streptavidin and biotin was chosen as a proof-of-principle bioassay to test the system. Streptavidin coated particles were deflected across the chamber such that they traversed a washing stream, a stream containing fluorescently labelled biotin and a final washing / detection stream. A method for detecting and analysing the particles was also developed.

Once the bioassay was optimised in terms of buffers and data acquisition, the effect of the concentration of biotin was investigated. The LOD of the system was 20 ng mL^{-1} and the dynamic range was 20 ng mL^{-1} to 200 ng mL^{-1} . The entire analytical procedure was performed within one minute with no manual intervention.

The system was shown to successfully perform a one-step bioassay in continuous flow. By generating the multiple laminar flow streams, all steps of the assay including

separation, washing, analyte binding and detection was performed in a single operation on one device requiring no intervention from the operator. The design and set-up of the device was extremely simple, with a single syringe pump and a small magnet. The entire procedure was performed in less than one minute, a reduction in the time usually required for a bioassay and with a reagent consumption of only 2 μL per experiment.

8.3 Two-step bioassays

The next stage of the project was to investigate whether the device could perform more reactions steps, usually required by conventional bioanalytical techniques such as immunoassays. A device capable of performing two washing steps and two reactions steps was demonstrated for a mouse IgG immunoassay and also a clinically relevant sandwich immunoassay for C-reactive protein.

A new chip design (MLF2) was used featuring five inlets and a longer reaction chamber was characterised. In bioanalytical procedures, cross contamination between reagents is undesirable and experiments were performed into the diffusion of reagents inside the chamber. This was investigated by using the reaction between iron and thiocyanate to produce a red complex on mixing. Diffusion between adjacent streams in the chamber was analysed and no mixing between reagents streams was observed.

The MLF2 chip design was then used to perform an immunoassay in which streptavidin coated M-270 particles were deflected across a stream containing biotinylated mouse IgG, a washing stream followed by a stream of fluorescently labelled anti-mouse IgG and then into a final wash / detect stream. Particles were videoed using a high sensitivity camera with a cooled CCD and analysed. The LOD for the mouse IgG

immunoassay was $0.1 \mu\text{g mL}^{-1}$, with a dynamic range between $0.1 \mu\text{g mL}^{-1}$ and $10 \mu\text{g mL}^{-1}$.

The device was then used to perform a more clinically relevant assay and the detection of CRP was chosen as the clinical range for the test was suitable to that of the device. M-270 particles surface functionalised with anti-CRP antibodies were deflected across a stream of, a washing stream, a stream of fluorescently labelled anti-CRP antibodies and a final wash / detect stream. Preliminary results were obtained for a CRP concentration of $10 \mu\text{g mL}^{-1}$. The reagent consumption of antibodies per experiment was $3.3 \mu\text{L}$.

The multi-laminar flow device was proven to be capable of performing two-step bioanalytical procedures in continuous flow. The entire immunoassay method, both for the mouse IgG and the CRP analytes, was executed in a single operation with a procedural time of less than one min, a fraction of the time required for conventional immunoassay techniques and an improvement on current on-chip times. Whilst the method is not as sensitive as some other on-chip methods, the extremely short procedural times would be desirable in a situation when a quick qualitative result is required or for tests with higher detection ranges. The simplicity of the system would be advantageous in developing a truly portable device as no bulky equipment is required for manipulating the magnetic particles compared to other particle handling techniques such as DEP or optical tweezers. In addition, magnetic particles are commercially available in a wide range of surface functionalities, and hence the system is potentially extremely versatile.

8.4 Diamagnetic repulsive forces for particle handling

The applicability of diamagnetic repulsion forces was investigated for performing two commonly used on-chip particle handling techniques; particle trapping and particle deflection, by suspending diamagnetic polystyrene particles in paramagnetic solutions of MnCl_2 . The particle trapping was utilised for a surface based bioreaction and the particle deflection for the size-selective diamagnetophoretic separation of two particle populations.

For the diamagnetic trapping of particles simple glass capillary was used with two magnets fixed either side, opposite poles facing and a suspension of diamagnetic particles was pumped into the capillary. Diamagnetic material is repelled by high magnetic field gradients and thus they were repelled by the high field gradient between the two magnets. As a result, a particle plug was formed upstream from the magnet set-up. The flow rate was optimised to achieve 100 % trapping efficiency, which was found to be $10 \mu\text{L h}^{-1}$ ($354 \mu\text{m s}^{-1}$). A second set of magnets was then added so that a second plug was formed upstream from the first. The optimum flow rate for 100 % trapping efficiency in the second plug was $7 \mu\text{L h}^{-1}$ ($247 \mu\text{m s}^{-1}$).

The system was then used for a surface based bioreaction by trapping a plug of plain polystyrene particles and a plug of streptavidin coated polystyrene particles. A solution of fluorescently labelled biotin was flushed over the surface of the particles and the biotin selectively bound to the plug of streptavidin particles such that a positive and a negative control were performed simultaneously.

In addition to this, the trapping of a mixture of diamagnetic and superparamagnetic particles was also investigated. The particle mixture was observed to separate out, with

diamagnetic particles being trapped upstream of the magnets and the superparamagnetic particles were trapped in the high field gradient between the magnets. Eight separate particle plugs were trapped with three magnet set-ups on one capillary and 100 % trapping efficiency was achieved at a flow rate of $8 \mu\text{L h}^{-1}$ in a time of 40 min.

Diamagnetic repulsion forces for the deflection of polystyrene particles was investigated using the FFM microchip device used for the particles selection experiments. A magnet was placed next to the particle inlet and a suspension of diamagnetic particles in MnCl_2 was pumped through the chamber. The polystyrene particles were repelled from the field produced by the magnet and were deflected from flow. The amount of diamagnetic repulsive force experienced by the particles depends on the volume of diamagnetic material and thus this system was used to investigate diamagnetic repulsion forces for the size-selective separation of a mixture of two particle populations of different sizes; $5 \mu\text{m}$ particles and $10 \mu\text{m}$ particles.

The effects of flow rate on the separation was investigated and at a flow rate of $20 \mu\text{L h}^{-1}$ the two particle populations were separated into different exits, with the $10 \mu\text{m}$ particles being deflected further than the $5 \mu\text{m}$ particles.

Diamagnetic repulsion forces for the manipulation of particles in microfluidic devices are label free, simple and rely on the intrinsic properties of the particles themselves. The work has proven these forces can be utilised for the on-chip handling of particles for use in bioanalytical procedures. In addition, water is a diamagnetic substance and because cells are made up mostly of water, diamagnetic forces could potentially be utilised for the label free handling of cells in microfluidic devices.

8.5 Outlook for the future

Continuous flow bioassays

A number of improvements could be made to the multi-laminar flow system, mainly in the area of magnetic particle handling. One of the main problems of the system was the sticking of particles in the chamber, probably due to both the inhomogeneous magnetic field and temperature fluctuations in the laboratory. The latter could be managed with a temperature control system on the chip, such as a Peltier element. The former could be addressed by a more detailed look into the magnetic set-up of the device. So far only small, simple permanent magnets have been used, but the field gradients produced by these devices are not only inhomogeneous in the y-direction, but also in x-direction along the chamber and in the z-direction, perpendicular to the plane of the device. Some effort was made to limit the gradient in the z-direction by drilling a hole into the device to place the magnet in such that the chamber is in the same plane as the magnet. However, in order to design and modify a homogenous magnetic gradient over the x- and y- direction over the chamber, accurate modelling of the field would be required.

Another area that could be improved is the sensitivity of the system which could be achieved by lengthening the residence time of the particles in the reagent streams. One way to do this would be simple modification of the field and the flow rate to slow the particles down as they traverse the chamber. Another would be to alter the chip design and widen the reagent streams but this would increase the amount of reagents consumed per experiment. Magnetic elements in conjunction with electromagnets could also be incorporated into the chamber to hold the particles in the stream for a specified length of time. However, this would require power supply and would increase the overall

procedural time.

Diamagnetic forces for particle handling

One of the limitations of using diamagnetic repulsion forces for on-chip particle handling is that the forces exerted on the particles are relatively weak compared to magnetic attraction forces. One way to increase the force would be to use a higher magnetic field gradient, such as those produced by a Halbach array or by focussing the magnetic field with intelligent field design. Another would be to suspend the particles in solutions of gadolinium, which is more paramagnetic than manganese and also more biocompatible.

Future experiments may include the manipulation of cells using diamagnetic repulsion forces or trying similar experiments to the continuous flow bioassays by repelling particles across multiple reagent streams.

References

- [1] Kawaguchi, H., *Progress in Polymer Science* 2000, 25, 1171-1210.
- [2] Peterson, D. S., *Lab on a Chip* 2005, 5, 132-139.
- [3] Verpoorte, E., *Lab on a Chip* 2003, 3, 60N-68N.
- [4] Manz, A., Graber, N., Widmer, H. M., *Sensors and Actuators B-Chemical* 1990, 1, 244-248.
- [5] Nilsson, J., Evander, M., Hammarstrom, B., Laurell, T., *Analytica Chimica Acta* 2009, 649, 141-157.
- [6] Sato, K., Tokeshi, M., Odake, T., Kimura, H., *et al.*, *Analytical Chemistry* 2000, 72, 1144-1147.
- [7] Sato, K., Tokeshi, M., Kimura, H., Kitamori, T., *Analytical Chemistry* 2001, 73, 1213-1218.
- [8] Sato, K., Yamanaka, M., Takahashi, H., Tokeshi, M., *et al.*, *Electrophoresis* 2002, 23, 734-739.
- [9] Sato, K., Yamanaka, M., Hagino, T., Tokeshi, M., *et al.*, *Lab on a Chip* 2004, 4, 570-575.
- [10] Oleschuk, R. D., Shultz-Lockyear, L. L., Ning, Y. B., Harrison, D. J., *Analytical Chemistry* 2000, 72, 585-590.
- [11] Andersson, H., van der Wijngaart, W., Enoksson, P., Stemme, G., *Sensors and Actuators B-Chemical* 2000, 67, 203-208.
- [12] Andersson, H., van der Wijngaart, W., Stemme, G., *Electrophoresis* 2001, 22, 249-257.
- [13] Satoh, T., Shinoda, Y., Tokonami, S., Hirota, R., *et al.*, *Sensors and Actuators B-Chemical* 2009, 142, 118-122.
- [14] Bergkvist, J., Ekstrom, S., Wallman, L., Lofgren, M., *et al.*, *Proteomics* 2002, 2, 422-429.
- [15] Seong, G. H., Zhan, W., Crooks, R. M., *Analytical Chemistry* 2002, 74, 3372-3377.
- [16] Russom, A., Tooke, N., Andersson, H., Stemme, G., *Analytical Chemistry* 2005, 77, 7505-7511.
- [17] Buranda, T., Huang, J. M., Perez-Luna, V. H., Schreyer, B., *et al.*, *Analytical Chemistry* 2002, 74, 1149-+.

References

- [18] Piyasena, M. E., Buranda, T., Wu, Y., Huang, J. M., *et al.*, *Analytical Chemistry* 2004, 76, 6266-6273.
- [19] Murakami, Y., Endo, T., Yamamura, S., Nagatani, N., *et al.*, *Analytical Biochemistry* 2004, 334, 111-116.
- [20] Jeong, Y., Choi, K., Kim, J., Chung, D. S., *et al.*, *Sensors and Actuators B-Chemical* 2008, 128, 349-358.
- [21] Malmstadt, N., Hoffman, A. S., Stayton, P. S., *Lab on a Chip* 2004, 4, 412-415.
- [22] Sivagnanam, V., Song, B., Vandevyver, C., Gijs, M. A. M., *Analytical Chemistry* 2009, 81, 6509-6515.
- [23] Velev, O. D., Bhatt, K. H., *Soft Matter* 2006, 2, 738-750.
- [24] Muller, T., Gradl, G., Howitz, S., Shirley, S., *et al.*, *Biosensors & Bioelectronics* 1999, 14, 247-256.
- [25] Li, H. B., Zheng, Y. N., Akin, D., Bashir, R., *Journal of Microelectromechanical Systems* 2005, 14, 103-112.
- [26] Yasukawa, T., Suzuki, M., Sekiya, T., Shiku, H., Matsue, T., *Biosensors & Bioelectronics* 2007, 22, 2730-2736.
- [27] Mela, P., van den Berg, A., Fintschenko, Y., Cummings, E. B., *et al.*, *Electrophoresis* 2005, 26, 1792-1799.
- [28] Ino, K., Shiku, H., Ozawa, F., Yasukawa, T., Matsue, T., *Biotechnology and Bioengineering* 2009, 104, 709-718.
- [29] Barbee, K. D., Hsiao, A. P., Heller, M. J., Huang, X. H., *Lab on a Chip* 2009, 9, 3268-3274.
- [30] Ashkin, A., Dziedzic, J. M., *Science* 1987, 235, 1517-1520.
- [31] Neuman, K. C., Block, S. M., *Review of Scientific Instruments* 2004, 75, 2787-2809.
- [32] Svoboda, K., Block, S. M., *Annual Reviews in Biophysical and Biomolecular Structures* 1994, 247 - 285.
- [33] Birkbeck, A. L., Flynn, R. A., Ozkan, M., Song, D. Q., *et al.*, *Biomedical Microdevices* 2003, 5, 47-54.
- [34] Ozkan, M., Wang, M., Ozkan, C., Flynn, R., *et al.*, *Biomedical Microdevices* 2003, 5, 61-67.
- [35] Ramser, K., Enger, J., Goksor, M., Hanstorp, D., *et al.*, *Lab on a Chip* 2005, 5, 431-436.
- [36] Jess, P. R. T., Garces-Chavez, V., Riches, A. C., Herrington, C. S., Dholakia, K.,

- Journal of Raman Spectroscopy* 2007, 38, 1082-1088.
- [37] Petrov, D. V., *Journal of Optics a-Pure and Applied Optics* 2007, 9, S139-S156.
- [38] Fuller, D. N., Gemmen, G. J., Rickgauer, J. P., Dupont, A., *et al.*, *Nucleic Acids Research* 2006, 34.
- [39] Applegate, R. W., Squier, J., Vestad, T., Oakey, J., Marr, D. W. M., *Optics Express* 2004, 12, 4390-4398.
- [40] Hart, S. J., Terray, A. V., Arnold, J., *Applied Physics Letters* 2007, 91.
- [41] Cran-McGreehin, S., Krauss, T. F., Dholakia, K., *Lab on a Chip* 2006, 6, 1122-1124.
- [42] Lai, C. W., Hsiung, S. K., Yeh, C. L., Chiou, A., Lee, G. B., *Sensors and Actuators B-Chemical* 2008, 135, 388-397.
- [43] Blakely, J. T., Gordon, R., Sinton, D., *Lab on a Chip* 2008, 8, 1350-1356.
- [44] Liu, Y., Yu, M., *Optics Express* 2009, 17, 21680 - 21690.
- [45] Yasuda, K., *Sensors and Actuators B-Chemical* 2000, 64, 128-135.
- [46] Lilliehorn, T., Simu, U., Nilsson, M., Almqvist, M., *et al.*, *Ultrasonics* 2005, 43, 293-303.
- [47] Svennebring, J., Manneberg, O., Skafte-Pedersen, P., Bruus, H., Wiklund, M., *Biotechnology and Bioengineering* 2009, 103, 323-328.
- [48] Manneberg, O., Vanherberghen, B., Svennebring, J., Hertz, H. M., *et al.*, *Applied Physics Letters* 2008, 93.
- [49] Lettieri, G. L., Dodge, A., Boer, G., de Rooij, N. F., Verpoorte, E., *Lab on a Chip* 2003, 3, 34-39.
- [50] Lin, C. M., Lai, Y. S., Liu, H. P., Chen, C. Y., Wo, A. M., *Analytical Chemistry* 2008, 80, 8937-8945.
- [51] Lutz, B. R., Chen, J., Schwartz, D. T., *Analytical Chemistry* 2006, 78, 5429-5435.
- [52] Gijs, M. A. M., *Microfluidics and Nanofluidics* 2004, 1, 22-40.
- [53] Pamme, N., *Lab on a Chip* 2006, 6, 24-38.
- [54] Fan, Z. H., Mangru, S., Granzow, R., Heaney, P., *et al.*, *Analytical Chemistry* 1999, 71, 4851-4859.
- [55] Hayes, M. A., Polson, N. A., Phayre, A. N., Garcia, A. A., *Analytical Chemistry* 2001, 73, 5896-5902.

- [56] Caulum, M. M., Henry, C. S., *Lab on a Chip* 2008, 8, 865-867.
- [57] Goral, V. N., Zaytseva, N. V., Baeumner, A. J., *Lab on a Chip* 2006, 6, 414-421.
- [58] Kwakye, S., Goral, V. N., Baeumner, A. J., *Biosensors & Bioelectronics* 2006, 21, 2217-2223.
- [59] Bronzeau, S., Pamme, N., *Analytica Chimica Acta* 2008, 609, 105-112.
- [60] Choi, J. W., Oh, K. W., Thomas, J. H., Heineman, W. R., *et al.*, *Lab on a Chip* 2002, 2, 27-30.
- [61] Choi, J. W., Liakopoulos, T. M., Ahn, C. H., *Biosensors & Bioelectronics* 2001, 16, 409-416.
- [62] Deng, T., Whitesides, G. M., Radhakrishnan, M., Zabow, G., Prentiss, M., *Applied Physics Letters* 2001, 78, 1775-1777.
- [63] Smistrup, K., Kjeldsen, B. G., Reimers, J. L., Dufva, M., *et al.*, *Lab on a Chip* 2005, 5, 1315-1319.
- [64] Smistrup, K., Lund-Olesen, T., Hansen, M. F., Tang, P. T., *Journal of Applied Physics* 2006, 99.
- [65] Abonnenc, M., Gassner, A. L., Morandini, J., Josserand, J., Girault, H. H., *Analytical and Bioanalytical Chemistry* 2009, 395, 747-757.
- [66] Doyle, P. S., Bibette, J., Bancaud, A., Viovy, J. L., *Science* 2002, 295, 2237-2237.
- [67] Minc, N., Bokov, P., Zeldovich, K. B., Futterer, C., *et al.*, *Electrophoresis* 2005, 26, 362-375.
- [68] Lacharme, F., Vandevyver, C., Gijs, M. A. M., *Analytical Chemistry* 2008, 80, 2905-2910.
- [69] Lacharme, F., Vandevyver, C., Gijs, M. A. M., *Microfluidics and Nanofluidics* 2009, 7, 479-487.
- [70] Watarai, H., Namba, M., *Analytical Sciences* 2001, 17, 1233-1236.
- [71] Watarai, H., Namba, M., *Journal of Chromatography A* 2002, 961, 3-8.
- [72] Winkleman, A., Gudiksen, K. L., Ryan, D., Whitesides, G. M., *et al.*, *Applied Physics Letters* 2004, 85, 2411-2413.
- [73] Peyman, S. A., Iwan, E. Y., Margaron, O., Iles, A., Pamme, N., *Journal of Chromatography A* 2009, 1216, 9055-9062.
- [74] Choi, S., Park, J. K., *Analytical Chemistry* 2008, 80, 3035-3039.
- [75] Armani, M. D., Chaudhary, S. V., Probst, R., Shapiro, B., *Journal of*

Microelectromechanical Systems 2006, 15, 945-956.

[76] Lee, G. B., Chang, C. C., Huang, S. B., Yang, R. J., *Journal of Micromechanics and Microengineering* 2006, 16, 1024-1032.

[77] Hsu, C. H., Di Carlo, D., Chen, C. C., Irimia, D., Toner, M., *Lab on a Chip* 2008, 8, 2128-2134.

[78] Park, J. S., Song, S. H., Jung, H. I., *Lab on a Chip* 2009, 9, 939-948.

[79] Mao, X. L., Lin, S. C. S., Dong, C., Huang, T. J., *Lab on a Chip* 2009, 9, 1583-1589.

[80] Aoki, R., Yamada, M., Yasuda, M., Seki, M., *Microfluidics and Nanofluidics* 2009, 6, 571-576.

[81] Choi, S., Song, S., Choi, C., Park, J. K., *Small* 2008, 4, 634-641.

[82] Schrum, D. P., Culbertson, C. T., Jacobson, S. C., Ramsey, J. M., *Analytical Chemistry* 1999, 71, 4173-4177.

[83] Yang, R. J., Chang, C. C., Huang, S. B., Lee, G. B., *Journal of Micromechanics and Microengineering* 2005, 15, 2141-2148.

[84] Zhu, J. J., Xuan, X. C., *Electrophoresis* 2009, 30, 2668-2675.

[85] Ozkan, M., Bhatia, S., Esener, S. C., *Sensors and Materials* 2002, 14, 189-197.

[86] Enger, J., Goksor, M., Ramser, K., Hagberg, P., Hanstorp, D., *Lab on a Chip* 2004, 4, 196-200.

[87] Arai, F., Ng, C., Maruyama, H., Ichikawa, A., *et al.*, *Lab on a Chip* 2005, 5, 1399-1403.

[88] Baumgartl, J., Hannappel, G. M., Stevenson, D. J., Day, D., *et al.*, *Lab on a Chip* 2009, 9, 1334-1336.

[89] Pamme, N., *Lab on a Chip* 2007, 7, 1644-1659.

[90] Chou, C. F., Austin, R. H., Bakajin, O., Tegenfeldt, J. O., *et al.*, *Electrophoresis* 2000, 21, 81-90.

[91] Huang, L. R., Cox, E. C., Austin, R. H., Sturm, J. C., *Science* 2004, 304, 987-990.

[92] Inglis, D. W., Davis, J. A., Austin, R. H., Sturm, J. C., *Lab on a Chip* 2006, 6, 655-658.

[93] Inglis, D. W., Davis, J. A., Zieziulewicz, T. J., Lawrence, D. A., *et al.*, *Journal of Immunological Methods* 2008, 329, 151-156.

[94] Inglis, D. W., *Applied Physics Letters* 2009, 94.

- [95] Louthback, K., Puchalla, J., Austin, R. H., Sturm, J. C., *Physical Review Letters* 2009, 102.
- [96] Vankrunkelsven, S., Clicq, D., Pappaert, K., Ranson, W., *et al.*, *Electrophoresis* 2004, 25, 1714-1722.
- [97] Schnelle, T., Muller, T., Gradl, G., Shirley, S. G., Fuhr, G., *Journal of Electrostatics* 1999, 47, 121-132.
- [98] Durr, M., Kentsch, J., Muller, T., Schnelle, T., Stelzle, M., *Electrophoresis* 2003, 24, 722-731.
- [99] Choi, S., Park, J. K., *Lab on a Chip* 2005, 5, 1161-1167.
- [100] Narayanan, N., Saldanha, A., Gale, B. K., *Lab on a Chip* 2006, 6, 105-114.
- [101] Li, Y. L., Dalton, C., Crabtree, H. J., Nilsson, G., Kaler, K., *Lab on a Chip* 2007, 7, 239-248.
- [102] Barrett, L. M., Skulan, A. J., Singh, A. K., Cummings, E. B., Fiechtner, G. J., *Analytical Chemistry* 2005, 77, 6798-6804.
- [103] Lewpiriyawong, N., Yang, C., Lam, Y. C., *Biomicrofluidics* 2008, 2.
- [104] MacDonald, M. P., Spalding, G. C., Dholakia, K., *Nature* 2003, 426, 421-424.
- [105] Milne, G., Rhodes, D., MacDonald, M., Dholakia, K., *Optics Letters* 2007, 32, 1144-1146.
- [106] Marchington, R. F., Mazilu, M., Kuriakose, S., Garces-Chavez, V., *et al.*, *Optics Express* 2008, 16, 3712-3726.
- [107] Hawkes, J. J., Coakley, W. T., *Sensors and Actuators B-Chemical* 2001, 75, 213-222.
- [108] Nilsson, A., Petersson, F., Jonsson, H., Laurell, T., *Lab on a Chip* 2004, 4, 131-135.
- [109] Petersson, F., Nilsson, A., Holm, C., Jonsson, H., Laurell, T., *Analyst* 2004, 129, 938-943.
- [110] Petersson, F., Nilsson, A., Holm, C., Jonsson, H., Laurell, T., *Lab on a Chip* 2005, 5, 20-22.
- [111] Petersson, F., Aberg, L., Sward-Nilsson, A. M., Laurell, T., *Analytical Chemistry* 2007, 79, 5117-5123.
- [112] Blom, M. T., Chmela, E., Oosterbroek, R. E., Tijssen, R., van den Berg, A., *Analytical Chemistry* 2003, 75, 6761-6768.
- [113] Yamada, M., Seki, M., *Lab on a Chip* 2005, 5, 1233-1239.

- [114] Yamada, M., Seki, M., *Analytical Chemistry* 2006, 78, 1357-1362.
- [115] Yamada, M., Nakashima, M., Seki, M., *Analytical Chemistry* 2004, 76, 5465-5471.
- [116] Takagi, J., Yamada, M., Yasuda, M., Seki, M., *Lab on a Chip* 2005, 5, 778-784.
- [117] Jain, A., Posner, J. D., *Analytical Chemistry* 2008, 80, 1641-1648.
- [118] Zhang, X. L., Cooper, J. M., Monaghan, P. B., Haswell, S. J., *Lab on a Chip* 2006, 6, 561-566.
- [119] Larsen, A. V., Poulsen, L., Birgens, H., Dufva, M., Kristensen, A., *Lab on a Chip* 2008, 8, 818-821.
- [120] Vig, A. L., Kristensen, A., *Applied Physics Letters* 2008, 93.
- [121] Bhagat, A. A. S., Kuntaegowdanahalli, S. S., Papautsky, I., *Lab on a Chip* 2008, 8, 1906-1914.
- [122] Kuntaegowdanahalli, S. S., Bhagat, A. A. S., Kumar, G., Papautsky, I., *Lab on a Chip* 2009, 9, 2973-2980.
- [123] Lin, C. H., Lee, C. Y., Tsai, C. H., Fu, L. M., *Microfluidics and Nanofluidics* 2009, 7, 499-508.
- [124] Yang, S., Undar, A., Zahn, J. D., *Lab on a Chip* 2006, 6, 871-880.
- [125] Park, J. S., Jung, H. I., *Analytical Chemistry* 2009, 81, 8280-8288.
- [126] Kim, K. S., Park, J. K., *Lab on a Chip* 2005, 5, 657-664.
- [127] Xia, N., Hunt, T. P., Mayers, B. T., Alsberg, E., *et al.*, *Biomedical Microdevices* 2006, 8, 299-308.
- [128] Siegel, A. C., Shevkoplyas, S. S., Weibel, D. B., Bruzewicz, D. A., *et al.*, *Angewandte Chemie-International Edition* 2006, 45, 6877-6882.
- [129] Lin, Y. A., Wong, T. S., Bhardwaj, U., Chen, J. M., *et al.*, *Journal of Micromechanics and Microengineering* 2007, 17, 1299-1306.
- [130] Song, S. H., Lee, H. L., Min, Y. H., Jung, H. I., *Sensors and Actuators B-Chemical* 2009, 141, 210-216.
- [131] Pamme, N., Manz, A., *Analytical Chemistry* 2004, 76, 7250-7256.
- [132] Pamme, N., Eijkel, J. C. T., Manz, A., *Journal of Magnetism and Magnetic Materials* 2006, 307, 237-244.
- [133] Pamme, N., Wilhelm, C., *Lab on a Chip* 2006, 6, 974-980.
- [134] Tarn, M. D., Peyman, S. A., Robert, D., Iles, A., *et al.*, *Journal of Magnetism and*

Magnetic Materials 2009, 321, 4115-4122.

[135] Tarn, M. D., Hirota, N., Iles, A., Pamme, N., *Science and Technology of Advanced Materials* 2009, 10.

[136] Liu, R. H., Yang, J. N., Lenigk, R., Bonanno, J., Grodzinski, P., *Analytical Chemistry* 2004, 76, 1824-1831.

[137] Eriksson, E., Enger, J., Nordlander, B., Erjavec, N., *et al.*, *Lab on a Chip* 2007, 7, 71-76.

[138] Boer, G., Johann, R., Rohner, J., Merenda, F., *et al.*, *Review of Scientific Instruments* 2007, 78.

[139] Augustsson, P., Aberg, L. B., Sward-Nilsson, A. M. K., Laurell, T., *Microchimica Acta* 2009, 164, 269-277.

[140] Morton, K. J., Louthback, K., Inglis, D. W., Tsui, O. K., *et al.*, *Lab on a Chip* 2008, 8, 1448-1453.

[141] Peyman, S. A., Iles, A., Pamme, N., *Chemical Communications* 2008, 1220-1222.

[142] Peyman, S. A., Iles, A., Pamme, N., *Lab on a Chip* 2009, 9.

[143] Tadmor, R., Hernandez-Zapata, E., Chen, N. H., Pincus, P., Israelachvili, J. N., *Macromolecules* 2002, 35, 2380-2388.

[144] Brett, C. M. A., Brett, A. M. O., *Electrochemistry: Principles, methods and applications*, Oxford University Press Inc., New York 2000.

[145] Jiles, D., *Introduction to Magnetism and Magnetic Material*, Chapman and Hall 1990.

[146] Morrish, A., *The Physical Principle of Magnetism*, IEEE Press, New York 2001.

[147] Duffin, W., *Electricity and Magnetism*, McGraw-Hill Book Company, Maidenhead 1990.

[148] Wild, D., Elsevier, Oxford 2005, p. 930.

[149] Diamandis, E. P., Christopoulos, T. K., *Clinical Chemistry* 1991, 625-636.

[150] Iiguni, Y., Suwa, M., Watarai, H., *Journal of Chromatography A* 2004, 1032, 165-171.

[151] Atkins, P., de Paula, J., *Elements of Physical Chemistry*, Oxford University Press Inc., New York 2009.

[152] Beebe, D. J., Mensing, G. A., Walker, G. M., *Annual Review of Biomedical Engineering* 2002, 4, 261-286.

[153] Gravesen, P., Branbjerg, J., Jensen, O., *Journal of Micromechanics and*

- Microengineering* 1993, 168-182.
- [154] White, F., *Viscous Fluid Flow*, McGraw - Hill 1974.
- [155] Buranda, T., Jones, G., Nolan, J., Keij, J., *et al.*, *Journal of physical Chemistry B* 1999, *103*, 3399-3410.
- [156] Wu, Y., Simons, P., Lopez, G. P., Sklar, L. A., Buranda, T., *Analytical Biochemistry* 2005, *342*, 221-228.
- [157] Li, Y. C., Ou, L. M. L., Yu, H. Z., *Analytical Chemistry* 2008, *80*, 8216-8223.
- [158] Manz, A., Pamme, N., Iossifidis, D., *Bioanalytical Chemistry*, Imperial College Press, London 2004.
- [159] L.D.R., *Handbook of Chemistry and Physics*, CRC Press 1997.
- [160] Gijs, M. A. M., Lacharme, F., Lehmann, U., *Chemical Reviews*, *110*, 1518-1563.
- [161] Vlahos, L., Gouliamos, A., Clauss, W., Kalovidouris, A., *et al.*, *Gastrointestinal Radiology* 1992, *17*, 300-304.

Appendix

- 1 **Paper # 1** – Rapid on-chip (bio)chemical procedures in continuous flow – manoeuvring through co-laminar reagent streams, *Chemical Communications*, 2008.
- 2 **Paper # 2** – The importance of particle type selection and temperature control for on-chip free-flow magnetophoresis, *Journal of Magnetism and Magnetic Materials*, 2009.
- 3 **Paper # 3** – Mobile magnetic particles as solid-supports for rapid surface-based bioanalysis in continuous flow, *Lab on a Chip*, 2009.
- 4 **Paper # 4** – A microfluidic system for performing fast, sequential biochemical procedures on the surface of mobile magnetic particles in continuous flow, *Magneto hydrodynamics*, 2009.
- 5 **Paper # 5** – Diamagnetic repulsion – a versatile tool for label-free particle handling in microfluidic devices, *Journal of Chromatography A*, 2009.

Rapid on-chip multi-step (bio)chemical procedures in continuous flow – manoeuvring particles through co-laminar reagent streams

Sally A. Peyman, Alexander Iles and Nicole Pamme*

Received (in Cambridge, UK) 29th October 2007, Accepted 17th December 2007

First published as an Advance Article on the web 18th January 2008

DOI: 10.1039/b716532c

We introduce a novel and extremely versatile microfluidic platform in which tedious multi-step biochemical processes can be performed in continuous flow within a fraction of the time required for conventional methods.

Tedious multi-step reaction processes are a common feature of many (bio)chemical procedures. A good example of this is oligonucleotide synthesis, where the addition of just a single base to a strand of DNA involves four reaction steps and four washing steps.¹ This form of synthesis is extremely important for the production of DNA primers and probes and it is of great significance to researchers interested in artificial genome production.² Other examples include bioassays, drug screening, chemical synthesis and catalyst screening.³ Despite the implementation of large scale automation, these procedures often involve highly repetitive processes that remain time consuming, labour intensive and wasteful of expensive reagents.

Microfluidics is revolutionising fluid handling in analytical chemistry and (bio)chemical synthesis.⁴ In micro devices, fluid flow behaviour is predictable and easy to control and, since diffusion distances are small, chemical processes can be performed far more quickly than with macroscale systems. Chemical analysis can be performed with reduced amounts of sample and reagents. Mass transfer can be further enhanced by the utilisation of surface functionalised particles⁵ inside microfluidic channels.^{6–8} Magnetic microparticles can be manipulated elegantly by external magnetic forces and many such particles are now commercially available with a range of different surface chemistries.⁹ A typical example of magnetic particle handling in microchannels is shown in Fig. 1a: the particles are trapped *via* an external magnet to form a ‘plug,’ different reagents are consecutively pumped through the plug. Once the desired reaction has been performed, the particles can be released for analysis or regeneration by removing the magnetic field. This concept has been demonstrated for nucleic acid hybridisation and recognition,^{10,11,12,13} immunoassays,^{14,15} and cell capture.¹⁶ Despite advantages in terms of fast and efficient binding, this process is still comparatively time consuming. Typically, such procedures take between 30 and 60 mins to complete, since reagent and washing buffers must be flushed consecutively.

Here, we present an innovative, dynamic concept for performing reactions on the surface of magnetic particles (Fig. 1b), by drawing particles through consecutive reagent streams. Due to laminar flow regimes in microfluidic devices, multiple reagent streams flowing in the *x*-direction can be generated across a chamber. Magnetic particles are introduced at one side of the chamber and a magnetic field applied perpendicular to the direction of flow. Particles experience a magnetic force in the *y*-direction and are deflected across the width of the chamber.¹⁷ Thus, the deflected particles are pulled through the different flow streams in a controlled movement and chemical reactions or binding processes can take place on their surface. This permits procedures involving multiple steps to be carried out extremely rapidly since reactions, washing steps, particle isolation and detection are all performed in one single operation in continuous flow on a particle by particle basis. To demonstrate the viability of this concept we have performed a simple binding assay and associated washing steps.

The microfluidic chip design featured four branched inlets, a rectangular reaction chamber 6 mm long and 3 mm wide and a single branched outlet (Fig. 2a). This design was suitable for

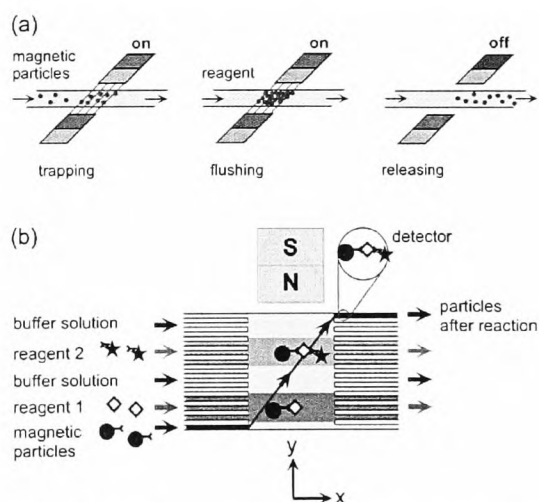


Fig. 1 (a) Surface chemistry on magnetic particles as performed conventionally: The particles are trapped and consecutively washed with reagents and washing buffers. (b) Here, a different principle is introduced whereby magnetic particles are continuously pulled through reagent streams. In the example shown above a sandwich assay is described, however, the same methodology could be applied to almost any surface based chemical process.

The University of Hull, Department of Chemistry, Cottingham Road, Hull, UK HU6 7RX. E-mail: n.pamme@hull.ac.uk; Fax: +44 1482 466416; Tel: +44 1482 465027

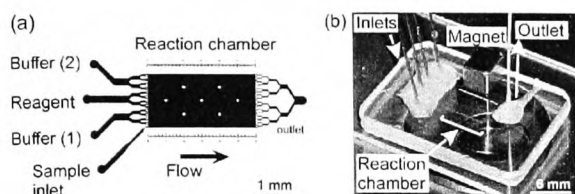


Fig. 2 (a) Schematic of the microfluidic chip design featuring a reaction chamber, four inlets and one outlet. (b) Photograph of the set-up showing the microfluidic chip and external magnet.

the introduction of particle suspension and three further liquid streams. The chip was fabricated in glass and etched to a depth of 20 μm . The magnetic field was generated by a permanent NdFeB magnet ($4 \times 5 \times 4 \text{ mm}^3$) placed on top of the chip, to the side of the chamber. Microcapillaries (i.d. 150 μm , Metal Composites, UK) were glued into the inlets and interfaced to four 1 mL Hamilton syringes (Fig. 2b). Reagent and buffer solutions and magnetic particle suspensions were pumped under positive pressure *via* a syringe pump as required (Harvard Applications, USA). The magnetic particles (2.8 μm diameter, Dynal, Invitrogen) were streptavidin coated for the binding assay or plain epoxy coated for the negative test. The buffer used was $0.1 \times \text{TBE}$ (0.1 M, pH 8.3, Sigma, UK) and the reagent was a solution of fluorescently labelled biotin (Molecular Probes, Invitrogen). The microchip was observed using an inverted fluorescence microscope (TE2000-U, Nikon, Japan) and images were captured using a CCD camera (WAT-221S, Watec, Japan) with the auto-adjustment disabled.

Initially, the generation of four parallel laminar flow streams was verified using alternating streams of yellow and blue ink such that the flow rate in the reaction chamber was $500 \mu\text{m s}^{-1}$. Since equal pressure was applied to the four syringes, the fluid streams had an equal width of 750 μm .

For the deflection of magnetic particles,¹⁷ streptavidin coated beads were pumped at a flow rate of $500 \mu\text{m s}^{-1}$ through the reaction chamber and the magnet was placed onto the device. The particles were deflected in the *y*-direction over the entire width of the chamber, crossing through the two central streams and leaving in the final stream. The force acting on the particle by the magnetic gradient was calculated to be in the pN range. A particle concentration of 6.7×10^6 beads mL^{-1} was used with an average particle throughput of 20 beads per min.

As a first example of a surface based biochemical process, a streptavidin–biotin binding assay was performed involving one binding step and two washing steps (Fig. 3). Streptavidin coated particles were introduced into inlet number 1, a buffer solution into inlet 2, a solution of fluorescently labelled biotin ($1 \mu\text{g mL}^{-1}$) into inlet 3 and a further buffer solution into inlet 4, so that the flow rate in the reaction chamber was $500 \mu\text{m s}^{-1}$. The magnetic particles were pulled through the first buffer stream and the fluorescent biotin stream and into the final buffer stream. Under fluorescent light, unreacted particles exhibited slight background fluorescence, which permitted them to be tracked in dark conditions (Fig. 3a). As the particles passed into the biotin stream, they began to fluoresce more strongly. Their fluorescence increased in intensity as they traversed the stream (Fig. 3b). After the particles left the biotin stream and moved into the last buffer stream, they continued to fluoresce, indicating that biotin had bound and been retained on their surface (Fig. 3c). The experiment was repeated using epoxy coated magnetic beads. For these beads, no change in their fluorescence was observed after traversing the biotin stream, indicating that there was little or no binding to their surface.

The experiment with streptavidin coated beads was also performed using a biotin concentration of $0.2 \mu\text{g mL}^{-1}$ and the fluorescence intensity of the particles prior to entering the biotin stream and after leaving the biotin stream was compared. Images taken from videos were analysed using ImageJ software. The relative intensities of 12 particles before and after passing through the biotin stream were averaged and plotted against distance across the particle image (Fig. 4). The residence time of the particles within the biotin stream was approximately 15 s, which is considerably longer than would be expected from the applied flow rate of $500 \mu\text{m s}^{-1}$. This was due to the placement of the magnet further towards the inlet end of the reaction chamber than the outlet end. Once the particles had passed the magnet, the field gradient was no longer perpendicular to the flow. Hence the magnet had a retarding effect on the particles, since at the point where the particles were in the biotin stream, the field was acting slightly in opposition to the flow. The time taken for each particle to cross the entire chamber was approximately 1 min. Reagent consumption of the system during an average 10 min experiment was approximately 3.6 μL of biotin and 13 μL in total including buffers and particle suspension.

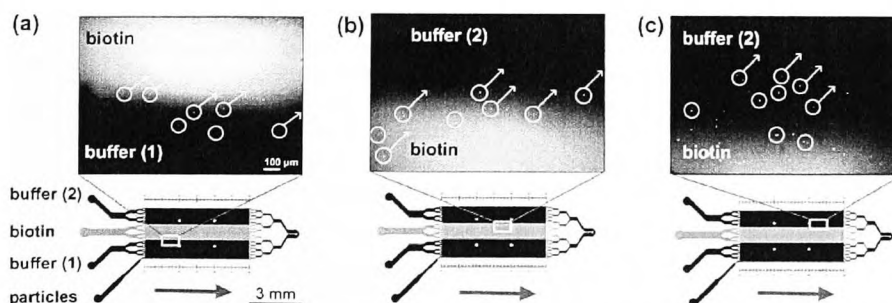


Fig. 3 Continuous flow binding, washing and isolation by pulling streptavidin coated magnetic particles through a stream of fluorescently labelled biotin into a buffer stream. (a) Particles before entering the biotin stream, (b) particles within biotin stream and (c) particles leaving biotin stream.

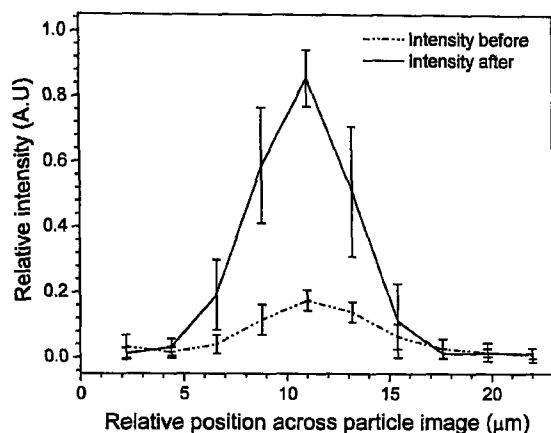


Fig. 4 Fluorescence intensity of particles before entering the biotin flow stream and after leaving the biotin flow stream.

The concentration of the biotin stream was $0.2 \mu\text{g mL}^{-1}$, therefore during the average residence time each particle spent in the biotin stream it was exposed to approximately 1.3×10^{-17} mol of biotin. According to the information supplied by the manufacturer each particle could bind 9.7×10^{-18} mol, so there is potential for the system to detect lower biotin concentrations. However, our detection was limited by the use of a primitive CCD camera with poor sensitivity. Particles became difficult to observe at lower biotin concentrations, thus to increase the sensitivity of the assay and to obtain more comprehensive quantitative results, a more sophisticated camera such as an intensified CCD could be employed.

Inter-diffusional mixing between different flow streams is extremely important for this microfluidic system. This will depend on the diffusivity of the reagents being used, the flow rate and the length of the reaction chamber. Ideally, two reagent streams should be separated by a buffer stream that is at least as wide as the maximum inter-diffusional distances of the neighbouring reagent streams. For example, in this case, for fluorescently labelled biotin in aqueous solution (diffusivity = $3.4 \times 10^{-6} \text{ cm}^2 \text{ s}^{-1}$)¹⁸ in a 6 mm long reaction chamber and a flow rate of $500 \mu\text{m s}^{-1}$, the maximum inter-diffusional distance at the end of the reaction chamber would be approximately 90 μm . Therefore, if there are two such streams separated by a buffer stream, then the buffer stream would have to be at least 180 μm wide to ensure the complete isolation of the two reagent streams.

These results successfully demonstrate the feasibility of fast sequential particle based (bio)chemistry in continuous flow. In one single operation over the course of approximately 1 min, the particles were isolated from the suspension liquid, mixed with reagent and then isolated from the reagent solution, washed and detected. This greatly reduces processing time from the 30 to 60 min in previously reported systems^{10–16} to ca. 1 min.

In this example, only four flow streams were used, however, with a suitable magnetic field design, many more flow streams could be employed.^{19,20} In addition to this, two or more devices could be connected in cascade, so that the particles from one device are fed into the next. Hence, multi-step

chemical reactions, such as sandwich immunoassays, multi-step syntheses (DNA synthesis, peptide synthesis), drug screening or even the processing of magnetically labeled cells could be performed. Limiting factors include the reaction kinetics and the number of sample molecules present in the stream that can interact with each particle as it passes through the reagent stream. These limitations could be overcome by modifying the magnetic field such that the particles are either temporarily stopped in flow,⁸ or are pulled to and fro through the reagent stream several times so that residence time is increased.

The controlled movement of particles is also not limited to magnetic forces. Many forces have been investigated for the deflection of particles in flow.²¹ These include dielectrophoretic, acoustic, optical or gravitational forces.

The reagent streams used in this work were aqueous based. However, this platform is also suitable for mixed phase systems. Therefore the streams could be for example, alternately organic and aqueous, or another combination of both.^{22–24}

A vast variety of chemical and bioanalytical reactions could be investigated in this fashion, by varying the surface chemistry of the particles and the composition of the reagent streams. Hence this novel, extremely versatile and dynamic system shows enormous potential for the fast and simple execution of multi-step processes and provides an alternative to the drudgery associated with many (bio)chemical procedures.

Notes and references

- Y. Hayakawa, S. Wakabayashi, H. Kato and R. Noyori, *J. Am. Chem. Soc.*, 1990, **112**, 1691.
- C. Zimmer, *Science*, 2003, **229**, 1006.
- P. Watts and C. Wiles, *Chem. Commun.*, 2007, 443.
- G. M. Whitesides, *Nature*, 2006, **442**, 368.
- H. Kawaguchi, *Prog. Polym. Sci.*, 2000, **25**, 1171.
- E. Verpoorte, *Lab Chip*, 2003, **3**, 60N.
- M. A. M. Gijs, *Microfluid. Nanofluid.*, 2004, **1**, 22.
- N. Pamme, *Lab Chip*, 2006, **6**, 24.
- Q. A. Pankhurst, J. Connolly, S. K. Jones and J. Dobson, *J. Phys. D: Appl. Phys.*, 2003, **36**, R167.
- Z. H. Fan, S. Mangru, R. Grazow, P. Heaney, W. Ho, Q. P. Dong and R. Kumar, *Anal. Chem.*, 1999, **71**, 4851.
- G. F. Jiang and D. J. Harrison, *Analyst*, 2000, **125**, 2176.
- S. Kwakye and A. Baeumner, *Anal. Bioanal. Chem.*, 2003, **376**, 1062.
- V. N. Goral, N. V. Zaytseva and A. J. Baeumner, *Lab Chip*, 2006, **6**, 414.
- J. W. Choi, K. W. Oh, J. H. Thomas, W. R. Heineman, H. B. Halsall, J. H. Nevin, A. J. Helmicki, H. Thurman Henderson and C. H. Ahn, *Lab Chip*, 2002, **2**, 27.
- M. A. Hayes, N. A. Polson, A. N. Phayre and A. A. Garcia, *Anal. Chem.*, 2001, **73**, 5896.
- V. I. Furdul and D. J. Harrison, *Lab Chip*, 2004, **4**, 614.
- N. Pamme and A. Manz, *Anal. Chem.*, 2004, **76**, 7250.
- A. E. Kamholz, E. A. Schilling and P. Yager, *Biophys. J.*, 2001, **80**, 1967.
- Y. Xu, F. G. Bessoth, J. C. T. Eijkel and A. Manz, *Analyst*, 2000, **125**, 677.
- D. B. Weibel, M. Kruthof, S. Potenta, S. K. Sia, A. Lee and G. M. Whitesides, *Anal. Chem.*, 2005, **77**, 4726.
- N. Pamme, *Lab Chip*, 2007, **7**, 1644.
- B. Zhao, J. S. Moore and D. J. Beebe, *Science*, 2001, **291**, 1023.
- Y. Kikutani, H. Hisamoto, M. Tokeshi and T. Kitamori, *Lab Chip*, 2004, **4**, 328.
- H. Xiao, D. Liang, G. Liu, M. Guo, W. Xing and J. Cheng, *Lab Chip*, 2006, **6**, 1067.



The importance of particle type selection and temperature control for on-chip free-flow magnetophoresis

Mark D. Tarn^a, Sally A. Peyman^a, Damien Robert^b, Alexander Iles^a, Claire Wilhelm^b, Nicole Pamme^{a,*}

^aThe University of Hull, Department of Chemistry, Cottingham Road, Hull HU6 7RX, UK

^bLaboratoire Matière et Systèmes Complexes (MSC), CNRS UMR 7057, Université Paris 7, Paris, France

ARTICLE INFO

Article history:

Received 7 October 2008

Received in revised form

29 April 2009

Available online 19 August 2009

Keywords:

Magnetic particle

Magnetophoresis

Microfluidic

Continuous flow

Separation

ABSTRACT

Free-flow magnetophoresis is becoming a popular technique for the separation and manipulation of magnetic particles and materials in microsystems. A wide variety of magnetic particles are commercially available that differ greatly in size and in magnetic properties. To investigate the suitability of different particle types for magnetophoretic operations in microfluidic devices, we compared a range of particles from three manufacturers by pumping them through a microfluidic separation chamber and deflecting them from the direction of laminar flow by applying an external magnetic field. The on-chip deflection of particles was compared to data provided by the manufacturers and magnetisation data obtained from vibrating sample magnetometer (VSM) measurements. Additionally, the extent of deflection was examined over a range of temperatures. Deflection distances were found to increase significantly with increasing temperature. Further to this, a separation of 2.8 and 1.0 μm magnetic particles was performed at different temperatures. Separation resolution was found to improve at higher temperatures. Hence, temperature manipulation provides a simple and effective means for improving a magnetic separation or for controlling the angle at which a particle is deflected from its hydrodynamic flow path.

© 2009 Elsevier B.V. All rights reserved.

1. Introduction

Magnetic microparticles have become increasingly popular as solid-supports for biomedical applications due to their high surface to volume ratio, versatility and ease of manipulation using an external magnetic field [1–4]. Most commercially available magnetic particles are composed of a polymer shell that contains either an iron oxide core or a dispersion of iron oxide nanoparticles. The presence of iron oxide nanoparticles gives rise to superparamagnetism in the particles; when a magnetic field is applied they become magnetised and are attracted to the field. When the field is removed they lose their magnetism and redisperse in solution, allowing them to be easily manipulated in small vessels such as Eppendorf tubes. Magnetic particles are widely available and can be functionalised to exhibit a variety of surface chemistries. Particles are often supplied with a particular biomolecule immobilised to their surface that is suitable for a specific reaction or assay, e.g. HIV immunoassays [5], mRNA isolation [6], and DNA hybridization [7]. Biologically active groups on the surface of the particles allow a number of binding reactions to occur that facilitate the magnetic labelling of a target material

in order for it to be separated from the bulk mixture. This is achieved simply by trapping the particles with the bound target material in a magnetic field, thus allowing separation of the target from the unwanted material which can then be removed. However, whilst this is an effective separation method, it is also time consuming and labour intensive due to the number of steps involved.

Continuous flow separations of magnetic particles [8,9] and cells labelled with magnetic nanoparticles [10] have been investigated since they have the potential to eliminate the inherent inefficiencies of batch methods. Several approaches have been suggested, including quadrupole magnetic field-flow fractionation [11] and split-flow thin (SPLITT) fractionation [12]. Magnetic separation techniques have recently gained attention due to their potential for integration into micro total analysis systems (μTAS) [3,13–17]. Such systems would facilitate the separation of target molecules or cells from a sample via the use of magnetic particles, allowing their detection and analysis downstream.

A method for continuous sorting of magnetic material, termed “on-chip free-flow magnetophoresis” has been developed (Fig. 1), and used to demonstrate the separation of magnetic particles of different sizes and magnetic susceptibilities from each other, as well as from non-magnetic particles [18,19]. The separation of cells has also been achieved using this system, by doping cells

* Corresponding author. Tel.: +44 1482 465027; fax: +44 1482 466410.
E-mail address: n.pamme@hull.ac.uk (N. Pamme).

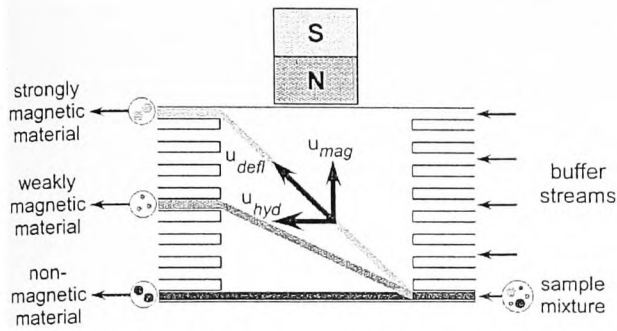


Fig. 1. The principle of free-flow magnetophoresis. Magnetic particles are deflected from the sample flow stream by the application of a magnetic field. For a given flow rate, liquid viscosity and magnetic field strength, the extent of the deflection is proportional to the volume of magnetic material present in the particle and its magnetic susceptibility.

with magnetic nanoparticles [20]. In addition to its use in magnetophoretic separations, the principles of magnetic deflection were recently utilised to perform rapid, multi-step (bio)chemical procedures in continuous flow [21], whereby a magnetic particle was deflected through laminar flow streams containing different reagents, utilising the surface groups on the particles for reaction. Hence, the extent of magnetic deflection of particles in microfluidic devices is fast becoming an important parameter.

Magnetic deflection is affected by parameters including magnetic composition of the particle, the particle size and the viscosity of the liquid. In previous work, only a small selection of commercially available microparticles has been studied. However, a wide range of magnetic particles are available from numerous manufacturers providing particles that differ greatly both in size and in their magnetic properties. Furthermore, it is expected that a change in temperature will have an impact on the carrier liquid viscosity, which in turn will significantly influence the extent of particle deflection. The effect of temperature on magnetic deflection has, to our knowledge, not yet been studied.

Here, we compare a selection of particles from three manufacturers in terms of their size, magnetic content, measured magnetisation values and on-chip deflection. Additionally, we explore the effect of temperature on the deflection of particles to determine its impact on particle manipulation in magnetophoresis. Furthermore, a separation of two particle types was undertaken at different temperatures to observe the effect of temperature on the resolution of the system.

2. Experimental section

2.1. Magnetic particles

Magnetic particles were purchased from three different manufacturers. Particles of 4.5 μm diameter (Dynabeads M-450 Epoxy) and 2.8 μm diameter (Dynabeads M-270 Epoxy), both featuring epoxy surface groups, were obtained from Invitrogen (Paisley, UK), as were particles of 1 μm diameter featuring carboxylic acid surface groups (Dynabeads MyOne Carboxylic acid). M-450 and MyOne particles were purchased as suspensions while the M-270 particles were supplied dry. Compel particles with 8 and 3 μm diameters and carboxylic acid surface groups were obtained from Bangs Laboratories Inc. (Fishers, IN, USA). Micromer particles of 10, 6 and 4 μm diameter, featuring carboxylic acid surface groups, were acquired from Micromod (Rostock-Warnemuende, Germany).

2.2. Preparation of particles for vibrating sample magnetometer

A sample of magnetic particles (1–3 mg) was dried in an oven for 2 h at 65 $^{\circ}\text{C}$, then placed in a pre-weighed nylon sample holder and the combined weight recorded. The sample holder was sealed with wood resin to ensure that the particles were fixed and attached to a vibrating sample magnetometer (VSM) probe (Lakeshore Cryotronics, USA). The magnetisation was adjusted from zero magnetic field to a field of 10,000 Oersteds (Oe) and the saturation magnetisation of the particles calculated from the resultant magnetisation versus magnetic field (M/H) loop.

2.3. Preparation of particles for on-chip magnetophoresis

Dynabeads M-270 particles were prepared according to manufacturer's specifications. 3 mg of dry Dynabeads M-270 particles (2×10^8 beads) were dispersed in 1 mL phosphate buffered saline and vortexed. The particles were collected via a magnet and the supernatant removed. This washing step was repeated twice and the particles were resuspended in 1 mL of $10 \times$ concentrated glycine saline (100 mM NaCl, 100 mM glycine, pH 8.3). All other particle solutions were obtained as aqueous suspensions and were prepared by diluting 10 μL of stock particle suspension in 990 μL of $10 \times$ glycine saline. The glycine was present to deactivate the reactive surface groups on the particles. Each solution was incubated overnight with agitation, then further diluted in $1 \times$ concentrated glycine saline buffer (10 mM glycine, 15 mM NaCl, pH 8.3) for storage at 4 $^{\circ}\text{C}$. Suspensions were diluted 1 in 10 with $0.1 \times$ concentrated glycine saline buffer solution prior to experiments, yielding particle concentrations between 2×10^5 and 6×10^9 particles mL^{-1} , depending on the particle batch.

2.4. Microchip fabrication and setup

The microchip design featured a 6 mm \times 6 mm separation chamber supported by 13 square posts of 200 μm \times 200 μm (Fig. 2). Sixteen buffer inlet channels and a single sample inlet channel were situated opposite to 16 outlet channels, and each channel was of 100 μm width. The buffer inlets were branched to allow introduction of the buffer from a single reservoir and to spread the buffer evenly throughout the chamber. The outlets were branched in a similar fashion to allow pumping via a single withdrawing syringe. The outlet branching system recombined any separated particles. For simplicity in these proof-of-principle experiments the isolation of particles at the end of the separation was not important, therefore the recombining of flows permitted the use of a single syringe pump.

The design in Fig. 2 was patterned onto a glass wafer coated with chromium and photoresist layers [22]. After photodevelopment and chrome-etching steps the exposed glass was wet etched to a depth of 20 μm . Chips were fabricated using either soda-lime (Nanofilm, Westlake Village, CA, USA) or B270 glass (Telic,

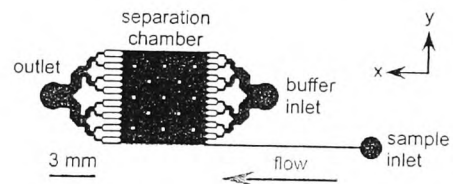


Fig. 2. Schematic of the microfluidic chip design, featuring a 6 mm \times 6 mm separation chamber, a single sample inlet channel, 16 buffer inlet channels and 16 outlet channels.

Valencia, CA, USA). Access holes were drilled into the etched plate that was subsequently pressure [23] or thermally-bonded [22] to a cover plate of soda-lime and B270, respectively. No difference in chip performance was observed between the different glass types or bonding methods.

Buffer and sample reservoirs were constructed from plastic pipette tips. These were glued around the inlet holes with epoxy, while a 10 mm section of PEEK tubing (0.5 mm i.d., Cole Parmer, London, UK) was glued into the outlet hole and interfaced to a syringe via a length of Tygon tubing (1.0 mm i.d. Cole Parmer, London, UK). Withdrawal rates between 100 and 500 $\mu\text{L}\cdot\text{h}^{-1}$ were employed by placing a 5 mL syringe in a syringe pump (Pump 11 Plus, Harvard Apparatus, Kent, UK).

The chip was pretreated for experiments by flushing with NaOH (100 mM), deionised water, and 0.1 \times concentrated glycine saline running buffer (1 mM glycine, 1.5 mM NaCl, pH 8.3) consecutively for 15 min each. Particle suspensions were introduced into the sample reservoir and glycine saline buffer into the buffer reservoir. Negative pressure was applied via the syringe pump to draw the buffer and particles through the separation chamber.

A 10 mm \times 5 mm cylindrical neodymium–iron–boron (NdFeB) magnet (Magnet Sales, Highworth, Swindon, UK) was situated on the surface of the microchip as indicated in Fig. 3(a). The

consistent positioning of the magnet was important as slight differences in placement would result in particles experiencing different forces from one experiment to another. The magnet was placed halfway over the chamber with the use of reference points in the chip design; rulers etched into the glass, the edges of the chamber and the support posts within it. The magnetic flux density, B , at the magnet surface was measured to be 320 mT, with a flux density of 47 mT at the sample inlet, using a Hall sensor (LOHET II, RS Components, Corby, UK). The magnetic flux density over the separation chamber (Fig. 3b) was simulated with FEMM 4.0 freeware (<http://femm.foster-miller.net>). For visualisation of magnetic particles inside the microchip, a zoom CCD camera (PV10, Olympus, Japan) was employed, and videos recorded on VHS. The particles were observed and counted from video footage as they exited the separation chamber via each outlet.

The temperature was controlled using a Peltier element (Thermo Module 127 TEC1-12708, Akizukidenshi, Tokyo, Japan) sandwiched between two aluminium blocks acting as heat sinks. The chip was placed on top of one of the aluminium blocks and the voltage to the Peltier element adjusted to achieve the desired temperature (Fig. 4). When temperatures below 20 °C were required, the Peltier setup was placed on top of a computer heatsink and cooling fan. The chip surface temperature was measured with a hand-held infrared sensor (Precision Gold,

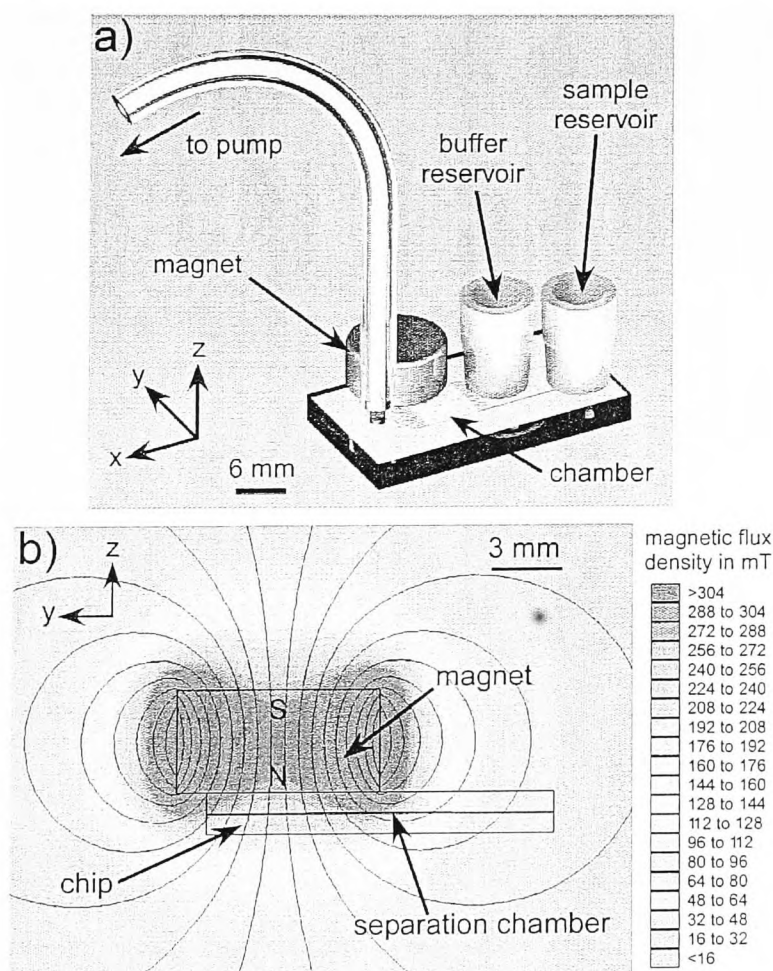


Fig. 3. (a) Chip setup, illustrating the sample and buffer reservoirs over the inlet holes, tubing for interfacing the outlet to a syringe pump, and the position of the NdFeB magnet, situated halfway over the chamber. (b) Two-dimensional simulation of the magnetic field from a side-view of the chip, demonstrating the gradient across the separation chamber. The model was generated using FEMM freeware.

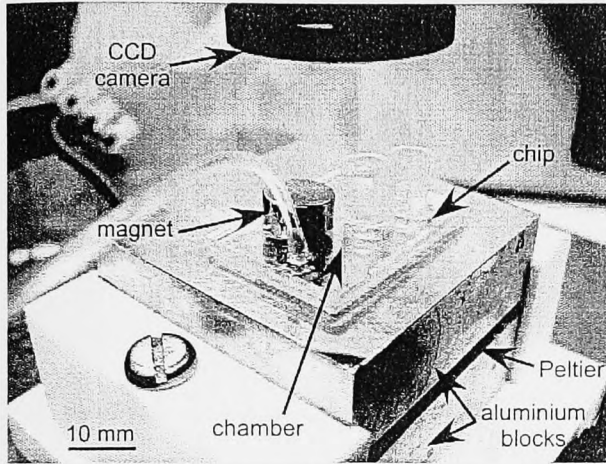


Fig. 4. Photograph of the experimental setup for determining the effect of temperature on particle deflection, utilising a Peltier element between two aluminium heat sinks. The magnetophoresis chip was fixed to one of the aluminium blocks, and an overhead CCD camera was used for observation.

Maplin Electronics, Barnsley, South Yorkshire, UK). The thermal emissivity was fixed at 0.95, suitable for glass. A thermocouple placed on the aluminium block surface was used, in combination with the chip surface readings, to estimate the temperature inside the chip.

3. Theory

3.1. Magnetic separation

The principle of free-flow magnetophoresis is shown in Fig. 1. Laminar flow is generated over a rectangular separation chamber in the x -direction. Perpendicular to the direction of flow a magnetic field is generated in the y -direction. Particles following the laminar flow experience a pull from the magnetic field and are deflected from the direction of flow. This observed velocity vector, \mathbf{u}_{defl} (m s^{-1}), of the magnetic particles is the sum of the magnetically induced movement in the y -direction due to the magnet, \mathbf{u}_{mag} and the hydrodynamic flow in the x -direction, \mathbf{u}_{hyd} :

$$\mathbf{u}_{defl} = \mathbf{u}_{mag} + \mathbf{u}_{hyd} \quad (1)$$

When the magnetic field is fixed, \mathbf{u}_{mag} remains constant and the degree of deflection depends only on the \mathbf{u}_{hyd} , which can be varied by changing the flow rate of the liquid. If the flow rate is too high, then \mathbf{u}_{hyd} dominates, particles move through the separation chamber very quickly and do not have sufficient time to interact with the magnetic field, and therefore are only deflected a short way from laminar flow. For a low flow rate, the opposite is true and particles interact strongly with the magnetic field. With extremely low flow rates, \mathbf{u}_{mag} dominates and particles become trapped in the magnetic field and therefore they do not exit the separation chamber. An optimal flow rate for a particular magnetic setting has to be established to achieve the best observed deflection for any given particle.

The magnetically induced movement, \mathbf{u}_{mag} , can be described as the ratio of the magnetic force acting on the particle, \mathbf{F}_{mag} , over the opposing viscous drag force produced as the particle passes

through the medium [19]:

$$\mathbf{u}_{mag} = \frac{\mathbf{F}_{mag}}{6\pi\eta r} = \frac{1}{6} \frac{\Delta\chi V_m (\nabla B^2) / \mu_0}{\pi\eta r} \quad (2)$$

where $\Delta\chi$ is the difference in magnetic susceptibility between the particle and surrounding medium (dimensionless), V_m is the volume of magnetic material per particle (m^3), B is the magnetic flux density of the applied magnetic field (T), μ_0 is the permeability constant of free space ($4\pi \cdot 10^{-7} \text{ V s A}^{-1} \text{ m}^{-1}$), η is the liquid viscosity ($\text{kg m}^{-1} \text{ s}^{-1}$) and r is the particle radius (m). Thus, for a given magnetic field and liquid viscosity, \mathbf{u}_{mag} becomes proportional to the volume of magnetic material in a particle over its radius:

$$\mathbf{u}_{mag} \propto \frac{V_m}{r} \quad (3)$$

Therefore, different particles can be separated from each other according to their size and the volume of magnetic material.

For a particle whose magnetic constituents have reached saturation in a magnetic field, which is generally the case for superparamagnetic particles in microfluidic devices, \mathbf{u}_{mag} can also be described in terms of saturation magnetisation, M_s , and the radius of the particle, r [20].

$$\mathbf{u}_{mag} = \frac{\mathbf{F}_{mag}}{6\pi\eta r} = \frac{\mu_0 M_s(\text{particle}) \text{grad } \mathbf{H}}{6\pi\eta r} \quad (4)$$

Again, particles can therefore be separated according to their size and saturation magnetisation, M_s .

$$\mathbf{u}_{mag} \propto \frac{M_s}{r} \quad (5)$$

This principle forms the basis of free-flow magnetophoresis and thus it was used in this work to compare a variety of magnetic particles from three different commercial manufacturers.

3.2. Temperature relation to viscosity

As shown in Eq. (2), the magnetically induced velocity, \mathbf{u}_{mag} , is inversely proportional to viscosity of the buffer medium. Hence, a change in viscosity will have a marked effect on the observed deflection behaviour. One parameter that changes viscosity is temperature. The correlation between temperature and viscosity is shown in the following equation [24]:

$$\eta = A \exp(\Delta E_{vis} / RT) \quad (6)$$

where η is the viscosity coefficient in $\text{kg m}^{-1} \text{ s}^{-1}$, A is a constant, ΔE_{vis} is the activation energy for viscous flow, R is the gas constant of $8.315 \text{ J K}^{-1} \text{ mol}^{-1}$, and T is the temperature in K. The absolute viscosity, η , of $0.1 \times$ glycine saline solution was determined over a range of temperatures to illustrate the relationship between the two parameters. The kinematic viscosity (in $\text{m}^2 \text{ s}^{-1}$) of the solution was determined at 5, 10, 20, 30 and 40°C using an Ostwald viscometer (Fisher Scientific, Loughborough, UK), and the density (in kg m^{-3}) at these temperatures was measured using a density meter (DMA 35N, Anton Paar Ltd., Hertford, Hertfordshire, UK). The temperature was controlled using a refrigerated circulator (LTD6G, Grant Instruments, Shepreth, Cambridgeshire, UK). Multiplication of the kinematic viscosity and density values yielded the absolute viscosity of the glycine buffer solution, after adjustment of the values using water as a reference. A plot of absolute viscosity versus temperature allowed the extrapolation of the best fit line to obtain a value of the absolute viscosity at 50°C , which could not be measured due to the limitations of the density meter. The relationship is shown in Fig. 5.

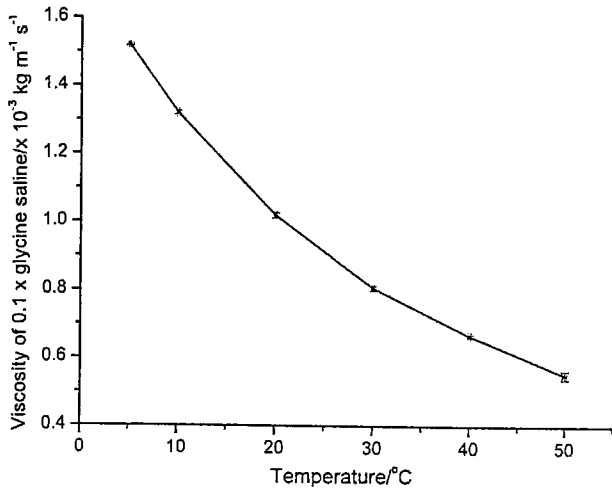


Fig. 5. The relationship between the viscosity of the 0.1 x glycine saline running buffer and the temperature of the solution. The viscosity decreases with increasing temperatures.

3.3. Theoretical particle trajectories

The expected paths of the particles were calculated from data on the magnetic field strength and gradient, particle properties, solution viscosity and flow rate. A map of the magnetic field gradient was determined across the separation chamber, as described by Pamme et al. [20].

4. Results and discussion

4.1. Comparison of particles

Eight different magnetic particles from three manufacturers were compared in terms of their magnetic loading, V_m , and magnetisation, M_s . Table 1 summarises the information provided by the manufacturers on the physical properties of the particles. In order to compare observations of deflection behaviour on-chip to theoretically expected observations the volume of magnetic material inside the particles had to be calculated (Eq. (3)). The volume of magnetic material for the Dynabeads and Compel particles could be calculated directly from the information provided on iron oxide content. The V_m/r values are listed in Table 2. However, this information was not available from Micromod. In order to obtain consistent magnetic information for all the particles, M/H curves for each particle were measured using a Vibrating Sample Magnetometer as outlined in the experimental section. From this curve the saturation

magnetisation, M_s , was calculated per particle. The corresponding M_s/r values (see Eq. (5)) are also listed in Table 2.

The deflection behaviour of the different particles was then investigated on-chip. Particle suspensions and buffer solution were pumped through the separation chamber as outlined in the experimental section. Without the influence of the magnetic field, particles were observed to follow laminar flow and exited the chamber via outlet 1, directly opposite the sample inlet channel. When a magnetic field was applied, particles were deflected from the direction of laminar flow. Fig. 6 shows the different deflection behaviour of each particle type at a flow velocity of $700 \mu\text{m s}^{-1}$, chosen as a typical example for these experiments. The Dynabeads M-270 particles deflected the furthest to outlet 5 while the MyOne particles reached outlet 4. Compel 3 μm particles, Micromod 4 and 6 μm particles exhibited similar deflection behaviour, reaching as far as outlet 3. Micromod 10 μm particles were deflected the least, leaving only via outlets 1 and 2. Dynabeads M-450 were not included in the graph because the particles showed such a strong interaction with the magnetic field at this flow velocity they became trapped in the field and did not leave the separation chamber.

By measuring the average distance travelled by the particle in the y -direction and the time taken to flow through the separation chamber, the magnetically induced velocity, u_{mag} , was calculated for each particle type (Table 3). For example, for the M-270 particles at a flow velocity of $700 \mu\text{m s}^{-1}$ the particles took an average of 8.6 s to cross the separation chamber. In that time the particles were deflected predominantly to outlet 5, corresponding to a distance of $1650 \mu\text{m}$ and an average u_{mag} of $310 \mu\text{m s}^{-1}$. The particles tended to be distributed across more than one exit (Fig. 6). Hence, the data in Table 3 refers to the average deflection observed for each particle population.

In order to compare theoretical and experimental results the values for u_{mag} , V_m/r and M_s/r were normalised with respect to the Dynabeads MyOne particles (Table 3). For the three Dynabeads particle types, the relative values clearly correlate with each other. As the magnetic content per particle increased, there was an increase in measured saturation magnetisation and an increase in

Table 2

Values for magnetic volume, V_m , over radius, r , as calculated from the information provided by the manufacturers together with values of magnetic saturation, M_s , over radius, r , as obtained from VSM measurements.

Particle	V_m/r (m^3)	M_s/r (A/m)
Dynabeads MyOne	9.4×10^{-14}	5.2×10^8
Dynabeads M-270	4.1×10^{-13}	1.4×10^7
Dynabeads M-450	1.3×10^{-12}	5.7×10^7
Compel 3 μm	3.3×10^{-13}	1.2×10^7
Compel 8 μm	3.5×10^{-13}	1.3×10^7
Micromer 4 μm	-	1.2×10^7
Micromer 6 μm	-	1.2×10^7
Micromod 10 μm	-	5.8×10^8

Table 1

Physical properties of the particles as supplied by the manufacturers.

Particle	Iron oxide content (% wt)	Mass susceptibility ($\text{m}^3 \text{kg}^{-1}$)	Saturation magnetization (emu/g)	Density (g/cm^3)
Dynabeads MyOne	20	$16 \pm 19 \times 10^{-9}$	-	1.6
Dynabeads M-270	15	$107 \pm 19 \times 10^{-9}$	-	1.6
Dynabeads M-450	26	-	-	1.8
Compel 3 μm	12	-	-	1.61
Compel 8 μm	2.4	-	-	1.09
Micromer 4 μm	-	-	3.6	1.1
Micromer 6 μm	-	-	3.6	1.1
Micromod 10 μm	-	-	-	1.1

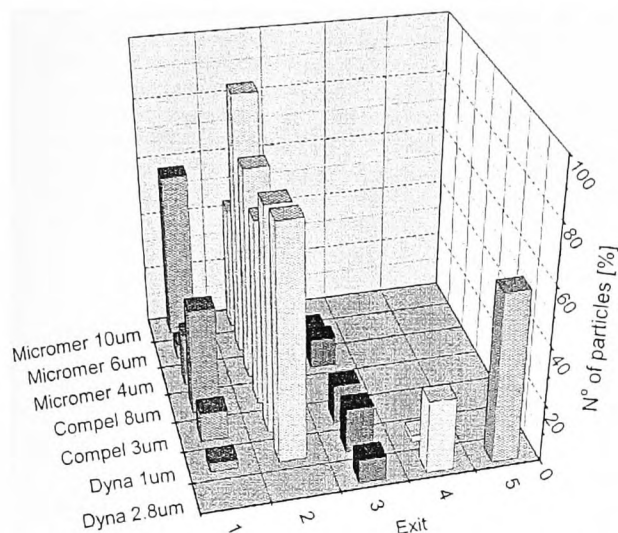


Fig. 6. Deflection behaviour of seven different particle types with corresponding exits. Dynabeads M-450 data is absent as particles became trapped in the magnetic field and did not exit the chamber.

Table 3

The observed values for magnetically induced velocity, u_{mag} , together with normalised values of u_{mag} , V_m/r and M_s/r with respect to the Dynabeads MyOne.

Particle	u_{mag} ($\mu\text{m/s}$)	Relative u_{mag}	Relative V_m/r	Relative M_s/r
Dynabeads MyOne	59	1	1	1
Dynabeads M-270	214	3.6	4.4	2.7
Dynabeads M-450	-	-	13.8	12.9
Compel 3 μm	56	0.9	4.2	2.3
Compel 8 μm	44	0.7	3.7	2.3
Micromer 4 μm	44	0.7	-	2.3
Micromer 6 μm	44	0.7	-	2.3
Micromer 10 μm	31	0.5	-	1.7

observed magnetic deflection. The same trend was observed for the two different Compel particles. However, the magnetisation values for the Dynabeads M-270 particles and the Compel 3 μm particles were slightly lower than suggested from the stated magnetic material content. This could be attributed to differences in constituent iron oxides, such as the ratio of magnetite (Fe_3O_4) to maghemite (Fe_2O_3).

As discussed in the theory section, the magnetically induced velocity is proportional to the magnetic content of the particle over the radius of the sphere (Eq. (3)). For Dynabeads particles, the observed u_{mag} values increased from the smaller particle type, MyOne, to the larger particle type, M-450. This observation is supported by the both the V_m and M_s values. The u_{mag} values for both Compel and Micromer particles remain similar despite changes in particle size which is consistent with the magnetisation results for these particles with only the Compel 3 μm particles showing a slightly higher u_{mag} value despite a similar saturation magnetisation to the Compel 8 μm particles.

However, when comparing observed u_{mag} values to magnetic content and magnetisation results for the Dynabeads against those of Compel and Micromer, it appears that the u_{mag} values for the MyOne particles and the M-270 particles far exceed the expected trends than their magnetic content and magnetisation values would suggest. MyOne, having the lowest magnetisation result, would be expected to be deflected the least of all the particles. However, they were observed to be deflected further than all of the Compel and Micromer particles used in this study. The M-270 particles had a similar

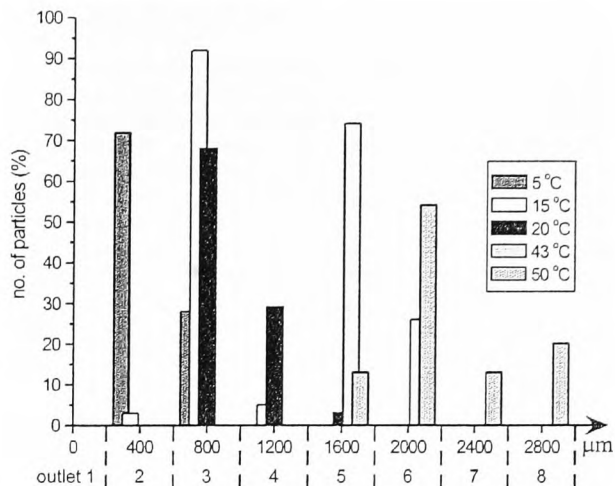


Fig. 7. The observed deflection in μm of Dynabeads M-270 at different temperatures between 5 and 50 $^{\circ}\text{C}$. The higher the temperature, the further the deflection.

magnetisation and magnetic content to the Compel 3 μm particles, however they were observed to deflect two outlets further than the Compel 3 μm . These observations are surprising and a more thorough investigation would have to be carried out to discover the reasons for such anomalous results.

4.2. Temperature dependent deflection of magnetic particles

Following the comparison of different types of magnetic particles, a study was conducted into the effect of temperature on particle deflection. The magnetically induced velocity u_{mag} is inversely proportional to the medium viscosity (Eq. (2)), which in turn changes with temperature (see Eq. (6) and Fig. 5). To determine the extent by which particle deflection is affected by changes in temperature, a series of experiments were undertaken in which a single particle type, Dynabeads M-270, was pumped through the microchamber and deflection was observed at five different temperatures between 5 and 50 $^{\circ}\text{C}$. The applied flow velocity was chosen to be 900 $\mu\text{m s}^{-1}$, as a typical example. The results for this are shown in Fig. 7. As expected, the least amount of deflection was seen at lower temperatures, whereas at higher temperatures greater deflection distances were observed. At room temperature, 20 $^{\circ}\text{C}$, the particles mostly exited via outlets 3 and 4, with some leaving the chamber at outlet 5. At a temperature of 50 $^{\circ}\text{C}$, the particles were deflected as far as outlet 8, with most exiting at outlet 6. The lower viscosity of the glycine saline, resulting from the increased temperature, exerted a lower drag force on the particles and this led to a higher degree of particle deflection. When lowering the temperature to 5 $^{\circ}\text{C}$, deflection distances were reduced, and the majority of particles exited the chamber at outlet 2 and some at outlet 3. The spread of the particles throughout the temperature range was relatively constant, with particles generally exiting via two or three adjacent exits, equivalent to a distribution across 200–400 μm . The exception to this was the spread at 50 $^{\circ}\text{C}$, where particles exited over four outlets, equivalent to a distribution across 600 μm .

The theoretically expected deflection was also calculated as described in Section 3.3. This is shown in Fig. 8, where the solid black lines represent the calculated particle paths, and the shaded areas around each line correspond to the observed trajectories. The figure shows that the calculated and experimental results match very well for the 20 and 50 $^{\circ}\text{C}$ temperatures. For 5 $^{\circ}\text{C}$ the

experimental results showed most particles exiting via outlet 2 rather than the expected outlet 3, possibly due to the starting position of the particles being different in the experiment. The spread of particles is not accounted for in the calculated paths as the particles are shown to enter the chamber from exactly the same position, and so only the outlet expected to have the highest percentage of particles exiting is shown. Generally however, these theoretical trajectories give a good indication of the distance a particle will travel due to the magnetic field.

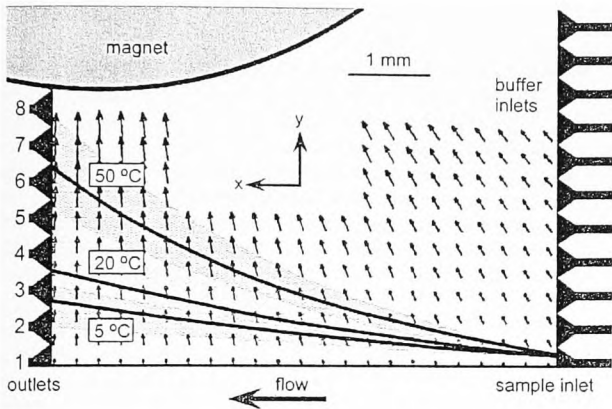


Fig. 8. Calculated trajectories of Dynabeads M-270 particles, shown as solid black lines, through the separation chamber at three temperatures. The shaded areas surrounding each trajectory line indicate the spread of the particle paths observed experimentally. The arrows indicate the direction and magnitude of the magnetic field gradient throughout the chamber. An arrow 1 mm in length on the given scale is equivalent to a gradient of 60 T m^{-1} , typical values in the chamber are therefore around 10 T m^{-1} .

4.3. Separation of particles

Having observed substantial differences in particle deflection over a range of temperatures, a separation of particles was performed to determine how temperature affects the resolution of the system. A mixture of Dynabeads M-270 particles and Dynabeads MyOne particles was pumped through the microchip at a flow rate of $900 \mu\text{m s}^{-1}$. The number of particles exiting each outlet was counted from CCD footage. The separation was performed at 5, 20 and 50 °C and the results are summarised in Fig. 9. The u_{mag} values were also determined and are summarised in Table 4. At 5 °C the majority of the two particle types were deflected into outlets 2 and outlet 3, respectively (Fig. 9a). There was some overlap of the two populations at outlet 2. The separation was improved by increasing the temperature to 20 °C, with most of the larger M-270 particles leaving via outlet 4 and most of the MyOne particles via outlet 2, although a small degree of crossover between particle types was still observed at outlet 3 (Fig. 9b). At 50 °C, full separation of the two particle populations was achieved, the majority of M-270 particles exited as far as outlet 6 and 7 whilst the MyOne particles mostly exited via outlets 2 and 3 (Fig. 9c). These results illustrate how increasing the temperature of the system can improve the resolution of the separation between different magnetic particles.

Table 4
The magnetically induced velocity, u_{mag} , of Dynabeads MyOne and M-270 particles at different temperatures.

Temperature (°C)	MyOne u_{mag} ($\mu\text{m s}^{-1}$)	M-270 u_{mag} ($\mu\text{m s}^{-1}$)
5	21 ± 1	92 ± 5
20	46 ± 5	125 ± 8
50	73 ± 6	342 ± 31

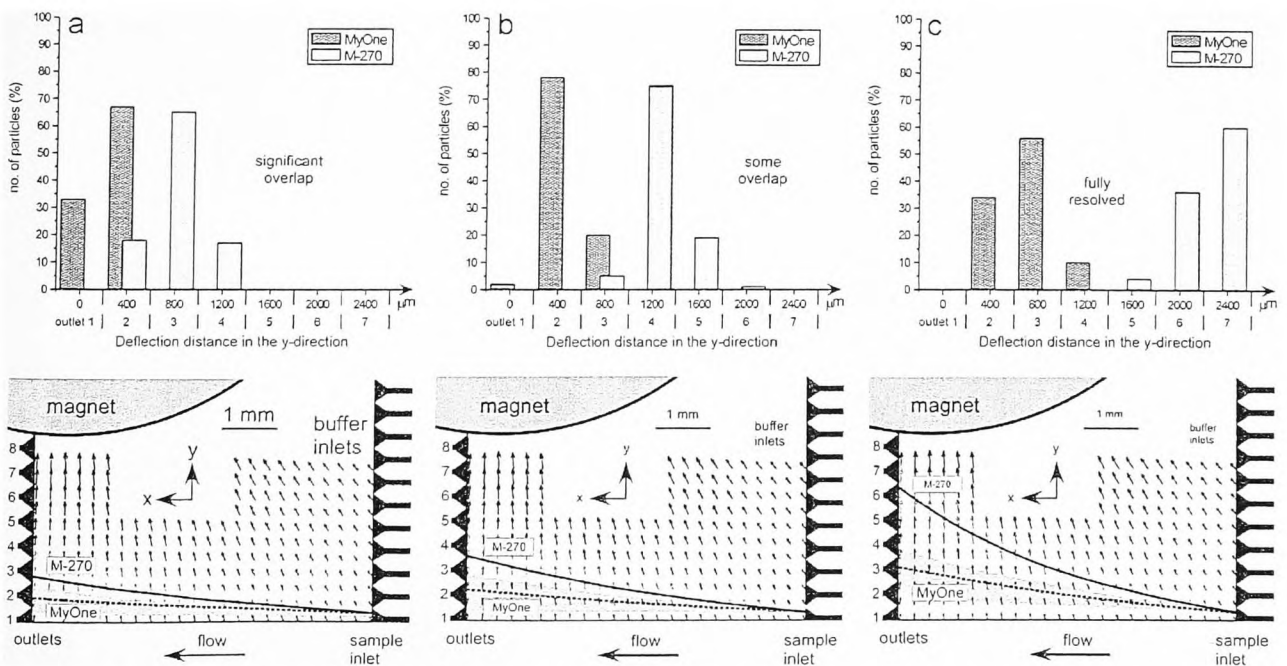


Fig. 9. Separation of Dynabeads MyOne and Dynabeads M-270 particles at (a) 5 °C, (b) 20 °C, and (c) 50 °C. The images below each graph illustrate the calculated particle trajectories for the smaller and larger particles in dotted and solid black lines, respectively. The shaded areas surrounding the lines demonstrate the spread of particles across the outlets observed experimentally.

Theoretical particle trajectories were calculated for the separation at the three temperatures. The experimental results compared well with the theoretical paths, particularly at the lower temperatures. At 5 and 20 °C (Fig. 9a, b) the majority of particles in the experiments were found to exit via the outlets expected by the theory. The calculated trajectory at 50 °C indicated that most particles should exit at outlet 6 whereas in the experiment most particles took outlet 7 (Fig. 9c). However, a large number of particles did leave the chamber at outlet 6, and the slight discrepancy may again be due to the position at which the particles entered the chip.

5. Conclusions

The magnetic deflection behaviour of eight different particle types from three companies was compared. The Dynabeads were found to feature the largest magnetically induced deflection from the direction of laminar flow and considerable variations in deflection behaviour between particles from different manufacturers was observed. This comparison shows the differences in the physical properties of the many commercially available magnetic particles and also highlights that some particle types are potentially more suitable than others for on-chip magnetophoresis. In a further study, the effect of temperature on the magnetic deflection behaviour of particles was investigated. It was found that increasing the temperature, and thus decreasing the viscosity of the carrier liquid, led to an increase in the extent by which a magnetic particle was deflected from the direction of laminar flow. Furthermore, it was shown how the separation of two particle populations can be optimised using temperature. These findings indicate that (i) in on-chip magnetophoresis, it is important to control temperature to obtain repeatable separations, and that (ii) as a variable, temperature can be easily manipulated to improve the resolution of a separation, or to achieve a specific particle deflection distance. This work exemplifies the fact that appropriate particle type selection and operating temperature are crucially important parameters for many on-chip magnetophoretic procedures.

Acknowledgements

The authors thank Neil Dearing for assistance with VSM measurements, Ibrahim Salama for help with the viscosity measurements, and the Engineering and Physical Sciences Research Council (EPSRC) for funding.

References

- [1] Q.A. Pankhurst, J. Connolly, S.K. Jones, J. Dobson, *J. Phys. D: Appl. Phys.* 36 (2003) R167–R181.
- [2] M.A.M. Gijs, *Microfluid. Nanofluid.* 1 (2004) 22–40.
- [3] N. Pamme, *Lab. Chip* 6 (2006) 24–38.
- [4] E. Verpoorte, *Lab. Chip* 3 (2003) 60N–68N.
- [5] M.A. Sommerfeld, I. Ohlsson, I. Flolid, R. Thorstensson, B. Sorensen, *J. Virol. Methods* 115 (2004) 191–198.
- [6] G.F. Jiang, D.J. Harrison, *Analyst* 125 (2000) 2176–2179.
- [7] Z.H. Fan, S. Mangru, R. Granzow, P. Heaney, W. Ho, Q.P. Dong, R. Kumar, *Anal. Chem.* 71 (1999) 4851–4859.
- [8] N. Pamme, *Lab. Chip* 7 (2007) 1644–1659.
- [9] M. Kersaudy-Kerhoas, R. Dhariwal, M.P.Y. Desmulliez, *IET Nanobiotechnol.* 2 (2008) 1–13.
- [10] N. Xia, T.P. Hunt, B.T. Mayers, E. Alsberg, G.M. Whitesides, R.M. Westervelt, D.E. Ingber, *Biomed. Microdev.* 8 (2006) 299–308.
- [11] F. Carpino, L.R. Moore, M. Zborowski, J.J. Chalmers, P.S. Williams, *J. Magn. Mater.* 293 (2005) 546–552.
- [12] C.B. Fuh, H.Y. Tsai, J.Z. Lai, *Anal. Chim. Acta* 497 (2003) 115–122.
- [13] D.R. Reyes, D. Iossifidis, P.A. Aurox, A. Manz, *Anal. Chem.* 74 (2002) 2623–2636.
- [14] P.A. Aurox, D. Iossifidis, D.R. Reyes, A. Manz, *Anal. Chem.* 74 (2002) 2637–2652.
- [15] T. Vilkner, D. Janasek, A. Manz, *Anal. Chem.* 76 (2004) 3373–3385.
- [16] P.S. Dittrich, K. Tachikawa, A. Manz, *Anal. Chem.* 78 (2006) 3887–3907.
- [17] J. West, M. Becker, S. Tombrink, A. Manz, *Anal. Chem.* 80 (2008) 4403–4419.
- [18] N. Pamme, A. Manz, *Anal. Chem.* 76 (2004) 7250–7256.
- [19] N. Pamme, J.C.T. Eijkel, A. Manz, *J. Magn. Mater.* 307 (2006) 237–244.
- [20] N. Pamme, C. Wilhelm, *Lab. Chip* 6 (2006) 974–980.
- [21] S.A. Peyman, A. Iles, N. Pamme, *Chem. Commun.* (2008) 1220–1222.
- [22] T. McCreedy, *Trends Anal. Chem.* 19 (2000) 396–401.
- [23] A. Iles, A. Oki, N. Pamme, *Microfluid. Nanofluid.* 3 (2007) 119–122.
- [24] W.J. Moore, *Physical Chemistry*, 4th ed., Longmans Green & Co. Ltd., London, 1962.

Mobile magnetic particles as solid-supports for rapid surface-based bioanalysis in continuous flow†

Sally A. Peyman, Alexander Iles and Nicole Pamme*

Received 9th March 2009, Accepted 31st July 2009

First published as an Advance Article on the web 21st August 2009

DOI: 10.1039/b904724g

An extremely versatile microfluidic device is demonstrated in which multi-step (bio)chemical procedures can be performed in continuous flow. The system operates by generating several co-laminar flow streams, which contain reagents for specific (bio)reactions across a rectangular reaction chamber. Functionalised magnetic microparticles are employed as mobile solid-supports and are pulled from one side of the reaction chamber to the other by use of an external magnetic field. As the particles traverse the co-laminar reagent streams, binding and washing steps are performed on their surface in one operation in continuous flow. The applicability of the platform was first demonstrated by performing a proof-of-principle binding assay between streptavidin coated magnetic particles and biotin in free solution with a limit of detection of 20 ng mL⁻¹ of free biotin. The system was then applied to a mouse IgG sandwich immunoassay as a first example of a process involving two binding steps and two washing steps, all performed within 60 s, a fraction of the time required for conventional testing.

Introduction

For many years micron-sized spherical particles have been utilised by scientists for various surface-based chemical and biochemical reactions. They feature a high surface-to-volume ratio and are commercially available with a variety of surface functionalities making them an ideal solid-support material for solution based reactions, as packing materials in chromatographic applications or as drug delivery vesicles.¹

The physical and chemical properties of microparticles have also been harnessed in microfluidic systems where they have been used as labels, cell substitutes in separation devices, flow indicators or as packing materials. Utilising particles inside channels can increase the available surface area for reactions such as binding assays and can improve sensitivity in analytical applications by preconcentrating small amounts of target analyte.²

A common method of manipulating particles is to retain them inside the microchannel by means of a physical barrier fabricated into the device such as dams and weirs^{3,4} or pillar arrays.^{5,6} Other physical methods of immobilising particles in channels include using gels to set particles in place⁷ or surface patterning of the channel wall.⁸ This has been demonstrated for on-chip immunoassays,^{9–11} protein digestion¹² and SNP analysis.¹³ Whilst barriers are an effective way of packing microchannels, they often require complex fabrication procedures. In addition, once particles have been retained, they are often difficult to remove.

There are also methods in which particles can be handled in a less permanent way, for instance, Malmstadt *et al.* used latex polymer particles modified with a temperature-sensitive polymer. In heated areas of the channel the particles aggregated and reversibly adhered to the channel walls.¹⁴ Particles can also be manipulated by use of external forces such as optical tweezers¹⁵ or acoustic forces.^{16,17} In another example, particles have been trapped in recirculating flows simply by manipulating pressure-driven flow and electro-osmotic flow together.¹⁸ Whilst these examples require simpler fabrication procedures, they often need complex or integrated instrumentation to generate forces and manipulate flow, respectively.

Magnetic particles are also widely used. They can be easily manipulated in fluidic environments by an externally applied magnetic field.^{19,20} The real advantage of these particles is that there is no requirement for complex or expensive instrumentation to handle them, a simple permanent magnet can generate a sufficient field gradient to move and trap particles inside a microfluidic device. A typical example of magnetic particle handling on-chip is the formation of plugs of magnetic particles inside channels. The functionalised particles are pumped through a microchannel and trapped by applying an external magnetic field. Plugs can also be easily released from the channel by removing the magnetic field. This handling has been demonstrated for nucleic acid hybridisation and recognition,^{21–23} DNA separation,²⁴ protein digestion,^{25,26} immunoassays^{27–30} and cell capture.³¹ However, despite advantages commonly associated with microfluidics such as reduced incubation time and reduced consumption of expensive reagents, this simple concept is still essentially a batch procedure with a fixed sample volume and can be relatively time consuming.

Due to the increasing demand for high through-put analysis systems, there has been a growing interest in continuous flow particle handling and, owing to their ease of manipulation in fluidic environments, magnetic particles are particularly well

Department of Chemistry, University of Hull, Cottingham road, Hull, HU6 7RX, United Kingdom. E-mail: n.pamme@hull.ac.uk; Fax: +441482466410; Tel: +441482465027

† Electronic supplementary information (ESI) available: Video of particles deflecting across a stream of fluorescently tagged biotin. Biotin concentration is 1 µg mL⁻¹ and the stream is narrower than in other assays to facilitate visualisation of the binding event in continuous flow. See DOI: 10.1039/b904724g

suitable for continuous flow procedures.³² For example, the continuous flow handling of magnetic particles has been utilised as a technique for separating magnetic particles and cells from a sample stream.^{33–36} A sample, such as a suspension of magnetic particles, was pumped continuously into a separation chamber. A magnetic field was applied, usually perpendicular to the fluid flow, and particles were deflected from their flow path.^{37,38} Despite their vast potential, magnetic continuous flow handling methods have so far only been used as separation techniques, and reactions on the particle surface usually have to be carried out off-chip before the on-chip separation is performed.^{36,39,40}

Our approach is to utilise magnetic particles for bioassays not as a static solid-support, but as a mobile platform on which multi-step procedures are performed in a continuous flow environment (Fig. 1). Several laminar flow streams are generated along a rectangular reaction chamber and functionalised magnetic particles are continuously deflected across the width of the chamber, passing through each of the flow streams. By incorporating streams with assay reagents, multi-step biochemical reactions can be performed on the particle surface. Previously, we demonstrated this principle for a single binding step streptavidin–biotin binding assay.⁴¹ Here we have significantly extended this work by investigating the platform's applicability to quantitative analysis. Furthermore, we introduce a new chip design to perform a two-binding step sandwich-type immunoassay. For this new chip design, we also investigated and characterised inter-diffusional mixing between co-laminar streams.

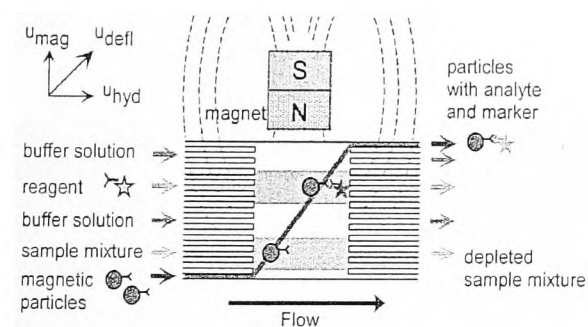


Fig. 1 The principle of the continuous flow reactor: magnetic particles are deflected through multi-laminar reagent streams and consecutive binding and washing steps are performed on their surface in continuous flow. The example shown above depicts a typical sandwich assay. Deflection of magnetic particles across the reaction chamber, u_{defl} is the sum of the flow vector for the hydrodynamic velocity of the liquid, u_{hyd} , and the flow vector resulting from the magnetic force, u_{mag} .

Experimental

Reagents and magnetic particle suspensions

Iron (III) sulfate and potassium thiocyanate were obtained from Sigma-Aldrich and were made up to 0.5 M and 0.75 M, respectively. Fluorescently labelled biotin (biotin-4-fluorescein, Molecular Probes, Invitrogen) was diluted in 0.1x TBE buffer (Tris-borate-EDTA, 0.1 M, pH 8.3, Sigma-Aldrich, UK). Biotinylated mouse anti-human CD4 IgG and goat anti-mouse IgG labelled with FITC were purchased from AbD-Serotec (UK) and diluted in PBS buffer (pH 7.45, Invitrogen).

Magnetic particle suspensions (2.8 μm diameter, Dynabeads M-270 streptavidin, Invitrogen) were prepared by diluting 10 μL of particle suspension in 990 μL of buffer, giving a stock particle concentration of 6×10^8 particles per mL. This suspension was further diluted by a factor of 2 prior to use in the chip, giving a final particle concentration of 3×10^8 particles per mL.

All working solutions contained 0.01% w/v BSA (Sigma-Aldrich, UK) to reduce non-specific binding.

Microfluidic device design and set-up

Two microfluidic designs were utilised for the work presented, and are referred to as design A and design B (Fig. 2). Both designs featured a flow chamber which was fed by several independent inlets for the generation of co-laminar streams inside the chamber, with each stream containing different reagents and buffer solutions.

Design A (Fig. 2a) was used for the streptavidin–biotin binding assay and featured four inlets, a reaction chamber 3 mm wide by 6 mm long and a single outlet. This design was suitable for the introduction of a suspension of streptavidin-coated magnetic particles through inlet 1, fluorescently labelled biotin through inlet 3 and washing buffer through inlets 2 and 4. A single outlet was sufficient for these experiments as detection was performed in real-time inside the chamber.

Design B (Fig. 2b) was used for the mouse IgG sandwich immunoassay and featured five inlets, a reaction chamber 3 mm wide by 8 mm long and two outlets. The branched outlet was primarily for reagent waste and the single narrower outlet for particle collection. A suspension of streptavidin-coated magnetic particles was introduced *via* inlet 1, biotinylated mouse IgG *via* inlet 2 and fluorescently labelled goat anti-mouse IgG *via* inlet 4. Washing buffer was pumped through inlets 3 and 5.

The chips were fabricated in glass and etched to a depth of 20 μm .^{42,43} They were connected to a syringe pump (Harvard PHD2000, Harvard Apparatus, USA) by gluing fused silica capillaries (i.d. 100 μm , o.d. 375 μm , Metal Composites, UK)

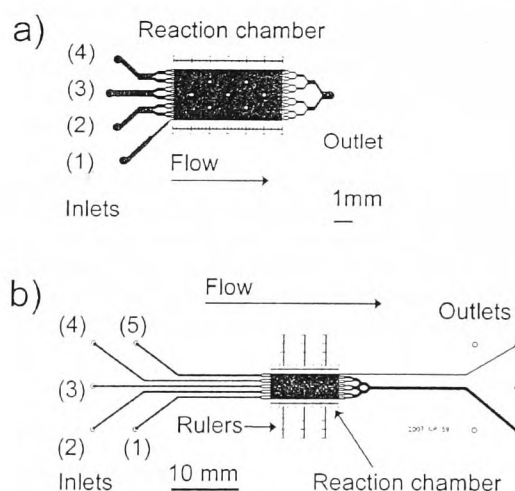


Fig. 2 a: Chip design A featured four inlets, a single outlet and a 6 mm long reaction chamber. b: Chip design B featured five inlets, two outlets and an extended 8 mm long chamber.

into the access holes and attaching them to glass syringes (SGE, Supelco, USA).

The magnetic field was generated by placing a small, rectangular neodymium-iron-boron magnet ($5 \times 4 \times 4 \text{ mm}^3$) on top of the microchip to the side of the reaction chamber (Fig. 3a and b). The magnetic field over the reaction chamber was modelled using Femm 4.0 software (<http://femm.foster-miller.net>) (Fig. 3c).

Observation and detection

Microchips were mounted on an inverted fluorescence microscope (TE2000, Nikon, Japan) and videos recorded using a CCD camera. For work on the streptavidin–biotin binding assay, a conventional CCD camera was used (MTV, Minitron, Taiwan) with relatively low sensitivity. Later, for the sandwich immunoassay, a more sophisticated camera with a cooled CCD was employed (EXL, QImaging, UK). In both cases, the auto-sensitivity adjustment on the camera was disabled. Image analysis of the particles before and after crossing reagent streams was performed manually using ImageJ software (<http://rsbweb.nih.gov/ij/>) and the average fluorescence intensity of particles was recorded with appropriate standard deviations. This software was also used to measure the greyscale intensities of diffusion bands across the reaction chamber.

Experimental procedures

Off-chip procedure for streptavidin–biotin

10 μL of streptavidin-coated magnetic particles ($6\text{--}7 \times 10^8 \text{ particles mL}^{-1}$) were mixed with 200 μL of fluorescently labelled biotin at a concentration of 20 $\mu\text{g mL}^{-1}$. The mixture was allowed to incubate for 10 min with protection from light to avoid photobleaching of the fluorescent tag. Particles were then collected using an external magnet and the supernatant was pipetted off. This was followed by three washing steps in which particles were resuspended in 200 μL of 0.1x TBE, collected and resuspended again. The particles were then placed on a microscope slide and observed under the fluorescence microscope.

Off-chip procedure for mouse IgG immunoassay. 10 μL of streptavidin coated magnetic particles ($6\text{--}7 \times 10^8 \text{ particles mL}^{-1}$) were mixed with 200 μL of biotinylated mouse IgG at a concentration of 10 $\mu\text{g mL}^{-1}$ and allowed to incubate for 30 minutes. Particles were collected and washed three times with PBS and resuspended in 200 μL of fluorescently labelled goat anti-mouse IgG. The suspension was allowed to incubate for 30 min (and protected from light). The particles were washed a further three times, resuspended in 100 μL of PBS and observed under the microscope.

On-chip procedure. Glass microchips were flushed with deionised water to remove air prior to experiments and then pretreated with potassium hydroxide to render the surface of the glass negatively charged. After a final wash with deionised water, the particles were introduced through inlet 1 and the other reagents and buffers were introduced as described in the results section. Equal pressure was applied to each syringe to generate stable and even multi-laminar flow streams inside the chamber. An applied flow rate of 25 $\mu\text{L h}^{-1}$, which corresponded to a flow velocity of 500 $\mu\text{m s}^{-1}$ was used in chip design A. For chip design B, a flow rate of 15 $\mu\text{L h}^{-1}$ was used, corresponding to a velocity of 350 $\mu\text{m s}^{-1}$. These flow rates were applied to achieve an optimum deflection of magnetic particles.

Diffusional mixing experiments. Diffusional mixing experiments were performed using chip design B (Fig. 2b) to investigate potential mixing between two reagent streams. Iron (III) sulfate and potassium thiocyanate were pumped into the chip through alternating inlets under positive pressure. Diffusion was observed using the 2x objective and still images taken for data analysis *via* ImageJ.

Theory

Magnetic particle deflection

The deflection of magnetic particles from one side of the reaction chamber to the opposite has been reported previously as a separation technique for magnetic and non-magnetic materials.^{36,38}

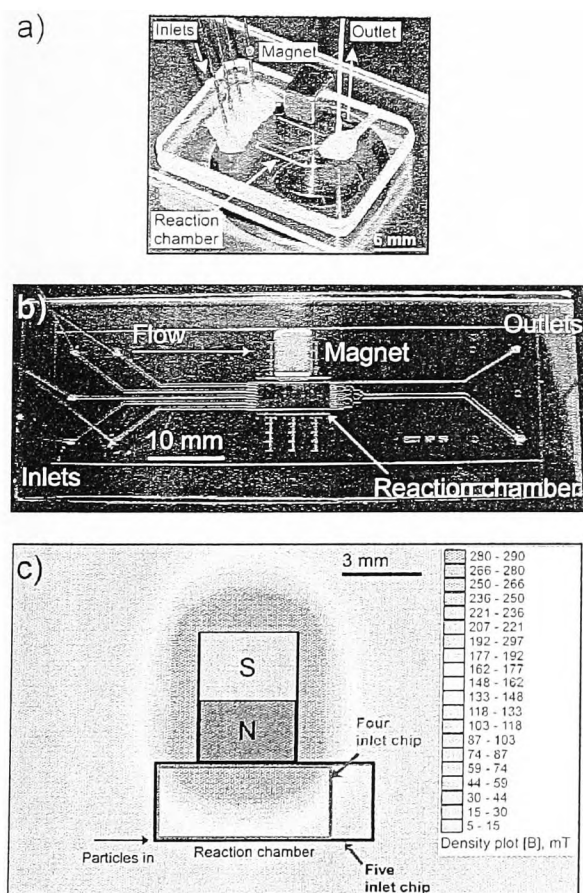


Fig. 3 a: Photograph of chip design A showing the position of the magnet on the chip surface. b: Photograph of chip design B showing the position of the magnet on the chip surface. c: A top view model of the magnetic field showing the magnetic field gradient generated across the chamber of chip design A (red) and chip design B (black).

Here we utilise the same principle to transport a single particle type across the entire width of a reaction chamber.

Laminar flow is generated across a rectangular chamber in the x -direction. Perpendicular to the direction of flow, a magnetic field is applied in the y -direction, generating a magnetic field gradient across the chamber. Particles introduced *via* inlet 1 (Fig. 2a and b) follow the laminar flow and, in the absence of the magnetic field, exit the chamber directly opposite the inlet. In the presence of an inhomogeneous field, the particles experience a force from the magnetic gradient and are pulled towards the magnet, traversing the chamber (Fig. 1). The observed velocity vector, u_{def} , of the magnetic particles is the sum of the hydrodynamic flow, u_{hyd} and the magnetically induced velocity, u_{mag} .³⁷

$$u_{\text{def}} = u_{\text{hyd}} + u_{\text{mag}} \quad (\text{Eqn 1})$$

As the particles are deflected across the chamber they pass through each of the reagent streams as shown in Fig. 1. The force acting on the particles from the magnetic field gradient, F_{mag} can be calculated according to:

$$F_{\text{mag}} = 6 \cdot \pi \cdot \eta \cdot r \cdot u_{\text{mag}} \quad (\text{Eqn 2})$$

where η is the viscosity of the medium ($\text{kg m}^{-1} \text{s}^{-1}$), r is the radius of the particle (m) and u_{mag} is the magnetically induced velocity of the particle (m s^{-1}). The force acting on the particle inside the chamber was calculated to be in the pN range.

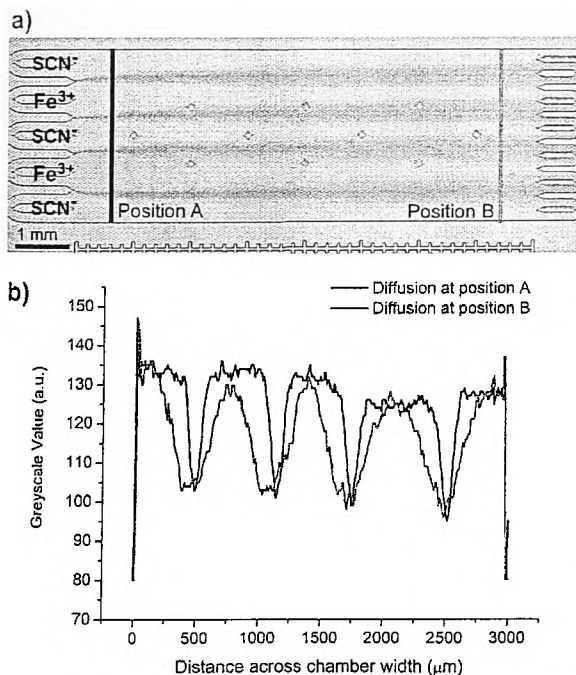


Fig. 4 a: Reaction chamber of chip design B with alternating streams of Fe^{3+} and SCN^- . The SCN^- was pumped through inlets 2 and 4 which would later be used for reagents at a flow velocity of $350 \mu\text{m s}^{-1}$. b: Greyscale intensity plot at position A and position B showing the inter-diffusion as dark bands.

Results and discussion

Diffusional mixing

It is crucial when performing biochemical assays such as immunoassays that there is no cross-contamination between reagents. In conventional assays this is ensured by repetitive washing steps between binding steps with an appropriate solution to remove any unbound reagent. For on-chip procedures, this was addressed by having washing streams containing buffer between reagent streams so that magnetic particles were washed before and after each binding step as they continued on towards the next reagent stream. The presence of washing streams also prevented direct mixing between two reagent streams by acting as a buffer zone. Previously, a simple theoretical calculation had demonstrated the minimum width a buffer stream would need to be to separate two reagent streams in chip design A.⁴¹ However, for chip design B (Fig. 2b), a longer chamber was employed with a slower flow rate for optimum particle deflection and, therefore, it was necessary to characterise the flow inside the chamber and to study any inter-diffusional mixing between streams. To visualise diffusion, alternating streams of iron (III) sulfate and potassium thiocyanate were generated along the reaction chamber at a flow velocity of $350 \mu\text{m s}^{-1}$. When these two colourless reagents diffused into each other, a dark red complex was formed (iron thiocyanate) which indicated the extent of diffusion between two adjacent streams as seen in Fig. 4a. Image analysis software was used to plot the greyscale intensity across the width of the chamber near the inlets and the outlets of the reaction chamber (Fig. 4b). The zone of diffusion appeared dark and gave a lower greyscale value than the colourless reagents which appeared light and, therefore, the width of diffusion was determined by the broadening of the darker regions. Greyscale intensities were plotted for position A near the inlets and position B (Fig. 4b) at a distance of $7200 \mu\text{m}$ along the chamber. The diffusion perpendicular to the direction of flow between position A and B was on average $340 \mu\text{m}$. At this flow rate, it took the liquid 20.6 s to travel $7200 \mu\text{m}$ through the chamber. Fe^{3+} ions and SCN^- ions have diffusion coefficients of $0.604 \times 10^{-9} \text{m}^2 \text{s}^{-1}$ and $1.758 \times 10^{-9} \text{m}^2 \text{s}^{-1}$, respectively.⁴⁴ The theoretical value for the diffusion distances can be calculated *via* the Einstein–Smoluchowski equation⁴⁵ (equation 3), where D is the diffusion coefficient ($\text{m}^2 \text{s}^{-1}$), t is time (s) and x is the diffusion distance (m). This was found to be $420 \mu\text{m}$.

$$t = \frac{x^2}{2D} \quad (\text{Eqn 3})$$

These two values correlate reasonably well. The slight discrepancy between observed diffusion and theoretical diffusion could be attributed to the diffusion coefficients being given at the standard room temperature of $25 \text{ }^\circ\text{C}$. The laboratory temperature during the experiments was at a maximum of $21 \text{ }^\circ\text{C}$, hence experimental ion diffusivity would be expected to be lower than the calculated diffusivity.⁴⁴

In this experiment, the thiocyanate solution was pumped through the same streams that reagents in the bioassay would later occupy. The iron (III) solution was pumped through the same inlets as the washing streams. It can be clearly seen in Fig. 4a that the two thiocyanate streams did not diffuse enough

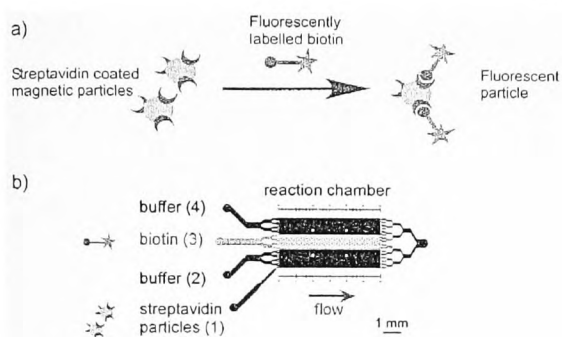


Fig. 5 a: Reaction scheme for the streptavidin–biotin binding assay involving streptavidin-coated magnetic particles and 100 ng mL^{-1} of fluorescently labelled biotin b: Schematic of the on-chip procedure with magnetic particles entering the chip *via* inlet 1 and fluorescently labelled biotin through inlet 3.

at a flow velocity of $350 \mu\text{m s}^{-1}$ to undergo any inter-diffusional mixing with each other. In addition, iron (III) and thiocyanate molecules are relatively small and have a large diffusion coefficient in the order of $10^{-9} \text{ m}^2 \text{ s}^{-1}$. Proteins such as antibodies, which are much larger and have a smaller diffusion coefficient in the range of $10^{-11} \text{ m}^2 \text{ s}^{-1}$, would diffuse even less than the Fe^{3+} and SCN^- ions and hence would not have the opportunity to mix in the chamber.

Streptavidin–biotin binding assay

As a first example of a surface-based biochemical process, a streptavidin–biotin binding assay to demonstrate the proof-of-principle was previously reported.⁴¹ This work has now been significantly extended to include a more comprehensive quantitative study.

The binding between fluorescently labelled biotin and streptavidin immobilised on the surface of the magnetic particles as depicted in the reaction scheme in Fig. 5a was first investigated off-chip, as detailed in the experimental section. The binding between the streptavidin particles and the fluorescein labelled biotin left the particles bright green in colour when observed under the fluorescence microscope with the 20x objective and easily identifiable on-screen using the CCD camera.

Once the assay had been successfully performed off-chip, the procedure was adapted for an on-chip continuous flow assay (Fig. 5b). Streptavidin-coated magnetic particles entering the chamber *via* inlet 1 were pulled through the first buffer washing stream and then into the fluorescently labelled biotin stream. As particles entered the biotin stream, they began to increase in fluorescence intensity and were observed as green streaks due to the relatively long exposure time on the CCD camera in low light conditions. Once the particles had been pulled out of the biotin stream by the magnet and into the final washing stream, so that any unbound biotin was washed off their surface, they exhibited a strong fluorescent signal. Particles observed before entering the biotin stream were found to give a slight background fluorescence due to their polystyrene shell which facilitated their tracking under UV illumination. The considerable increase in fluorescent signal after passing through the biotin stream and

washing stream confirmed the fluorescent biotin had successfully bound to the streptavidin on the surface of the particle. An on-chip negative control was also performed in which epoxy-coated magnetic particles were deflected through the biotin stream and there was no measurable increase in fluorescent signal, indicating little or no non-specific binding. This also indicated that no ‘boundary layer’ of reagent coating the particle surface was carried between adjacent streams. In addition, no mixing of reagents was observed as the particle passed between liquid interfaces, as can be seen from the supplementary video (ESI).[†] The Reynolds number for a particle depends on the size of the particle, its velocity relative to the liquid and the liquid viscosity.^{46,47} For a small particle moving relatively slowly, the Reynolds number of the particle is extremely low ($\text{Re} \ll 1$) and, therefore, the flow regime around the particle is laminar.

The residence time of the particle inside the biotin stream at a flow velocity of $500 \mu\text{m s}^{-1}$ was approximately 16 s, which is an extremely short incubation time compared to off-chip procedures which took 10 min in an Eppendorf tube. The continuous flow nature of the device allows the reagent molecules to be delivered directly to the particle’s surface as it traverses the reagent stream. Also, because the magnetic particle is free-flowing through the reagent, maximum exposure of available binding sites over the entire particle surface to the reagent is ensured in contrast to an immobilised particle such as particles trapped in a plug, which would have a certain amount of surface area interacting with the vessel wall and adjacent particles. The entire procedure from injection of the particles to detection of the signal was performed on-chip within one minute, the time taken for the particle to cross from one side of the reaction chamber to the other, a significant reduction in procedural time from 30 minutes for an off-chip Eppendorf tube experiment, as washing and separation steps are performed in one operation. In addition, the entire procedure was performed without any need for manual intervention (ESI).[†]

In order to perform quantitative analysis, the fluorescent intensity of particle streaks prior to entering the biotin stream and after leaving the biotin stream were compared using ImageJ software. The sensitivity of the system to concentrations of free biotin was investigated by lowering the concentration of biotin until the fluorescence signal of the particles after the biotin stream was indistinguishable from the background fluorescence on analysis. The limit of detection for the system using this method was 20 ng mL^{-1} of biotin. This sensitivity is comparable for other on-chip methods for detecting biotin,^{48,49} but was performed in a fraction of the time.

A calibration range was also investigated with four biotin concentrations ranging from 20 ng mL^{-1} to 200 ng mL^{-1} . Particle fluorescence intensities from the four concentrations were analysed and the average peak areas of 16 particles before and after the binding step along with standard deviations were plotted against the biotin concentration (Fig. 6). The graph in Fig. 6 shows an increase in fluorescence signal as the concentration of free biotin was increased. The significant variance in fluorescence signal could be attributed to several factors. Firstly, the reaction chamber was $20 \mu\text{m}$ deep and the M-270 particles have a diameter of $2.8 \mu\text{m}$. Therefore, when analysing videos of the particles, not all of them were at the same depth within the chamber and because of this some were in the focal plane of the microscope whilst others lay just outside. This can cause a lower fluorescence

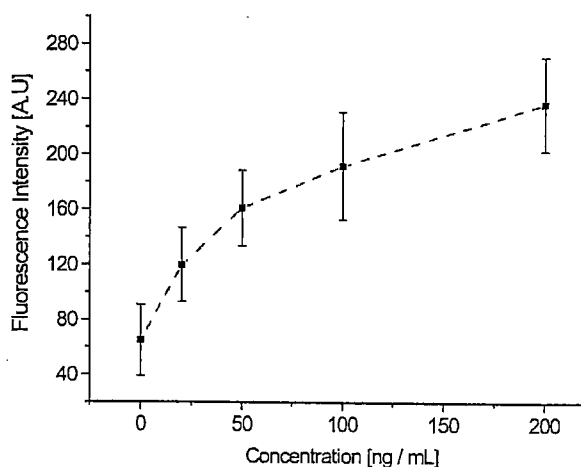


Fig. 6 Calibration graph of peak area of fluorescence intensity versus concentration of biotin in free solution for 16 particles.

intensity for particles slightly out of focus compared to those that are focused sharply. Also, some of the particles travelling through the chip occasionally stuck momentarily to the chamber walls. If a particle paused within the biotin stream, even for a millisecond, then that particle would have been exposed to slightly more biotin than a particle that had passed straight through and, hence, the need to analyse more than one particle per assay.

This work demonstrated the potential applicability of the system to sensitive, real-time quantitative analysis and the reduction of lengthy procedural times commonly associated with conventional biochemical procedures.

Mouse IgG sandwich immunoassay

In order to test the platform's applicability to perform biochemical procedures with more than one binding step, a mouse IgG sandwich immunoassay involving two binding steps and two washing steps (Fig. 7a) was investigated as an example. Again, off-chip experiments were performed to investigate the binding between complementary antibodies according to the procedure outlined in the experimental section. After incubation with the primary (biotinylated mouse IgG) and secondary antibody (goat anti-mouse IgG tagged with FITC), the magnetic particles appeared a very bright green under observation on the microscope and were easily identifiable using the CCD camera.

Once the two binding steps had been successfully performed off-chip, the procedure was adapted for an on-chip assay. Streptavidin-coated particles were introduced through inlet 1 of chip design B and were deflected across a stream initially containing $1 \mu\text{g mL}^{-1}$ solution of primary antibody in stream 2. This was followed by a washing stream (3) to remove any unbound primary antibody before the next binding step. The particles were then pulled into $10 \mu\text{g mL}^{-1}$ of the secondary labelled antibody in stream 4, followed by a final washing stream (5). Thus, the deflection of particles across two reagent streams and two washing streams was achieved. Image analysis was performed on particles before entering the primary antibody stream

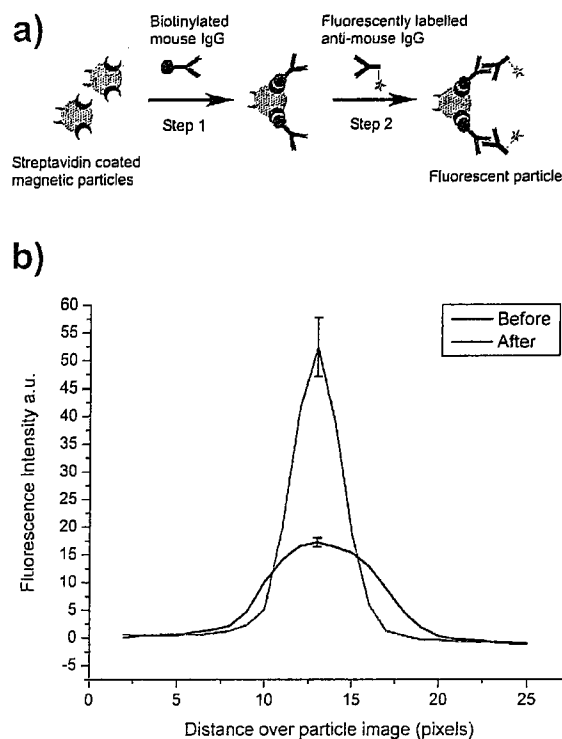


Fig. 7 a: Reaction schematic for a sandwich mouse IgG assay b: Average fluorescence intensity of particles before passing through the two reagent streams and after passing through the secondary antibody stream. The primary antibody concentration was $1 \mu\text{g mL}^{-1}$.

and after leaving the secondary antibody stream. The average fluorescence intensity of particles before and after is plotted in Fig. 7b. The analysis showed a clear increase in the fluorescence signal, indicating that an immunocomplex had been formed successfully. Again, an on-chip negative control was performed in which the primary antibody stream was left away and the particles deflected across the secondary antibody stream only. There was no detectable increase in fluorescence intensity after passing through the fluorescent stream, indicating no non-specific binding or transference of reagents *via* the boundary layer. Once more the residence time of the particles within the chamber, from injection to detection and hence the time required for the entire reaction procedure, was approximately one minute. This represents a dramatic reduction in time compared to both conventional sandwich assays, which can often take several hours, and existing on-chip immunoassay procedures. In addition, reagent consumption including magnetic particle suspension during an average 10 minute assay was only $7.5 \mu\text{L}$ ($2.5 \mu\text{L}$ for each reagent), which is a massive reduction in the volumes used compared to conventional methods.

A dose response range for the two-step sandwich immunoassay was also investigated using five different concentrations of the primary antibody ranging from 0.1 to $10 \mu\text{g mL}^{-1}$. Particle fluorescence intensities at the five concentrations were analysed and the average intensities of 16 particles before and after the two binding events were plotted against the primary antibody

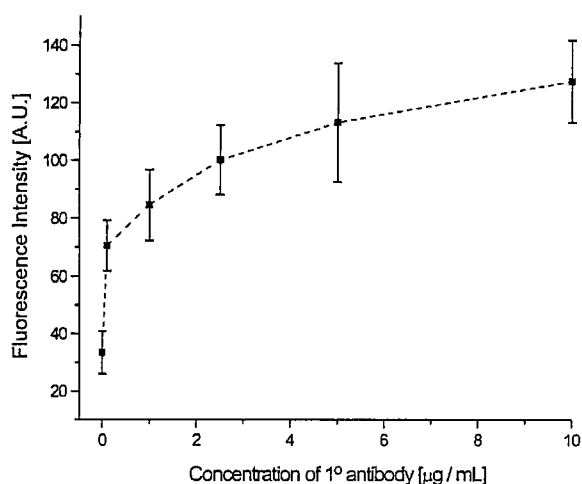


Fig. 8 Average fluorescence intensity of particles at different concentrations of primary antibody for the two-step sandwich immunoassay.

concentration (Fig. 8). As can be seen from the figure, the fluorescence intensity of the particles increased as the concentration of primary antibody was increased. There was also a notable difference between signals from the $0.1 \mu\text{g mL}^{-1}$ and the blank, suggesting that a further decrease in primary antibody concentration would still be distinguishable from the background. Despite the short incubation times associated with the current set-up, the system achieved the detection of target analytes at around $0.1 \mu\text{g mL}^{-1}$, indicating the potential for clinical relevance. For example, the system could be used to test for disease markers such as the inflammatory marker C-reactive protein, which is detected in the $0.1\text{--}1 \mu\text{g mL}^{-1}$ range.⁵⁰ However, should the sensitivity of the system require a further increase, a number of strategies could be employed. The residence time of the particle in the reagent stream could be lengthened by reducing the particle velocity, by widening the reagent streams or by modifying the magnetic field. Furthermore, a different fluorescent tag could be employed, which is less prone to photobleaching, such as the Alexa Fluor dye range. Future work would include measures to increase the sensitivity of the system and also the use of real biological samples.

Conclusions

We have successfully demonstrated a simple microfluidic platform for executing fast sequential particle-based (bio)reactions in continuous flow. Combining multi-laminar reagent streams and magnetic particles as mobile solid-supports has created a rapid, dynamic system that has greatly reduced procedural times to a fraction of those required for conventional bench top assays, as well as volume consumption of expensive reagents. Magnetic particles are extremely versatile¹⁹ and by varying their surface functionality our system could be used to perform many useful multi-step analytical and synthetic procedures.

References

- 1 H. Kawaguchi, *Prog. Polym. Sci.*, 2000, **25**, 1171.
- 2 E. Verpoorte, *Lab Chip*, 2003, **3**, 60N.

- 3 K. Sato, M. Tokeshi, T. Odake, H. Kimura, T. Ooi, M. Nakao and T. Kitamori, *Anal. Chem.*, 2000, **72**, 1144.
- 4 R. D. Oleschuk, L. L. Shultz-Lockyear, Y. B. Ning and D. J. Harrison, *Anal. Chem.*, 2000, **72**, 585.
- 5 H. Andersson, W. van der Wijngaart, P. Enoksson and G. Stemme, *Sens. Actuators, B*, 2000, **67**, 203.
- 6 H. Andersson, W. van der Wijngaart and G. Stemme, *Electrophoresis*, 2001, **22**, 249.
- 7 M. C. Breadmore, K. A. Wolfe, I. G. Arcibal, W. K. Leung, D. Dickenson, B. C. Giordano, M. E. Power, J. P. Ferrance, S. H. Feldman, P. M. Norris and J. P. Landers, *Anal. Chem.*, 2003, **75**, 1880.
- 8 H. Andersson, C. Jonsson, C. Moberg and G. Stemme, *Electrophoresis*, 2001, **22**, 3876.
- 9 K. Sato, M. Tokeshi, H. Kimura and T. Kitamori, *Anal. Chem.*, 2001, **73**, 1213.
- 10 K. Sato, M. Yamanaka, T. Hagino, M. Tokeshi, H. Kimura and T. Kitamori, *Lab Chip*, 2004, **4**, 570.
- 11 Y. Jeong, K. Choi, J. Kim, D. S. Chung, B. Kim, H. C. Kim and K. Chun, *Sens. Actuators, B*, 2008, **128**, 349.
- 12 C. Wang, R. Oleschuk, F. Ouchen, J. J. Li, P. Thibault and D. J. Harrison, *Rapid Commun. Mass Spectrom.*, 2000, **14**, 1377.
- 13 A. Russom, A. Ahmadian, H. Andersson, P. Nilsson and G. Stemme, *Electrophoresis*, 2003, **24**, 158.
- 14 N. Malmstadt, A. S. Hoffman and P. S. Stayton, *Lab Chip*, 2004, **4**, 412.
- 15 M. Ozkan, M. Wang, C. Ozkan, R. Flynn, A. Birkbeck and S. Esener, *Biomed. Microdevices*, 2003, **5**, 61.
- 16 T. Laurell, F. Petersson and A. Nilsson, *Chem. Soc. Rev.*, 2007, **36**, 492.
- 17 M. Evander, L. Johansson, T. Lilliehorn, J. Piskur, M. Lindvall, S. Johansson, M. Almqvist, T. Laurell and J. Nilsson, *Anal. Chem.*, 2007, **79**, 2984.
- 18 G. L. Lettieri, A. Dodge, G. Boer, N. F. de Rooij and E. Verpoorte, *Lab Chip*, 2003, **3**, 34.
- 19 M. A. M. Gijs, *Microfluidics and Nanofluidics*, 2004, **1**, 22.
- 20 N. Pamme, *Lab Chip*, 2006, **6**, 24.
- 21 Z. H. Fan, S. Mangru, R. Granzow, P. Heaney, W. Ho, Q. P. Dong and R. Kumar, *Anal. Chem.*, 1999, **71**, 4851.
- 22 G. F. Jiang and D. J. Harrison, *Analyst*, 2000, **125**, 2176.
- 23 S. Kwakye and A. Baeumner, *Anal. Bioanal. Chem.*, 2003, **376**, 1062.
- 24 P. S. Doyle, J. Bibette, A. Bancaud and J. L. Viovy, *Science*, 2002, **295**, 2237.
- 25 M. Slovakova, N. Minc, Z. Bilkova, C. Smadja, W. Faigle, C. Futterer, M. Taverna and J. L. Viovy, *Lab Chip*, 2005, **5**, 935.
- 26 A. Le Nel, J. Krenkova, K. Kleparnik, C. Smadja, M. Taverna, J. L. Viovy and F. Foret, *Electrophoresis*, 2008, **29**, 4944.
- 27 J. W. Choi, K. W. Oh, J. H. Thomas, W. R. Heineman, H. B. Halsall, J. H. Nevin, A. J. Helmicki, H. T. Henderson and C. H. Ahn, *Lab Chip*, 2002, **2**, 27.
- 28 M. A. Hayes, N. A. Polson, A. N. Phayre and A. A. Garcia, *Anal. Chem.*, 2001, **73**, 5896.
- 29 S. Bronzeau and N. Pamme, *Anal. Chim. Acta*, 2008, **609**, 105.
- 30 F. Lacharme, C. Vandevyver and M. A. M. Gijs, *Anal. Chem.*, 2008, **80**, 2905.
- 31 V. I. Furdul and D. J. Harrison, *Lab Chip*, 2004, **4**, 614.
- 32 N. Pamme, *Lab Chip*, 2007, **7**, 1644.
- 33 G. Blankenstein and U. D. Larsen, *Biosens. Bioelectron.*, 1998, **13**, 427.
- 34 K. S. Kim and J. K. Park, *Lab Chip*, 2005, **5**, 657.
- 35 A. C. Siegel, S. S. Shevkoplyas, D. B. Weibel, D. A. Bruzewicz, A. W. Martinez and G. M. Whitesides, *Angew. Chem., Int. Ed.*, 2006, **45**, 6877.
- 36 N. Pamme and C. Wilhelm, *Lab Chip*, 2006, **6**, 974.
- 37 N. Pamme and A. Manz, *Anal. Chem.*, 2004, **76**, 7250.
- 38 N. Pamme, J. C. T. Eijkel and A. Manz, *J. Magn. Magn. Mater.*, 2006, **307**, 237.
- 39 K. H. Han and A. B. Frazier, *Lab Chip*, 2006, **6**, 265.
- 40 D. W. Inglis, R. Riehn, R. H. Austin and J. C. Sturm, *Appl. Phys. Lett.*, 2004, **85**, 5093.
- 41 S. A. Peyman, A. Iles and N. Pamme, *Chem. Commun.*, 2008, 1220.
- 42 T. McCreedy, *TrAC Trends Anal. Chem.*, 2000, **19**, 396.
- 43 A. Iles, A. Oki and N. Pamme, *Microfluid. Nanofluid.*, 2007, **3**, 119.
- 44 L.D.R. *Handbook of Chemistry and Physics*, 78th edition ed., CRC Press, 1997.

-
- 45 P. Atkins, J. de Paula *Elements of physical chemistry*, Fourth Edition ed., Oxford University Press, 2006.
- 46 J. S. Park, S. H. Song and H. I. Jung, *Lab Chip*, 2009, 9, 939.
- 47 J. Berthier, S. Pascal *Microfluidics for biotechnology*, Artech House: Boston London, 2006.
- 48 D. A. Markov, K. Swinney and D. J. Bornhop, *J. Am. Chem. Soc.*, 2004, 126, 16659.
- 49 Y. C. Li, L. M. L. Ou and H. Z. Yu, *Anal. Chem.*, 2008, 80, 8216.
- 50 D. Wild, *The Immunoassay Handbook*, 3rd ed., Elsevier B. V., Amsterdam, Netherlands, 2005.

A MICROFLUIDIC SYSTEM FOR PERFORMING FAST, SEQUENTIAL BIOCHEMICAL PROCEDURES ON THE SURFACE OF MOBILE MAGNETIC PARTICLES IN CONTINUOUS FLOW

S.A. Peyman, H. Patel, N. Belli, A. Iles, N. Pamme

Department of Chemistry, University of Hull, Cottingham Road, Hull, HU6 7RX, UK

A rapid, highly versatile microfluidic platform is demonstrated for performing multi-step (bio)reactions on the surface of single magnetic particles in continuous flow. Functionalised magnetic particles were deflected across the width of a reaction chamber along which multiple laminar reagent streams had been generated. As the particles traversed the reagent streams, several operations were performed on their surface including washing, incubation and detection, all within a fraction of the time required for conventional assaying methods. The microfluidic platform was applied to a mouse IgG immunoassay and a DNA hybridisation assay, both involving two washing steps and one reaction step. These continuous flow procedures were performed in less than one minute and could be adapted for many other analytical measurements.

1. Introduction. Biochemical assays such as immunoassays and DNA hybridisation play an integral part in clinical diagnostics, forensic analysis and environmental monitoring. Their high specificity and sensitivity make them an ideal analytical tool for detecting small concentrations of analyte, often in complex matrices such as bodily fluids, scene-of-crime or soil samples. Immunoassays are based on the highly specific recognition between antibodies and their complementary antigen and are widely in the diagnosis of disease markers [1]. The detection and analysis of samples of DNA has become increasingly important with the onset of forensic technology but also in the use of genomic information in the diagnosis and treatment of congenital diseases. In the laboratory, conventional biochemical procedures often take several hours or even days for sample preparation, incubation and detection. Each stage of the conventional bioassay usually involves multiple incubation and washing steps that are labour intensive, time consuming and require large amounts of expensive reagents. Hence, there is a great demand for fast, high through-put, automated point-of-care instrumentation.

Microfluidic technology can address some of these issues [2]. In recent years many biochemical procedures have been developed in microfluidic devices. The Reynolds numbers of fluid flows in micron scale channels are low, typically < 1 . Hence, flow in is laminar and mixing occurs by diffusion alone. Despite being diffusion limited, when biochemical procedures are performed inside microchannels, diffusion distances are short and so reagents can mix rapidly. Therefore, in microsystems incubation times can be much shorter than in macroscale systems. In addition, microdevices have a working volume that is generally in the nL to μ L range and so reagent consumption is significantly reduced [3]. Many groups working in microfluidics have utilised micron-sized spherical particles to increase the available surface area for reaction. These particles have been packed or trapped inside the channels using physical barriers, such as weirs or frits or external forces, such as optical or acoustic forces [4]. Another convenient way to immobilise particles reversibly inside a channel is to use magnetic microparticles. These particles are usually superparamagnetic and can be easily manipulated in

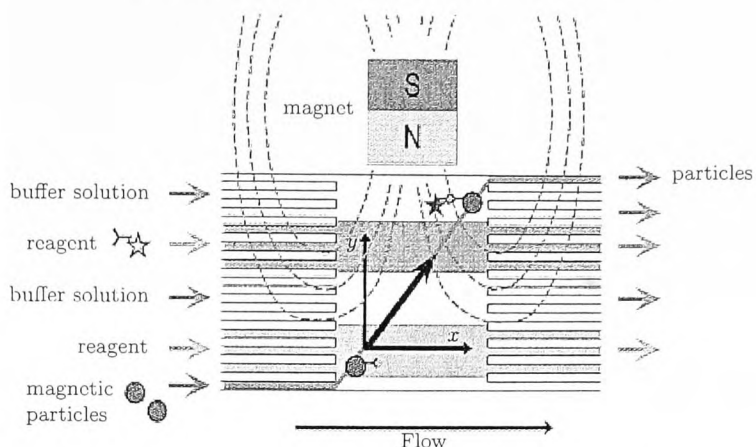


Fig. 1. Principle of the continuous flow reactor. Fluid flow is pumped in the x -direction and a magnetic field is applied in the y -direction. Magnetic particles are pulled across multilaminar reagent streams and assays performed on their surface in continuous flow.

fluidic environments by an external magnetic field [5]. Conventionally, magnetic particles functionalised with a particular biomolecule are pumped into a channel and an external magnetic field is applied. Particles become trapped in a plug like formation [6]. Reagents can then be pumped over the surface of the particles and once the assay has been completed they can be released by removing the field. This simple concept has been demonstrated for nucleic acid hybridisation and recognition [7]–[10], immunoassays [11]–[13] and cell capture [14]. However, despite these miniaturised approaches having a significant effect on incubation times and reagent consumption compared to conventional assaying methods, they are still essentially batch processes and require the consecutive changing of reagents for each assay step. Therefore these on-chip procedures remain relatively labour intensive and can still take between 30 and 60 minutes to complete.

Here we demonstrate a highly versatile microfluidic device that is capable of performing entire multi-step procedures including washing, incubation and detection in a very short time frame, typically within one minute. The system utilises functionalised magnetic particles as free-flow mobile solid supports for biochemical reactions (Figure 1). Several laminar flow streams are generated along a reaction chamber in the x -direction. A magnetic field gradient is applied perpendicular to flow in the y -direction. Particles entering the chamber can be continuously deflected across these laminar flow streams by the external magnetic field [15]. Multiple sequential assay steps are thus performed on their surface. We have previously demonstrated this principle for a biotin–streptavidin binding assay [16]. Here we significantly extend the work by characterising the flow inside the reaction chamber and by demonstrating an immunoassay and DNA hybridisation assay techniques.

2. Experimental.

2.1. Reagents and particle suspensions. For the flow characterisation inside the chamber streams were visualised using acidified eosin Y and sodium hydroxide (Sigma-Aldrich, UK). For the mouse IgG assay biotinylated mouse IgG and fluorescently labelled goat anti-mouse IgG (AbD-Serotec, UK) were diluted 1/10 and 1/100, respectively, in PBS (pH 7.45, Invitrogen) to a concentration

Table 1. Base sequence of the biotinylated DNA and the fluorescently tagged complementary DNA strand.

DNA	Base sequence
Biotinylated DNA primer	3 GGG ACC CGA GAC ATT TCT TAT CAC 5 - Biotin
Complimentary DNA primer with fluorophore label	5 CCC TGG GCT CTG TAA AGA ATA GTG 3 - Joe Green

of $10 \mu\text{g mL}^{-1}$ according to manufacturers recommendations. Magnetic particle suspensions ($2.8 \mu\text{m}$ in diameter, Dynabead M-270 streptavidin, Invitrogen) were prepared by diluting $10 \mu\text{L}$ of particle suspension in 990 L of PBS giving a stock particle concentration of 6×10^8 particles mL^{-1} . This suspension was further diluted to 3×10^8 particles mL^{-1} prior to use in the chip.

For the DNA hybridisation assay Biotinylated DNA probe primers and complimentary DNA primer with fluorophore JOE GREEN (MWG Eurofins, UK) were purchased in hydrolysed form (Table 1). Stock solutions were made up using $151 \mu\text{L}$ of purified water ($18.2 \text{ M}\Omega$ at 25°C , $0.05 \mu\text{m}$ filtered). The DNA stock solution was diluted 1/10 in purified water to give the working stock solutions. A final 1/10 dilution of this stock was made prior to experiments with TE hybridisation buffer (Tris-EDTA, Sigma-Aldrich) to a working concentration of $100 \mu\text{M}$. All DNA solutions were kept at 4°C .

2.2. Microchip design and set-up. The microchip design (Figure 2) featured four inlets, a rectangular reaction chamber 3 mm wide by 6 mm long and a single outlet. This design was suitable for introduction of a suspension of functionalised magnetic particles through inlet 1, an appropriate reagent solution through inlet 3 and washing buffer through inlets 2 and 4. A single outlet was sufficient for these experiments as detection was performed in real-time inside the chamber. The microfluidic device was fabricated in glass and etched to a depth of $20 \mu\text{m}$ [17, 18].

The device was interfaced to a syringe pump (Harvard PHD2000, Harvard Applications, USA) by gluing fused silica capillaries (i.d. $100 \mu\text{m}$, o.d. $375 \mu\text{m}$, Metal Composites, UK) into the drill holes and connecting them to glass syringes (SGE, Supelco, USA).

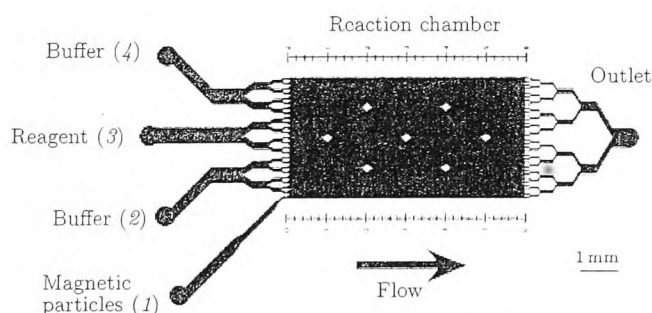


Fig. 2. Microchip design featuring four branched inlets, a rectangle reaction chamber and a single branched outlet, etched to a depth of $20 \mu\text{m}$.

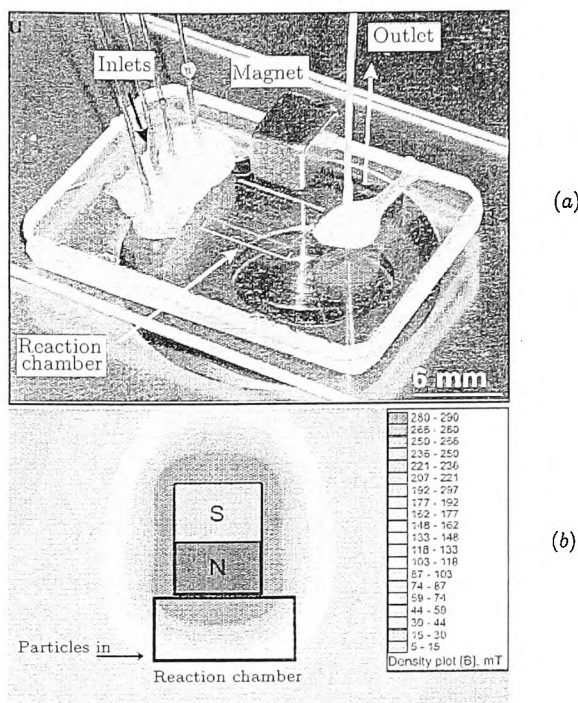


Fig. 3. (a) Photograph of the microchip set-up showing the position of the magnet. (b) Model of the magnetic field generated by the magnet and the relative position of the reaction chamber.

The magnetic field was provided by a small permanent neodymium-iron-boron magnet $5 \times 4 \times 4 \text{ mm}^3$ (MagnetSales, UK). The magnet was placed on top of the glass chip, to the opposite side of the reaction chamber to the particle inlet as seen in Figure 3a. The magnetic field generated by this magnet was modelled using Femm.4.0 software (<http://femm.foster-miller.net>) and the position of the reaction chamber in relation to the inhomogeneous field is shown in Figure 3b.

The microfluidic device was observed using an inverted fluorescence microscope (TE2000-U, Nikon, Japan) with a 20x objective. Videos were taken using a CCD camera (EXL, Qimaging, UK) with the auto-exposure adjustment on the camera disabled for experiments. Image analysis of the particles before and after crossing reagent streams was performed using ImageJ software (<http://rsnweb.nih.gov/ij/>) and the fluorescence intensity plotted across the particle image. For the DNA hybridisation assay a microscope heating plate was set prior to the start of the assay to 42°C and allowed to reach temperature.

2.3. Experimental procedures.

Off-chip procedures.

Mouse IgG immunoassay: $10 \mu\text{L}$ of streptavidin coated magnetic particles ($6 \div 7 \times 10^8 \text{ particles mL}^{-1}$) were mixed with $200 \mu\text{L}$ of biotinylated mouse IgG at a concentration of $10 \mu\text{L mL}^{-1}$ and allowed to incubate for 30 minutes. Particles were collected and washed three times with PBS and re-suspended in $200 \mu\text{L}$ of fluorescently labelled goat anti-mouse IgG. The suspension was allowed to incubate for 30 minutes and protected from light. The particles were washed a further

A microfluidic system for performing fast, sequential biochemical procedures

three times, re-suspended in 100 μL of PBS and observed on the microscope. The fluorescence intensity of particles before the reaction and after were compared using image analysis software.

DNA hybridisation assay: 100 μL of biotinylated DNA working stock solution was added to a 50 μL stock suspension of magnetic particles, vortexed and allowed to incubate for 15 minutes. To this mixture 100 μL of fluorescently tagged DNA working stock solution was added and incubated for a further 15 minutes in a heated water bath set to an optimal calculated temperature of 42°C for hybridisation. After incubation the magnetic particles were collected using an external magnet and the supernatant removed. The particles were then re-suspended in hybridisation buffer and the mixture vortexed. This washing process was repeated a further two times and then 10 μL of the final solution was placed onto a microscope slide for observation.

On-chip procedures.

General microchip pre-treatment: glass microchips were flushed with deionised water to remove air prior to experiments and then pre-treated with a base to render the surface of the glass negative. Equal pressure was applied to each syringe to generate stable and even multi-laminar flow streams inside the chamber.

Flow characterisation: acidified eosin and sodium hydroxide were pumped into the microchip through alternating inlets at a flow velocity of 500 μms^{-1} . Acidified eosin has a very low fluorescent signal below pH 3, but above this value it becomes strongly fluorescent. As two adjacent streams of acidified eosin and sodium hydroxide diffused into each other the cone of diffusion could be visualised on the microscope. The width of these bands were measured using image analysis software.

Mouse IgG immunoassay: mouse IgG was immobilised to the surface of the streptavidin coated particles by incubating 10 μL of particles ($6 \div 7 \times 10^8$ particles per mL) with 200 μL of biotinylated mouse IgG for 30 minutes. Particles were then collected using a magnet and washed three times with PBS buffer. Mouse IgG coated magnetic particles were then re-suspended in 1 mL of PBS and diluted to the working particle concentration before introduction into the microfluidic device. Fluorescently tagged anti-mouse IgG antibodies at a concentration of 1 $\mu\text{g mL}^{-1}$ were pumped through inlet 3 and PBS through inlets 2 and 4 at a flow velocity of 500 μms^{-1} (see Figure 2).

DNA hybridisation assay: 100 μL of biotinylated DNA working stock solution was added to a 50 μL stock suspension of magnetic particles, vortexed and allowed to incubate for 15 minutes. Magnetic particles coated in ssDNA were then diluted to a working on-chip concentration of 6.7×10^6 particles mL^{-1} before introduction into the microchip. Fluorescently tagged complementary ssDNA was pumped through inlet 3, with hybridisation buffer pumped through inlets 2 and 4 at a flow velocity of 500 μms^{-1} .

3. Results and discussion.

3.1. Flow characterisation. It is imperative when performing biochemical assays such as immunoassays and DNA hybridisation that there is no cross-contamination between reagents. In conventional assays this is ensured by repetitive washing steps with an appropriate buffer between reaction steps. On-chip this is addressed by having washing streams before and after reagent streams so any unbound material is washed off the particle surface before it continues on to the next step of the assay. However, at the relatively low flow rates required to deflect the particles over the full width of the chamber it was essential to characterise the flow inside the chamber and to investigate any inter-diffusional mixing

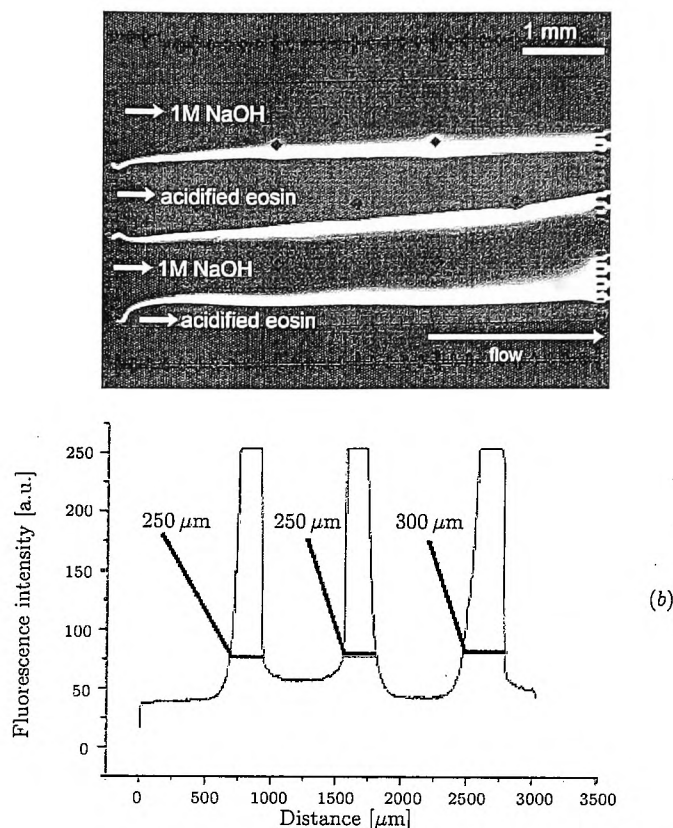


Fig. 4. (a) Visualisation of diffusion in the reaction chamber at $500 \mu\text{ms}^{-1}$. Area of bright fluorescence is result of diffusion between acidified eosin and sodium hydroxide. (b) Measurement of diffusion distances between each stream.

between streams. Experiments utilising a pH sensitive fluorophore were performed to visualise the inter-stream diffusion. Figure 4a clearly shows that the level of inter-stream diffusion in the reaction chamber at a flow rate of $500 \mu\text{ms}^{-1}$ is not sufficient to cause inter-diffusion mixing between neighbouring reagent streams. The diffusion between streams was measured at an average of $260 \mu\text{m}$ (Figure 4b). If equal pressure was applied to each of the four glass syringes then each stream is approximately $750 \mu\text{m}$ wide at the inlet end of the chamber. Therefore, the presence of the washing streams between reagent streams is sufficient to keep the two reagent streams separate and avoid any cross contamination.

3.2. Mouse IgG assay. The assay between mouse and anti-mouse IgG antibodies was first investigated off chip to ensure immuno-recognition would take place according to the procedure outlined in section 2.3. The binding between mouse IgG antibodies immobilised on the surface of the magnetic particles and the fluorescently tagged anti-mouse IgG in solution was determined by comparing the fluorescence intensities of particles before and after incubation. Particles appeared a very bright green after incubation with fluorescently labelled anti-mouse IgG when observed under UV illumination at a 20x magnification indicating immune-recognition was successful. A negative control was also carried out

A microfluidic system for performing fast, sequential biochemical procedures

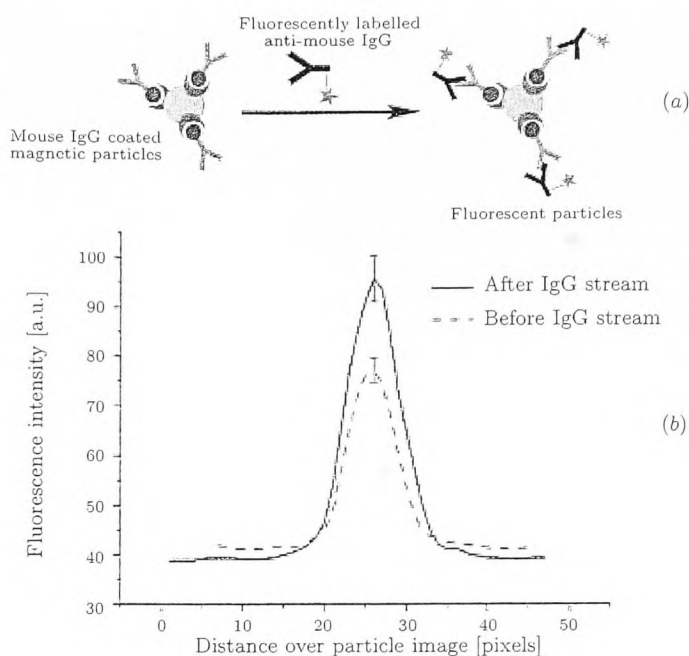


Fig. 5. (a) Reaction scheme for the mouse IgG immunoassay. (b) Fluorescence intensity of particles before and after passing through anti-mouse IgG stream showing an increase in fluorescence signal.

in which plain streptavidin coated particles were incubated with the fluorescently tagged anti-mouse IgG. There was no measurable increase in fluorescence intensity in this case indicating little or no non-specific binding.

Once the assay had been successfully performed off chip the procedure could be adapted for an on-chip continuous flow assay according to section 2.3. The on-chip immunoassay was performed using magnetic particles with mouse IgG antibodies already immobilised to their surface and fluorescently labelled anti-mouse IgG in free solution, the reaction schematic is shown in Figure 5a. Antibody coated particles were pumped into the chip via inlet 1. Fluorescently labelled goat anti-mouse IgG was introduced to the chip via inlet 3, with PBS washing buffer pumped through inlets 2 and 4. When the magnetic field was applied particles were pulled from the particle stream, through the first washing stream and into the stream containing anti-mouse IgG. Finally the particles were pulled into the final washing buffer in stream 4. Image analysis was performed on particle images taken before the reagent stream and after particles entered the final washing stream. From Figure 5b it can be seen that the particles showed an increase in fluorescence intensity after passing through the reagent stream, thus indicating that a successful immunoassay had been performed on the surface of the particle in continuous flow. At a flow rate of $500 \mu\text{ms}^{-1}$ the residence time of the particle inside the anti-mouse IgG stream was approximately 16 s which is an extremely short incubation time in comparison to conventional and other microfluidic assays. The continuous flow nature of the device allows antibody molecules to be delivered directly to the particle surface as it traverses the reagent stream whereas in a static fluid situation

such as an Eppendorf tube, the assay is limited by the length of time it takes for the antibodies to diffuse to the surface of the particle to find their target through a relatively large volume of liquid. Also, because the magnetic particle is free-flowing through the reagent stream this ensures maximum exposure of available binding sites over the entire particle surface to the reagent stream in contrast to an immobilised particle, which would have a certain amount of surface area interacting with the vessel wall and adjacent particles. The total residence time of the particles in the reaction chamber, i.e. the time it takes for a particle to pass through both washing streams and the reagent streams was approximately 60s and so the entire immunoassay procedure, including washing steps, reagent incubation and detection was performed within 1 min in continuous flow without any need for manual intervention. In addition, the reagent consumption for an average 10 min assay, including magnetic particle suspension was approximately 8.3 μL , which is a huge reduction compared to reagent consumption for an off-chip bench-top procedure.

3.3. DNA hybridisation. The hybridisation assay between single-stranded DNA, ssDNA, and its fluorescently tagged complementary strand, cDNA was first investigated off chip according to the procedure outlined in section 2.4 to ensure hybridisation between the two strands was successful. Magnetic particles were observed under the microscope. Fluorescence intensities of particles before and after hybridisation were then analysed and compared and it was found that magnetic particles after hybridisation showed an increase in fluorescence intensity compared

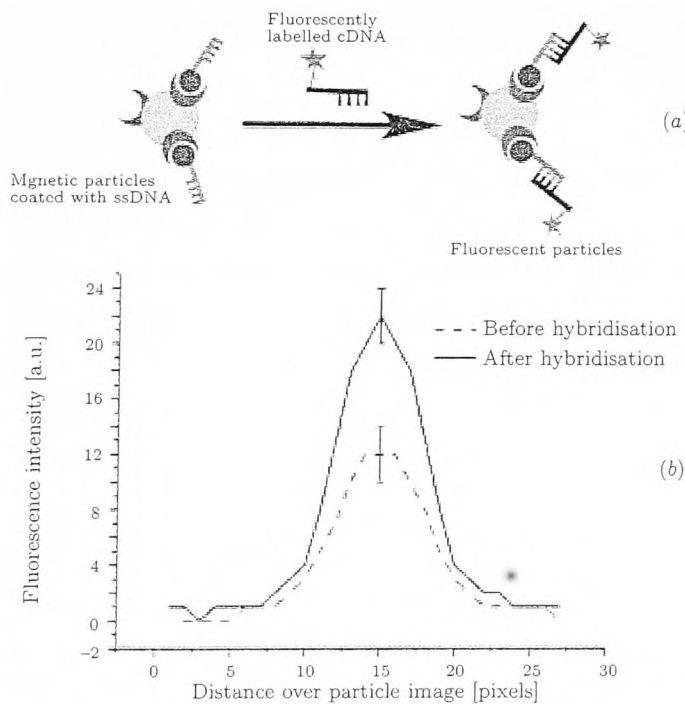


Fig. 6. (a) Reaction scheme for the DNA hybridisation. (b) Fluorescence intensity of particles before the fluorescently tagged cDNA stream and afterwards showing an increase in fluorescent signal.

to unreacted magnetic particles indicating successful hybridisation between ssDNA on the surface of the particle and the fluorescently tagged cDNA in free solution.

Again, once the hybridisation had been successfully demonstrated off chip, the procedure was then adapted for a continuous flow on-chip assay. For the on-chip assay ssDNA was immobilised to the surface of the particle according to the procedure in section 2.3 and the fluorescently tagged cDNA probe was in free solution, the reaction schematic for the hybridisation is shown in Figure 6a. The magnetic particles were pumped into the chamber via inlet 1. The fluorescently tagged cDNA probe was introduced via inlet 3, buffer was pumped through inlets 2 and 4. When the magnetic field was applied, magnetic particles were pulled from the particle stream across first buffer stream, the cDNA stream and into the final buffer stream where any unbound cDNA was washed away. Images were taken of particles before entering and after leaving the cDNA stream. Particles showed an increase in fluorescence intensity as shown in Figure 6b. Again the residence time of the particle inside the cDNA stream was approximately 16 s, indicating that hybridisation between ssDNA and cDNA was successfully performed on the surface of the particle in continuous flow. The short time required to complete the hybridisation procedure is a considerable reduction in the time required for conventional hybridisation procedures, which can often take several hours.

4. Conclusion. We have demonstrated a dynamic, versatile microfluidic platform that is capable of performing continuous flow multi-step biochemical procedures in a fraction of the time required for conventional procedures. Hence, this work brings within our grasp the promise of low cost, real-time point-of-care analysis and diagnostics. Furthermore, the by utilising different functionalised magnetic particles and increasing the number of reagent streams, the platform could also be applied to an enormous variety of different analytical and synthetic applications.

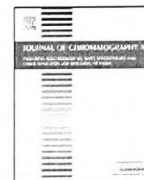
REFERENCES

- [1] D. WILD. *The Immunoassay Handbook* (3rd ed., Elsevier, 2005).
- [2] G.M. WHITESIDES. *Nature*, Vol. 442 (2006), pp. 368.
- [3] D. JANASEK, J. FRANZKE, A. MANZ. *Nature*, Vol. 442 (2006), pp. 374.
- [4] E. VERPOORTE. *Lab on a Chip*, Vol. 3 (2003), pp. 60N.
- [5] M.A.M. GIJS. *Microfluidics and Nanofluidics*, Vol. 1 (2004), pp. 22.
- [6] N. PAMME. *Lab on a Chip*, Vol. 6 (2006), pp. 24.
- [7] Z.H. FAN, S. MANGRU, R. GRANZOW, P. HEANEY, W. HO, Q.P. DONG, R. KUMAR. *Analytical Chemistry*, Vol. 71 (1999), pp. 4851.
- [8] S. KWAKYE, A. BAEUMNER. *Analytical and Bioanalytical Chemistry*, Vol. 376 (2003), pp. 1062.
- [9] G.F. JIANG, D.J. HARRISON. *Analyst*, Vol. 125 (2000), pp. 2176.
- [10] V.N. GORAL, N.V. ZAYTSEVA, A.J. BAEUMNER. *Lab on a Chip*, Vol. 6 (2006), pp. 414.
- [11] J.W. CHOI, K.W. OH, J.H. THOMAS, W.R. HEINEMAN, H.B. HALSALL, J.H. NEVIN, A.J. HELMICKI, H.T. HENDERSON, C.H. AHN. *Lab on a Chip*, Vol. 2 (2002), pp. 27.

S.A. Peyman, H. Patel, N. Belli, A. Iles, N. Pamme

- [12] M.A. HAYES, N.A. POLSON, A.N. PHAYRE, A.A. GARCIA. *Analytical Chemistry*, Vol. 73 (2001), pp. 5896.
- [13] S. BRONZEAU, N. PAMME. *Analytica Chimica Acta*, Vol. 609 (2008), pp. 105
- [14] V.I. FURDUI, D.J. HARRISON. *Lab on a Chip*, Vol. 4 (2004), pp. 614.
- [15] N. PAMME, A. MANZ. *Analytical Chemistry*, Vol. 76 (2004), pp. 7250.
- [16] S.A. PEYMAN, A. ILES, N. PAMME. *Chemical Communications* (2008), pp. 1220.
- [17] T. MCCREEDY. *Trac-Trends in Analytical Chemistry*, Vol. 19 (2000), pp. 396.
- [18] A. ILES, A. OKI, N. PAMME. *Microfluidics and Nanofluidics*, Vol. 3 (2007), pp. 119.

Received 21.05.2009



Diamagnetic repulsion—A versatile tool for label-free particle handling in microfluidic devices

Sally A. Peyman, Er Yee Kwan, Oliver Margaron, Alexander Iles, Nicole Pamme*

The University of Hull, Department of Chemistry, Cottingham Road, Hull HU6 7RX, UK

ARTICLE INFO

Article history:

Available online 18 June 2009

Keywords:

Microparticles
Diamagnetic repulsion
Microfluidic
Separation

ABSTRACT

We report the exploration of diamagnetic repulsion forces for the selective manipulation of microparticles inside microfluidic devices. Diamagnetic materials such as polymers are repelled from magnetic fields, an effect greatly enhanced by suspending a diamagnetic object in a paramagnetic Mn^{2+} solution. The versatility of diamagnetic repulsion is demonstrated for the trapping, focussing and deflection of polystyrene particles for three example applications. Firstly, magnet pairs with unlike poles facing each other were arranged along a microcapillary to trap plugs of differently functionalised particles for a simultaneous surface-based assay in which biotin was selectively bound to a plug of streptavidin coated particles utilising only 22 nL of reagent. Secondly, by slightly modifying the magnetic field design, the rapid focussing of particles into a narrow central stream at a flow rate of $650 \mu m s^{-1}$ was accomplished for particle pre-concentration. In a third application, 5 and $10 \mu m$ polystyrene particles were separated from each other in continuous flow by passing the particle mixture through a microfluidic chamber with a perpendicular magnetic field, a method termed diamagnetophoresis. The separation was investigated between flow rates of $20\text{--}100 \mu L h^{-1}$, with full resolution of the particle populations being achieved at $20 \mu L h^{-1}$. These experiments show the potential of diamagnetic repulsion for simple, label-free manipulation of particles and other diamagnetic objects such as cells for a range of bioanalytical techniques.

© 2009 Elsevier B.V. All rights reserved.

1. Introduction

Microfluidic technology is an increasingly popular area of research that involves the manipulation of small amounts of fluids, typically within the nano-litre range, inside micron-sized channels [1]. Reynolds numbers in such channels are very low resulting in laminar fluid flow which is highly predictable and controllable. Microfluidic devices have been used extensively as platforms for the analysis and separation of cells, and for particle-based reactions and therefore the manipulation of micron-sized objects inside these channels has become of particular interest [2]. A popular way of manipulating cells and particles inside microchannels is to use externally applied forces such as dielectrophoresis [3,4], acoustic forces [5,6] and optical tweezers [7]. While these methods allow the direct and contactless manipulation of single objects they often require complex or integrated instrumentation.

Another common method of particle and cell manipulation inside microchannels is the use of magnetic forces [8,9]. Particles and cells that have been doped with iron oxide nanoparticles can be easily and elegantly manipulated using simple magnet set-ups. Magnetic forces are ideal as they do not require large instrumen-

tation and are generally independent of pH, ionic strength, surface charges or temperature. For example, magnetic forces have been utilised to trap particles inside microchannels to form plugs for biochemical assays [10,11], to isolate magnetically labelled cells [12] and to separate or sort magnetic material according to size and magnetic properties in continuous flow [13]. Recently, magnetic particles have also been utilised as a mobile solid-support for continuous flow bioanalysis in which a magnetic field was used to deflect functionalised particles through multiple laminar reagent streams [14].

A less commonly known method for particle manipulation, which has so far received relatively little attention, is the phenomenon of diamagnetic repulsion. In the same way as a magnetic material is attracted towards a magnetic field, a non-magnetic or diamagnetic material experiences a repulsive force. Diamagnetic forces are much weaker than magnetic forces and therefore generally go un-noticed. However, by applying very high magnetic fields and gradients such as those generated by super-conducting magnets, diamagnetic repulsion forces have been used to manipulate large diamagnetic objects. This was first demonstrated by Beaugnion and Tournier who levitated a variety of diamagnetic materials in the bore of a hybrid magnet [15]. Another interesting study concerned the diamagnetic levitation of a living frog [16]. While these initial examples have highlighted the potential of diamagnetic repulsion as a means of object manipulation, they required the use of special-

* Corresponding author. Tel.: +44 1482 465027; fax: +44 1482 466416.
E-mail address: n.pamme@hull.ac.uk (N. Pamme).

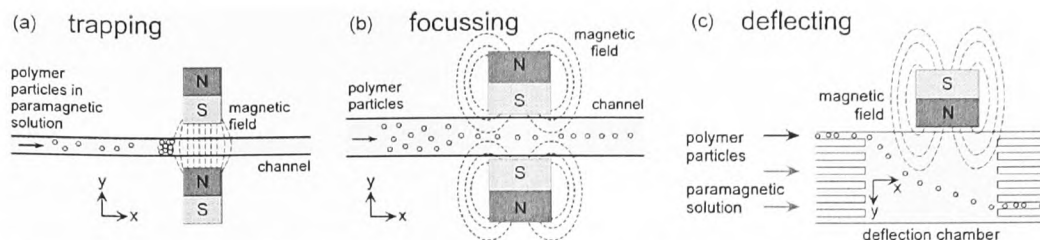


Fig. 1. Principle of particle handling using diamagnetic repulsion forces: (a) trapping of particles in flow by exclusion from an area of high magnetic field; (b) focussing of particles into a narrow stream between two opposing magnet poles; (c) deflection of particles from the direction of laminar flow by a perpendicular magnetic field.

ist equipment to generate the very high magnetic fields necessary. More recently, diamagnetic repulsion has been applied to smaller scale devices in which magnetic fields can be brought closer to the object of interest, reducing the need for the extremely high magnetic fields used previously. In addition, the repulsive effect of diamagnetism can also be greatly enhanced by suspending the diamagnetic material in a paramagnetic solution such as those containing ions of manganese or gadolinium. Watarai et al. have used conventional permanent magnets to perform studies on the behaviour of diamagnetic polystyrene particles in paramagnetic manganese(II) solutions in fused-silica capillaries under stop-flow conditions by arranging the magnets around the capillary and monitoring particle velocities. The same set-up was also used to trap diamagnetic blood cells [17]. Salts of manganese are considered to be harmful to biological material, however by employing the more stable and less toxic paramagnetic MRI contrast agent gadolinium DPTA, Winkleman et al. trapped living cells in a magnetic field minimum generated between two permanent magnets [18]. In another example, polymer particles of different densities were separated by balancing diamagnetic levitation and gravitational forces inside a device with denser particles exiting via a lower outlet than those that were less dense [19]. Recently, we have demonstrated the effect of diamagnetic repulsion forces on 5 and 10 μm sized polystyrene particles in different concentrations of manganese solution in a continuous flow microfluidic device [20,21].

Here, we expand the field to demonstrate the versatility of diamagnetic repulsion for a range of label-free particle manipulation methods (Fig. 1). Firstly, we use diamagnetic trapping of polymer particles to form a series of plugs along a capillary in order to perform simultaneous bioanalytical procedures. We also report the use of diamagnetic repulsion to focus and pre-concentrate polymer particles into a narrow stream along a capillary in continuous flow. Furthermore, we demonstrate how diamagnetic forces can be used to deflect and separate two particle populations of differing diameters in continuous flow using size selective diamagnetophoresis.

2. Theory – diamagnetic repulsion

The magnetic force (F_{mag}) acting on a particle (Eq. (1)) depends on the difference between the magnetic susceptibility of the particle, χ_p , and the magnetic susceptibility of the medium, χ_m , as well as the volume of the particle, V_p , the magnetic flux density and gradient of the magnetic field ($\mathbf{B} \cdot \nabla \mathbf{B}$), and μ_0 , the permeability of free space ($4\pi \times 10^{-7} \text{ H m}^{-1}$):

$$F_{\text{mag}} = \frac{(\chi_p - \chi_m)V_p}{\mu_0} (\mathbf{B} \cdot \nabla) \mathbf{B} \quad (1)$$

For a magnetic particle ($\chi_p > 0$) suspended in an aqueous diamagnetic medium ($\chi_m < 0$) the difference between the two values becomes positive and the particle is attracted to the magnetic field. If the particle is diamagnetic ($\chi_p < 0$) and the medium is paramagnetic ($\chi_m > 0$) then the difference becomes negative and the particle is repelled from the magnetic field towards an area of field minima.

These two magnetic effects are summarised in Fig. 2. Thus diamagnetic forces can be used to direct or trap diamagnetic particles in areas of magnetic field minima.

As the particle is repelled through the paramagnetic medium it also experiences an opposing viscous drag force, F_{vis} , in N:

$$F_{\text{vis}} = 6\pi\eta r \mathbf{u}_{\text{mag}} C_W \quad (2)$$

where η is the liquid viscosity, r is the radius of the particle, \mathbf{u}_{mag} is the magnetically induced velocity of the particle, and C_W is the viscous drag coefficient due to the surface of the top and bottom chamber walls [22,23]. The force acting on a particle as it is repelled through a medium is equal to that of the opposing viscous drag force and therefore F_{mag} can also be determined experimentally using Eq. (2) by measuring the magnetically induced velocity, \mathbf{u}_{mag} .

In the case of diamagnetophoresis (Fig. 1c), particles are pumped into a rectangular chamber and follow the hydrodynamic flow in the x -direction, \mathbf{u}_{hyd} . The particles also have a velocity in the y -direction, \mathbf{u}_{mag} , induced by the repellent force of the magnetic field. The sum of these two vectors results in the deflection of the particle through the chamber with a velocity, \mathbf{u}_{defl} :

$$\mathbf{u}_{\text{defl}} = \mathbf{u}_{\text{hyd}} + \mathbf{u}_{\text{mag}} \quad (3)$$

Therefore, when \mathbf{u}_{hyd} is fixed, the extent of deflection of the particle depends entirely on \mathbf{u}_{mag} . In turn, when the magnetic field and the

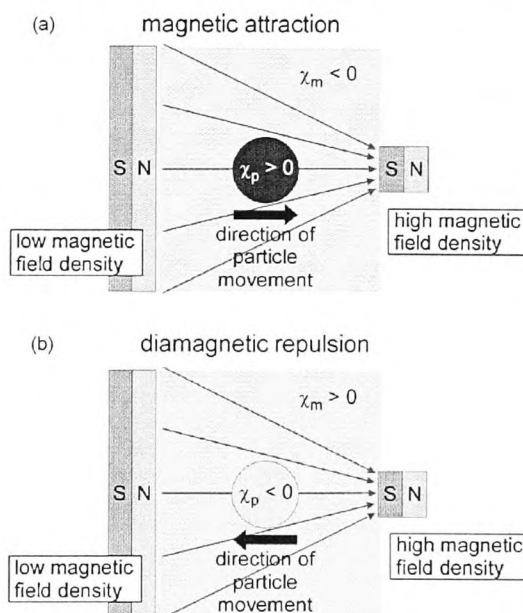


Fig. 2. Schematic of the two types of magnetic effects. (a) A magnetic particle ($\chi_p > 0$) suspended in a diamagnetic medium ($\chi_m < 0$) experiences an attraction towards a magnetic field. (b) A diamagnetic particle ($\chi_p < 0$) suspended in a paramagnetic medium ($\chi_m > 0$) experiences a repulsive force from the magnetic field.

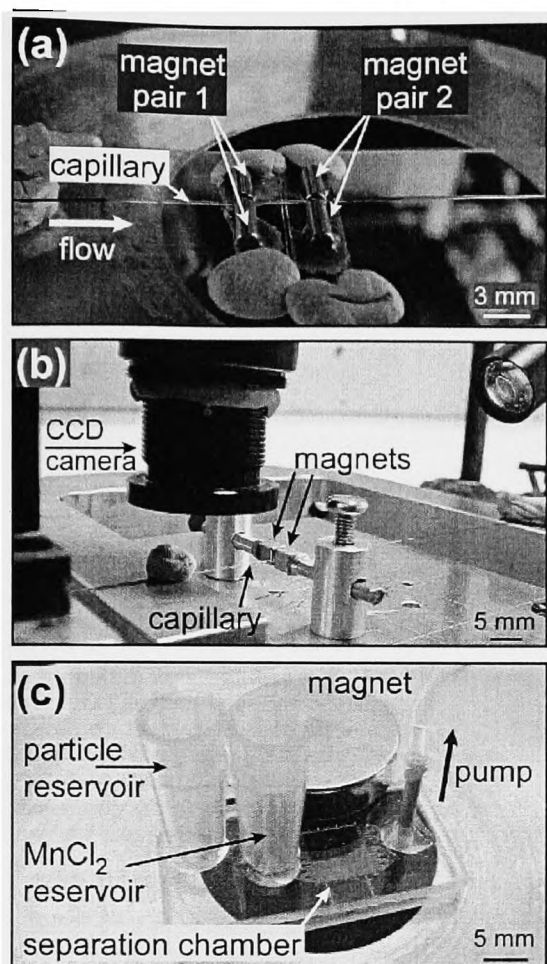


Fig. 3. Photographs of experimental set-up. (a) Trapping: a capillary was positioned between two pairs of magnets with unlike poles facing each other. (b) Focussing: a capillary was positioned between a single pair of magnets, fixed into position with like poles facing each other. (c) Deflection: microfluidic device with pipette tip reservoirs and magnet placed on the surface of the chip.

magnetic susceptibility of both the particles and the medium are kept constant, the value of u_{mag} depends only on the size of the particle.

3. Experimental

3.1. Reagents and polystyrene particle suspensions

Manganese(II) chloride tetrahydrate and gadolinium(III) chloride hexahydrate were purchased from Sigma–Aldrich (Dorset, UK) and solutions were prepared by dissolving the salts in deionised water. Fluorescently labelled biotin (biotin-4-fluorescein) was sourced from MolecularProbes (Invitrogen, Paisley, UK). Bovine serum albumin (BSA) and Tween20 were purchased from Sigma–Aldrich.

Diamagnetic plain polystyrene particles ($\chi_p = -8.21 \times 10^{-6}$) of 5 μm diameter (Microbead NIST Traceable Size Standard) and 10 μm diameter (Megabead NIST Traceable Size Standard) were purchased as aqueous suspensions from Polysciences Europe GmbH (Eppenheim, Germany), with concentrations of 1.21×10^8 and 1.87×10^7 particles mL^{-1} , respectively. Streptavidin coated polymer particles were purchased as an aqueous suspension from Micromer Partikeltechnologie GmbH (Micromod, Germany) with a particle

concentration of 4.6×10^7 particles mL^{-1} . All particle suspensions were diluted in paramagnetic solution; the relevant concentrations are detailed in Sections 3.2–3.4.

All solutions contained 0.01% (w/v) Tween20 to prevent particle agglomeration and sticking. In addition to Tween20, particle suspensions utilised in the particle-based assay also contained 0.01% (w/v) BSA to reduce non-specific binding.

3.2. Diamagnetic trapping for particle-based assays

For the particle-based assay, particle suspensions of plain 10 μm polymer particles and streptavidin coated 10 μm particles were diluted in MnCl_2 (10 wt.%, 0.79 M), to concentrations of 1.9×10^5 and 4.6×10^5 particles mL^{-1} , respectively. Solutions of biotin-4-fluorescein were prepared by dissolving 1 mg of biotin in 100 mL of MnCl_2 solution (10 wt.%), giving a concentration of $1 \mu\text{g mL}^{-1}$.

Particle trapping experiments were carried out using a fused silica capillary with a 100 μm internal diameter (o.d. 363 μm , Polymicro Technologies, Phoenix, USA). The polyimide coating was partly removed using a flame to create a window for observation and the capillary was fixed to a glass slide for support. Tygon tubing (i.d. 254 μm , o.d. 762 μm , Cole-Parmer, London, UK) was used to interface the capillary to a syringe on one end while the other end was dipped into a sample tube. Particle suspensions were pulled into the capillary by applying negative pressure to the syringe with a pump (PHD2000 infuse/withdraw, Harvard Apparatus, USA).

3.2.1. Off-capillary procedure

200 μL of streptavidin coated polystyrene particles were mixed with 200 μL of fluorescently labelled biotin ($1 \mu\text{g mL}^{-1}$). The mixture was allowed to incubate for 30 min and protected from light to avoid photobleaching of the fluorescent tag. Particles were then collected by centrifuging the mixture for 5 min at 5000 rpm and the supernatant removed. The particles were washed by re-suspending them in MnCl_2 solution. This procedure was repeated a further three times before particles were placed on a microscope slide and observed on the fluorescence microscope.

3.2.2. On-capillary procedure

A pair of permanent cylindrical neodymium–iron–boron magnets (1.5 mm in diameter, 5 mm in length) was placed across the 100 μm internal diameter capillary with opposite poles facing each other (Fig. 3a). The capillary was first flushed with MnCl_2 solution using positive pressure to remove any air bubbles from the system. A suspension of streptavidin coated polystyrene particles was then pumped into the capillary under negative pressure at a flow rate of $10 \mu\text{L h}^{-1}$ ($350 \mu\text{m s}^{-1}$) until a plug of particles was formed. A flush of MnCl_2 solution followed, to ensure all particles in the system were trapped in the plug. A second pair of magnets was placed 5 mm upstream along the capillary and a second particle suspension of plain polymer particles was introduced at $7 \mu\text{L h}^{-1}$ ($250 \mu\text{m s}^{-1}$) to form a control plug. After pumping any solution into the capillary, the system was allowed to equilibrate for 5 min to avoid the introduction of air bubbles into the tubing. To perform a particle-based assay, a solution of fluorescently labelled biotin was pumped through the capillary for 13 min at a flow rate of $6 \mu\text{L h}^{-1}$ ($210 \mu\text{m s}^{-1}$) followed by MnCl_2 solution for 20 min. Fluorescence detection was then performed on both the streptavidin and control plugs.

3.3. Diamagnetic focussing of polymer particles

A suspension of 10 μm particles was prepared by diluting stock suspension in MnCl_2 (10 wt.%, 0.79 M) to give a particle concentration of 1.9×10^6 particles mL^{-1} .

A fused silica capillary with an internal diameter of 150 μm was set-up as described in Section 3.2. The capillary was first flushed with MnCl₂ using positive pressure to remove any air bubbles from the system. The suspension of 10 μm particles was then pumped into the capillary under negative pressure at a flow rate 40 μL h⁻¹ (670 μm s⁻¹) and a pair of rectangular NdFeB magnets (3 mm × 3 mm × 4 mm) was fixed either side of the capillary with like poles facing each other 0.7 mm apart (Fig. 3b). The set-up of the camera allowed videos of particles inside the capillary to be taken 10 mm upstream and 5 mm downstream of the magnet position and particle positions were plotted using image analysis software.

3.4. Diamagnetophoresis

A mixed suspension of 5 and 10 μm diameter polymer particles was prepared by diluting stock particle suspensions in MnCl₂ (10 wt.%, 0.79 M) solution to yield final particle concentrations of 6 × 10⁵ and 3.7 × 10⁵ particles mL⁻¹, respectively.

The microchip design featured a 6 mm × 6 mm separation chamber supported by 13 square posts of 200 μm × 200 μm. 16 buffer inlet channels and a single sample inlet channel were situated opposite to 16 outlet channels, and each channel was of 100 μm width. The buffer inlets were branched to allow introduction from a single reservoir and to spread the buffer evenly throughout the chamber. The outlets were branched in a similar fashion to allow pumping via a single withdrawing syringe. Buffer and particle reservoirs were constructed from plastic pipette tips. These were glued around the inlet holes with epoxy resin glue, while a 10 mm section of PEEK tubing (0.5 mm i.d., Cole Parmer, London, UK) was glued into the outlet hole and interfaced to a 1 mL syringe via Tygon tubing (1.0 mm i.d., Cole Parmer, London, UK). Negative pressure was

applied using a syringe pump (Pump 11 Plus, Harvard Apparatus, Kent, UK) to draw the buffer and particles through the separation chamber with withdrawal rates between 20 and 100 μL h⁻¹.

A disc neodymium–iron–boron (NdFeB) magnet 20 mm in diameter by 5 mm in depth (Magnet Sales, Highworth, Swindon, UK) was placed on the surface of the microchip as indicated in Fig. 3c. Videos were taken at the exit area of the deflection chamber and particle positions in the y-direction were recorded using image analysis software approximately 160 μm upstream from the exits.

3.5. Observation and analysis

Capillaries and microchips were observed using either an inverted fluorescence microscope (TE2000-U, Nikon, Japan) with videos recorded using a colour CCD camera (Minitron, Taiwan) or a zoom CCD camera (PV10, Olympus, Japan). Where required, image analysis software (ImageJ, <http://rsnweb.nih.gov/ij/>) was used to plot particle positions and trajectories.

4. Results and discussion

4.1. Diamagnetic trapping for particle-based assays

Diamagnetic particles suspended in a paramagnetic solution such as MnCl₂ are repelled from magnetic fields. This principle was utilised in the trapping of particles along a capillary. Two NdFeB magnets were placed either side of the capillary with opposite poles facing each other, creating an area of high magnetic field gradient in the x-direction. As shown in Fig. 1a, the diamagnetic particles flowing in the x-direction are thus repelled by the magnetic field and should not pass between the two magnets. Initial

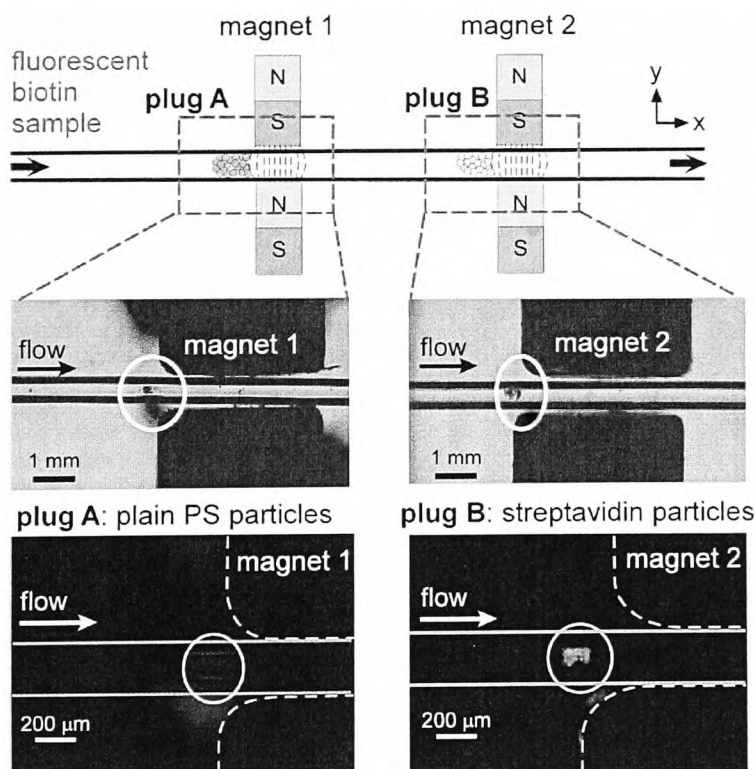


Fig. 4. Diamagnetic trapping of particles showing the location of the formed plugs relative to the magnet pair position and the fluorescence observed from the particle plugs after flushing with fluorescently labelled biotin. The streptavidin functionalised plug was on the right of the image and the negative control on the left.

experiments proved successful in trapping diamagnetic particles in flow using this technique. Control experiments were also performed in which particles were suspended in water without MnCl_2 . Particles in these experiments were not trapped by the magnets indicating the trapping of particles in the paramagnetic buffer was a result of diamagnetic repulsive forces. However the efficiency of the capture depended on the flow rate at which the particles were travelling. At high flow rates some particles were not stopped by the field and would pass through the two magnets. In order to perform simultaneous particle-based analysis a series of different plugs should be formed along the capillary, with different surface functionalities. Hence, it was imperative that there was no particle cross-contamination between the plugs and so the plugs must be formed with a 100% trapping efficiency. Experiments were performed to investigate the optimum flow rate at which 100% trapping efficiency was achieved and this was found to be $10 \mu\text{L h}^{-1}$ ($350 \mu\text{m s}^{-1}$). For the formation of a second plug in the capillary the flow rate was $7 \mu\text{L h}^{-1}$ ($250 \mu\text{m s}^{-1}$) for 100% trapping efficiency.

Once the trapping of particles with 100% efficiency was achieved, the system could be applied to simultaneous particle-based analysis, similar to our method demonstrated previously with magnetic particles [11]. The binding between two molecules such as biotin and streptavidin is commonly performed in a biological buffer, such as phosphate buffered saline. It was therefore necessary to first test the binding between fluorescently labelled biotin and streptavidin in the paramagnetic MnCl_2 solution and to confirm a fluorescent signal could be detected. The off-chip binding of fluorescently labelled biotin and streptavidin on the surface of the particles, as outlined in Section 3.2, left the particles bright green in colour when observed using the fluorescence microscope, indicating that the binding had been successful in the MnCl_2 solution. A negative control was also performed using plain polystyrene particles and there was no measurable increase in fluorescent signal, indicating little or non-specific binding.

Once the assay had been successfully performed off capillary in MnCl_2 , the procedure was moved to the capillary as outlined in Section 3.2. Two plugs were formed along the capillary approximately 6.5 mm apart, one made from streptavidin coated particles and the other from plain polystyrene particles for the negative control. Fig. 4 shows the position of the two plugs relative to the arrangement of the two magnet pairs. The formation took approximately 10 min per plug. The particle plugs were flushed with a solution of fluorescent biotin followed by MnCl_2 and the fluorescent signal from the two plugs was monitored. At the bottom of Fig. 4 the two particle plugs are shown after flushing with the biotin solution. The plug consisting of streptavidin-coated particles appeared a very bright green when observed on the microscope, whereas the plug of plain polystyrene particles exhibited no fluorescence. The two plugs were flushed with biotin for 13 min at a flow rate of $6 \mu\text{L h}^{-1}$, which corresponded to a fluid volume of just 22 nL. The biotin concentration was $1.6 \mu\text{M}$, hence, in a fluid volume of 22 nL the number of moles of biotin used in this assay was 35 fmol. These results show the ease at which diamagnetic manipulation can be used to form plugs of surface functionalised polymer particles for simultaneous bioanalytical procedures and confirmed that such binding events between biological molecules were successful in paramagnetic MnCl_2 solutions. An alternative to MnCl_2 solution for experiments involving biological material would be the use of the paramagnetic ion gadolinium. Gadolinium complexes are not only more paramagnetic than manganese compounds; they are also generally considered less toxic and are used as a contrast agent in MRI applications. Our initial experiments show the potential of diamagnetic trapping for particle-based analysis in which many plugs could be formed along one capillary to do a variety of simultaneous bioanalytical procedures such as immunoassays or DNA hybridisation.

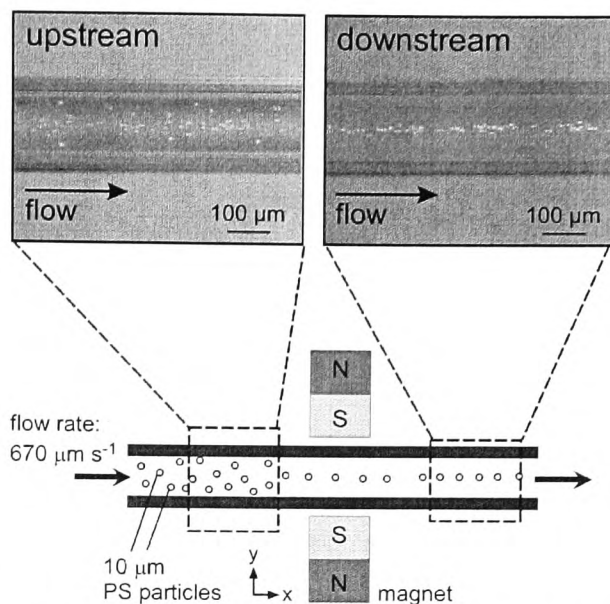


Fig. 5. Diamagnetic repulsion for focussing of $10 \mu\text{m}$ polystyrene particles into the centre of a $150 \mu\text{m}$ diameter capillary: The photograph on the left was taken 10 mm upstream from the magnet pair and clearly shows the distribution of particles across the entire width of the capillary. The photograph on the right was taken 5 mm downstream from the magnet pair, showing the particles focussed into the centre.

4.2. Diamagnetic focussing for sample pre-concentration

Diamagnetic manipulation can be used to stop particles in flow to form plugs as discussed in Section 4.1. A similar set-up was used to investigate the use of diamagnetic forces to continuously focus particles dispersed in solution into a narrow stream. In this application the magnets were arranged such that they had like poles facing each other 0.7 mm apart. Such an arrangement creates an area of zero magnetic field between the two magnet surfaces, as magnetic field lines cannot cross (Fig. 1b). Diamagnetic particles dispersed across the capillary in the y -direction would be repelled from the area of high magnetic field and, as discussed in Section 2, particles

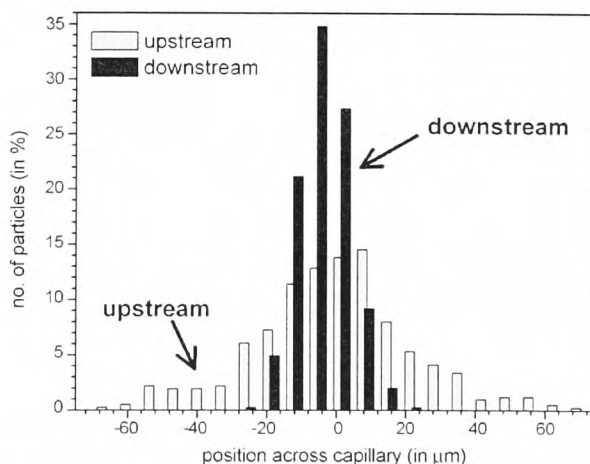


Fig. 6. Histogram of the particle distribution across the capillary width showing the focussing of polymer particles into the centre of the $150 \mu\text{m}$ diameter capillary. Upstream, the $10 \mu\text{m}$ diameter particles were distributed over the entire width of the capillary. After passing the magnet pair, the particles were focussed into a narrow band $\pm 20 \mu\text{m}$ from the centre of the capillary.

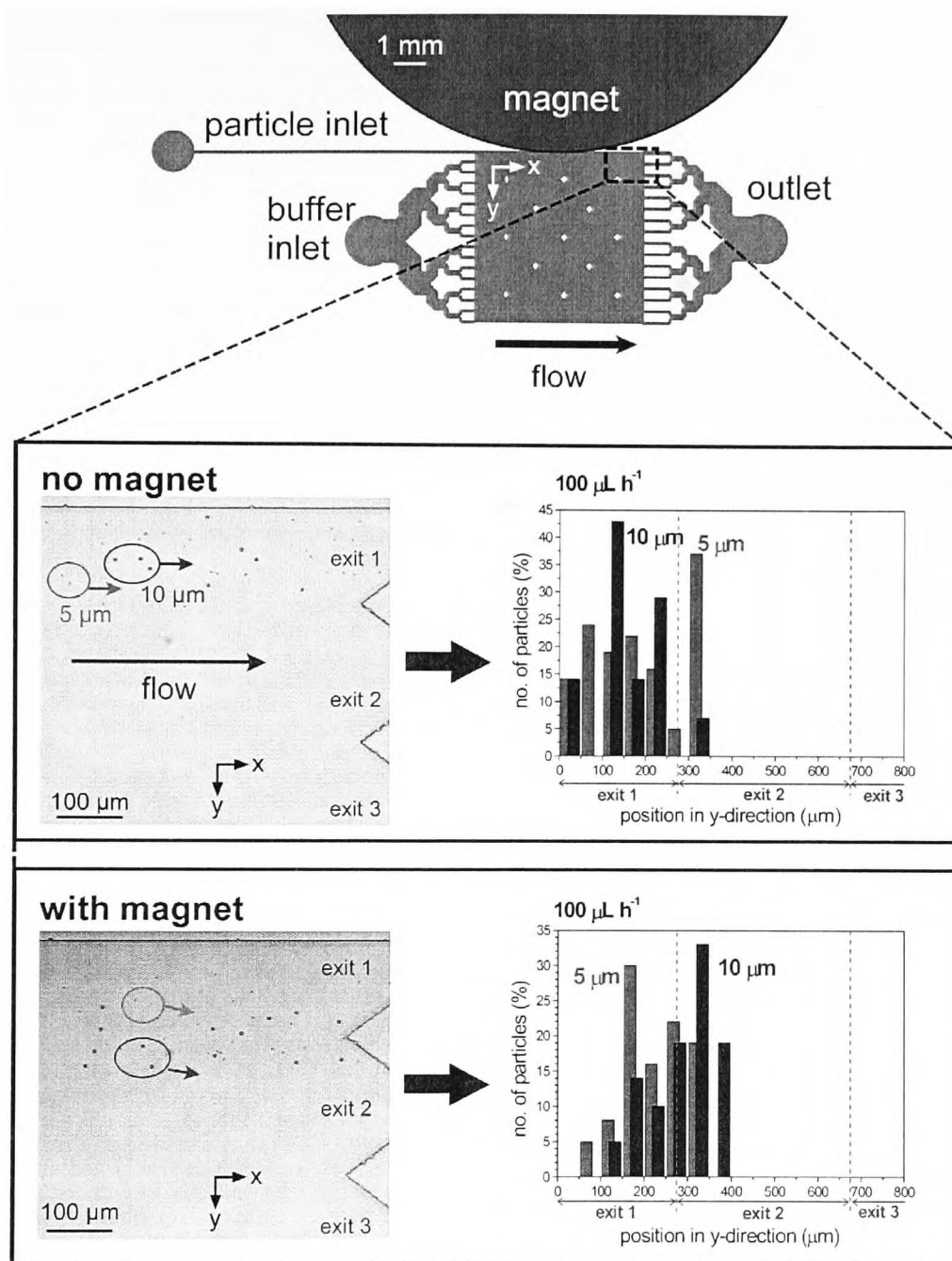


Fig. 7. The microfluidic chip used for diamagnetophoresis experiments featuring a 6 mm × 6 mm deflection chamber supported by a number of posts, a single particle inlet, 16 buffer inlets and 16 exits merging into a common outlet. In the absence of a magnetic field, the particles were found to follow the direction of laminar flow and left the chamber directly opposite the inlet via exit 1. When the NdFeB magnet was placed near the microfluidic chamber, the particles were deflected and depleted from the chamber wall. The 10 μm particles were deflected to a larger extent than the 5 μm particles. The photographs on the left were generated by overlaying seven still images from the video footage.

should move to the magnetic field minimum in the centre of the capillary and thus should be focused into the centre stream.

A fused silica capillary (i.d. 150 μm) was prepared according to Section 3.3. A suspension of 10 μm polymer particles was pumped into the capillary under negative pressure and videos were taken upstream and downstream of the magnet pair. Fig. 5 shows the particle distribution inside the capillary upstream and downstream from the magnet position. Particles were distributed across the

entire capillary width before they reached the magnet pair. As the particles approached the magnets they were repelled by the magnetic field gradient close to the magnet surface and into the area of zero field in the centre of the capillary. The diamagnetic particles were continuously focused into this area as they passed between the two magnets. Fig. 6 shows a histogram of the relative particle positions in μm along the width of the capillary 10 mm upstream and 5 mm downstream of the magnet pair. The yellow bars indicate

that upstream of the magnets the particles occupied $\pm 70 \mu\text{m}$ of the centre of the capillary, a spread of $140 \mu\text{m}$. The blue bars signify the positions of the particles after passing through the two magnets. The particles were focused to within $\pm 20 \mu\text{m}$ of the centre of the capillary by the magnetic field, a reduction of over 1/3 of the original particle distribution. Again, control experiments were performed in which particles were suspended in water without MnCl_2 present and particles were not observed to focus between the two magnets.

These results demonstrate that diamagnetic forces can be used to rapidly focus and pre-concentrate polymer particles into a narrow particle stream at relatively high flow rates ($650 \mu\text{m s}^{-1}$) using a simple magnetic set-up, without the need for particle doping or a specific flow focussing microfluidic design with a large number of pumps such as those used in flow cytometry applications. Due to the set-up of the camera in these experiments the focussing of particles could only be investigated in one plane, future work would include the exploration of three-dimensional focussing using this system. In addition, work will include investigations into the focussing of different sizes of particles.

4.3. Diamagnetophoresis – diamagnetic separation of particles sizes

Diamagnetic repulsion could also be used to deflect particles from the direction of laminar flow inside microfluidic devices (Fig. 1c). In this application a microfluidic chip with a relatively large square deflection chamber was utilised. Particles entering the chamber in the absence of a magnetic field would follow the laminar flow in the x -direction and should exit the chamber directly opposite to its entrance position. If a magnetic field is applied perpendicular to the fluid flow in the y -direction then diamagnetic particles should be repelled from the field and deflected in the y -direction away from the magnet surface. This principle was investigated by studying the deflection behaviour of 5 and $10 \mu\text{m}$ diameter particles in 10 wt.% MnCl_2 .

As outlined in Section 3.4, a mixture of 5 and $10 \mu\text{m}$ sized particles was pumped through the chamber and their flow paths at the exits of the chamber were recorded in the absence and presence of a magnetic field. From the videos the position of each particle in the y -direction was measured and plotted as a histogram. Particle numbers of between 10 and 30 depending on particle throughput were analysed for each experiment. Fig. 7 shows the flow paths of 5 and $10 \mu\text{m}$ particles at a flow rate of $100 \mu\text{L h}^{-1}$ ($230 \mu\text{m s}^{-1}$). In the absence of a magnetic field both the 5 and the $10 \mu\text{m}$ particles followed the laminar flow and exited the chamber via exit 1, directly opposite the particle inlet. The histogram signifies the particle position in the y -direction for both particle sizes. Without the magnet, the two particle populations were randomly distributed between 0 and $300 \mu\text{m}$, corresponding to exit 1 of the chamber. When a magnetic field was applied, particles were slightly deflected from the direction of laminar flow as can be seen at the bottom of Fig. 7. The histogram shows that at the applied flow rate of $100 \mu\text{L h}^{-1}$ the $5 \mu\text{m}$ particles were depleted from the chamber wall with no particles seen within the first $50 \mu\text{m}$. The $10 \mu\text{m}$ particles were deflected slightly further than the $5 \mu\text{m}$ particles, between 100 and $400 \mu\text{m}$. The histogram also indicates the distribution of the two particle populations as they begin to separate according to size, with the $10 \mu\text{m}$ particle population being deflected further than the $5 \mu\text{m}$ population. Control experiments performed in water without the presence of MnCl_2 showed no deflection of either particle size confirming that the deflection in paramagnetic buffer was based on diamagnetic repulsion forces.

Following this initial investigation, the effect of flow rate on the deflection behaviour of diamagnetic particles was studied. Fig. 8a shows deflection of the 5 and $10 \mu\text{m}$ particles at a range of flow

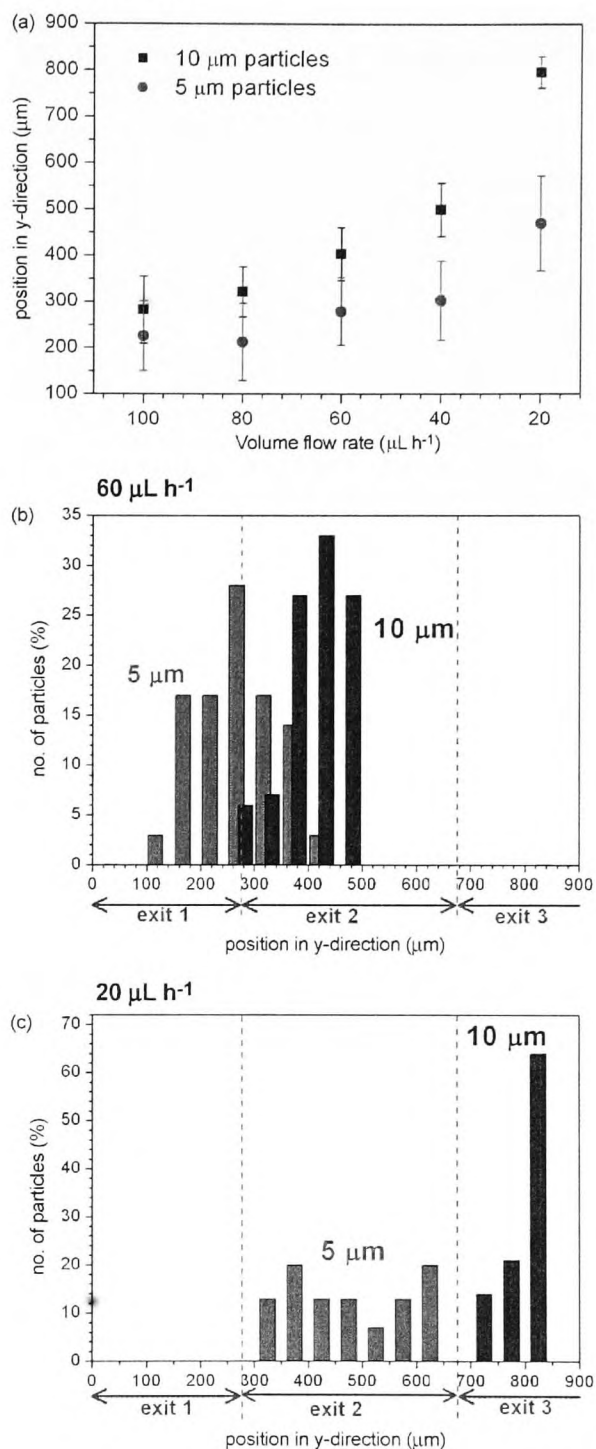


Fig. 8. (a) Diamagnetophoresis of 5 and $10 \mu\text{m}$ diameter polystyrene particles a flow rates from 100 to $20 \mu\text{L h}^{-1}$. The extent of deflection in the y -direction was found to increase with decreasing flow rate and the two particle populations were completely separated at the lower flow rates. (b) Histogram for an applied flow rate of $60 \mu\text{L h}^{-1}$ showing some overlap. (c) Histogram at a flow rate of $20 \mu\text{L h}^{-1}$ showing the complete separation of the $5 \mu\text{m}$ particles leaving the chamber through exit 2 and the $10 \mu\text{m}$ particles leaving through exit 3.

Table 1
Theoretically calculated and observed results for F_{mag} for 5 and 10 μm particles.

Particle size (μm)	Theoretical F_{mag} (N)	Observed F_{mag} (N)
5	-3.2×10^{-16}	$-2 (\pm 0.06) \times 10^{-13}$
10	-2.5×10^{-15}	$-1.2 (\pm 0.07) \times 10^{-12}$

rates between 100 and 20 $\mu\text{L h}^{-1}$, corresponding to a flow velocity between 230 and 45 $\mu\text{m s}^{-1}$. As the flow rate decreased, both particle populations were deflected further due to the smaller contribution of u_{hyd} to the particle trajectory (Eq. (3)). More notably, as the flow rate decreased the two particle populations could be separated from each other. A histogram of the particle positions at 60 $\mu\text{L h}^{-1}$ (Fig. 8b) indicates that the 5 μm particles were deflected between 100 and 400 μm while the 10 μm particles were deflected between 250 and 500 μm . A further decrease in flow rate to 20 $\mu\text{L h}^{-1}$ (Fig. 8c) improved the separation even more with the 5 μm particles being deflected between 300 and 650 μm (exit 2) and the 10 μm particles being deflected 700 μm or more (exit 3). At this flow rate the two particle populations were fully resolved with no overlap in particle positions.

The deflection of 10 μm particles was greater than that of the 5 μm particles as was expected from Eq. (1), where a larger particle volume (V_p) leads into an increase in the force acting on the particle (F_{mag}). The F_{mag} values can be calculated theoretically from Eq. (1). The observed F_{mag} was calculated from the experiments using Eq. (2) and the measured u_{mag} values by noting the y -deflection of each particle over a given time. Table 1 shows values for calculated and observed F_{mag} values for the 5 and 10 μm sized particles at 20 $\mu\text{L h}^{-1}$. The theoretical values indicate that the force acting on the 10 μm particles from the magnetic field is eight times larger than the force acting on the 5 μm particles. The observed F_{mag} values from the experiment at 20 $\mu\text{L h}^{-1}$ show good correlation with expected values in that the observed force on the 10 μm particles was six times greater than the force acting on the 5 μm particles. It should be noted that the observed F_{mag} values were much higher than the calculated values. However, the theoretical F_{mag} values are an approximation as the magnetic field gradient was not known exactly, a factor that may account for the discrepancy between observed and calculated F_{mag} values. In summary, the 10 μm particles have a larger volume than the 5 μm particles and were found to experience six times greater force from the magnetic field in comparison. At lower flow rates the particles spend longer under the influence of the magnetic field and therefore a size selective separation of the two particle populations in continuous flow was possible. Future work could include the separation of different particles or substances with differing magnetic susceptibilities. Also this system could potentially be applied to the label-free sorting

and isolation of cells in continuous flow as almost all biological cells have high water content. As water is diamagnetic [24] cells could therefore be sorted according to size and volume.

5. Conclusions

We have successfully demonstrated the use of diamagnetic forces as a versatile tool for the manipulation of micron-sized polymer microparticles suspended in paramagnetic buffer in microfluidic devices. Polymer particles were trapped in plugs at specific locations along a capillary and utilised in a simultaneous particle-based bioassay to selectively bind an analyte of interest. Diamagnetic forces were also used to rapidly focus and pre-concentrate polymer particles at high flow rates. Furthermore, a size selective diamagnetophoretic separation of 5 and 10 μm particles was successfully demonstrated in continuous flow. This work highlights the potential of diamagnetic repulsion forces for the simple, label-free manipulation of particles and other diamagnetic materials such as cells for a range of bioanalytical and separation techniques.

References

- [1] G.M. Whitesides, *Nature* 442 (2006) 368.
- [2] E. Verpoorte, *Lab Chip* 3 (2003) 60N.
- [3] B.M. Taff, J. Voldman, *Anal. Chem.* 77 (2005) 7976.
- [4] X.Y. Hu, P.H. Bessette, J.R. Qian, C.D. Meinhart, P.S. Daugherty, H.T. Soh, *Proc. Natl. Acad. Sci. U.S.A.* 102 (2005) 15757.
- [5] T. Laurell, F. Petersson, A. Nilsson, *Chem. Soc. Rev.* 36 (2007) 492.
- [6] M. Evander, L. Johansson, T. Lilliehorn, J. Piskur, M. Lindvall, S. Johansson, M. Almquist, T. Laurell, J. Nilsson, *Anal. Chem.* 79 (2007) 2984.
- [7] M. Ozkan, M. Wang, C. Ozkan, R. Flynn, A. Birkbeck, S. Esener, *Biomed. Microdev.* 5 (2003) 61.
- [8] M.A.M. Gijss, *Microfluid Nanofluid* 1 (2004) 22.
- [9] N. Pamme, *Lab Chip* 6 (2006) 24.
- [10] Z.H. Fan, S. Mangru, R. Granzow, P. Heaney, W. Ho, Q.P. Dong, R. Kumar, *Anal. Chem.* 71 (1999) 4851.
- [11] S. Bronzeau, N. Pamme, *Anal. Chim. Acta* 609 (2008) 105.
- [12] N. Pamme, C. Wilhelm, *Lab Chip* 6 (2006) 974.
- [13] N. Pamme, J.C.T. Eijkel, A. Manz, *J. Magn. Magn. Mater.* 307 (2006) 237.
- [14] S.A. Peyman, A. Iles, N. Pamme, *Chem. Commun.* (2008) 1220.
- [15] E. Beaunon, R. Tournier, *Nature* 349 (1991) 470.
- [16] M.V. Berry, M.K. Geim, *Eur. J. Phys.* 18 (1997) 307.
- [17] H. Watarai, M. Namba, *J. Chromatogr. A* 961 (2002) 3.
- [18] A. Winkleman, K.L. Gudiksen, D. Ryan, G.M. Whitesides, D. Greenfield, M. Prentiss, *Appl. Phys. Lett.* 85 (2004) 2411.
- [19] A. Winkleman, R. Perez-Castillejos, K.L. Gudiksen, S.T. Phillips, M. Prentiss, G.M. Whitesides, *Anal. Chem.* 79 (2007) 6542.
- [20] N. Pamme, A. Iles, N. Hirota, *Micro Total Analysis Systems 2007*, vol. 1, 2007, 212.
- [21] M.D. Tarn, N. Hirota, A. Iles, N. Pamme, *Sci. Technol. Adv. Mater.* 10 (2009) 014611.
- [22] J. Happel, H. Brenner, *Low Reynolds Number Hydrodynamics*, Noordhoff International Publishing, 1973.
- [23] Y. Iiguni, M. Suwa, H. Watarai, *J. Chromatogr. A* 1032 (2004) 165.
- [24] N. Hirota, T. Homma, H. Sugawara, K. Kitazawa, M. Iwasaka, S. Ueno, H. Yokoi, Y. Kakudate, S. Fujiwara, M. Kawamura, *Jpn. J. Appl. Phys.* 34 (1995) L991.